ABSTRACT

Title of Document: EXPERIMENTAL STUDIES TO INVESTIGATE PRESSURE LOADING ON TARGET PLATES.

Hans Ulrich Leiste, Ph.D., 2012

Directed By: Professor W.L. Fourney, Department of Mechanical Engineering

The pressure distribution on the bottom of an armored vehicle caused by a detonating explosive buried in soil has been long of interest in the community of the Armed Services. This experimental study discusses results from small-scale tests conducted to determine the distribution of pressure on target plates when subjected to loading due to the detonation of buried mines. A new methodology has been developed in order to measure the pressure – time profiles on the bottom of a vehicle. The tests are conducted by using water, saturated sand, and dry sand as the loading media. Different stand off distances are investigated using saturated sand. Kolsky bars and pressure sensors, on the target plate, are used to determine the free-field pressure - time profile of the output of the charge at any location for the vehicle bottom. For verification of the pressure results at certain distances, the specific impulse measured by utilizing different size round plates are employed. In order to investigate the loading mechanisms, high speed cameras are applied. The small-scale test results can be scaled to full scale by using verified scaling laws. The results of this research are of interest to the U.S NAVY and U.S ARMY in order to develop and evaluate computer codes which are mainly used in soil models. These computer codes are to be used to design mine resistant personnel carriers and in the field to predict the threat assessments.

EXPERIMENTAL STUDIES TO INVESTIGATE PRESSURE LOADING ON TARGET PLATES

By

Hans Ulrich Leiste

Dissertation submitted to the Faculty of the Graduate School of the
University of Maryland, College Park, in partial fulfillment
of the requirements for the degree of
Doctor of Philosophy
2012

Advisory Committee:
Professor W. L. Fourney, Chair
Professor B. Balachandran
Professor H. A. Bruck
Professor H. W. Haslach
Professor C. W. Schwartz

© Copyright by
Hans Ulrich Leiste
2012

Dedication

This work is dedicated to Isabel Maria Rodriguez Andrades.

A missed mother and grandmother who gave so much and demanded so little.

Acknowledgements

First and foremost, I would like to express my gratitude to my advisor Professor William L. Fourney (Assoc. Dean ENME) for his continued guidance and the unconditional support throughout the conducted research.

In addition I would like to thank the members of the committee, Professor B. Balachandran (Chair ENME), Professor H. A. Bruck (ENME), Professor H. W. Haslach (ENME), Professor C. W. Schwartz (ENCE) and the honorary member Professor J. Forbes for their support.

Part of the work was started under the contract to the Office of Naval Research (ONR Indian Head Division) as part of a larger effort. General direction of the overall effort was provided by Mr. Lee Mastroianni (ONR) and Mr. Timothy Hennessey (ONR) (Contract ONR N000140610335).

The main body of work was completed under the supervision of my advisor Professor William L. Fourney at the University of Maryland.

Last but not least I would like to thank Mr. Leslie Taylor and the numerous undergraduate and graduate students of the Dynamic Effects Laboratory at the University of Maryland for helping conducting the numerous experiments.

In addition I would like to thank my family for their full support during the last years.

Table of Contents

List of Figures

Chapter 4

Chapter 5

Chapter 6

List of Tables

PAGES

Chapter *3*

Chapter 4

Chapter 5

Chapter 1: Introduction

Improvised explosive devices (IED) are one of the biggest threats of the wars in Iraq and Afghanistan. Both the U.S NAVY and U.S ARMY are seeking results that could be applied on a large scale to detonations of buried explosives. In order to improve the survivability of a personnel carrier subjected to an improvised explosive device, the pressure applied at the vehicle floor should be known. The results of this study will be used by both organizations in order to develop and improve computer codes which are used to predict pressure time profiles in the field. Additionally, the pressure – time history at any given location at the bottom of a vehicle floor can be used in order to design an armored floor pan for personnel carriers. Pressure time profiles this close to detonating explosive charges have never been measured before. Approximately 500 small scale tests have been conducted at the University of Maryland to determine pressure time profiles and explosive loading mechanisms.

The conducted tests are based on the Cube Root Scaling Law so that the results of the small-scale testing can be extended to field testing. Small scale testing is inexpensive when compared to full scale testing, and in addition, it provides more insight into the mechanisms of explosive loading applied on target plates. Furthermore, small scale testing is time-saving compared to full scale testing and test issues can be resolved prior conducting a field test. It has been shown in the past that results from small scale testing can be scaled up to full scale results [**1**].

The pressure-time profiles measured at different distances are integrated in order to compute the specific impulse. The accumulated impulse is calculated from the specific impulse values using the cylindrical shell method. The computed impulse is then compared to the measured impulse using different diameters of round plates. A series of tests were conducted in the past by using round target plates of different diameters keeping the mass of the target constant. As shown in past

research [**2**] it is important to keep the mass of the target plates constant in order to compare the impulse delivered by the explosive loading.

Chapter 2: Background

Mine Resistant Ambush Protected (MRAP) vehicles, see **Figure 2.1**, are a family of vehicles produced by a variety of domestic and international companies that generally incorporate a V-shaped hull and armor plating designed to provide protection against mines and IEDs. DOD is currently procuring three types of MRAPs. These include Category I vehicles, capable of carrying up to 7 personnel and intended for urban operations; Category II vehicles, capable of carrying up to 11 personnel and intended for a variety of missions such as supporting security, convoy escort, troop or cargo transport, medical, explosive ordnance disposal, or combat engineer operations; and Category III vehicles, intended to be used primarily to clear mines and IEDs, which are capable of carrying up to 13 personnel. The Army and Marines first employed MRAPs in limited numbers in Iraq and Afghanistan in 2003, primarily for route clearance and explosive ordnance disposal (EOD) operations. These route clearance MRAPs quickly gained a reputation for providing superior protection for their crews, and some suggested that MRAPs might be a better alternative for transporting troops in combat than up-armored High Mobility, Multi-Wheeled Vehicles (HMMWV).

Figure 2.1 Mine Resistant Ambush Protected (MRAP) vehicles

MRAPs have been described as providing significantly more protection against IEDs than up-armored HMMWVs. Congressional support for MRAPs, as well as fully funding the program, has been credited with getting these vehicles to Iraq and Afghanistan in a relatively short timeframe, thereby helping to reduce casualties (**Figure 2.2**) [**3**]. A statistic shown in **Figure 2.2** proves the effectiveness of the new vehicle. The IED caused fatalities declined from 60% to below 10% per month with increasing number of MRAPs (1,000 to 10,000) employed in total. **Figure 2.3** shows a MRAP hit by an IED. The vehicle hull stays intact and hence protects the occupants. The double V-shape has proven its advantage compared to the flat vehicle bottom. The V-shape concept was tested in the Dynamic effects laboratory in the past and demonstrated its superiority in small scale tests conducted (**Figure 2.4**).

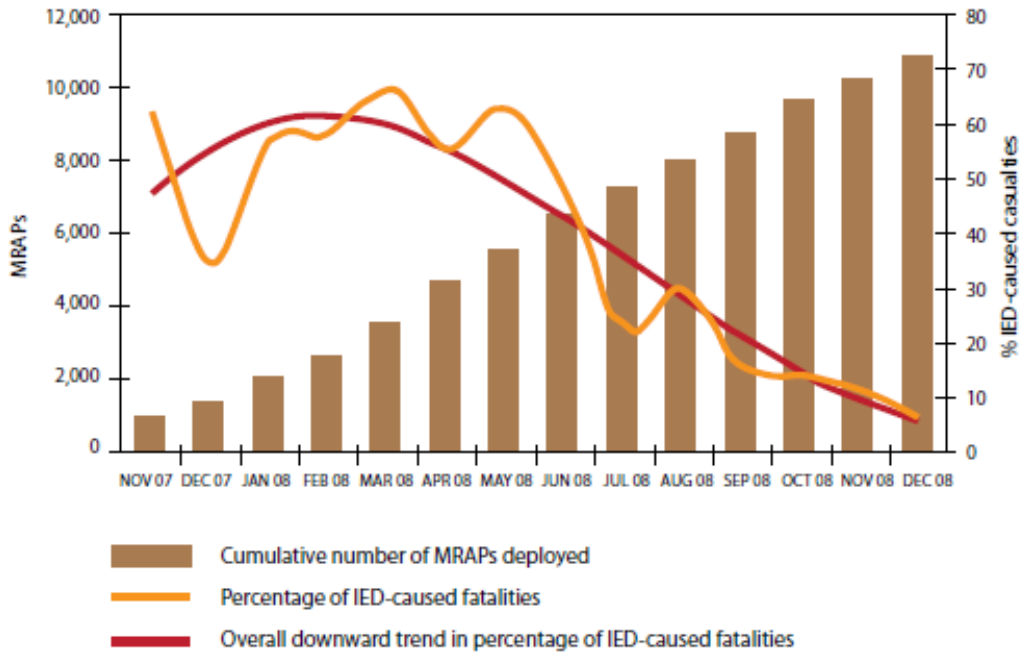

Figure 2.2 MRAPs employed versus casualties between November 2007 and December 2008 **[3]**

Figure 2.3 MRAP incident **[63]**

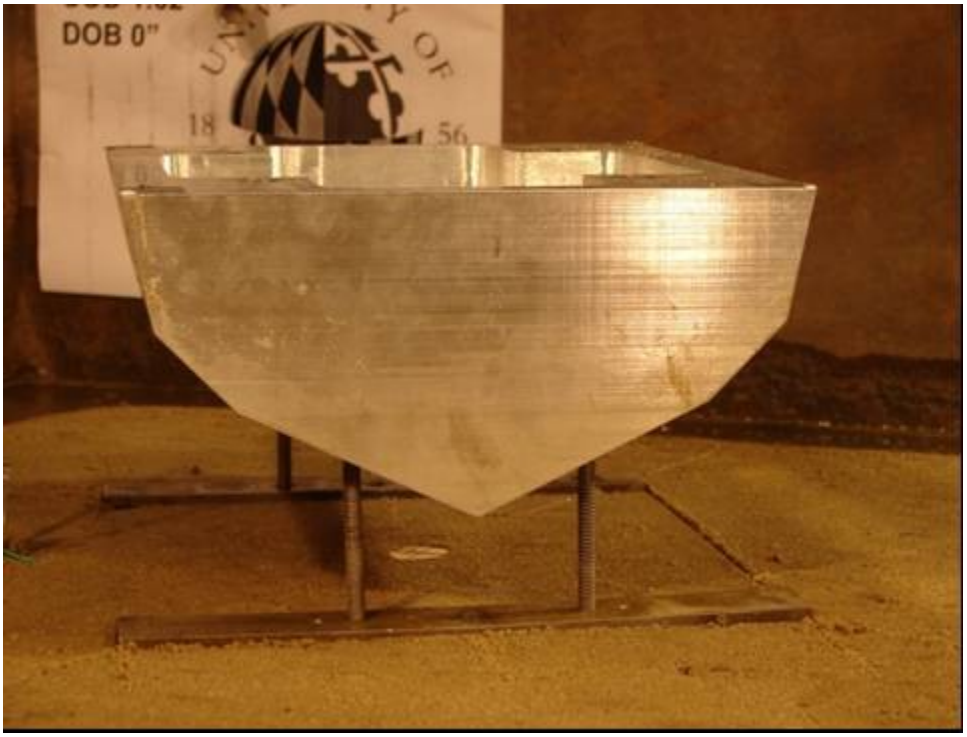

Figure 2.4 Double V-shape tests at UMD

DOD reports that as of January 6, 2011, 13,624 MRAPs had been delivered to Afghanistan, including more than 6,500 M-ATVs. The Army has recently said that it will begin development of yet another MRAP version—the "Ultra-Lite MRAP". The full FY2011 DOD budget request of $3.4 billion for the MRAP Vehicle Fund has been authorized by the Ike Skelton National Defense Authorization Act for FY2011 (P.L. 111-383) **[4]**.

The Dynamics Effects Laboratory at the University of Maryland has been involved during the last 8 years in a type of research that studies the effects of detonation of a buried mine on target plates of different shapes. The shapes tested include flat, pocket, and V-shape plates of a variety of angles (**Figure 2.4**). The basic research conducted resulted in impulse, acceleration, plastic deformation, and pressure measurements. A huge effort is made in understanding the effects of explosive loading on target plates. The established data base represents a valuable contribution to the research conducted in the field of explosive loading.

Chapter 3: Experimental Apparatus and Instrumentation

This chapter describes the set of instruments that is used in the tests conducted. It refers to all technical equipment used except the Kolsky bars and the Instrumentation used with the bars. Since the Kolsky bars are a crucial part of the instrumentation for the pressure measurements taken, they will be discussed in **Chapter 4**. The innovation is to introduce a new technique to measure high pressure profiles very close to buried explosive charges.

3.1 Technical Specifications of Explosives Used

Different types of explosives and charge sizes were used in order to conduct the small scale tests. In certain test set-ups, only single detonators were employed. The main charge utilized contained Deta sheet or Pentolite as output explosive and was designed in the laboratory for specific test set-ups. These charges have an RP detonator attached as the initiating explosive charge. The RP detonators contain RDX (cyclotrimethylenetrinitramine) an explosive nitroamine and PETN (Pentaerythritol tetranitrate). Both components are among the most powerful high explosives known. In the following all types of charges used will be described.

3.1.1 The Function of the RP-3, RP-87, and RP-80 EBW Detonator

In an explosive bridge wire detonator, the explosive is pressed in two increments of different density, with both increments consisting of a secondary type, less sensitive, explosive. The first increment (PETN), or the increment next to the bridge wire, is pressed into the header at a density of approximately 50% of crystal density. The second increment consists of a different type of secondary explosive (RDX) which has been pressed to approximately 90% of crystal density. This

increment is called the output charge of the detonator. The first increment is called the initial pressing. To function as an EBW detonator, electrical energy is applied to the bridge wire. A capacitor is discharged into the bridge wire circuit. The rate of this energy application and its magnitude, results in the sublimation of the bridge wire in the detonator. As the bridge wire sublimates, the shock wave and thermal energy are transferred into the low-density secondary explosive from the wire at about 1500 meters/sec. As the wave travels into the explosive, a detonation of the explosive is initiated and builds up the normal detonation velocity of the initial pressing explosive. This velocity is approximately 5000 meters/sec., since the initial pressing of the explosive is only 50% of crystal density. As the shock wave moves through the initial pressing into the output pressing, the velocity of the wave increases to approximately 8000 meters/sec., due to the higher density of the output pellet.

3.1.2 The RP-3 EBW Detonator

The RP-3 EBW (Exploding Bridge Wire) detonator is manufactured by Reynolds Industries. This detonator is the smallest detonator of all used. It contains 29 mg of PETN explosive and has a very thin stainless steel case which is open towards its end surrounding its explosive train. The dimensions of the detonator are given in **Figure 3.1**.

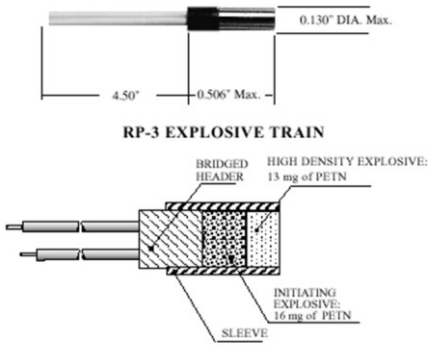

Figure 3.1 The RP-3 EBW explosive train

3.1.3 The RP-87 EBW Detonator

The RP-87 EBW (Exploding Bridge Wire) detonator is manufactured by Reynolds Industries. The explosive is contained in a 0.152 mm thick stainless steel case which is crimped onto the plastic head. It is for use where small size is important. The cross section of the explosive train is shown in **Figure 3.2**. The stainless steel case contains 26 mg PETN (initiating explosive) and 43 mg RDX (output explosive).

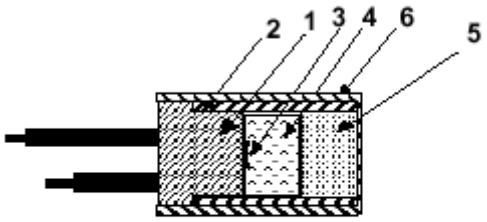

Figure 3.2 The RP-87 EBW explosive train 1. Plastic molded head
2. Brass sleeve
3. Bridge wire (gold)
4. Initiating explosive: 26 mg PETN
5. Output explosive: 43 mg RDX
6. Stainless steel cup 0.152 mm thick

The overall dimensions of the RP-87 are shown in **Figure 3.3**.

Figure 3.3 Dimensions of the RP-87 1. Diameter 4.88 mm
2. Length 10.41 mm

The specific dimensions of all components of the RP-87 detonator are given in detail in **Figure 3.4**.

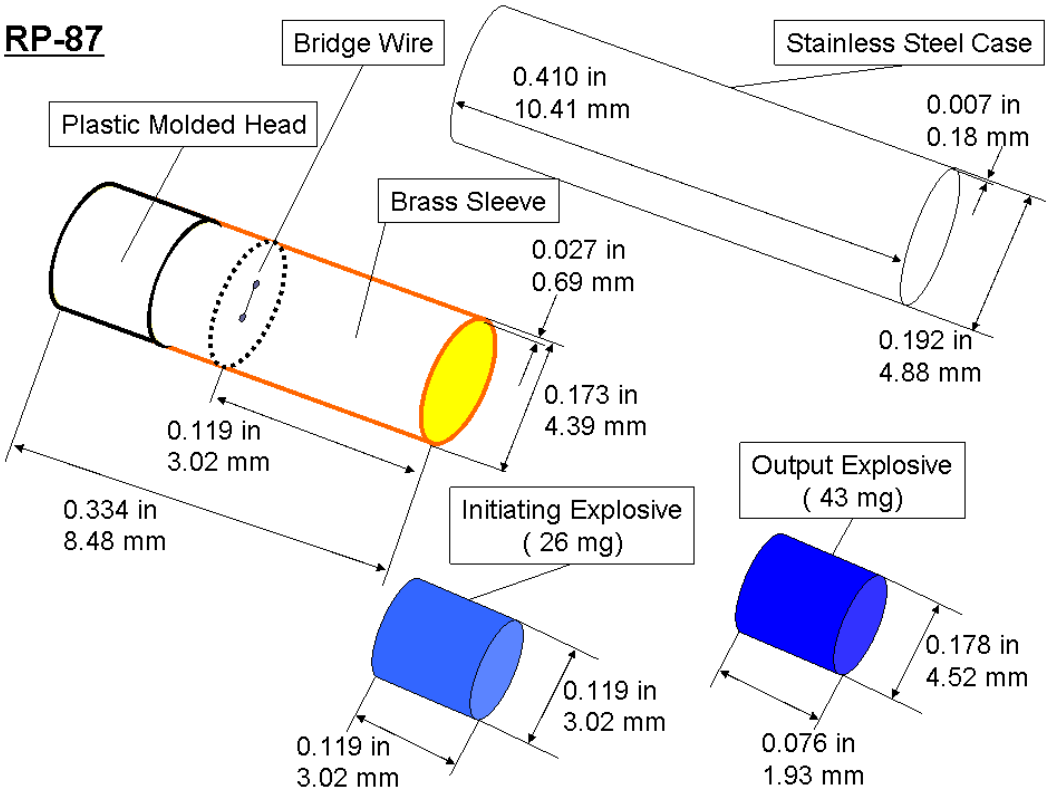

Figure 3.4 Specific dimensions of the RP-87 detonator

3.1.4 The RP-80 EBW Detonator

The RP-80 EBW (Exploding Bridge Wire) detonator, manufactured as well by Reynolds Industries, is a standard end lighting detonator. It is housed in an aluminum cup to provide sealing and strength to the explosive charge. **Figure 3.5** shows a cross section of its explosive train. The aluminum cup contains 80 mg PETN and 123 mg RDX. The PETN initiates the RDX, and the RDX is the output explosive.

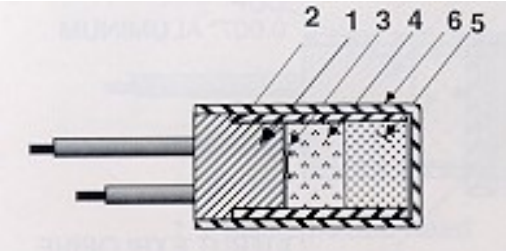

Figure 3.5 The RP-80 EBW explosive train 1. Plastic molded head
2. Brass sleeve
3. Bridge wire (gold)
4. Initiating explosive: 80 mg PETN
5. Output explosive: 123 mg RDX
6. Aluminum cup 0.007" thick

The dimensions of the RP-80 are shown in **Figure 3.6**.

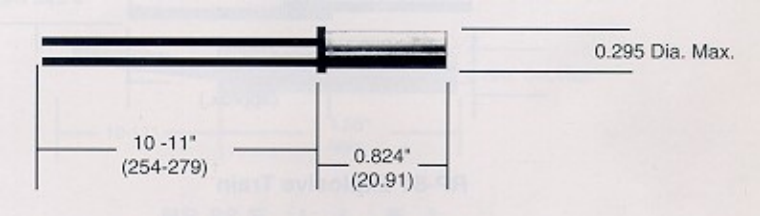

Figure 3.6 Dimensions of the RP-80 1. Diameter 7.49 mm
2. Length 20.93 mm

The specific dimensions of all components of the RP-80 detonator are given in detail in **Figure 3.7**. Note that the case is made out of aluminum.

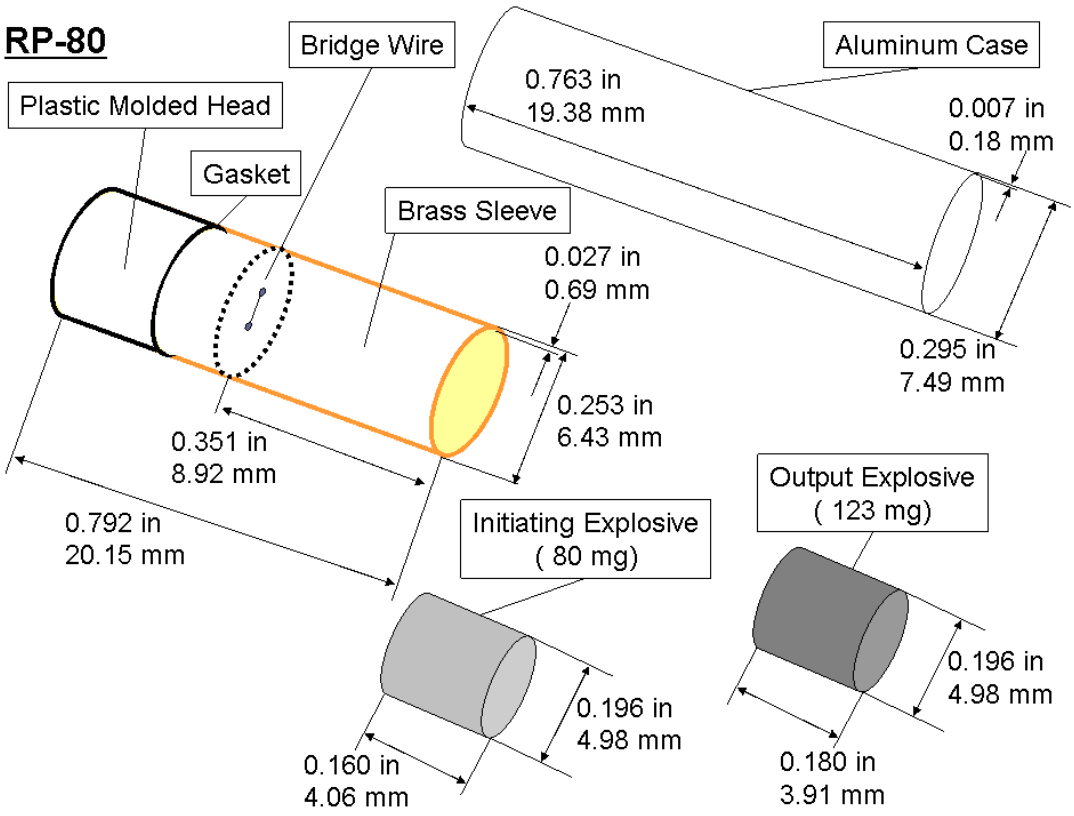

Figure 3.7 Specific dimensions of the RP-80 detonator

Figures 3.8 and **3.9** show the actual components of an RP-80 detonator: The aluminum cup, the plastic molded head, the brass sleeve, the sealing gasket, the initiating explosive (80 mg PTN powder), the output explosive (123 mg RDX pellet), see Figure 1.8 Exploding Bridge Wire.

Figure 3.8 Components of an RP-80 detonator

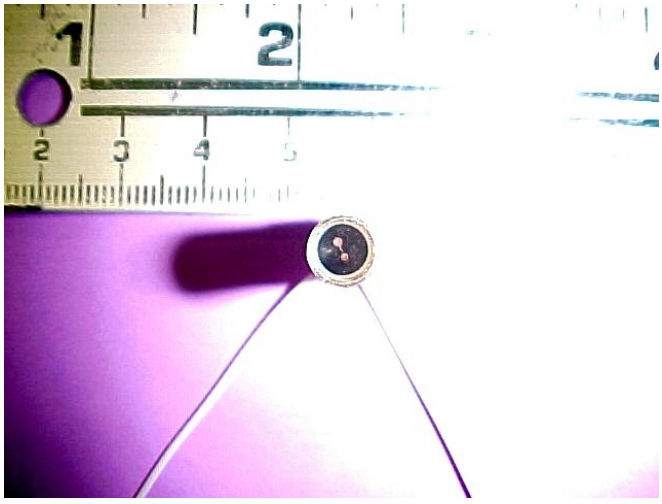

Figure 3.9 Exploding Bridge Wire of an RP-80 detonator

3.1.5 Pentolite Charges

The Pentolite charges were supplied by the NSWC Indian Head Division. Pentolite consists of a composition of 50% TNT (Trinitrotoluene) and 50% PETN (Pentaerythritol tetranitrate) and is considered as a military explosive. In order to develop and evaluate computer codes the U.S NAVY and U.S ARMY needed a well characterized type of explosive. For Pentolite the equation of states are validated. The energy output and the gaseous products are well known.

The charge density of Pentolite is between 1.64 and 1.68 g/cc. The corresponding detonation velocity is between 7,530 and 7650 m/sec.

Three different sizes of Pentolite charges were used. **Figure 3.10** shows the 8.0g, 4.4g, and 0.8g charges from left to right. The total amount of explosive used includes the explosive mass of the booster (69 mg). The charge casings are made out of cardboard. In order to detonate the charge an RP-87 Booster is used and glued into an indentation in the center of the back side of the charge. **Table 3.1** contains the specifics of the Pentolite charges used.

The charge casings were made out of 0.65 mm thick cardboard as shown in **Figure 3.11**. Basically a cardboard ring was used to surround the charge and the top was closed using a cardboard circle with a cut-out in order to attach a detonator.

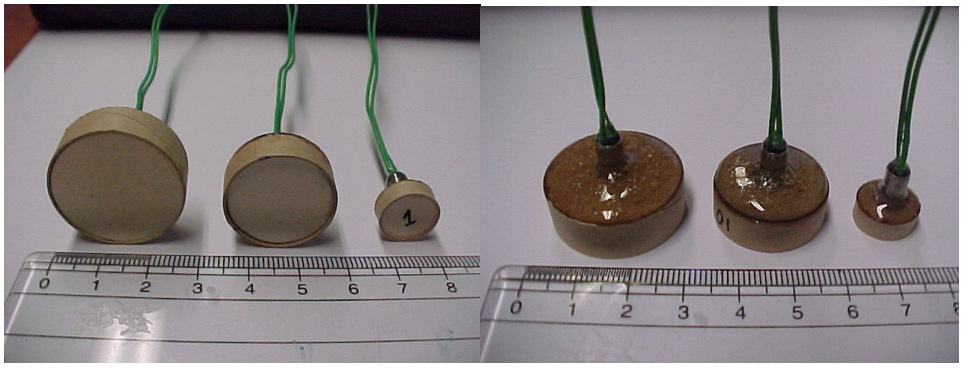

Figure 3.10 Pentolite charges

Pentolite Charge Main Disk Dimensions:	D	H	Volume		Weight
	inches	inches	in^3	cm^3	grams
0.8g Charge	0.474	0.158	0.027881	0.457	0.7310
4.4g Charge	0.858	0.286	0.16536	2.710	4.3356
8.0g Charge	1.049	0.350	0.302489	4.957	7.9310

Detent Dimensions:	D	H	Volume		Weight
	inches	inches	in^3	cm^3	grams
0.8g Charge	0.193	0.020	0.000585	0.010	0.0153
4.4g Charge	0.193	0.020	0.000585	0.010	0.0153
8.0g Charge	0.193	0.020	0.000585	0.010	0.0153

	Actual Explosive Weight Without RP-87 Booster grams:	Volume		Charge Weight
		in^3	cm^3	grams
0.8g Charge	0.731	0.027295	0.447288	0.7157
4.4g Charge	4.331	0.164599	2.697291	4.3157
8.0g Charge	7.931	0.301902	4.947294	7.9157

Table 3.1 Pentolite charge specifics

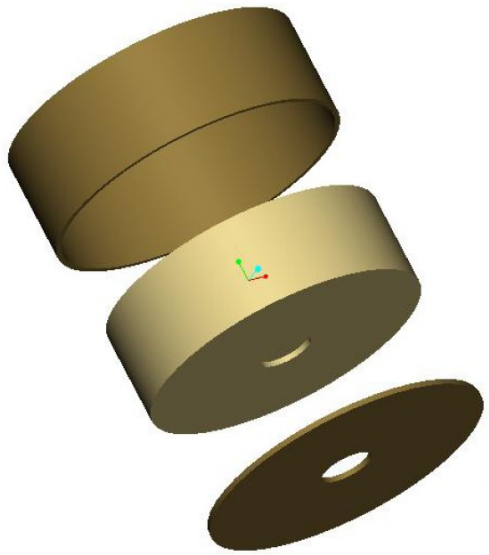

Figure 3.11 Cardboard casing for Pentolite charges

3.1.6 The Detasheet Charges

The Deta sheet charges were designed in our laboratory. Deta sheet charges with explosive masses of 0.8, 1.6, 4.4, 8.0, 13.0, and 16.0 g were used in the conducted tests. The used Datasheet contains 63% PETN and 37% plasticizer which makes it moldable. Therefore any desired charge size could be manufactured. The height to diameter ratio of the charges ranged from about 1.1 to 0.3. The masses listed above only include the masses of explosive components (PETN of the Deta sheet + explosive mass of detonator) used. They do not include the mass of the plasticizer or the charge casings.

As material for the charge casings POM (Polyoxymethylene) also known as acetal or Delrin was used. Acetal rod was machined in order to meet the desired dimensions. The wall thickness of the casings happened to be between 1 and 2 millimeters. The height of the charge casing was chosen accordingly to the amount of explosive used. It exceeded the charge height by approximately 5 millimeters in order to be filled with epoxy. The epoxy was utilized to hold the detonator in place which was inserted in the middle of the charge with a depth of 1/3 of the detonator length. **Figure 3.12** shows the Deta sheet charges of 0.8, 4.4, and 8.0 g having an RP-87 detonator inserted.

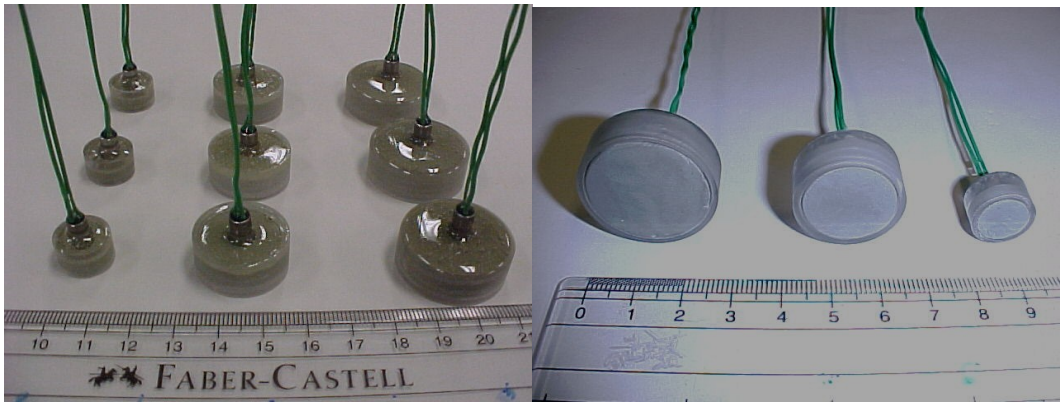

Figure 3.12 Deta sheet charges (8.0g, 4.4g, 0.8g)

Table 3.2 contains the specifics of the Deta sheet charges used in the small scale testing.

Deta-sheet Charge Main Disk Dimensions:	**Diameter**	**Height**	**Volume**		**Total Weight**
	inches	inches	in^3	cm^3	grams
0.8g Charge	0.474	0.276	0.04870	0.798	1.160
4.4g Charge	0.858	0.512	0.29603	4.851	6.875
8.0g Charge	1.205	0.551	0.62837	10.297	12.589
13.0g Charge	1.430	0.560	0.89939	14.738	20.525
16.0g Charge	1.430	0.600	0.96364	15.791	25.287

Table 3.2 Deta sheet charge specifics

In order to prove the cube root scaling laws for pressure measured, the 4.4 and 16.0g Deta sheet charges were scaled in two ways as can be seen in **Figure 3.13**. Since the 16.0g Pentolite charges were two 8.0g charges stacked on top of each other, the Deta sheet charges were scaled accordingly keeping the diameter constant. The added plasticizer contributes to the larger volume of the charges which increases their height. Some tests were conducted using 4.4g Deta sheet charges which have the same diameter as the 4.4g Pentolite charges. This will be covered in detail under the section pressure scaling.

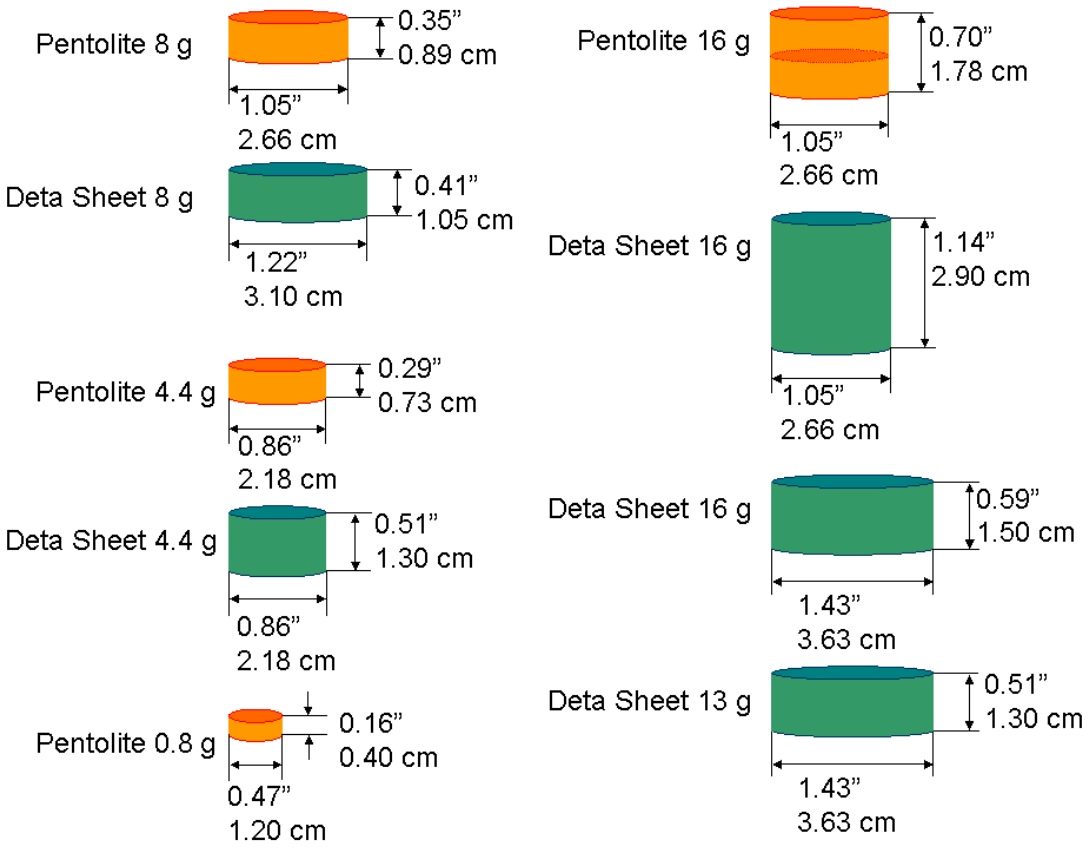

Figure 3.13 Dimensions of scaled charges

3.2 The EBW Firing System FS-10

The FS-10 firing system, manufactured by Reynolds Industries, Inc., is designed to generate and deliver an electrical energy pulse to fire EBW type detonators. The FS-10 is designed to safely initiate EBW detonators, and to fire EBW type detonators only, and should not be used to detonate any other type of detonator (**Figure 3.14**).

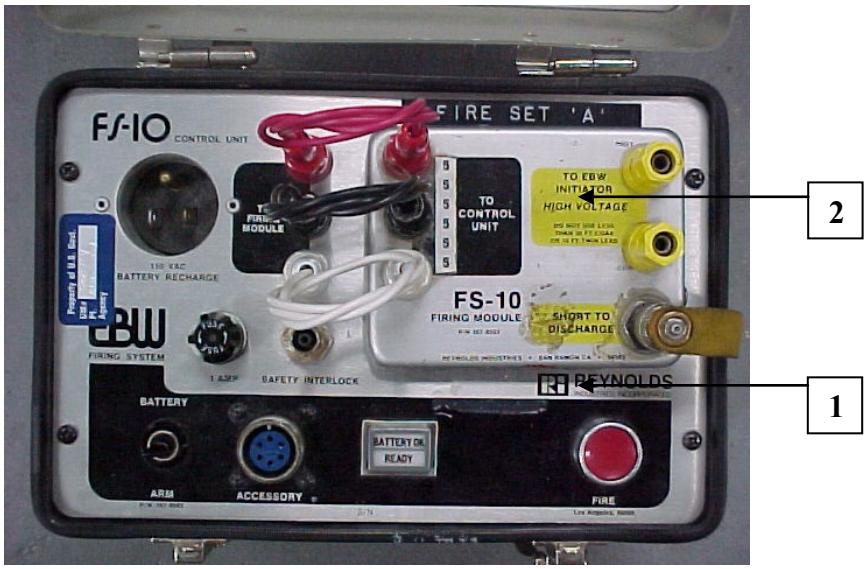

Figure 3.14 The FS-10 firing system: 1. FS-10 control unit
2. FS-10 firing module

The purpose of the FS-10 control unit is to provide low voltage electrical energy to the firing module. The output from the control unit to the firing module is 40 volts when the batteries are fully charged. The input to charge the FS-10 firing module system must be between 32 and 40 volts. This low voltage input charges a one-microfarad capacitor. When this capacitor reaches 3000 volts, the firing module is ready to be fired. Triggering of the triggered spark gap occurs by applying a 30-volt pulse to the red terminal. This discharges the one-microfarad capacitor into the yellow terminals, which will fire the EBW detonator. The detonation will occur in

less than 10 microseconds from the time that the 30-volt pulse is applied to the red binding post. Safety is guaranteed until the shorting plug is mated into the control unit "safety interlock" connection.

To test the equipment set-up prior to the actual test, it is required to use a bridge wire without explosive powder (**Figure 3.15**). The bridge wire operates with electrical energy. An overleaping spark shows that the system operates correctly.

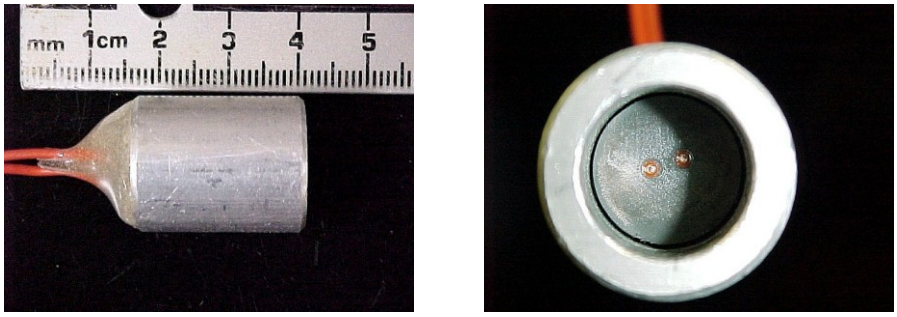

Figure 3.15 Bridge wire top and insight view

3.3 Test Boxes

Two different test boxes were used conducting the tests in saturated sand, dry sand and water.

3.3.1 The Dry Sand / Water Test Box

The test box used (**Figure 3.16**) is designed for conducting dry sand tests and water tests. The test box dimensions are 1220 mm × 610 mm × 610 mm. For the water tests, the sand was removed and a rubber liner was used in order to prevent leaking. The soil samples were compacted using a cinder block and leveled using a scraper which can be seen in **Figure 3.17**. After leveling the soil the charges were buried accordingly to the scaled test set-up. For the water tests conducted the charges

were held in place using a wooden stick which was anchored in an aluminum block on the bottom of the tank.

Figure 3.16 Dry sand / water test box:

Test box length:	1220 mm
Test box width:	610 mm
Test box depth:	610 mm
Soil bed thickness:	300 mm

3.3.2 The Saturated Sand Test Box

The test box used (**Figure 3.17**) is designed for conducting saturated sand tests. The test box dimensions are 1520 mm × 1520 mm × 610 mm. The water inlet in order to saturate the sand is in the bottom of the tank. A layer of gravel and a filter cloth in the bottom of the tank ensures even saturation from the bottom up.

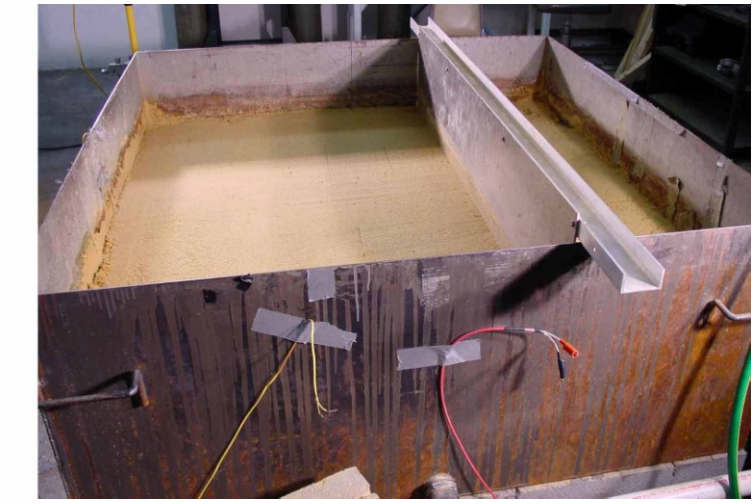

Figure 3.17 Saturated sand test box:

Test box length:	1520 mm
Test box width:	1520 mm
Test box depth:	610 mm
Soil bed thickness:	300 mm

3.4 The High Speed Cameras

In certain test set-ups The Phantom V 7.2 high-speed camera or two Phantom V 12.1 high speed cameras (**Figure 3.18**) were used for visualization purpose. These cameras are a product from Vision Research. The cameras are monochrome models that offer high sensitivity and image resolution. They use a high-speed digital imaging system based on SR-CMOS sensors. The CMOS cameras offer rates of up to one million frames per second. Selections for higher frame rates reduce the image sizes. The digital cameras generate "ciné" image files, which are transferred over an Ethernet cable to an external computer. Basic camera operation requires only a connection to a common laptop or desktop PC for setup, plus power and trigger connections. The pictures taken can be digitally edited, shown as movies or printed out separately. The play back speed is variable and a zoom is available. Several

types of zoom lenses were used to document the process of target loading mechanisms. The Phantom software provides the user with controls to setup camera-operating parameters while viewing the "live" image on the control monitor of the computer. Frame rate, shutter speed, and EDR (Extreme Dynamic Range) functions are set before the shot. This software may also be run on a desktop PC for additional analysis.

The Phantom V 12.1 cameras provide a roughly three times higher image rate using the same resolution compared to the camera V 7.2. Table 1.3 contains the specifications of both camera systems.

Figure 3.18 Phantom V 7.2 (left) and 12.1 (right) cameras

Camera Type	Phantom V 7.2	Phantom V 12.1
Resolution max [# of Pixels]	800 x 600	1,280 x 800
Frame Rate (max Resolution)	6,688	6,200
Frame Rate max	220,000	1,000,000
Pixel Size [µm]	22	20
Exposure Time min [µs]	2	0.3
Shutter min [µs]	1.5	0.3

Table 3.3 Specs of Phantom cameras

3.5 Dynamic Pressure Sensors

The ICP (Integrated Circuit Piezoelectric) Dynamic Pressure Sensors (made by PCB Piezotronics) are specifically designed for shock tube and blast wave measurements and for other applications requiring very high frequency response. Two types of sensors are used in the experiments conducted. Both types are acceleration compensated.

3.5.1 Dynamic Pressure Sensor Model 109C11

The pressure sensor Model 109C11 is able to measure pressure in the range of up to 550 mega Pascal (80,000 PSI) and was used for verification of pressure measurements taken by the Kolsky bar in the very beginning of the test program. This sensor has a sensitivity of 0.01 mV/kPa (0.07 mV/PSI) and a rise time of 1 µs. A general schematic can be seen in **Figure 3.19**. The Model 109 contains a very rigid acceleration compensated quartz element coupled to a tiny amplifier located near the electrical connector. Additionally the diaphragm is ceramic coated in order to withstand abrasion caused by the harsh testing environment.

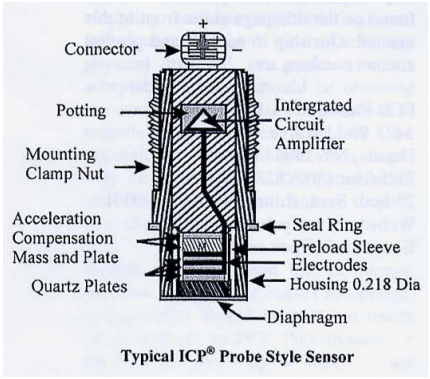

Figure 3.19 Dynamic pressure sensor Model 109C11

3.5.2 Dynamic Pressure Sensor Models 113B24, S102B

Due to their higher sensitivity, the PCB Piezotronics ICP Dynamic Pressure Sensor Models 113B24 and Model S102B are used for pressure measurements in tests conducted in dry sand at distances of three inches or more from the target plate center instead of the Kolsky bars. The pressure sensor Model 113B24 is able to measure pressure in the range of up to 6.9 mega Pascal (1,000 PSI) and Model S102B 34.5 mega Pascal (5,000 PSI). Sensor 113B24 has a sensitivity of 0.725 mV/kPa (5.0 mV/PSI) and sensor S102B has a sensitivity of 0.15 mV/kPa (1.0 mV/PSI). Both have a rise time of 1 μs.

Since the thread of the sensors is shorter than the target plate, they have to be attached into the target plate using specially manufactured casings (**Figure 3.20**). This allows the diaphragm of the sensor to be level with the bottom of the target plate.

Figure 3.20 Dynamic pressure sensor Model 113B24 and casing

3.6 PCB Piezotronics Amplifier Model 483A

The PCB-Piezotronics Amplifier is a 12 channel amplifier (**Figure 3.21**). It is used to amplify the signals of the PCB-Piezotronics pressure sensors. The frequency response of the signal conditioner is 1,000 kHz which reflects a measurement taken every micro second. In order to record the signals measured, the outputs are be connected to the oscilloscopes.

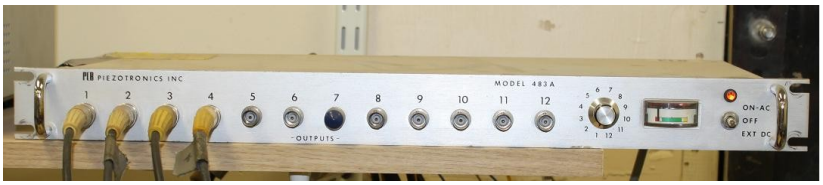

Figure 3.21 Signal conditioner Model 483A used in combination with pressure sensors Model 109C11, 113B24, and S102B

As mentioned in the beginning of this chapter the Kolky bars are covered in **Chapter 4** since they will be described in more detail. Specifically, the design, the use, and the set-up will be explained. Additionally in order to understand the pressure-time profiles measured using the bars, the loading mechanisms for target plates will be explained.

Chapter 4: Kolsky Bar and Pressure Measurements

This chapter describes the method used in order to measure the pressure applied to the bottom of a target plate using Kolsky bars.

Mainly the test results will be obtained using the Kolsky bars due to the severeness of the impact close to an explosive charge. The commercial available pressure transducers don not withstand much testing under these conditions. They usually fail after approximately 8 tests. They respond to temperature change and hence tend to not give good results after the pressure peak was measured. Additionally they are expensive whereas the Kolsky bar is a low-priced solution. The latest developed model of the Kolsky bar is very durable, reusable and works very reliably in harsh environments.

The propagation of elastic waves in solids has long been an area of interest. The stress waves provide a powerful tool for studying the mechanical properties of solids. A technique to measure the shape of a stress pulse in a long elastic bar was first described in 1914 by Bertram Hopkinson **[5]**. He investigated experimentally the propagation of stress pulses in long bars. He developed the Hopkinson pressure bar, an application of the theory of stress propagation of elastic pulses in a cylindrical bar. Later Herbert Kolsky **[6]** introduced the Kolsky (split Hopkinson) pressure bar technique. In this application the specimen is sandwiched and dynamically compressed between two pressure bars. He measured the displacement profiles in both bars by adding displacement gages and oscillographic recording techniques. He was able to obtain complete pulse amplitude wave forms. He used a one-dimensional elastic wave analysis in order to show how stress and strain within the deforming specimen are related to displacements in the pressure bars.

In the following the technique of using the modified Kolsky bar will be explained. Details of the test set-up will be revealed in this chapter. **Figure 4.1** shows how the measurements taken were obtained. The Kolsky bars sense the pressure signal at various points caused by the detonated buried explosive. The circuit box completes the Wheatstone bridge needed by the strain gages mounted on

the Kolsky bar. The eight signal conditioning units amplify the signals which are recorded by 2 oscilloscopes. The test set-up is shown in **Figure 4.1**. The depth of burial (DOB) of the charge and the stand-off distance (SOD) of the target are defined for the standard case of testing in **Figure 4.1**. The cube root scaling law **[12], [64], [65]** is used in order to scale the experiment with respect to the corresponding prototype. The scaling factor of 10.1 is calculated, taking the cube root of the explosive mass of the prototype over the explosive mass of the model. The field conditions (prototype) were assumed to be a SOD of 40.64 cm (16 inches) and a DOD of 10.16 cm (4 inches) for a 4.536 kg (10 lb) charge. Using a 4.4 gram charge in the model testing, the SOD of 4 cm (1.58 inches) and a DOB of 1 cm (0.39 inches) can be calculated.

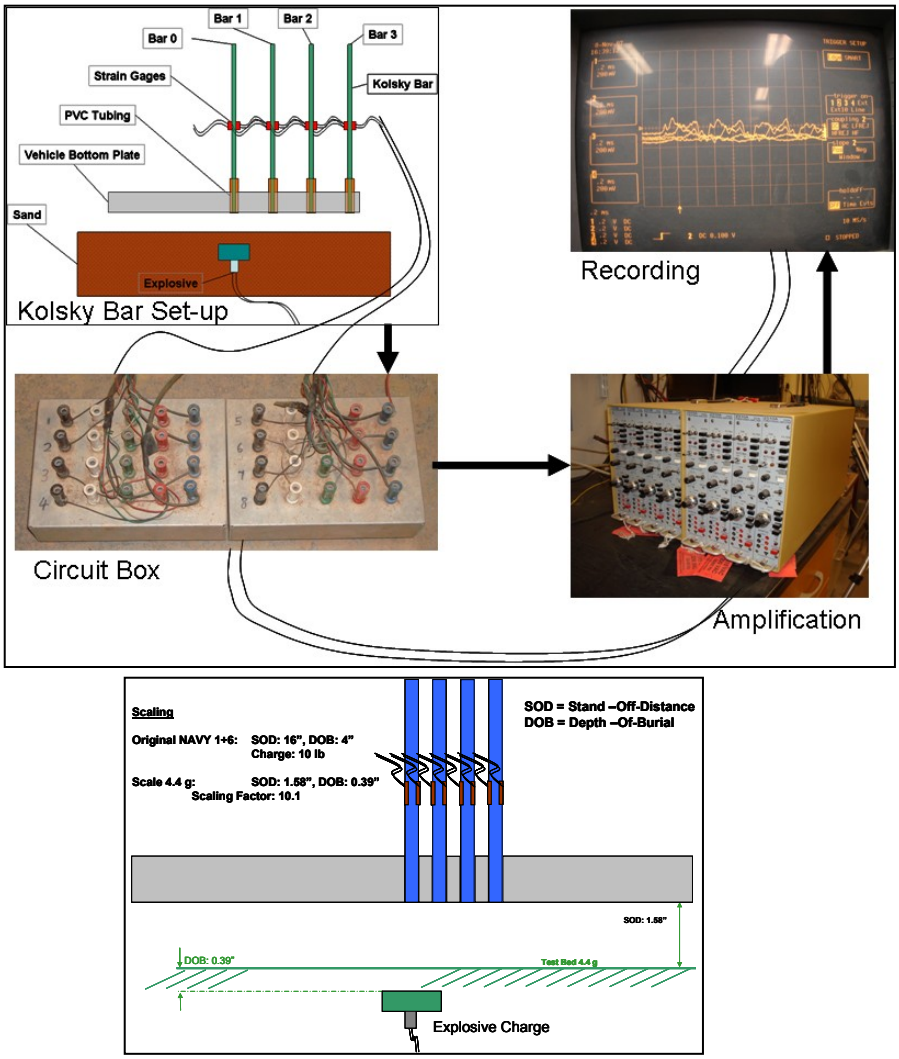

Figure 4.1 Obtaining the test results and some definitions

4.1 Introduction to the Kolsky Bar Use

We modified the Kolsky bar test set-up in order to introduce a new technique for measuring a local pressure applied to a target plate. Usually in a typical Split Hopkinson bar set-up a specimen is placed between the ends of 2 straight bars. These bars are called incident bar and transmitter bar. Here we used only the incident bar. The incident bar is exposed to the blast and a stress wave is created which propagates through the bar until it reaches the upper end and there it gets reflected. Note that the bar does not suffer any plastic deformation during the loading process. Strain gages are used to measure strain caused by the stress waves.

In the beginning of the test program we used Kolsky bars as shown in **Figure 4.2**. The detonation of the buried explosive charge ejects the sand-water mixture forming the crater. The ejected material impacts the target plate hence the Kolsky bars which are mounted flush to the bottom of the target plate (**Figure 4.3**). The stress waves caused by the impact travel up the bars and pass the electrical resistance strain gages which are mounted at certain heights above the impacted end of the Kolsky bar. The change in electrical resistance will be measured and recorded using an oscilloscope. Then using experimental stress analyses techniques the pressure which was applied to the bottom of the plate and hence the rods mounted at a certain location can be calculated.

The Kolsky bars used here are made out of stainless steel, 1.22 meters long (4 Feet) and have strain gages mounted at typically 30.5 centimeters (1 foot) from the bottom of the bar if not mentioned otherwise. Two gages are placed opposing each other and wired into a Whetstone Bridge circuit so as to double the axial strain reading and cancel any bending strain. **Figure 4.3** shows a schematic of the early test set-up using the Kolsky bars placed at a distance of 0, 1, 2, and 3 inches from the center of impact. Later we used a different layout which shows the view from the bottom in **Figure 4.4**. Details of why it was changed will be explained in **Section 4.7**. The signals are amplified using a signal conditioning amplifier from Vishay. For recording the signals, two oscilloscopes made by LeCroy are used.

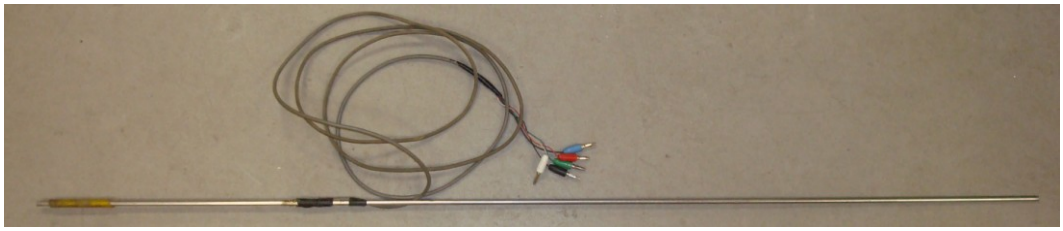

Figure 4.2 Kolsky bar

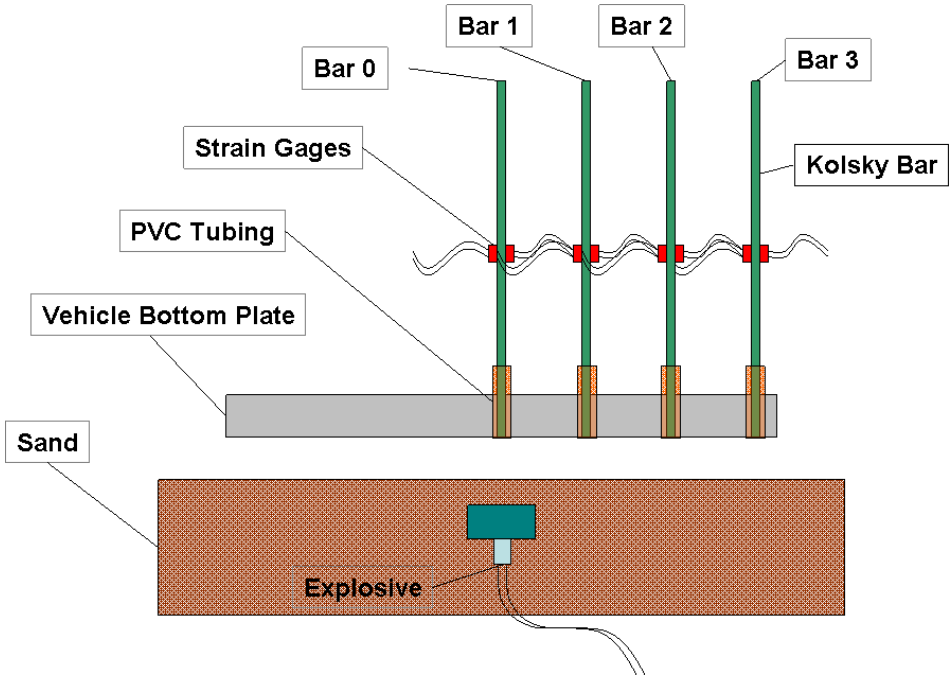

Figure 4.3 Schematic of the early test set-up

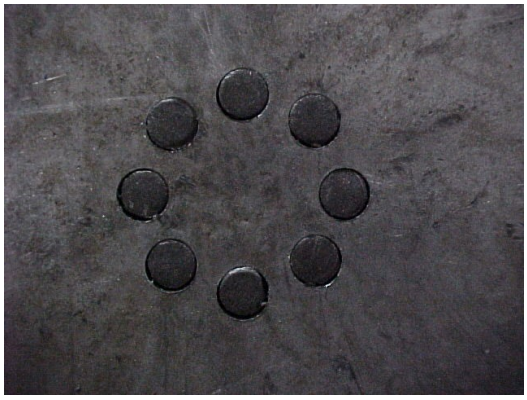

Figure 4.4 Bottom view of target plate of the test set-up at 0.5 inches from center

4.2 The Strain Gages Used

Strain is by definition the amount of the elastic deformation per unit length of a body due to an applied force which is in our case the explosive loading of the bottom end of the Kolsky bar **(Figure 4.5)**. More specifically, strain (ε) is defined as the fractional change in length (**Equation 4.1**). In practice, the magnitude of the measured strain is very small. Therefore, strain is expressed as micro strain (με). The electrical resistance of the strain gage varies in a proportion of the change of ΔL/L. The metallic strain gage used here consists of a metallic foil arranged in a grid pattern **(Figure 4.6)**. The grid is bonded to a thin backing which is called the carrier. The carrier is directly attached to the Kolsky bar using M-bond adhesive resin. Hence the strain experienced by the bar is transferred through the active grid length into the strain gage. The small compression of the Kolsky bar causes a linear change in electrical resistance of the gage taking advantage of the physical property of electrical conductance.

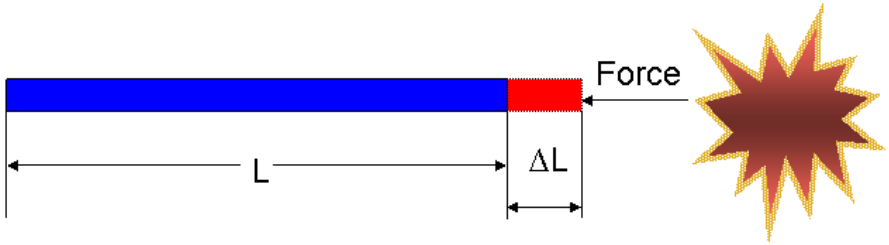

Figure 4.5 Loading of the bottom of a Kolsky bar

$$\varepsilon = \frac{\Delta}{L}$$

Equation 4.1 Definition for strain

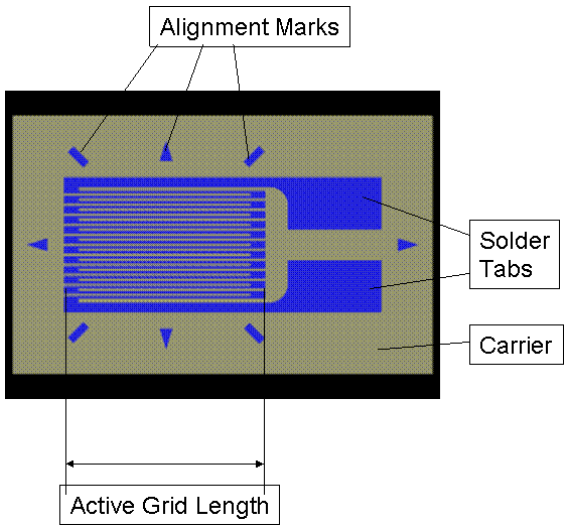

Figure 4.6 Grid pattern of a metallic foil strain gage

4.2.1 Strain Gages Type CEA-06-062UW-350

The strain gage used in almost all of the experiments conducted is shown in **Figure 4.7**. The CEA-series gage is a general purpose gage made by Vishay Micro-Measurements. The gages are supplied with a fully encapsulated grid and exposed copper coated integral solder tabs as seen in **Figure 4.7**. The nominal resistance value of the strain gage is 350 ohm. Two bridge wires connect the strain gage to the bonded terminal as seen in **Figure 4.8**. The terminal accommodates the wires which connect the strain gages with the amplifier. It is advisable to keep the length of the connecting wires as short as possible since the wires will add some resistance to the resistance of 350 ohm of the gages. Because of the way the bridge circuit is set-up using precision resistors of 350 ohm, the amplifier can not balance the difference in resistance. This will be explained in more detail in the following chapter. Here the length of the connecting wires used is about 2.5 meter (8 feet). The bridge wires are necessary in order to keep the force applied on the solder tabs of the gages due to the explosive loading as low as possible. Connecting the wires directly to the solder tab

will lead inevitably to a damage of the strain gage. Both the terminals and the strain gages are bonded using M-Bond adhesive resin type AE from the Measurements Group, Inc to the Kolsky bar. It is very important that the strain gages are properly mounted onto the Kolsky bar in order that the strain is accurately transferred from the bar through the adhesive and the strain gage backing to the foil itself. The gage length is 1.57mm, overall length 5.59 mm, grid width and overall width is 3.05 mm, carrier length is 7.9 mm, and carrier width is 4.8 mm.

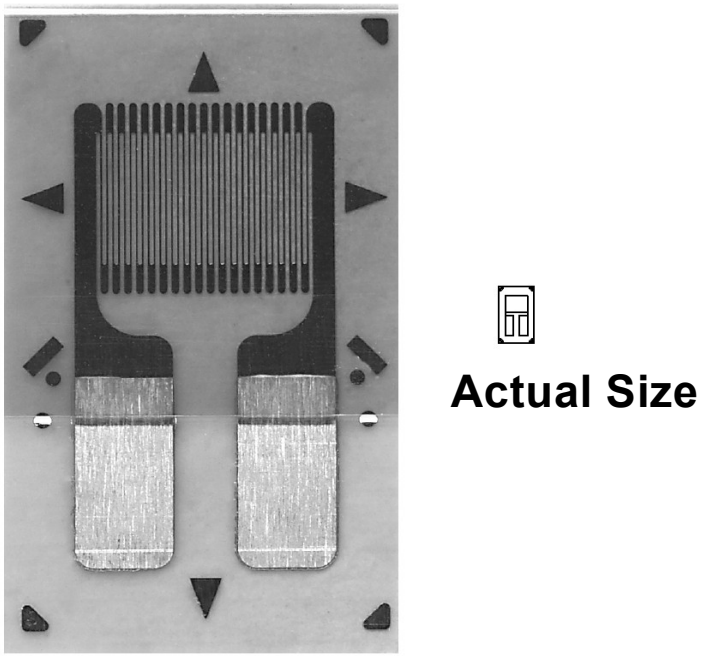

Figure 4.7 Strain gage CEA-06-062UW-350 image magnification and actual size

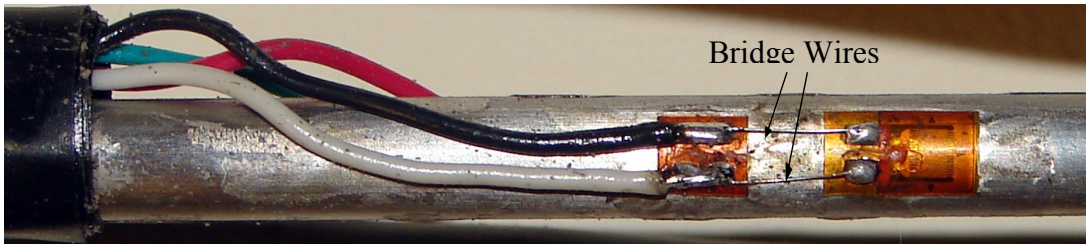

Figure 4.8 Strain gage and terminal mounted on 0.25 inches Kolsky bar

4.2.2 Strain Gages Type EA-06-062AQ-350

The strain gage used in some of the experiments conducted using a 3.4 mm (0.135 inches) diameter Kolsky bar is shown in **Figure 4.9**. The EA-series gage is a very small Constantan (copper-nickel alloy) foil gage made by Vishay Micro-Measurements. The reason for using this type of gage is simply that the CEA series gage as described before does not fit on the bar which is the smallest we ever used. The gages are supplied with an exposed grid and exposed copper coated integral solder tabs as seen in **Figure 4.9**. Therefore the grid of the gage has to be protected during soldering using an installation tape in order not to cover the grid with excessive solder changing its resistance. Again two bridge wires connect the strain gage to the bonded terminal as seen in **Figure 4.10**. The procedure used to bond the gages on the Kolsky bar is the same as described before. The gage length is 1.57mm, overall length 2.90 mm, grid width and overall width is 1.57 mm, carrier length is 6.6 mm, and carrier width is 3.8 mm.

Additional information about strain gage bonding on Kolsky bars can be found in the appendix since there are some specific characteristics which have been observed.

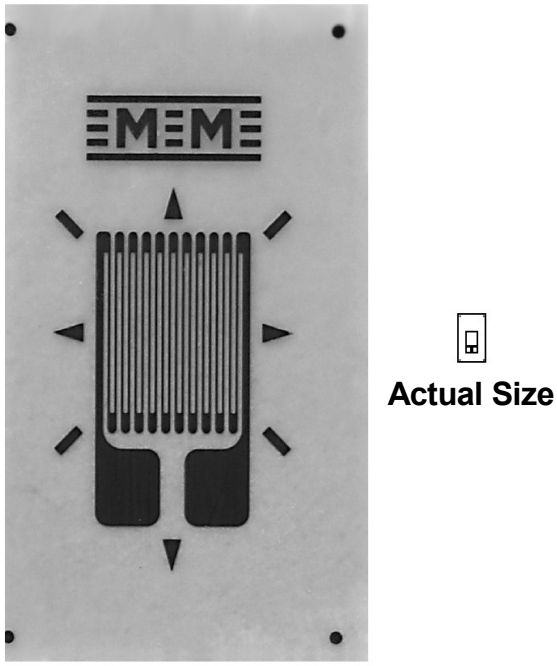

Figure 4.9 Strain gage EA-06-062AQ-350 image magnification and actual size

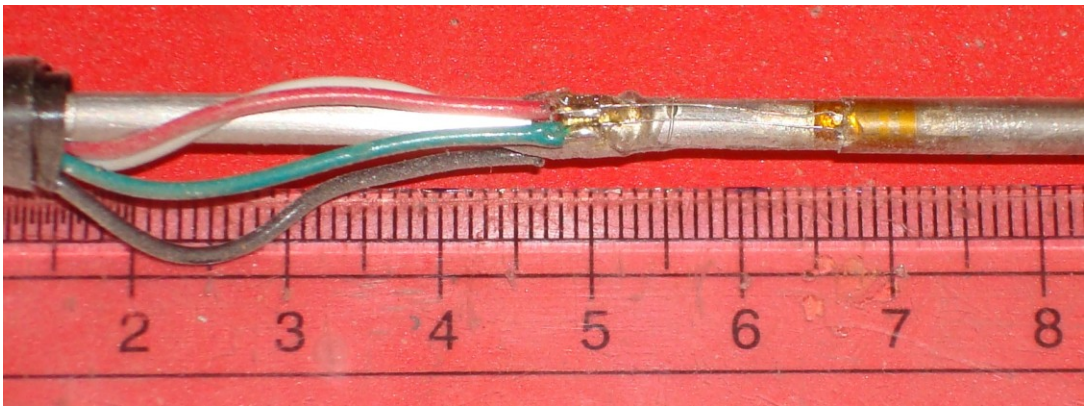

Figure 4.10 Strain gage and terminal mounted on 0.135 inches Kolsky bar

4.3 The Bridge Circuit

A Wheatstone bridge was used as a gage input configuration for the signal conditioning amplifier. All strain indicators employ some form of Wheatstone bridge circuit in order to detect the resistance change in the gage with strain. In this case two active strain gages are used in compression and two dummy resistors to complete the bridge. The two active gages in this configuration grant twice the sensitivity compared to one single gage used. The gage configuration and the connection ports used on the signal conditioning amplifier (SCA) are shown in **Figure 4.11**. The letters J, L and K, A indicate the input plug pin arrangement of the SCA for an external full bridge set-up. The letter P is the input plug pin for the ground. The shielding surrounding the connecting cables is typically connected only to the input plug pin P and not to the Kolsky bar.

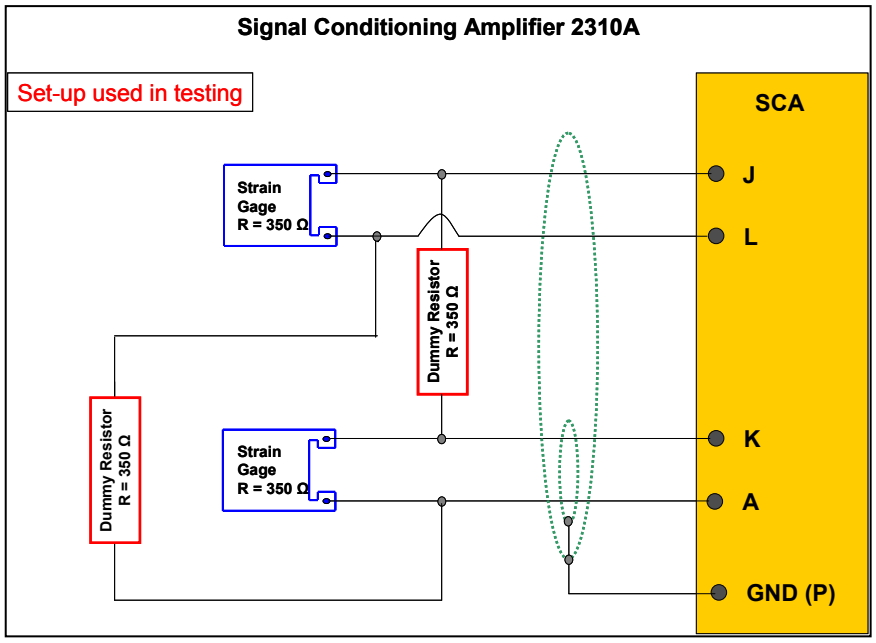

Figure 4.11 Strain gage and dummy resistor configuration

Two precision dummy resistors of the type S-350-01 (manufactured by Vishay Micro Measurements) were used in order to complete the bridge as described for each Kolsky bar. The dummy resistors are accommodated in the circuit box shown in **Figure 4.12**. The Cables connecting the Kolsky bars are simply plugged in which makes the change of a non functional bar easy and fast. As described earlier it is essential not to exceed a length of approximately 2.5 meter (8 feet) of the cable connecting the Kolsky bar to the box in order not to add too much electrical resistance. Otherwise the bridge can not be balanced by the signal conditioning amplifier used.

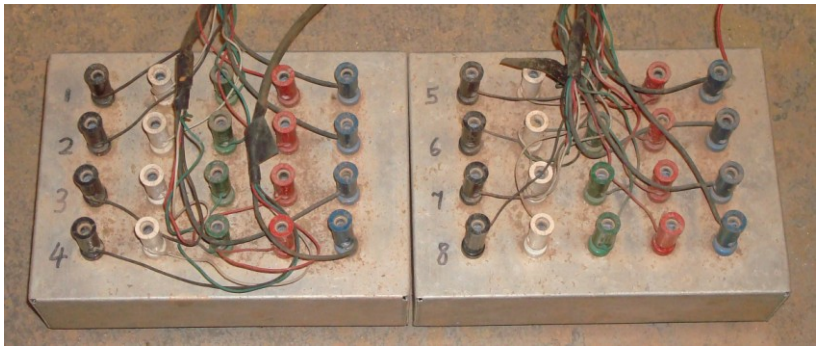

Figure 4.12 Circuit box completing the bridge circuit for 8 Kolsky bars

4.4 The Signal Conditioning Amplifier (SCA)

In total eight signal conditioning amplifiers of the 2300 series (manufactured by Vishay Micro Measurements) were used for the amplification of the signals measured by the strain gages. Consequently eight Kolsky bars were used in each test conducted like in the configuration shown in **Figure 4.4**.

The 110 Volts powered portable enclosure accepts 4 amplifiers as shown in **Figure 4.13**. In total two units were used to accommodate the eight amplifiers. Each SCA is electrically isolated from the other and provides features essential for accurate stress analysis data in a wide range of measurement applications.

We used in the first enclosure 4 SCAs of the type 2310 B which is a slightly improved version of the SCA type 2310 A. The second unit used contained 4 SCAs of the type 2310 A. Therefore the Kolsky bar 1 to 4 (signal 1 to 4) is amplified by an SCA 2310 type B. For Kolsky bar 5 to 8 (signal 5 to 8) a SCA type A was used. The main difference between the two types of amplifiers is the frequency response shown in **Table 4.1**. The filter buttons can be used to reduce the upper frequency cut-off (10-10.000 Hz) in order to reject undesired noise. We used the depressed "WB" (Wide-Band) button to achieve wide-band operation. The excitation control allows selecting the desired bridge excitation which was selected to be 10 for all conducted tests. The amplifier gain reading of the 10 turn control was set to 4.00 and multiplied by the selected push button by 10. (4.00 X 10). The indicated gain is the gain from the input to the +/- 10V output, see **Figure 4.14**. The sampling rate used was 170 kHz for the SCA 2310 type A and 250 kHz for the SCA 2310 type B. This sampling rate correlates to 1 pressure measurement taken every 5.88 microseconds for the SCA 2310 type A and to 1 pressure measurement taken every 4 microseconds for the SCA 2310 type B. The described settings were used on each type of amplifier in all conducted tests.

Figure 4.13 Two portable enclosures accept 8 amplifiers in total

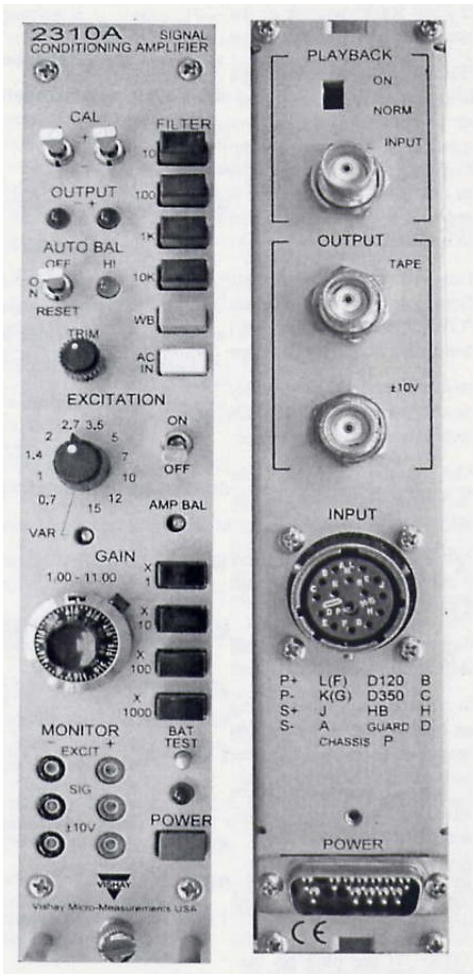

Figure 4.14 Front and rear panel of an SCA type 2300 A

SCA Type	2310 B	2310 A
Filter	WB	WB
Excitation	10	10
Gain	4.00 X 10	4.00 X 10
Frequency Response	250 kHz	170 kHz

Table 4.1 SCA settings used during all conducted tests

4.5 Calibration of the Kolsky Bar Using the SCA

Before the calibration can be carried out, the system has to be switched on for a duration of at least 20 minutes to allow the bridge to warm up. The temperature change and hence the resistance change in the strain gages caused by the current flow is noticeable. Until the warm-up of the gages is not terminated, the bridges can not be balanced. The warm-up time needed is around 30 minutes. The output indicators show permanently the balance condition of the bridges (**Figure 4.14**). After approximately 20 minutes the toggle switches for the calibration control can be used to auto balance the bridges. Note that if "HI" lamp in the front panel lights up even after balancing the bridge, the bridge can not be balanced and a technical defect has been detected. For further fine adjustment of the balance for the bridges, the trim control has to be used until just before the test is conducted.

The toggle switches (CAL) A and B are used in order to place shunt-calibration resistors across the arms of the input bridge. For all calibrations which were done before each test, the toggle switch B was used. In general, one arm of the input bridge is shunted using a specific resistance, which introduces a specific change in resistance into this arm. This specific change simulates a compressive strain in the strain gage. The SCA output responds as if that specific change in resistance actually had occurred using the existing bridge excitation and SCA gain. Recording these calibration signals using the oscilloscopes is needed in order to later on calculate the pressure which was applied to each Kolsky bar.

In order to calculate the compressive micro strain applied through toggle switch B, **Equation 4.1** is used. The number of the full active gages is 2.0. The gage factor of the gages used equals 2.145. The factor 1000 is used to convert Volt into millivolt and the factor of ½ is needed in order to account for the double sensitivity of the configured bridge.

$$\frac{2.0}{2.145} * 000 * \frac{1}{2} = 166\mu\varepsilon$$

Equation 4.2 Calculation of the compressive micro strain for calibration

Equation 4.2 and the result of the calibration signal for each channel recorded is used for calculating the strain rate per millivolt. For calculating the calibration factor **Equation 4.3** is used.

$$Cal.Factor = \frac{466}{Amplitude} \frac{\mu\varepsilon}{mV}$$

Equation 4.3 Calculation of the calibration factor

4.6 Converting Strain to Pressure

Young's modulus of elasticity describes the ratio of uniaxial stress (units of psi) to uniaxial strain (dimensionless) in the range of stress in which Hooke's Law can be applied. Using the calibration factor in strain, Young's modulus for stainless steel ($30*10^6$) and the measured amplitude in millivolt, the pressure measured by the Kolsky bar can be calculated (**Equation 4.4**).

$$P = Cal.Factor * 10^{-6} * 30 * 10^6 * Amplitude$$

Equation 4.4 Pressure Calculation

Figure 4.15 shows a typical measurement taken by a 0.635 cm (0.25 inches) diameter Kolsky bar using a RP-3 detonator attached to a small specimen and the specimen attached to the Kolsky bar. The first peak at the time of 0.2 milliseconds

shows a peak pressure of 241 MPa (35,000 PSI). All the other peaks measured show the reflection of the stress wave on the top and the bottom travelling up and down the Kolsky bar. The specimen which was attached to the Kolsky bar is shown in **Figure 4.16**. It measured 13.86 mm (0.55 inches) in length and the diameter was the same as the Kolsky bar. As it can be seen in **Figure 4.16** the specimen was dented by the detonation of the RP-3.

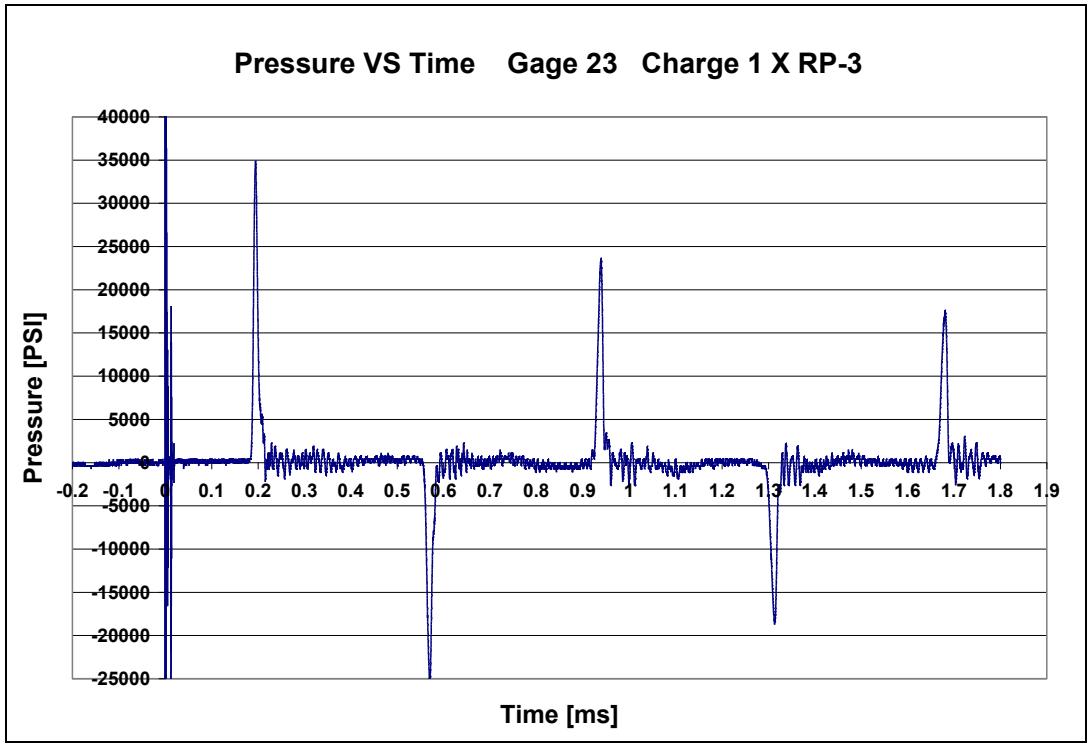

Figure 4.15 Typical signal of a Kolsky bar using an attached detonator and a test specimen

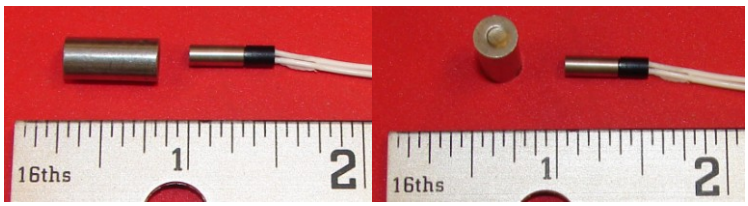

Figure 4.16 Specimen attached to the Kolsky bar

The specimen got plastically deformed but since this setting (**Figure 4.17**) was mainly used to determine the wave speed of the stress wave travelling up and down the Kolsky bar, the peak pressure values were not of interest. The wave speed was measured several times. The results agreed very well and the value of the velocity was determined to be 4864 m/sec (191.5 inches/msec).

Figure 4.17 Test set-up for determination of the stress wave velocity

4.7 Oscilloscopes Used for Recording Measured Signals

Two types of oscilloscopes were used for recording the signals. The LeCroy 9314 AM 400 MHz and the LeCroy 9354 AM 500 MHz (**Figure 4.18**). The main difference is the maximum sample rate both oscilloscopes can offer. The sample rate chosen for all tests conducted was 10 mega samples per second if not mentioned otherwise. The recording time for each test was 2 milliseconds which started 0.2 milliseconds before triggering the detonation. This sampling rate correlates to 1 pressure measurement taken every 0.1 microseconds and hence exceeds the sampling rate of the SCAs. The limitation of sampling frequency is therefore given by the signal conditioning amplifier. The vertical setting of each channel was chosen accordingly to the expected pressure measured. During the first test series conducted,

the oscilloscopes were triggered by the noise of the charge. Later the trigger was changed to the output of the firing set.

Figure 4.18 Oscilloscopes used for recording the signals

4.8 Sizes of Kolsky bars

Five different diameters of Kolsky bars made out of stainless steel were used during the test program. The length of all bars is identical at 122 cm (4 feet). The diameters used are 2.45 cm (1 inch), 1.27 cm (0.5 inches), 0.635 cm (0.25 inches), 0.476 cm (3/16 inch), 0.318 cm (1/8 inch) (**Figure 4.19**). In order to establish the pressure profiles over distance on the target plate, the 0.635 cm (0.25 inches) diameter Kolsky bars were used. The other diameters were employed to investigate the differences in peak pressures measured. Keeping the test set-up the same and using a different diameter Kolsky bar results in a change of peak pressure measured. Since the size of the impact area of the bar changes, the pressure measured will be averaged accordingly. In order to explain the method of loading the bottom of the bar, it is important to look at the ejecta leaving the crater area. Visualization testing, which will be explained in a later section, is needed in order to look at the loading mechanisms.

Figure 4.19 Kolsky bar diameters used from the top: 2.45 cm (1 inch)
1.27 cm (0.5 inches)
0.635 cm (0.25 inches)
0.476 cm (3/16 inch)
0.318 cm (1/8 inch)

4.9 Improvement of the Kolsky bar

During the test program the Kolsky bar was improved from its early layout to the last version used. In the very beginning of the testing the bridge wires and the connecting wires were not protected against the harsh environment they were tested in. As mentioned earlier the balanced bridge is very sensitive to temperature changes. If tested was in very dry sand or water, dust or water particles will settle on the gages and connecting wires. Even though the wires and the solder joints are protected by a polyurethane coating, the impact of the particles changes the resistance of the bridge and will result in a faulty pressure measurement. In order to protect the wires, solder joints and the gages, a heat shrink tube was applied on the previously polyurethane coated wires and solder joints. The coating is important to prevent any short circuit in the wiring. Additionally PVC tubing was fitted embedding the heat shrink tube and the gage set-up see **Figure 4.20**. Using a target plate as seen in **Figure 4.3** a first generation Kolsky bar can be used since the plate protects the bar against immediate impact of particles being ejected by the detonation, but they need to be cleaned before being used again since dust will settle on the connecting wires and gages. It is recommended to use the improved Kolsky bar as well in this set-up since the bar

location will be changed frequently depending at which distance the pressure will be measured. The improved bar is much more durable both during testing and in switching locations.

The enhanced Kolsky bar has to be used in any testing, where no target plate is used and the ejecta is allowed to travel alongside the bar. The ejected media will impact the gages and the connecting wires and change the measured result as described.

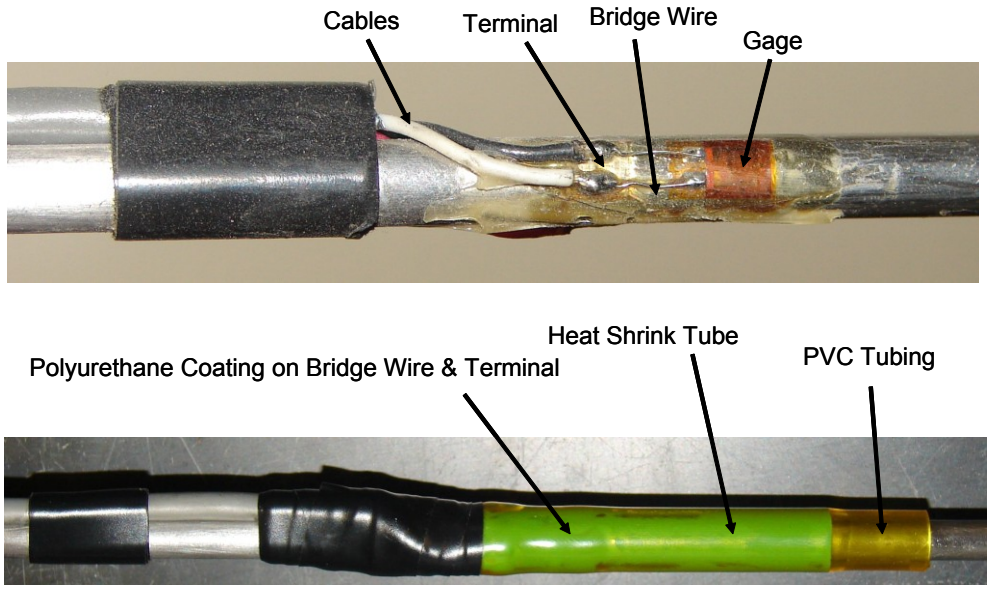

Figure 4.20 Kolsky bar first generation (top) and second generation (bottom)

The quality of the signal improved as well by adding the heat shrink and the tubing to the bar. **Figure 4.21** shows qualitatively the change of the signal. The high frequency noise is mechanically filtered out by the enhancement.

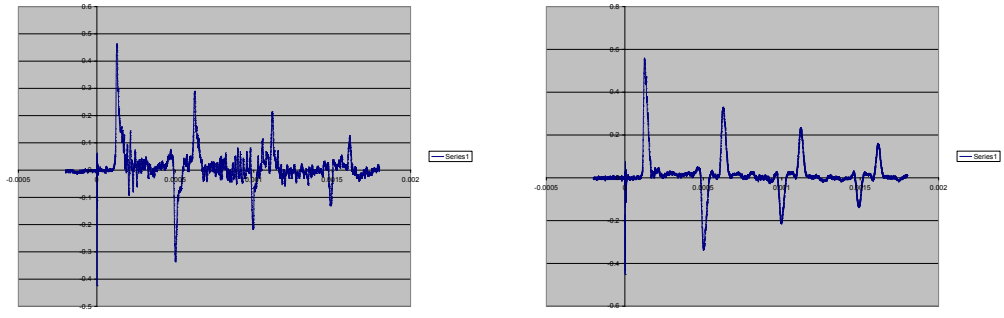

Figure 4.21 Kolsky bar signal improvement before (left), after (right)

4.10 Plate Layouts Used

The plate layout was changed several times during the test program due to improvements.

The first tests conducted used a frame holding a target plate shown in **Figure 4.22**. The frame allows adjusting the SOD (Stand-Off Distance)as needed and was employed in all conducted tests. The spacing of the Kolsky bars on the plate was chosen to be 1.27 cm (0.5 inches) starting at the center of the plate. The bars were held in place using a rim of electric tape on the bar. This configuration was changed quickly for two reasons. First, the stress waves generated in the plate by the loading from the bottom could be transmitted into the Kolsky bars. This causes some interference with the stress wave generated by the loading of the bar. Second, one pressure measurement taken at one specific location does not reveal the final answer. Since the pressure values can differ up to 100% at certain locations, a lot of pressure values have to be recorded in order to come up with a statistical distribution. It is very important in this context to look at the loading mechanisms of the target plate which are involved and will be discussed in the next chapter.

The set-up was accordingly improved to collect up to 8 pressure values at a certain distance from the center. **Figure 4.23** shows the test set-up in which 8 Kolsky bars are used at a distance of 3.1 cm (1.22 inches) from the center of the plate. Also note the rubber tubing surrounding the bottom of the Kolsky bar was used from then on. In order to align the bars and keep them from impacting each other, foam blocks were used as seen in **Figure 4.23**.

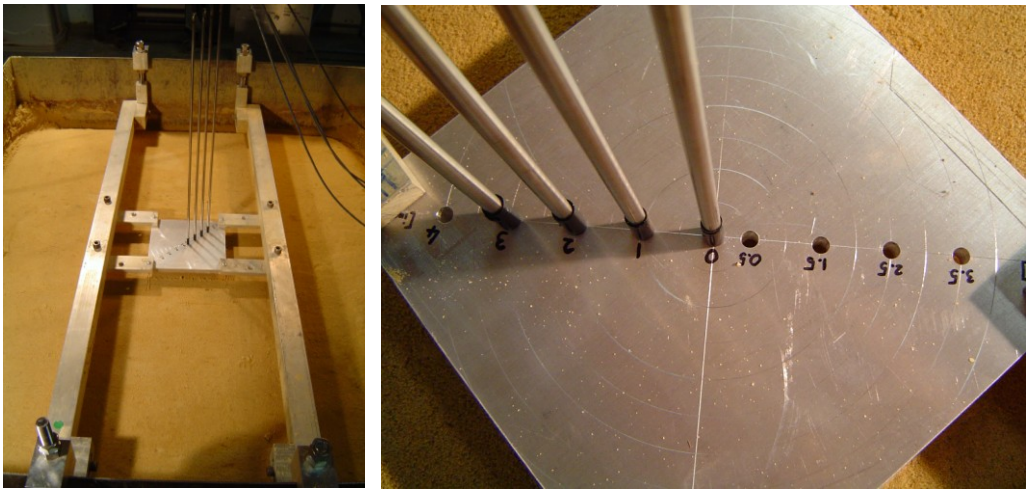

Figure 4.22 Kolsky bar set-up frame and plate (left), detail of the plate (right)

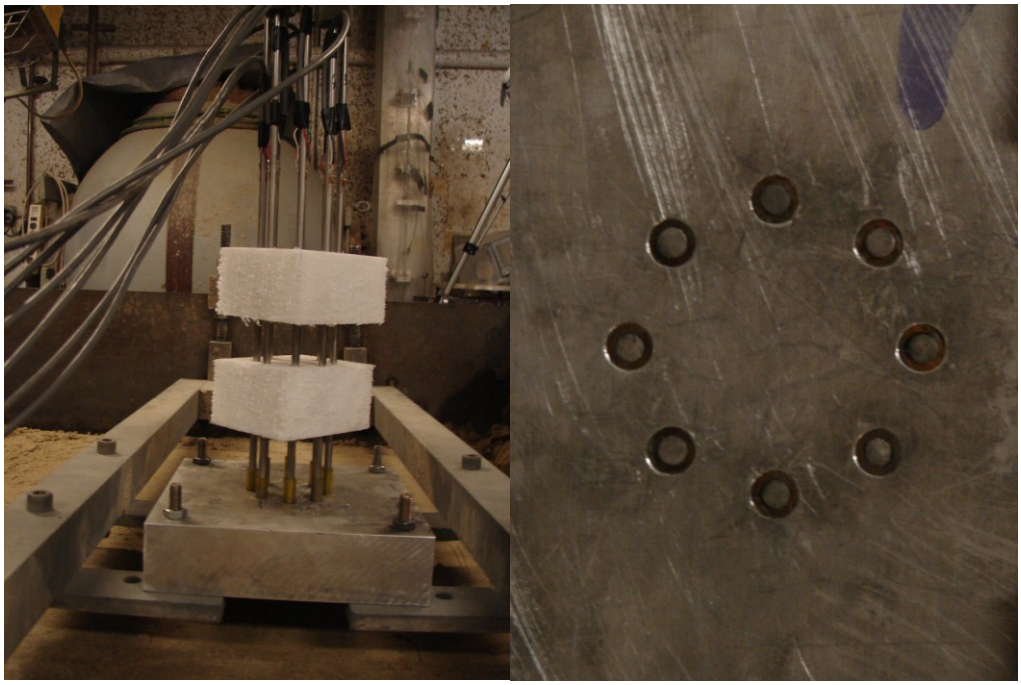

Figure 4.23 Circular Kolsky bar set-up frame, plate, and foam blocks (left), detail of the bottom of the plate (right)

Figure 4.24 shows the pressure distribution of 6 tests conducted. Gage 112, 117, 118 were conducted using the set-up shown in **Figure 4.22**. All 3 tests were conducted using the same test conditions which are a DOB of 0.991 cm (0.39 inches), a SOD of 4.013 cm (1.58 inches), and a Pentolite charge of 4.4g. The distances the pressure was measured was 0 cm, 0.762 cm (0.3 inches), 0.889 cm (0.35 inches), 1.016 cm (0.4 inches), 1.27 cm (0.5 inches), 1.702 cm (0.67 inches), 2.134 (0.84 inches), and 2.54 cm (1 inch). As can be seen in the test results of the 3 tests there is little agreement in the peak pressures measured. In certain locations the results are off by 70% and basically show that test results are not repeatable using this Kolsky bar set-up. Changing to the new Kolsky bar set-up in a circular pattern like shown in **Figure 4.23**, another 3 tests were conducted at the same conditions. Two tests (Gage 127, 128) had the Kolsky bars placed at a distance of 1.27 cm (0.5 inches) and one test (Gage 158) at 2.54 cm (1 inch). The two repeats Gage 127 and 128 cover the pressure spectrum at the distance of 1.27 cm (0.5 inches). This suggests that the pressure measured in test Gage 118 at this location shows a maximum and in test Gage 112 and 117 a minimum pressure. The test result of Gage 158 shows a pressure spectrum which exceeds the pressure measured of Gage 112, 117, and 118 in both directions for the minimum and maximum. Therefore it has to be concluded that the measured pressure deviation at any location requires multiple measurements taken in order to collect enough data to show the pressure distribution.

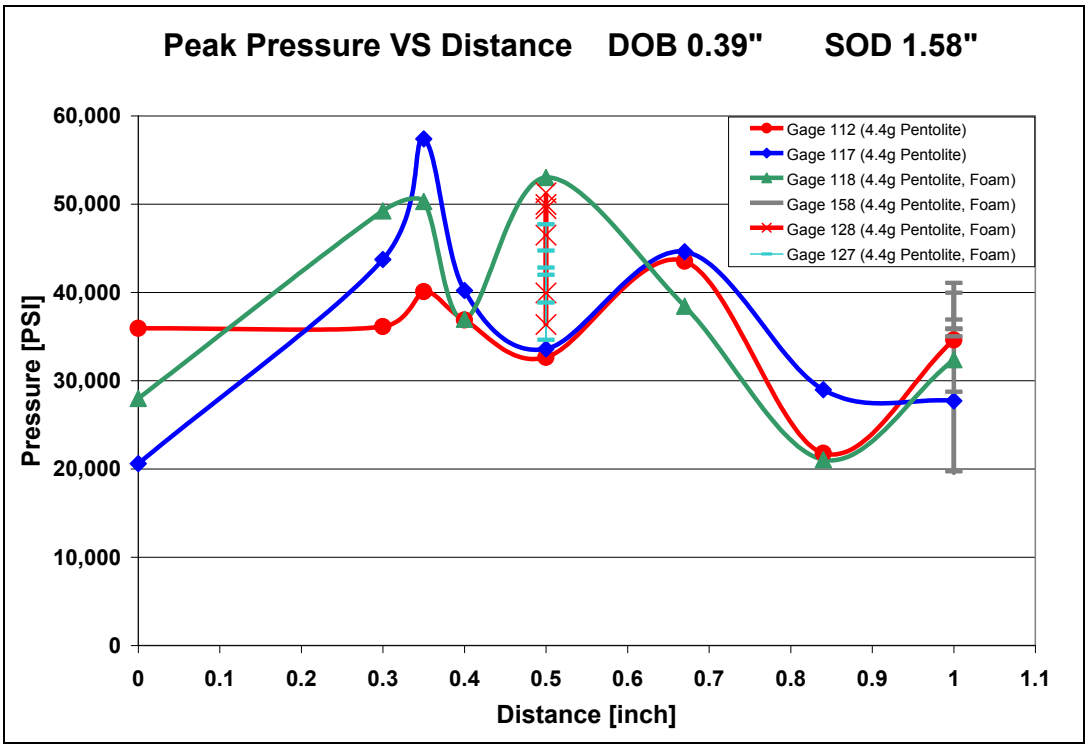

Figure 4.24 Results of test Gage 112, 117, 118, 127, 128, and 158

Since there was a need to measure the pressure in each test conducted at the center of the plate, the configuration was changed to one Kolsky bar at the center and seven bars surrounding the center equally spaced at different distances from the center of the target plate. Hence in each test carried out, one measurement was taken at the center to generate a data basis for the impact directly above the charge. **Figure 4.25** shows a layout as an example using one Kolsky bar at the center and seven at a distance of 10.16 mm (0.4 inches) from the center of impact.

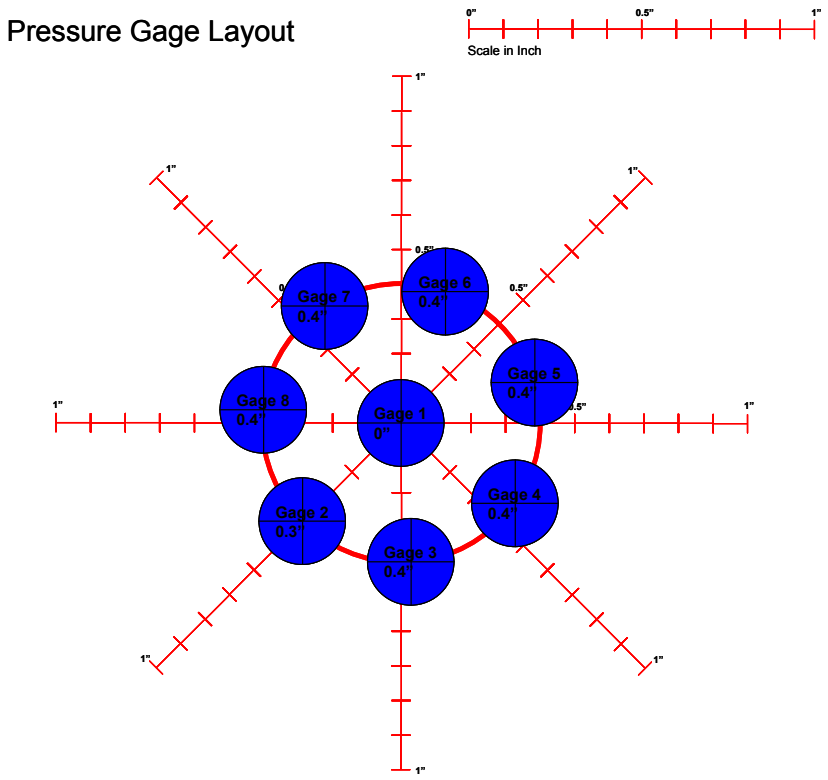

Figure 4.25 Kolsky bar lay-out for pressure measurement at the center of impact and at a distance of 10.16 mm (0.4 inches)

4.11 Loading Mechanisms of the Target Plate

In order to explain the results in the peak pressure measured, it is necessary to examine the loading mechanisms of the target plate. The pressure time curve recorded is a function of type of material the charge is buried in, the impact velocity, and the mass of the matter impacting at a specific point of interest. Since the gas driven soil cap expanding above the detonated charge can be described as non-uniformly distributed in density, the pressure measurements are not repeatable. Several papers have been published in the past **[7], [8], [9]** about the so-called Richtmeyer – Meshkov instabilities and soil cap density distribution. In the following, three different types of loading will be examined keeping the DOB, SOD, and the charge size scaled for each type of loading to a 4.536 kg (10 lb) charge used at a DOB of 10.16 cm (4 inches) and a SOD 40.64 cm (of 16 inches).

4.11.1 Loading Mechanism of the Target Plate Using Saturated Sand

The high speed camera is used to record the dome which is generated by the explosive charge in saturated sand. **Figure 4.26** shows the side view of the dome development over time of an 8 grams Deta Sheet charge buried at DOB 1.219 cm (0.48 inches) in saturated sand. The first image taken shows the soil surface after 16 microseconds of the detonation of the charge. Every following image is taken at an interval of 14.93 microseconds, hence the last image shows the dome at 150.43 microseconds. At the time of 16 microseconds the charge detonated and jets start to develop on top of the sand surface. At 31 microseconds the dome begins to form and the jets are well pronounced. Between 46 and 91 microseconds the jets still have the needle-point shape and the dome resembles a cylinder with an almost spherical top. The jets are different in diameter and length and travel faster than the dome. Between 106 and 150 microseconds the jets do not show the needle-point tip anymore. The dome resembles a cupcake shape with a very ragged surface.

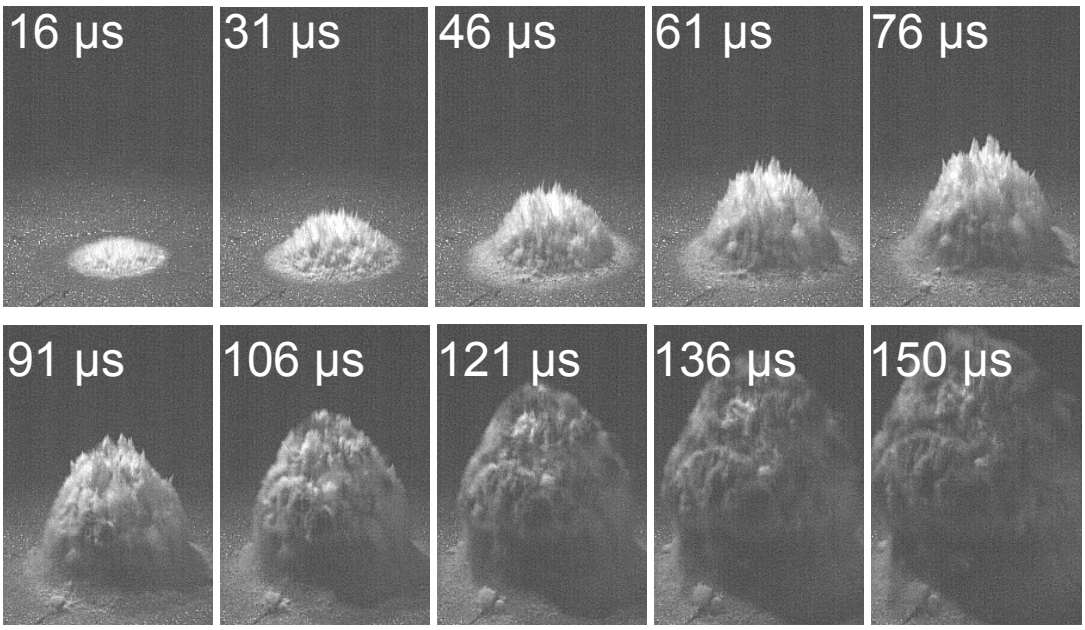

Figure 4.26 Side view: rising dome of a shallow buried charge in saturated sand

Figure 4.27 shows the top view of the dome development over time of the same test as shown in **Figure 4.26** using an 8 gram Deta Sheet charge. The first image taken shows the soil surface after 13.14 microseconds of the detonation of the charge. The time sequence shown in **Figure 4.27** is comparable to the time sequenced (14.93 microseconds between images) of **Figure 4.26**. It shows the change of the dome qualitatively over time and reveals areas between the jets which do not have a regular pattern. Over progressing time, the sand spreads out and the pockets between the jets become larger.

Since in almost all the tests conducted for pressure measurement the charge is buried shallow, the loading of the target plate can be considered as non-uniform, thus the peak pressure measured at a certain location above the dome changes the magnitude depending on if the Kolsky bar gets impacted by a jet or a pocket.

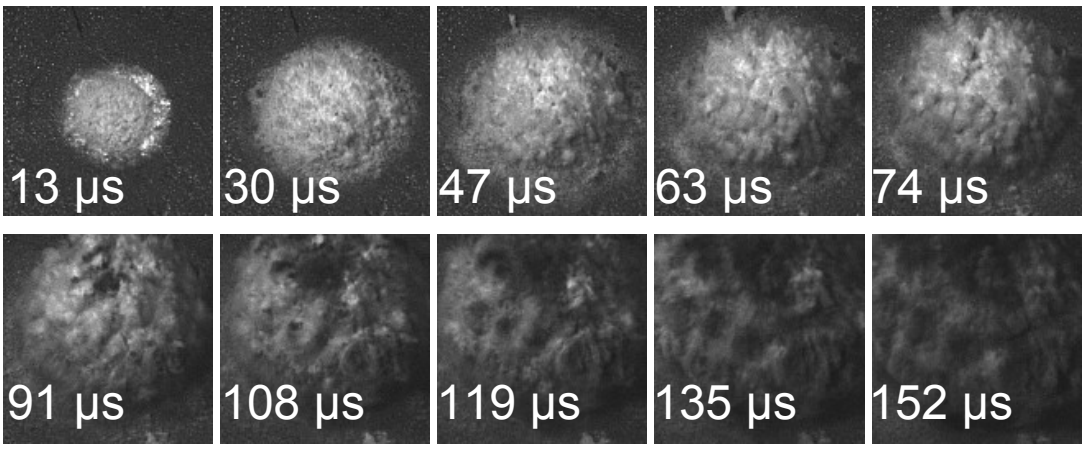

Figure 4.27 Top view of a rising dome of a shallow buried charge in saturated sand

Introducing a target plate made out of 1.27 cm (0.5 inches) thick clear gel rubber stretchable up to 1200% was used at a SOD of 5.08 cm (2 inches) in order to visualize a flexible target response. The sheet was held in place being clamped between two steel frames. The explosive employed was a 1gram Deta Sheet charge at a DOB of 0.762 cm (0.3 inches). **Figure 4.28** shows images recorded at certain times. The first image taken at 35 µs shows the dome rising up under and starting to impact the clear gel rubber sheet. At a 106 µs the irregularities of the dome develop

pouches in the rubber sheet. At a 177 µs, certain pouches have climbed higher than others. At the left rear end the first pouch starts to break open due to the high velocity impact of the saturated sand. Note that the pouches in the center didn't climb highest. A ring around the pouches can be clearly seen formed by the spray of the dome. These are particles which did not have enough force to penetrate the rubber and were mainly thrown up by the shock wave reflected at the soil - air interface. At 319 µs, more pouches opened up and the diameter of the impact zone expanded further. At 426 µs, the pouches developed at the outer edge do not open up anymore since the impact of the saturated sand does not have enough force. From than on the diameter of impact belt increases and slows down significantly.

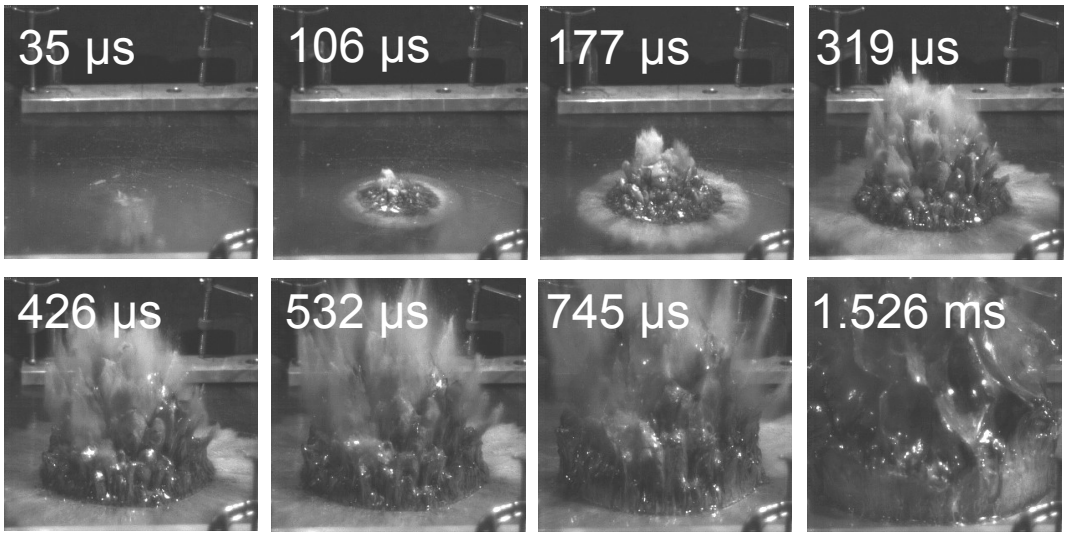

Figure 4.28 Side view of a dome impacting a clear gel rubber sheet

Investigating the dome impacting a 4 inches thick acrylic (PMMA) sheet allows discovering what happens under a ridged target plate. **Figure 4.29** shows the test set-up for the acrylic sheet. The plate is held in place at a SOD of 4 cm (1.58 inches) using a frame which is clamped onto the frame of the test box. The high speed camera is mounted above the sheet facing downwards allowing the impact to be seen. The charge used is the standard size of 4.4 g of Deta Sheet at a DOB of 1 cm (0.39 inches).

Figure 4.29 Test set-up for a clear acrylic (PMMA) sheet

Figure 4.30 shows the recorded images of the test set-up described. The spots on the acrylic sheet which are marked with an X in the image at 0 µs are positions where the Kolsky bars will be positioned in a following test in order to verify the pressure recording. This will be described in one the following sections. Note that there are 2 X's on top of each other, one on the bottom of the plate and one on the top. At 13 µs the charge has detonated and the dome begins to form. At 52 µs the dome is very close to impacting the bottom of the target plate. At 68 µs the center has been impacted and there is a ring visible which expands in the first few microseconds very rapidly and slows down later on. The ring is very bright due to the ionized gas in the impact zone. Tests have been conducted without any light source and the ring was clearly pronounced until it has reached the diameter of approximately 7.6 cm (3 inches). At that distance the saturated sand impacts at a lower velocity and is therefore not able to ionize the gas any more. Inside the ring the gas bubble caused by the reacted explosive is trapped and driving the ring outwards due to the overpressure inside the ring. Also note that there is no excavated material impacting after the ring has passed the area. It is only the gas bubble still applying pressure at that point. Also note that the spots marked with an X on the bottom of the

plate are erased after the ring passed by, see image at 68 µs and further on in time. At 81 µs the ring is still very well pronounced. It has approximately the thickness of 0.64 cm (0.25 inches), see the two red arrows which mark the ring thickness. At the outside of the ring a corona is formed by the saturated sand travelling away from the center of the impact forming needle-like jets. At 94 µs the corona expanded further and the ring shows less light intensity. The applied pressure at the impact decreases as it will be explained in a later section and therefore causes less ionization. Also note that the ring is not perfectly round. At 133 µs the ring diameter has increased and the ionization has almost died out. The ring thickness has increased as well. The corona and the jets are very well pronounced. At 172 µs the ring starts to break up. The rim at the inside is not as uniformly shaped as it was before and neither is the rim at the outside. The ionization has disappeared. At 211 µs the collapse of the ring and its rims has increased.

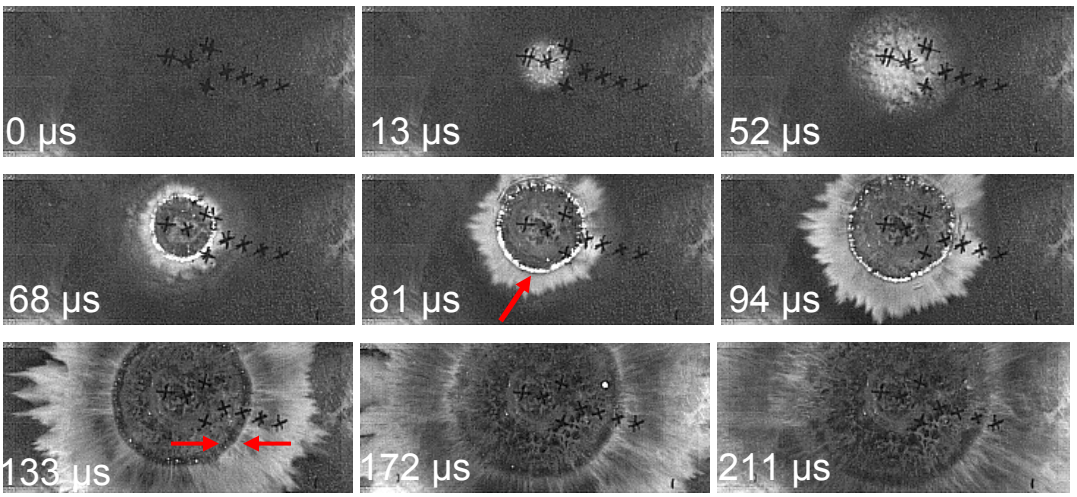

Figure 4.30 Images of saturated sand impacting an acrylic sheet

4.11.2 Loading Mechanism of the Target Plate Using Dry Sand

Once again the high speed camera is employed to record the dome which is generated by the explosive charge in dry sand. **Figure 4.31** shows the side view of the dome development over time of a 4.4 g Deta Sheet charge buried at DOB 0.991 cm (0.39 inches) in dry sand. The first image taken shows the soil surface after 13 microseconds of the detonation of the charge. Every following image is taken at an interval of 24.11 microseconds, hence the last image shows the dome at 205 microseconds. At the time of 13 microseconds the charge detonates. At 37 microseconds the dome seems to be transparent, the charge casing is still visible, and the shock wave has propelled already some sand in the air. At 61 microseconds the dome starts to form and black clouds show up at its surface which indicates that some of the gaseous reaction products penetrated the sand in this early stage. From this early state on the dome has a shape of ball, compare with the more cylindrical shape of the dome in **Figure 4.26** (saturated sand). There are no needle-shaped jets visible at any time. At 85 microseconds, the dome color has changed completely into black indicating that the gaseous products have mixed well with the sand particles. By now the dome shows the spherical imperfections at its surface. The dome surface stays the same until the end of the image sequence shown expanding in all directions equally.

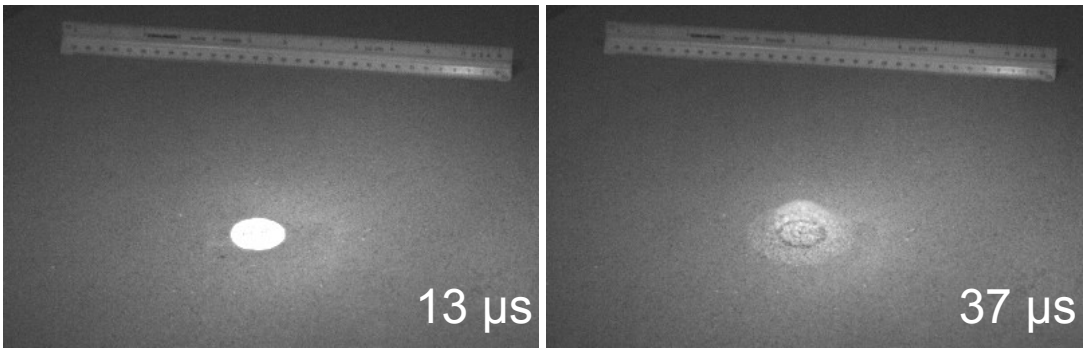

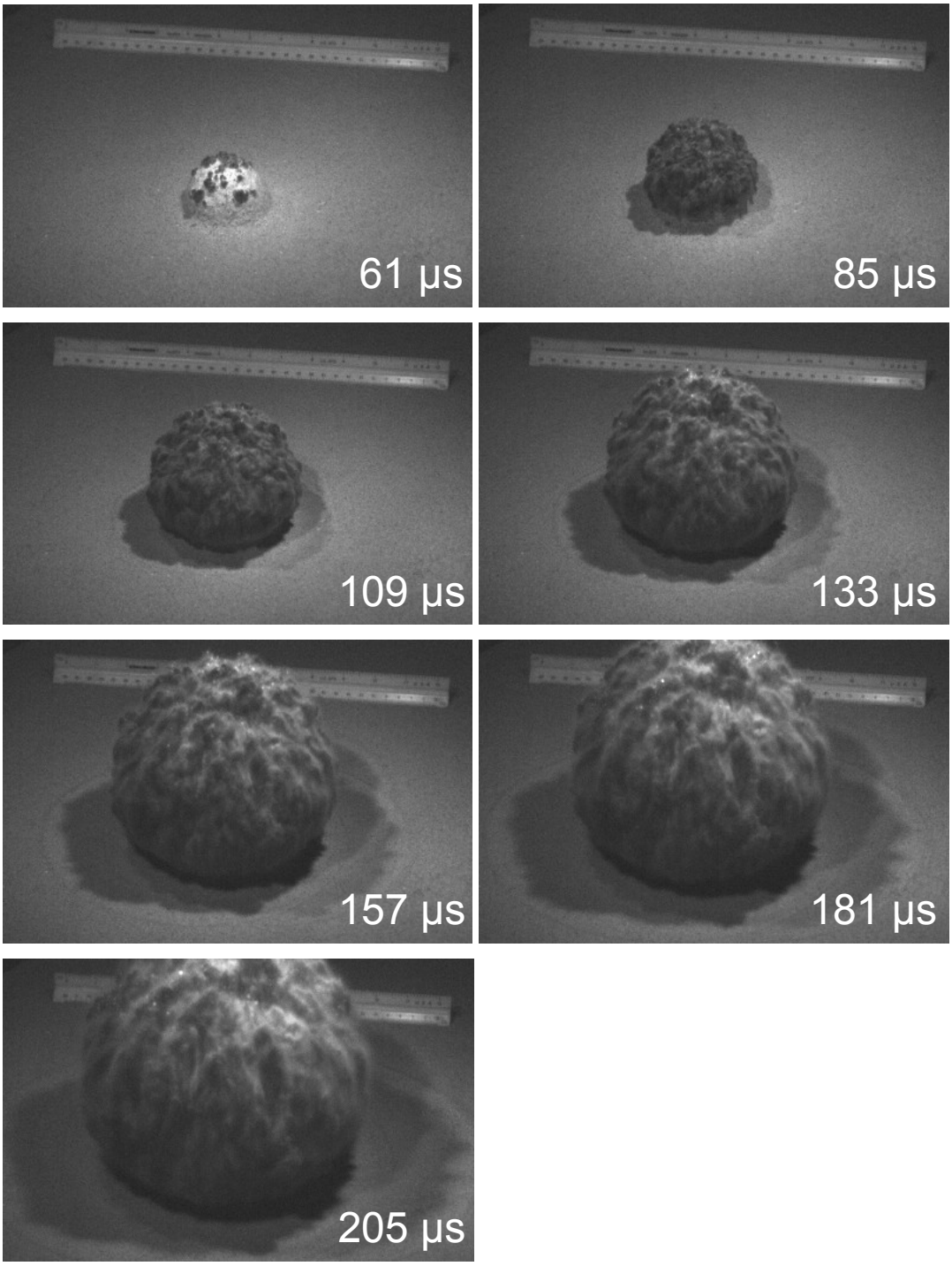

Figure 4.31 Side view of a rising dome of a shallow buried charge in dry sand

Figure 4.32 shows the top view of the dome development over time in dry sand using the same test set-up as shown in **Figure 4.29** using a glass plate as target. The 4.45 cm (1.75 inches) thick bullet-proof glass plate is held in place at a SOD of 4.013 cm (1.58 inches) using a frame as described before. The charge used is the standard size of 4.4 g of Deta Sheet at a DOB of 0.991 cm (0.39 inches). The first image taken shows the soil surface after 10 microseconds of the detonation of the charge. At 24 microseconds the charge is completely detonated and there appears to be a ring in the dry sand showing ionization. The voids between the sand particles are filled with air and therefore allow the ionization while the sand particles are smashed into each other in close range to the detonation. At the time of 38 microseconds the dome is visible. At 52 microseconds the dome shows its irregularities. At 66 microseconds the center of the dome crashes into the surface of the glass plate causing ionization. At 80 microseconds pockets of the dome arrive and crash into the plate surface observable by the ionized areas. At 94 microseconds sand particles still impact the center of the plate again highlighted by the ionization. From 109 to 165 microseconds the dome opens up in a very irregular manner not at all comparable to the loading mechanism of the saturated sand. Clearly there is no ring expanding like is seen in **Figure 4.30**. Studying the images where no plate is employed for saturated and dry sand, the difference in the overall shape of the dome is reflected in the images where a transparent target plate is used. The more cylindrical shape of the dome using saturated sand leads to the ring type loading while the ball shaped dome of the dry sand results in a more randomly dominated loading mechanism.

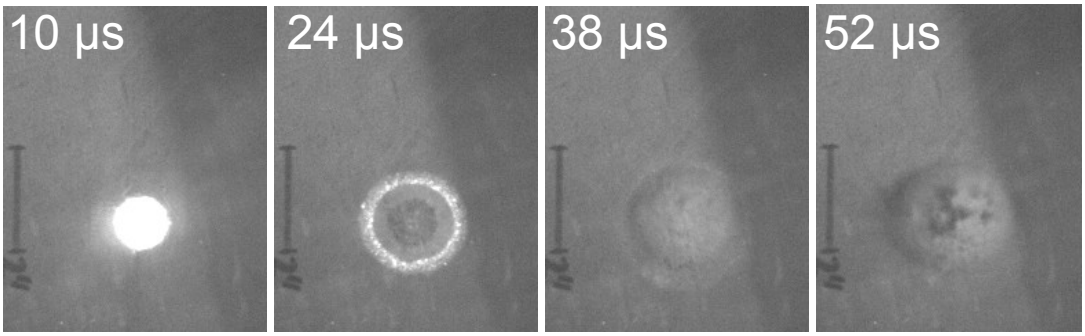

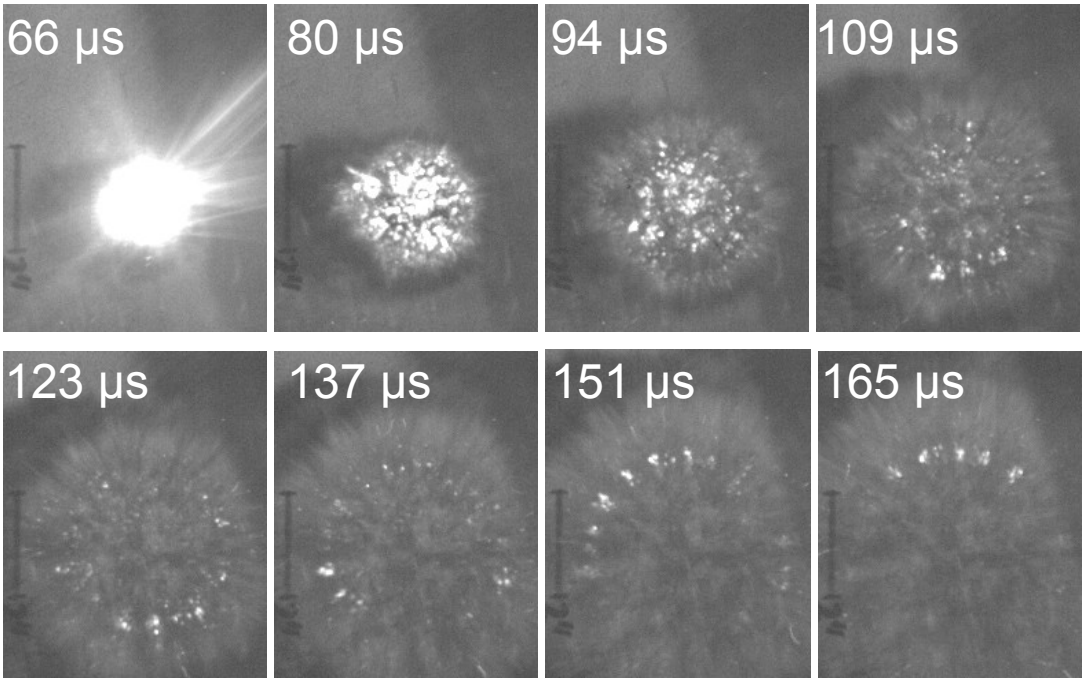

Figure 4.32 Images of dry sand impacting a glass sheet

4.11.3 Loading Mechanism of the Target Plate Using Water

The high speed camera reveals the loading mechanism using water as an impacting media. **Figure 4.33** shows the side view of the dome development over time of an 8 g Deta Sheet charge buried at DOB 1.219 cm (0.48 inches) in water without any target employed. The first image taken shows the charge before the detonation. At 4 microseconds the charge started to detonate at the center. At 9 microseconds after triggering the detonation, the charge detonated to the outer casing. In the center the gaseous reaction products begin to form the dome. At 15 microseconds a ring of a donut shape is formed around the center of the detonated charge. In the middle of the donut, the top of a ball shaped gas bubble can be seen. At 20 microseconds the donut shaped dome starts rising and the sudden pressure drop in the surrounding water causes cavitation forming a second donut shaped ring in the water. Between 26 and 37 microseconds the dome kept rising and the ring of

cavitation expanded further. The overall shape of the dome is kept the same with the exception of a further expansion. From 43 to 59 microseconds the dome keeps rising without significant change besides overall expansion. The shape of the rising dome is best characterized by a cylindrical profile containing a ball shaped cap on the top.

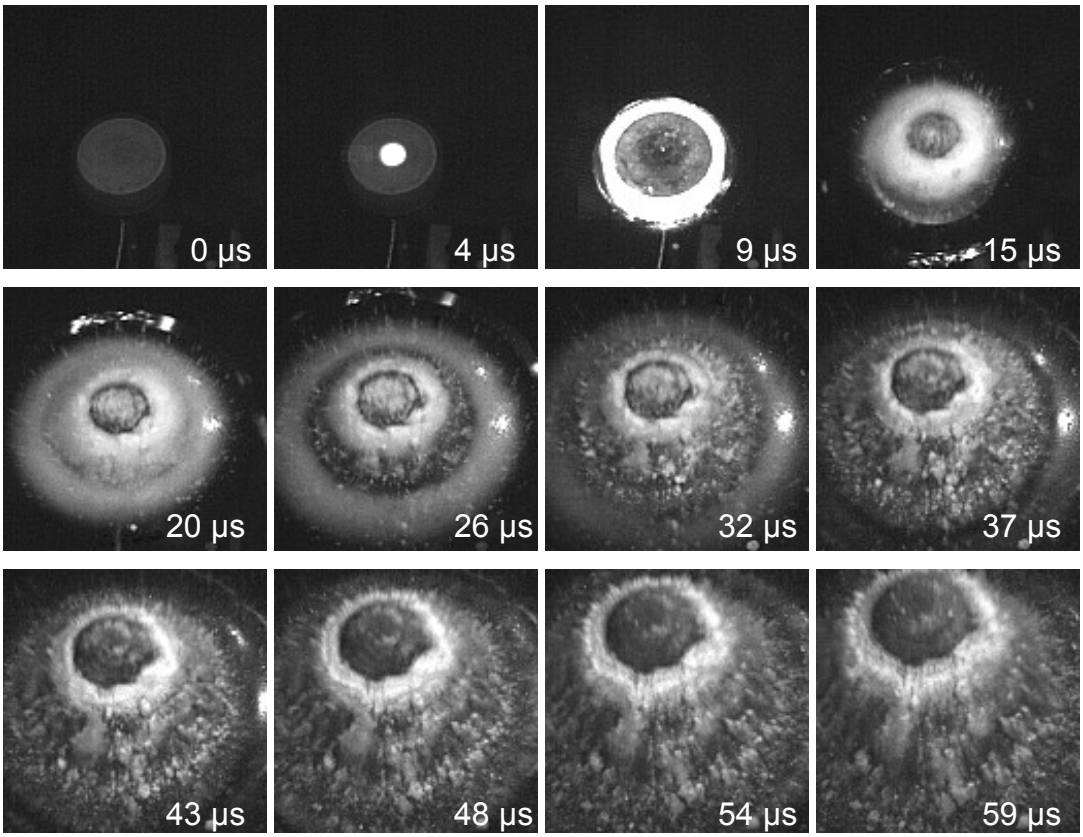

Figure 4.33 Side view of a rising dome of a shallow buried charge in water

Using the same test set-up as shown in **Figure 4.33** but adding a target plate at a SOD of 4.9 cm (1.93 inches), the test was repeated. The target plate utilized was a 10.16 cm (4 inches) thick transparent acrylic sheet. The high speed camera recorded the loading using a frame rate of 114,450 images per second. **Figure 4.34** shows the first images taken at an interval of 8.73 microseconds. Again the first image taken shows the charge before the detonation. At 12 microseconds the donut shape was formed and at 21 microseconds the dome started rising. Note the black cross marks the center where the acrylic sheet will be impacted. At 30 microseconds the cavitation in the water is visible. Between 39 and 47 microseconds the dome continues to rise until it impacts at 56 microseconds on the target plate. Compare the images taken until 47 microseconds with the images shown in **Figure 4.33**. At 56 microseconds the ionization shows the main impact of the donut shaped dome. At 65 microseconds the corona of the deflected water is shown. Note that the acrylic sheet started cracking in a circular manner inside the radius of the corona and the black cross is erased by the impacting water. Between 74 and 82 microseconds the corona expands rapidly and the circular crack in the acrylic sheet started forming a bowl shape. This process continuous until the end of the growth of the crack is reached at 135 microseconds.

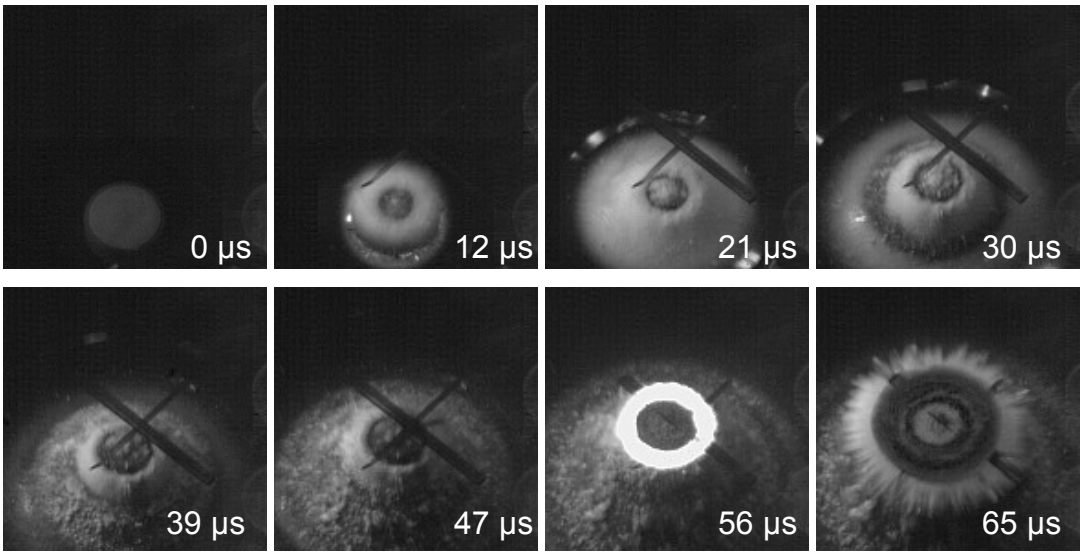

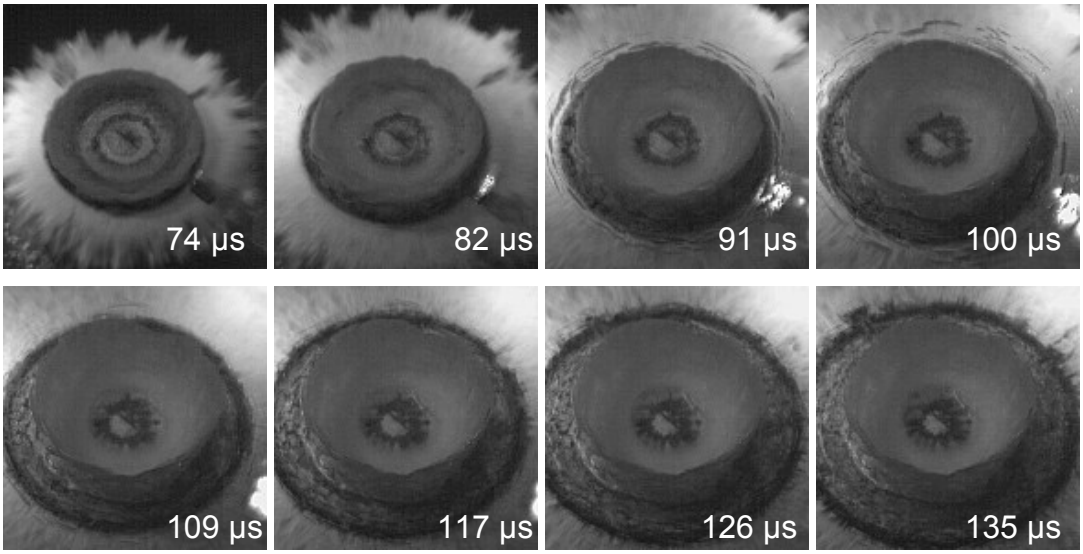

Figure 4.34 Side view of a rising dome of a shallow buried charge in water and impacting an acrylic sheet

During the same test set-up as shown in **Figure 4.34** a second high speed camera was used in order to record the propagating crack in the acrylic sheet from a side view. The camera was set-up looking through the side of the polished acrylic sheet. The high speed camera was set to a frame rate of 180,064 images per second. **Figure 4.35** shows the first images taken at an interval of 5.55 microseconds. At 52 microseconds the sheet was impacted at the center. At 58 microseconds the donut shaped dome impacted the bottom of the acrylic sheet. At 63 microseconds the acrylic sheet shows a circular fracture pattern shaped like a donut. From 69 to 113 microseconds the crack propagated in a circular pattern forming a bowl shape. At 113 microseconds the crack growth arrested. All tests conducted in water using an acrylic sheet as a target plate showed the same results. The crack pattern and the crack shape are very repeatable. The overall crack dimensions are almost the same.

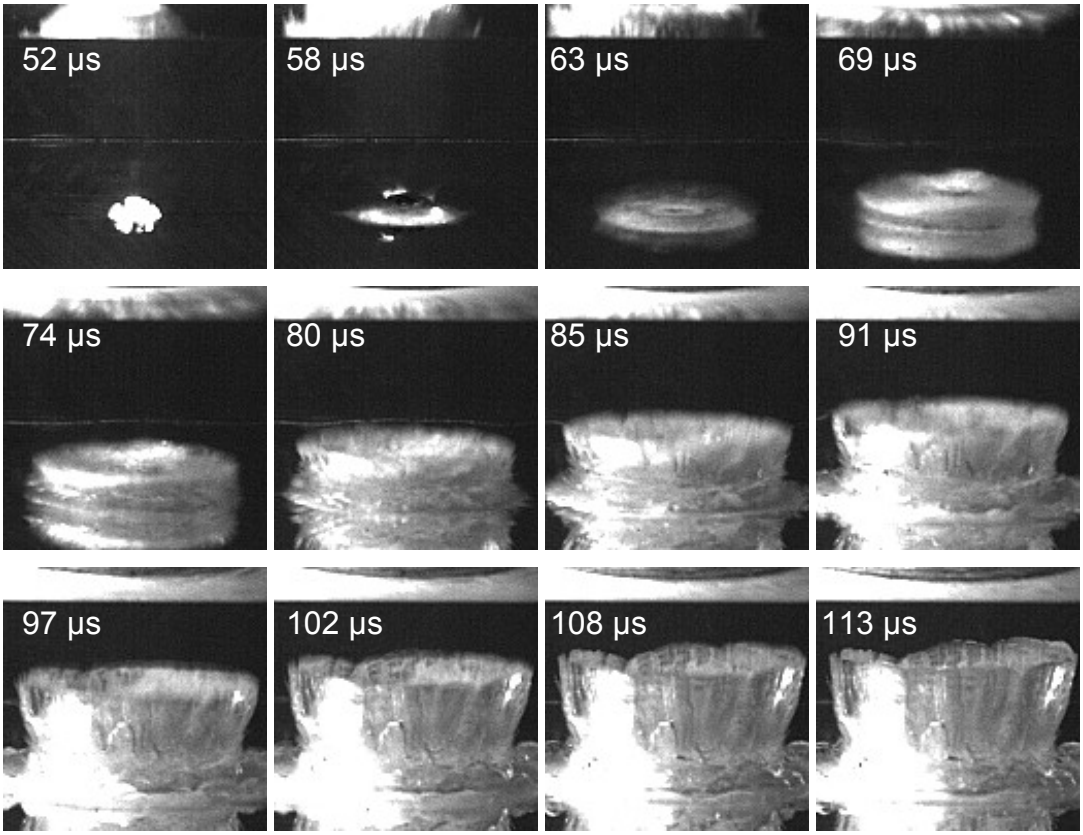

Figure 4.35 Side view of a propagating circular fracture pattern in an acrylic sheet

Using water as impacting media results in a more uniformly shaped dome. The main force is introduced into the acrylic sheet by the donut shaped ring impacting the sheet. Water travels at almost double the velocity compared to saturated sand since the density is roughly half of the density of saturated sand. Tracking the crack propagation using the software provided by the high speed camera provided the results shown in **Figure 4.36**. The graph contains the data for the distance versus the time of the tip of a crack forming the bowl shape. Plotting a linear trend line shows a crack velocity of 631 meters per second (24,841 inches per second). This approaches the low shear wave speed in acrylic materials of 750 to 1,000 meters per second (30 to 40,000 inches/sec).

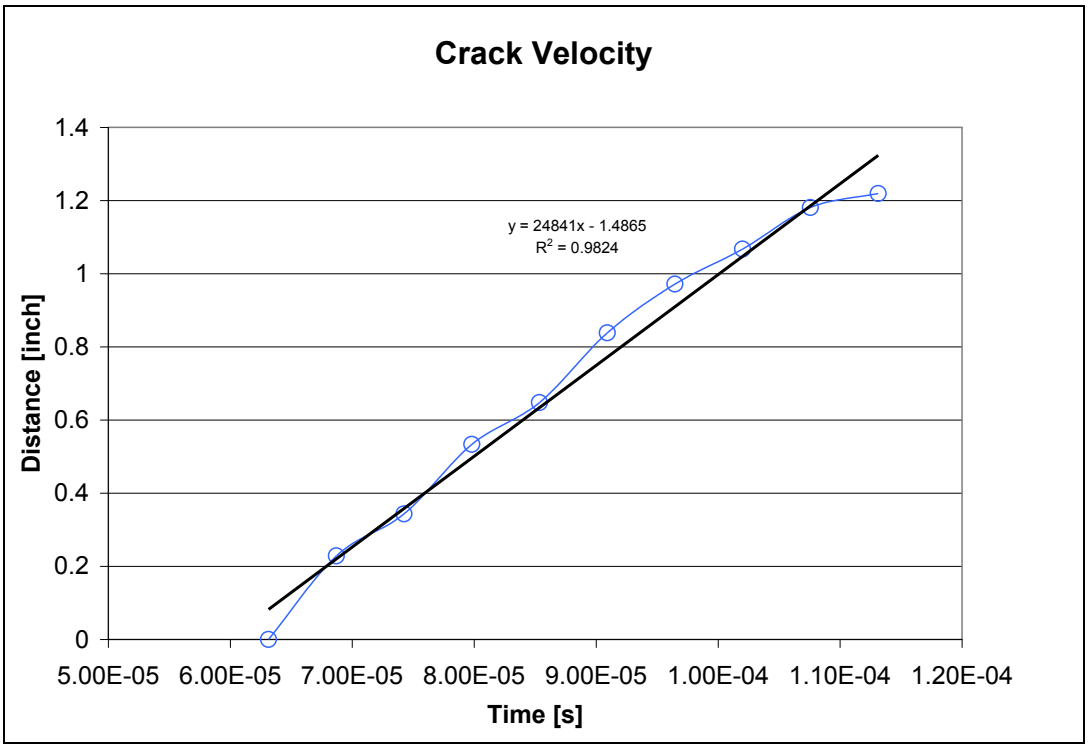

Figure 4.36 Crack propagation velocity in an acrylic sheet

The fracture caused by the water impact is shown in **Figure 4.37** from the top. The bowl shaped crack pattern is surrounded by smaller fractures in a circular configuration. Compare the difference in fracture pattern caused by saturated sand loading using an identical test set-up (**Figure 4.38** red arrow). The bowl shaped fracture reveals a much more irregular bowl containing areas where no fracture appears at all (compare red arrow in **Figure 4.39**). Also the overall length of the cracks is very different (**Figure 4.38**). This can be taken as a result of the difference in loading applied to the target plate. Compare the two fracture pattern in **Figure 4.38** directly. The center one (red arrow) is caused by saturated sand and the one on the left in the rear by water. The test conditions for both tests conducted were identical. This result has to be kept in mind looking at the pressure profiles over time presented in the following sections.

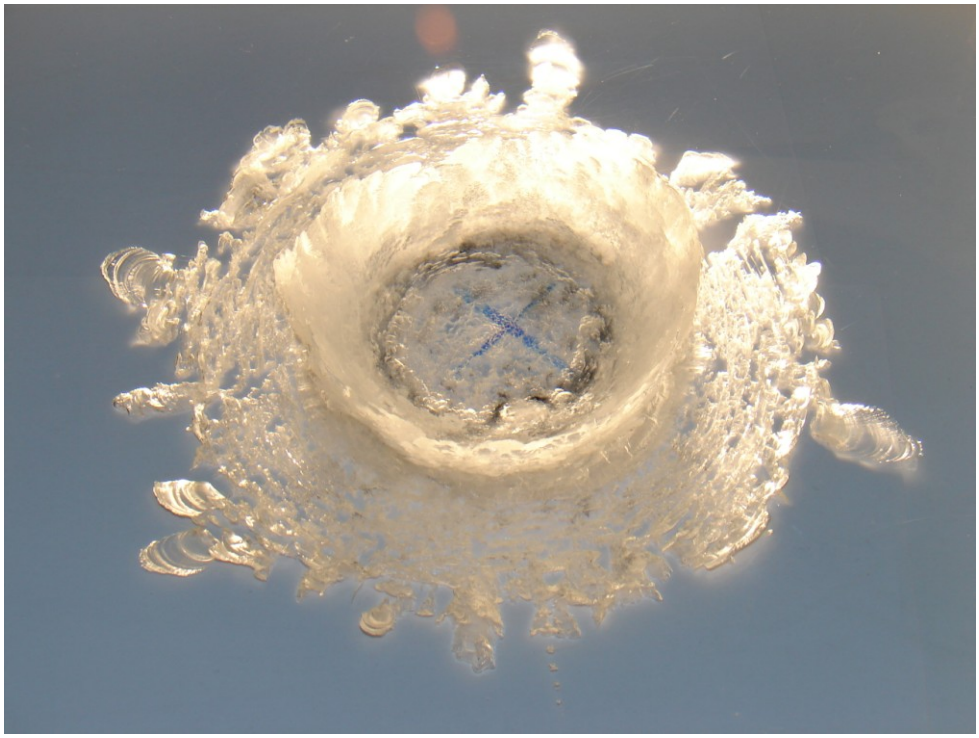

Figure 4.37 Fracture pattern in an acrylic sheet caused by water impact top view

Figure 4.38 Fracture pattern in an acrylic sheet caused by saturated sand impact top view

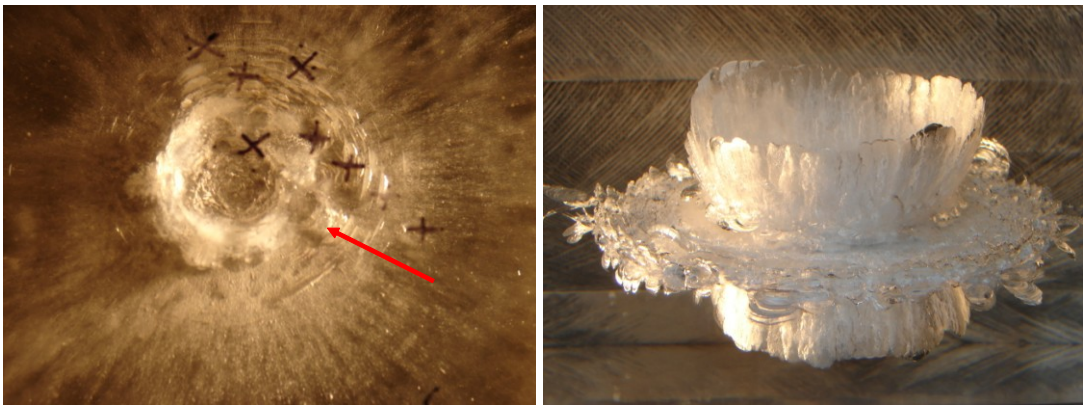

Figure 4.39 Fracture pattern in an acrylic sheet caused by saturated sand (left) top view and by water (right) side view

4.12 Verification of Pressure Measurement and Signal Conditioning

In order to relate the pressure measured using the Kolsky bar to the loading time interval, the high speed camera was applied and the Kolsky bars were mounted using an acrylic sheet (Thickness of 10.16 cm (4 inches)) as a target plate. The SOD used in Gage Test 310 was 4 cm (1.58 inches) and the DOB 1 cm (0.39 inches). The charge used was a 4.4 g Deta Sheet charge in combination with an RP-87 booster. The Kolsky bar distribution over distance is shown in **Figure 4.40**. The distances the Kolsky bars were mounted from the center of the impact are the following: Kolsky bar number 1 at 0 cm (0 inches), number 2 at 1.45 cm (0.57 inches), number 3 at 2.54 cm (1 inch), number 4 at 3.10 cm (1.22 inch), number 5 at 3.91 cm (1.54 inches), number 6 at 5.08 cm (2 inches), number 7 at 6.35 cm (2.5 inches), and number 8 at 7.62 cm (3 inches). Note that the red numbers in the photograph of Figure 2.38 represent the Kolsky bar number as shown in the schematic above. Also the red arrow pointing at Kolsky bar number 4 shows where the bar penetrates the clear acrylic sheet. Below the arrow it shows a reflection of the bar. Bar number 3 is difficult to see since it is covered by bar number 4.

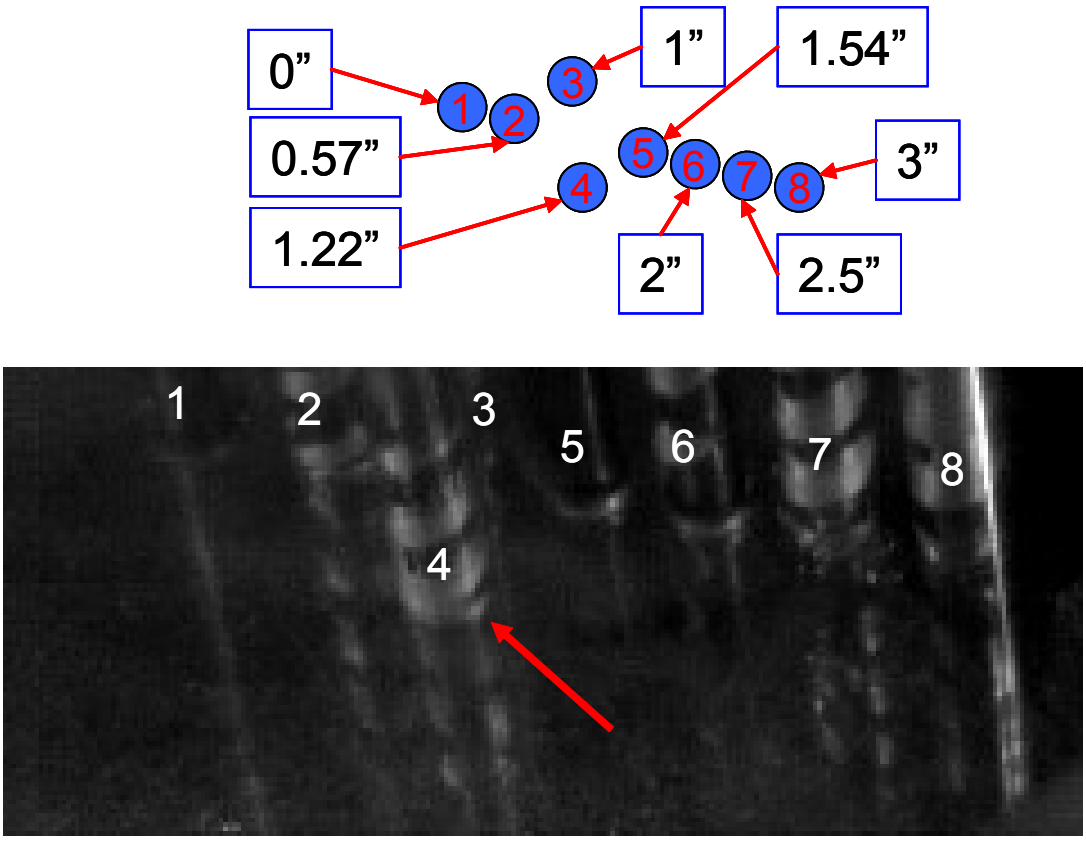

Figure 4.40 Test set-up for visualization of pressure measurement

The pressure – time signal recorded is shown in **Figure 4.41**. The time shown in the graph is adjusted to the time of impact at the plate (that is to say that the time in which the signal travels up to the strain gages is subtracted in all signals measured). The signal noise was reduced calculating a 20 point running average throughout the recording time. The peak pressure recorded at the center (0 cm, gage 1) is measured to be around 258 mega Pascal (37,400 PSI) and arrives first in time. The pressure at the distance of 1.45 cm (0.57 inches, Gage 2) reaches its peak at around 300 mega Pascal (43,500 PSI) and is the highest measured in this test. The pressure measured at the distance of 2.54 cm (1 inch, Gage 3) reaches about the same peak like the Gage 1 at the center (260 mega Pascal, 37,700 PSI). All other pressure peaks measured for the other bars decrease vastly over increasing distance from the center. **Table 4.2** contains the results of the measured pressure - time data.

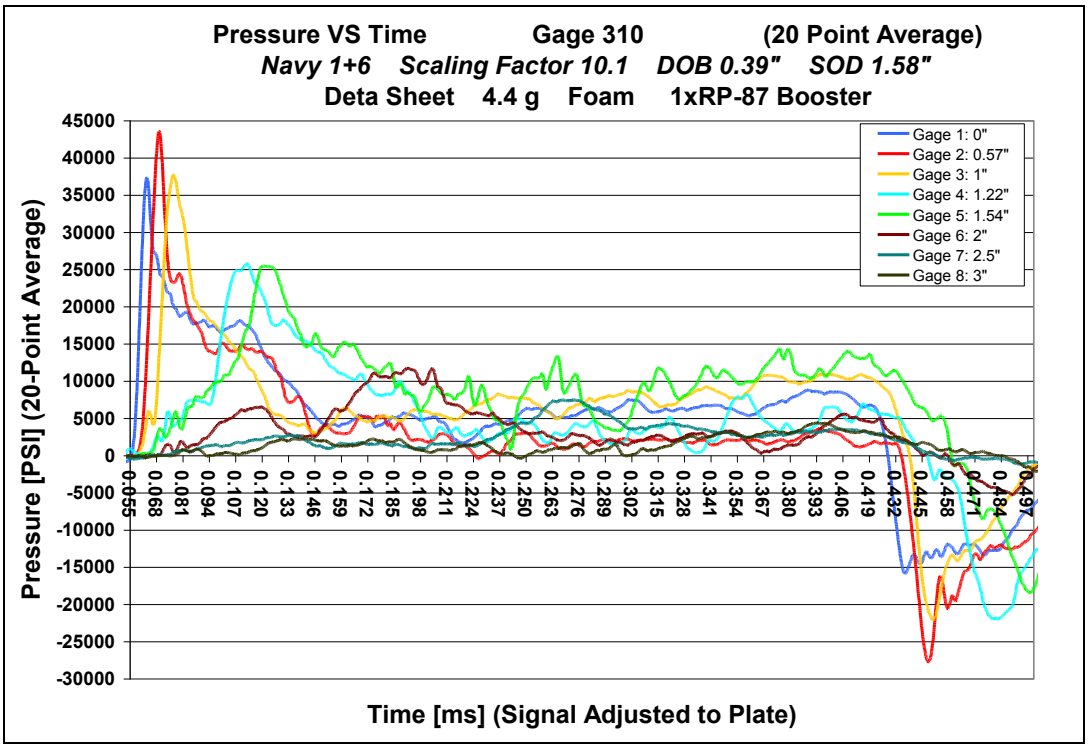

Figure 4.41 Pressure – time profile recorded of Gage Test 310

	Peak Pressure [PSI]	Peak Pressure [MPa]	Time of Arrival [ms]
Last Run	Gage8		Gage8
Gage 1	37,391	258	0.063318129
Gage 2	43,568	300	0.069318129
Gage 3	37,718	260	0.076518129
Gage 4	25,753	178	0.11251813
Gage 5	25,470	176	0.12061813
Gage 6	11,727	81	0.19221814
Gage 7	7,496	52	0.27301814
Gage 8	4,415	30	0.39251814

Table 4.2 Test results for pressure measurement of Test Gage 310

The correlation of time and impact using the high speed camera and the measurement recorded for the center Kolsky bar number 1 at 0 cm (0 inches) can be seen in **Figure 4.42**. The recording interval for the images taken was set to 13 microseconds. At 55 microseconds the first impact at the center of the plate close to Kolsky bar number 1 is visible, compare red arrow pointing at the ionization in **Figure 4.42**. At that time Kolsky bar number 1 starts to pick up the impact, see red bar in the diagram at 0.055 milliseconds in **Figure 4.42**.

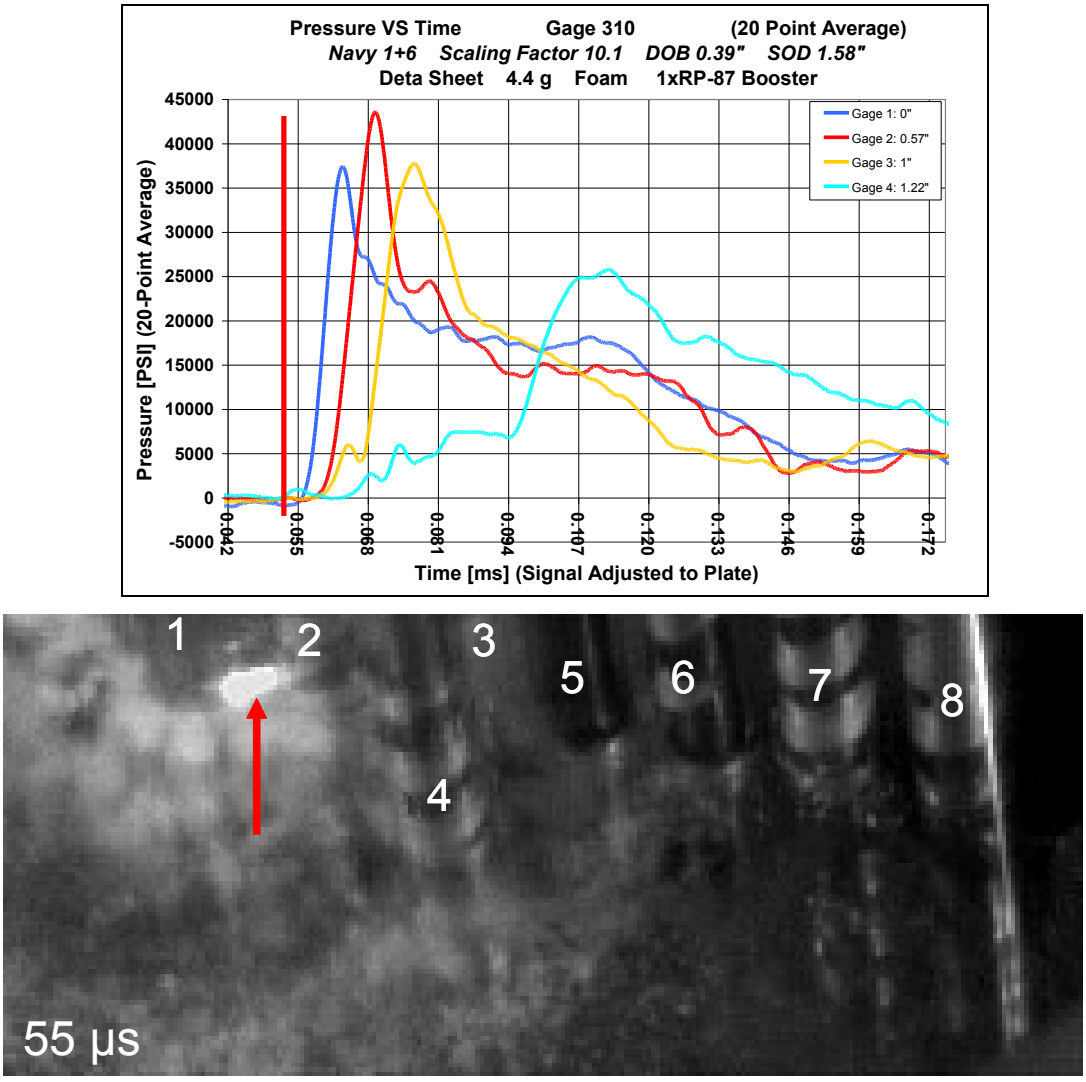

Figure 4.42 Pressure–time profile recorded of Kolsky bar 1 to 4 and image at the time of 55µs

At 68 microseconds the main loading has passed Kolsky bar number 1 at the center, compare the graph (red bar) and the image (red arrow) in **Figure 4.43**. Kolsky bar number 2 at 1.45 cm (0.57 inches) is just about to measure the peak pressure caused by the ring of the applied loading. The outer ring of the loading has just passed Kolsky bar number 2 and about to reach Kolsky bar number 3 which is difficult to see since it is partially covered by Kolsky bar number 4. Kolsky bar number 4 picks up some noise but did not get impacted yet.

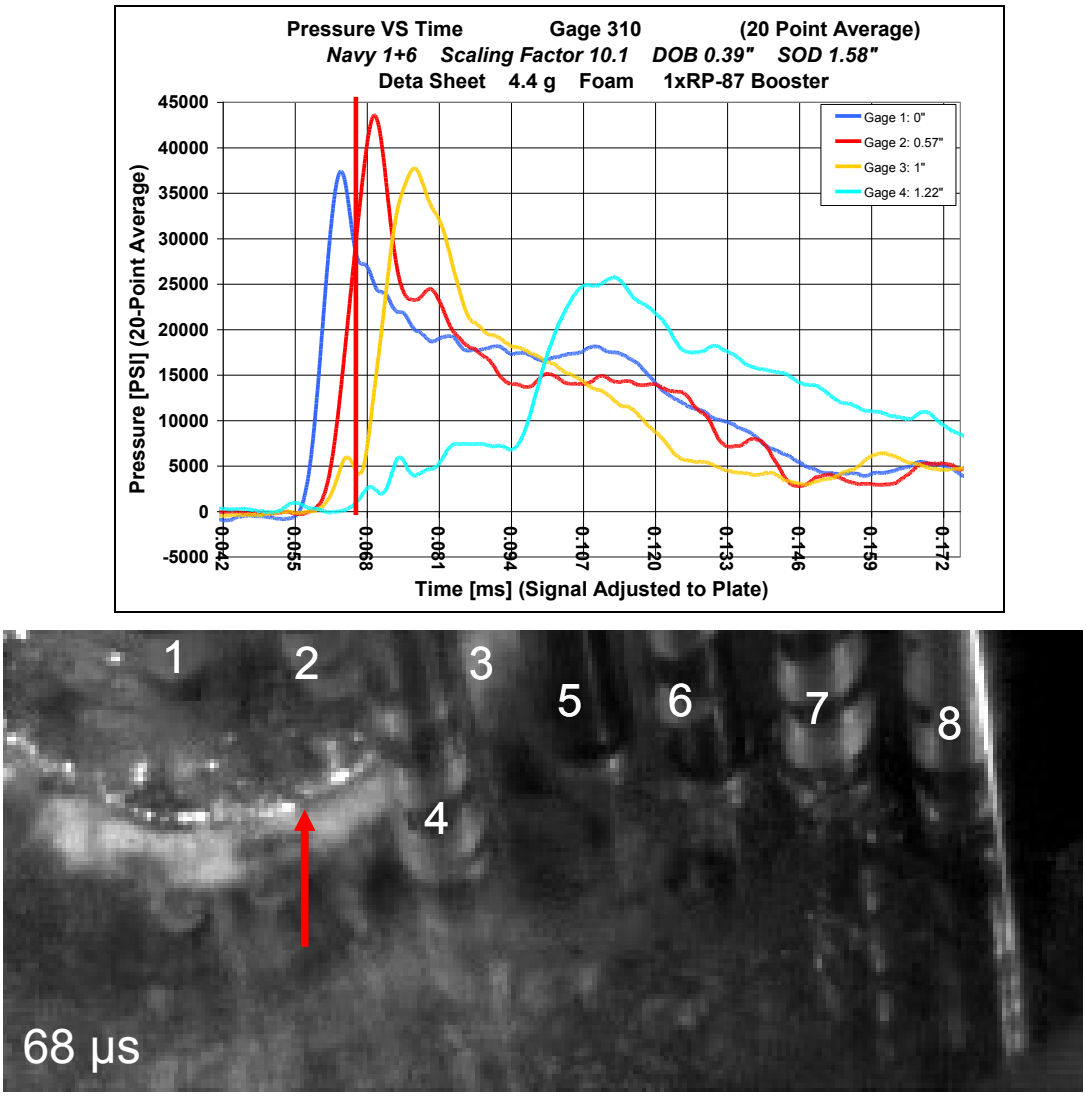

Figure 4.43 Pressure – time profile recorded of Kolsky bar 1 to 4 and image at the time of 68 µs

At 81 microseconds the main loading has passed Kolsky bar number 1, 2, and almost 3. Kolsky bar number 4 at 3.10 cm (1.22 inches) and 5 at 3.91 cm (1.54 inches) has just started to get impacted, compare the graph (red bar) and the image (red arrow) in **Figure 4.44**. Kolsky bar number 3 still gets impacted but the pressure is declining. Kolsky bar number 6, 7, and 8 are not impacted yet. But all 3 Kolsky bars already notice some excitation which is due to the stress waves introduced into the acrylic plate. This stress waves travel very fast and reach the bars before the saturated sand impacts the bottom.

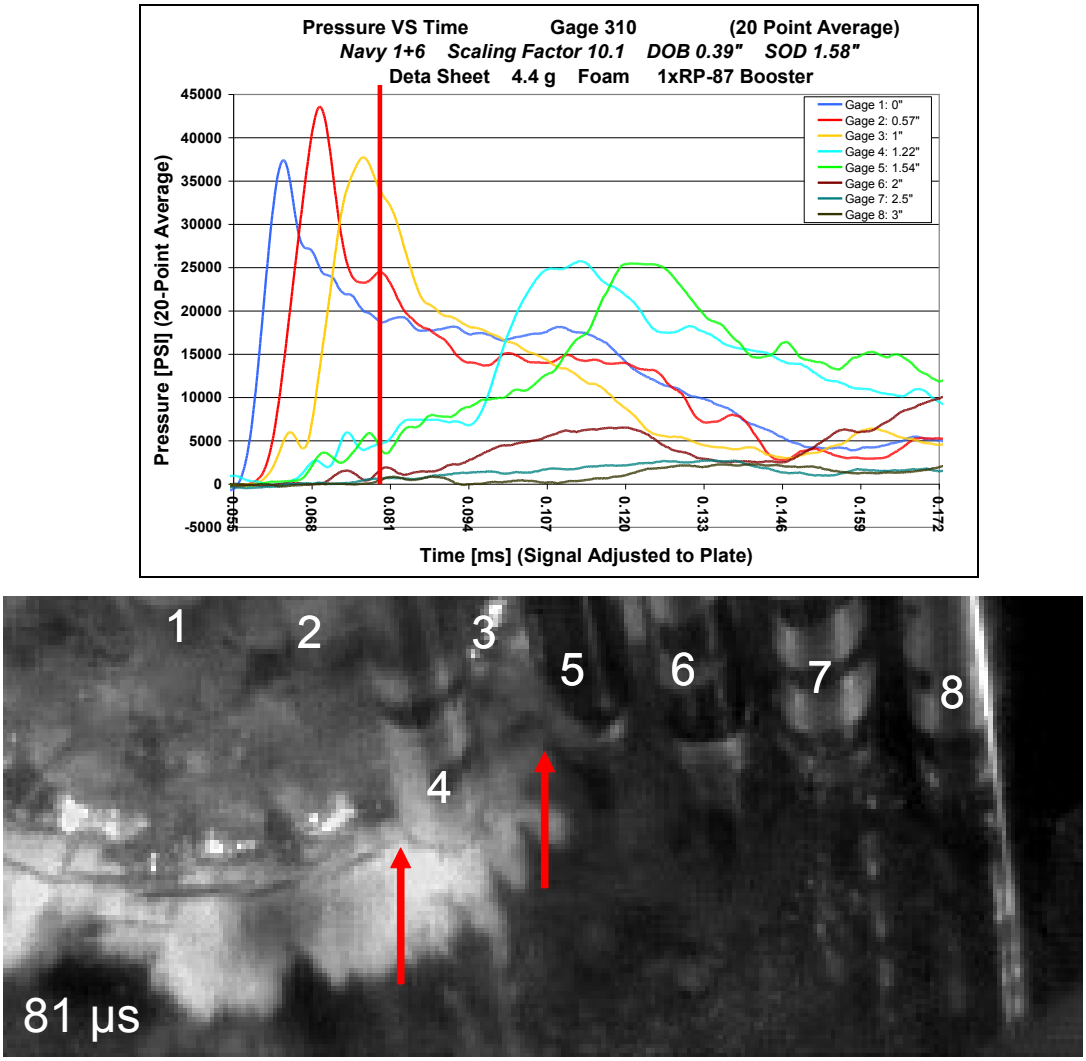

Figure 4.44 Pressure – time profile recorded of Kolsky bar 1 to 8 and image at the time of 81 µs

At 94 microseconds the main loading is about to impact Kolsky bar number 4, see red arrow in **Figure 4.45** in the image taken at 94 microseconds. Kolsky bar number 4 is just short of measuring the steep rise in pressure towards its peak. At 107 microseconds bar number 4 has almost measured the peak pressure. Compare the loading shown in the image (red arrow at 107 microseconds) and the graph at this time in **Figure 4.45**. From 120 to 133 microseconds the loading still continues but at a much lower pressure. Notice that the ring of the applied load slows down during its expansion, see red arrow in image at 120 and 133 microseconds in **Figure 4.45**. That gives the pressure – time curve of Kolsky bar number 4 a distinctive character compared to bar number 1, 2, and 3. The pressure – time curve decreases slowly until the loading has passed. Still after the loading has stopped there is an off-set noticeable in the pressure – time curve. This is typical for all Kolsky bars since the gages warmed up during the measurement taken and the gages changed therefore the resistance slightly.

The same characteristics as described for bar number 4 can be stated for Kolsky bar number 5. It gets impacted a little later in time and therefore it reaches the peak pressure measured later in time. The pressure decreases comparable to bar number 4. Bar number 4 and 5 always show these characteristics at their distances from the center using a 4.4 g charge.

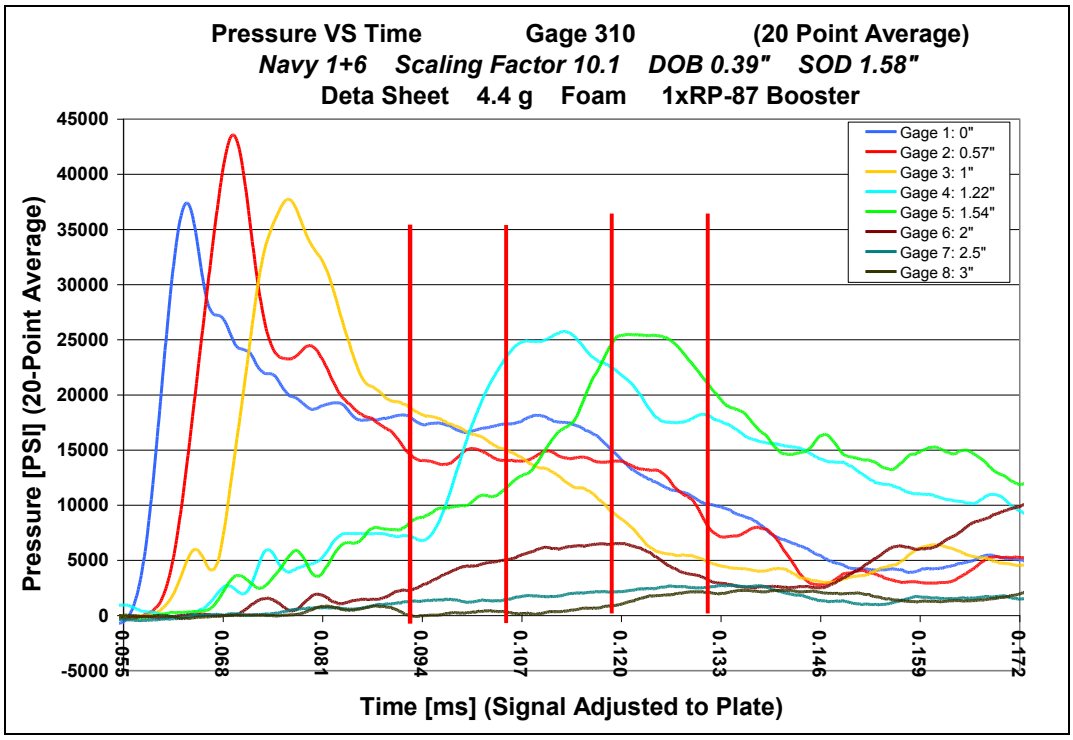

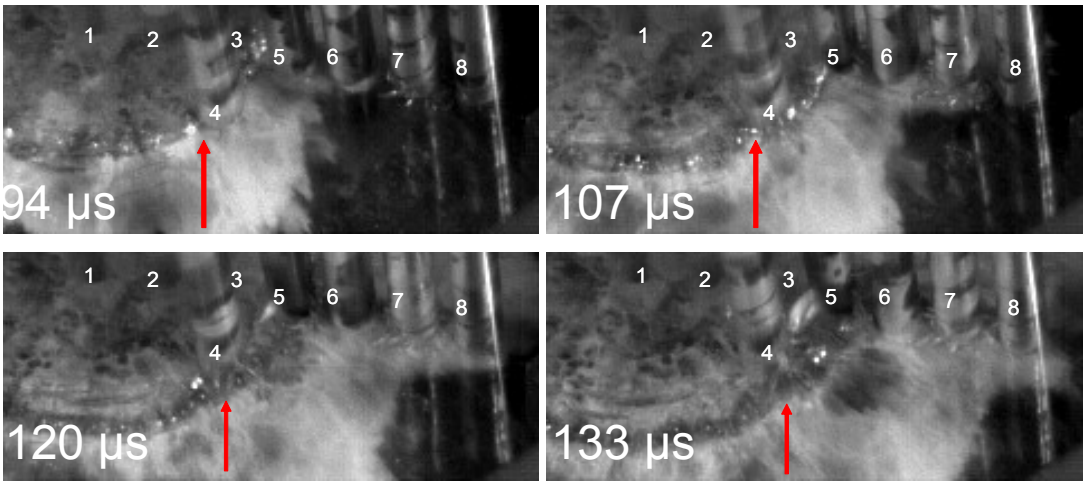

Figure 4.45 Pressure – time profile recorded of Kolsky bar 1 to 8 and image at the time of 94,107, 120, and 133 µs

Kolsky bar number 6 at the time of 107 microseconds picks up a precursor of the loading even though the ring of the loading did not arrive yet. Compare again the red arrow at 107 microseconds and the pressure – time curve at this time in **Figure 4.46**. The loading arrives at the bottom of the bar at 146 microseconds which is clearly documented in **Figure 4.46**. From then on, the bar measures the peak of the pressure loading until the ring has arrived at the center of the bar at the time of 172 microseconds (compare the red arrows and the red bars at each time step). Hence there is an off-set of 17 mega Pascal (2500 PSI) before the ring of loading arrives. Later in the next chapter signals will be shifted in order to calculate the specific impulse at certain locations. What causes the off-set is not proven. A possibility might be that the Kolsky bar absorbs a small side impact from the material which impacted first at the center of the target plate, got redirected, and forms by now the corona. This can happen if the Kolsky bars are not perfectly flush mounted at the bottom of the target plate. Since the whole set-up gets mounted on the test box, it is possible that during handling the Kolsky bars move slightly. Before testing the bars locations get checked but it is nearly impossible to correct their positions to be precisely mounted flush to the bottom of the target plate.

At the time of 263 Microseconds the ring of loading has passed Kolsky bar number 6, compare red arrow at the time 263 microseconds in the image with the red bar at the same time in the pressure – time plot in **Figure 4.46**. The ring has moved on to the middle of Kolsky bar number 7 mounted at the distance of 6.35 cm (2.5 inches) from the center. Compare blue arrow in the image at the time of 263 microseconds and the blue bar at the same time in the pressure – time plot in **Figure 4.46**. The bar measures the peak pressure at this time.

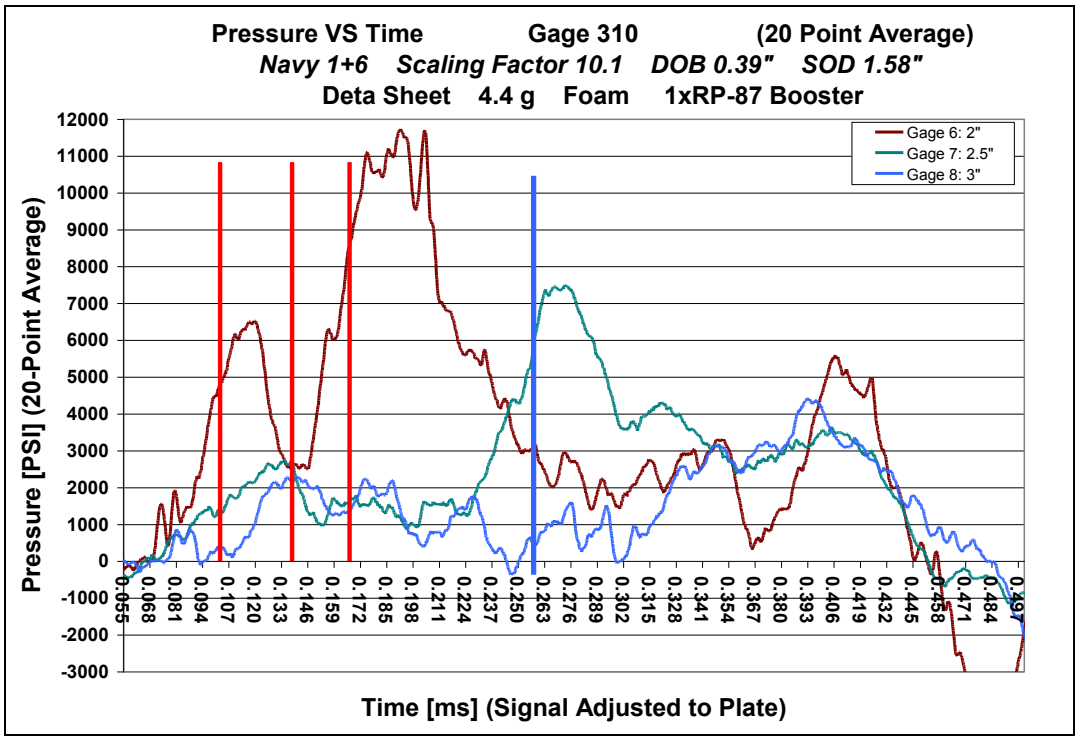

Figure 4.46 Pressure – time profile recorded of Kolsky bar 6 to 8 and image at the time of 107, 146, 172, and 263 µs

In order to point out certain signal conditioning which has to be performed after recording the pressure – time profiles, Kolsky bar number 7 is a good example to look at. At the time of 94 microseconds bar number 7 picks up the precursor as described before. Again comparing the red bar in the pressure – time profile and the red arrow in the image at 94 microseconds in **Figure 4.47** nothing is impacting the bar yet. Shortly before the time of 237 microseconds is reached, the bar gets impacted (compare the green bar and the green arrow in **Figure 4.47**). The pressure starts rising abruptly. There is an off-set of approximately 8.3 mega Pascal (1200 PSI) (compare **Figure 4.47** in the graph) caused probably by stress waves traveling through the plate. This suggests that the peak pressure value is instead of 51.7 mega Pascal (7500 PSI), see **Figure 4.47**, 8.3 mega Pascal (1200 PSI) lower. The solution is shifting the signal for 8.3 mega Pascal (1200 PSI) down. Shortly before the time of 276 microseconds is reached, the peak pressure is measured; compare the blue bar in the pressure – time profile and the blue arrow in the image at the time of 276 microseconds of **Figure 4.47**.

By the time of 354 microseconds the ring of loading has passed bar number 7, see yellow arrow in the image at that time and the yellow bar in the pressure – time profile in **Figure 4.47**. Even though the Kolsky bar seems to be still measuring pressure, it is quite possible that it is noise recorded which is generated by the stress waves travelling through the set-up. Therefore it is suggested to cut of the signal at this point especially for the calculation of the specific impulse which will be shown later. Also this suggests that many signals have to be recorded at each distance from the center of the target plate in order to generate an average signal at each location. In this case the signal of Kolsky bar number 7 is valid from 224 microseconds on until the time of 354 microseconds is reached. In order to evaluate all the signals the recorded images are very helpful for each set-up in which the SOD and the DOB are different. Every single signal has to be manually evaluated for the length of the recording time and the shift of the amplitude.

Finally note that the ring of loading changes its thickness in this particular set-up. Comparing its thickness in **Figure 4.47** at the time of 276 and at 354 microseconds

the dark zone characterizing the ring of loading widens up later in time, see the yellow mark in the image at the time of 354 microseconds.

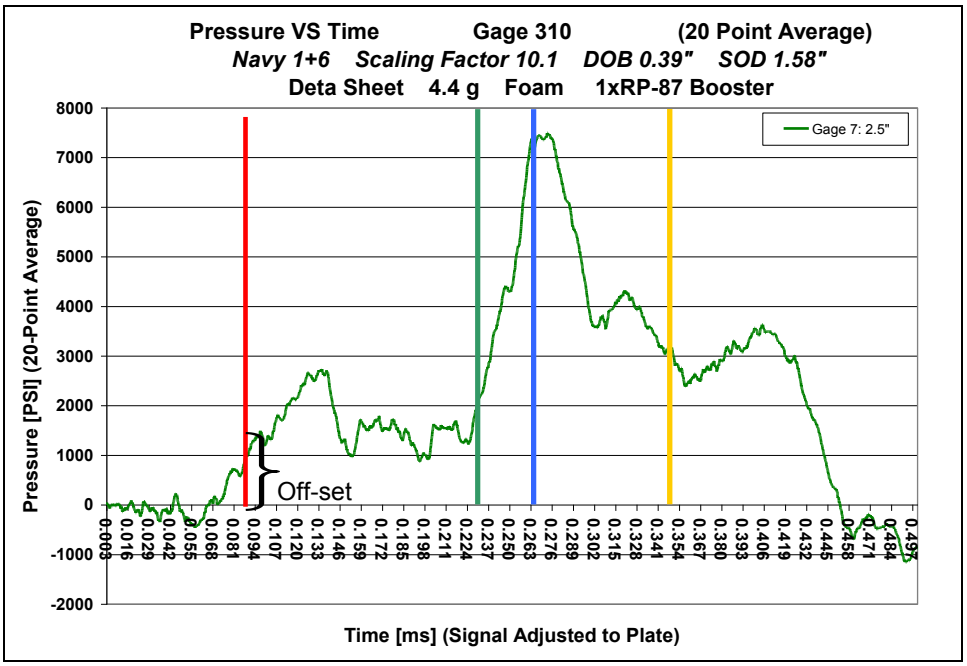

Figure 4.47 Pressure - time profile recorded of Kolsky bar 7 and image at the time of 94, 237, and 276 µs

Looking at Kolsky bar number 8, the pressure – time profile shows a precursor as described before (**Figure 4.48**). At the time of 302 microseconds the Kolsky bar started to get impacted by the ring of the loading compare the red bar in the pressure – time profile and the red arrow in the image at 302 microseconds in **Figure 4.48**. In this case there is no shift in the pressure amplitude necessary since the off-set died out. At the time of 393 microseconds the peak pressure of 30.4 mega Pascal (4,400 PSI) is obtained and the ring of loading has covered the whole bar, compare **Figure 4.48** at 393 microseconds. By the time of 484 microseconds the ring of loading has passed bar number 8 and the reflections of the precursor start to appear in the measurement see **Figure 4.48** at the time of 484 microseconds.

The distance of 7.62 cm (3 inches) from the center of impact is the last location the 122 cm (4 feet) long Kolsky bars can be used for two reasons. First the reflections of the noise measured will superimpose the measurement of the loading and second the sensitivity of the Kolsky bar will be too low.

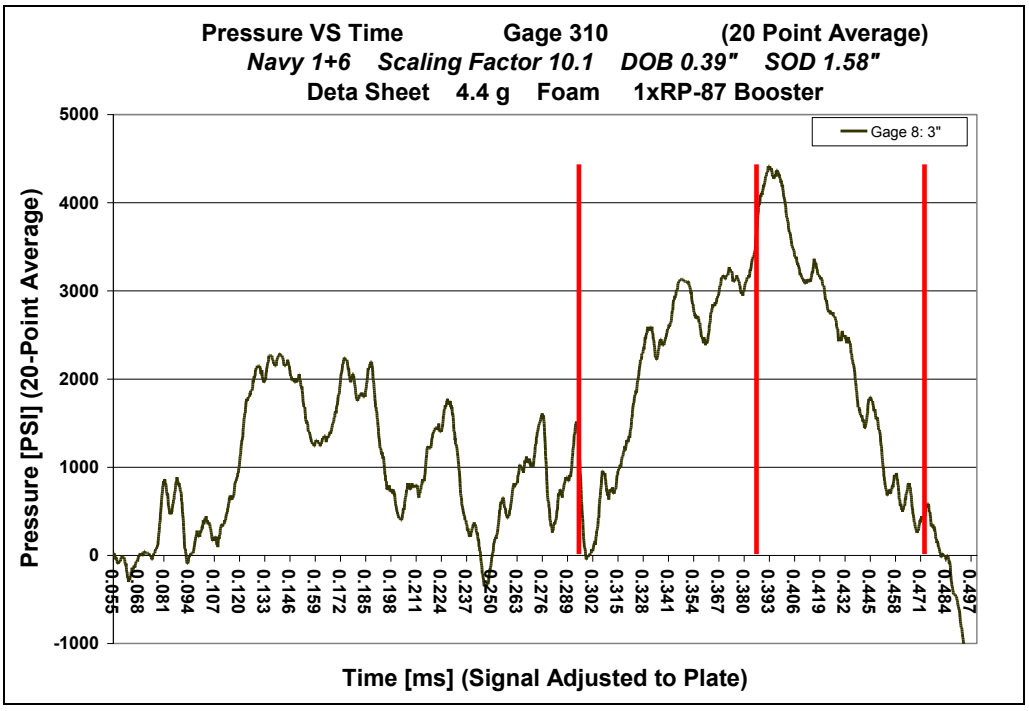

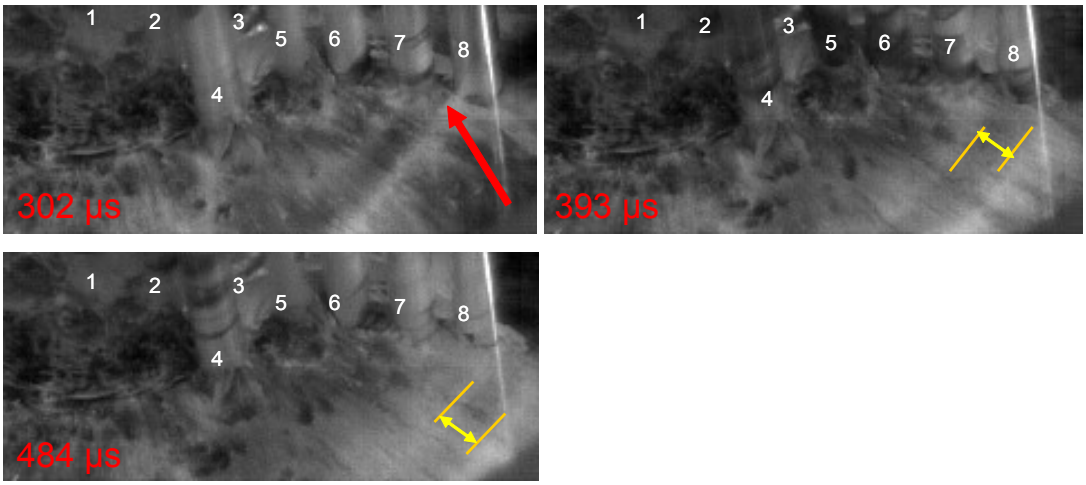

Figure 4.48 Pressure-time profile recorded of Kolsky bar number 8 and image at the time of 302, 393, and 484 µs

4.13 Time Correction for Pressure Measurement

As discussed in section 2.6 several tests were conducted measuring the wave speed in the Kolsky bar. The test set-up used is shown in **Figure 4.17**. The wave speed determined was 4864 m/sec (191.5 inches/msec). In order to adjust the time of arrival in each test and for each Kolsky bar used, the time of travel of the signal has to be taken into account. In almost all cases 122 cm (4 feet) long Kolsky bars were used where the strain gages were mounted at a distance of 30.48 cm (12 inches) from the bottom of the bar. In order to adjust the time of impact to the bottom of the plate (bottom of the Kolsky bar), the travel time for 30.48 cm (12 inches) for the wave in the Kolsky bar has to be subtracted. The travel time for this distance is typically 63.2 microseconds. Applying this calculation including the filtering of the 20 point running average for the amplitude the curve changes little its overall appearance. **Figure 4.49** shows both curves. The blue curve is the original recorded one and the red curve contains the time adjusted and amplitude filtered data.

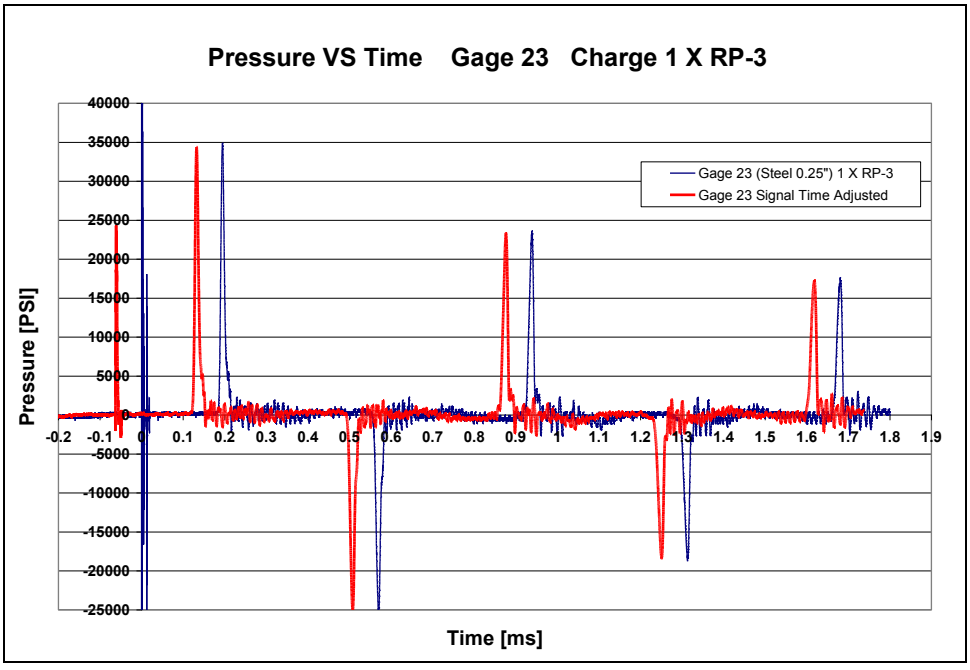

Figure 4.49 Pressure-time profile showing original and time adjusted plot

4.14 Pressure Adjustment to the Bottom of the Kolsky Bar

As mentioned, technically it is not possible to mount the strain gages at the very bottom end of the Kolsky bar. First because the trigger noise of the explosive charge has to vanish over time and second the bar is mounted using a thick target plate so there is no access at the very end to the bar. Since the strain gages are mounted 30.48 cm (12 inches) up from the bottom of the bar, the stress wave has to travel for 30.48 cm (12 inches) before the gages measure the amplitude of the stress wave. In that distance the magnitude of the amplitude has changed.

A total of 3 tests were conducted using a 2.44 meter (8 foot) long Kolsky bar with 8 pairs of strain gages mounted on it. An identical test set-up was employed in all tests. The bar was mounted in the center of the target plate which had a SOD of 4 cm (1.58 inches). The charge used was a 4.4 g charge buried at 0.99 cm (0.39 inches) in saturated sand. One test was conducted using the same set-up as described except the charge was buried at 1.98 cm (0.78 inches). Strain gages were mounted on the Kolsky bar at distances of 15.24 cm (6 inches), 30.48 cm (12 inches), 60.96 cm (24 inches), 91.44 cm (36 inches), 121.92 cm (48 inches), 152.4 cm (60 inches), 182.88 cm (72 inches), and 213.36 cm (84 inches) measured from the bottom of the bar.

Exemplarily Gage Test 301 is shown in **Figure 4.50** which was conducted at a DOB of 1.98 cm (0.78 inches). As can be seen the recorded amplitude of the pressure – time profile declines with increasing travel distance. Note that the recorded noise of the first pair of strain gages (blue curve) mounted at a distance of 15.24 cm (6 inches) from the bottom of the Kolsky bar at a time of 0.2 milliseconds is typical for strain gages mounted too close to the bottom of the bar. **Figure 4.50** shows the pressure – time plot for 8 pairs of gages including the first reflection.

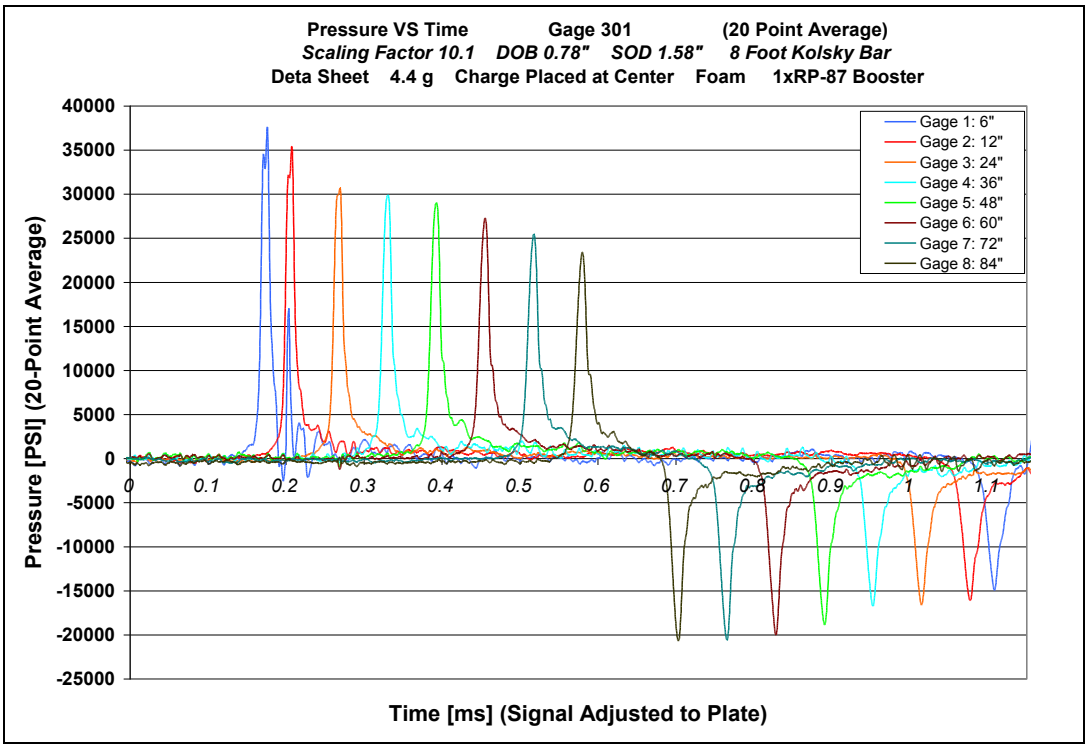

Figure 4.50 Pressure-time profile for a Kolsky bar using multiple pairs of strain gages

Shifting the individual curves as described in section 2.13, the change in shape of the pressure – time curve over distance becomes obvious, see **Figure 4.51**. There is little change comparing the signal recorded at a travel distance of 15.24 cm (6 inches) (blue curve) and 30.48 cm (12 inches) (red curve). The major difference is the peak pressure measured drops and the slop of the rising pressure decreases with increasing stress wave travel distance. This trend can be observed with increasing distance for the other measurements taken at the other locations of the Kolsky bars. The double peak recorded by the gages at the distance of 15.24 cm (6 inches) (blue curve) changes its shape eventually to a single peak at the distance of 121.92 cm (48 inches) (light green curve) since the larger travel distance of the stress waves smoothen the pressure – time profile.

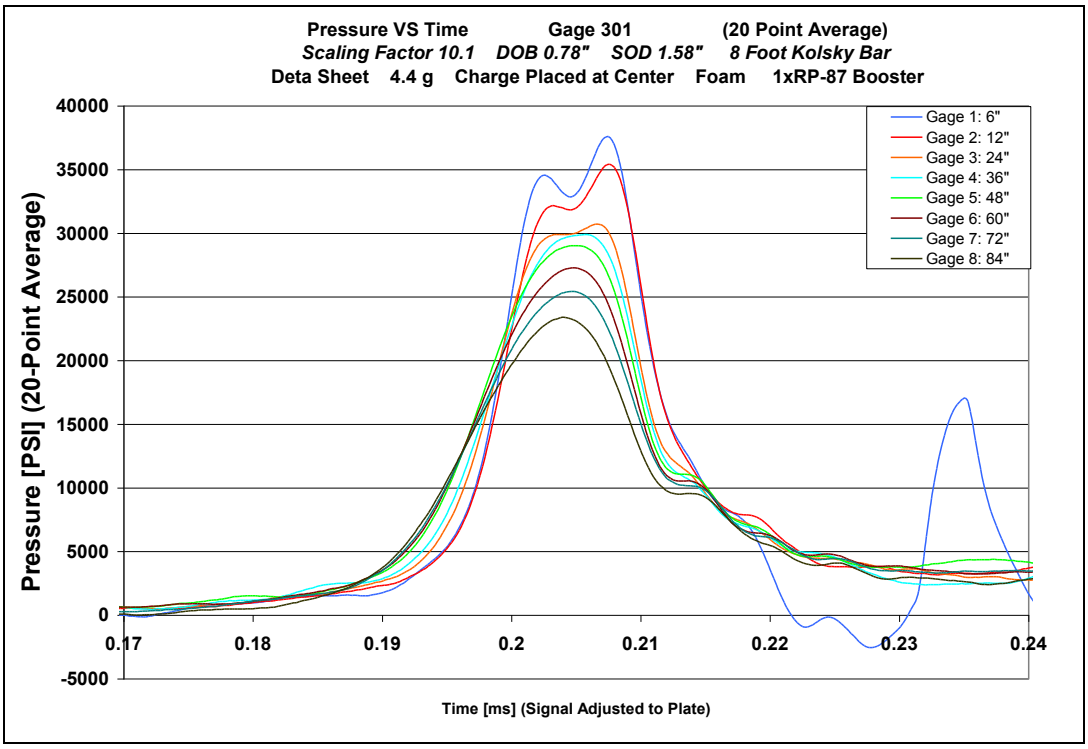

Figure 4.51 Shifted pressure-time profile for a Kolsky bar using multiple pairs of strain gages

The pressure – time profile at the bottom of the Kolsky bar is not known. The profile has to be predicted using the data from the profiles generated by the strain gages mounted further up the Kolsky bar.

In order to calculate the pressure – time profile at the bottom of the Kolsky bar, the logarithmic decrement method is used. The logarithmic decrement is the natural log of the amplitudes of any two successive peaks. **Equation 4.5** is used to calculate the logarithmic decrement δ. A_0 is the greater of the two amplitudes and A_n is the amplitude n periods away. There are two unknown in the equation. The first one is the greater amplitude A_0, the pressure – time profile which has to be calculated. The second one is the logarithmic decrement δ which has to be predicted.

$$\delta = \frac{1}{n} * \ln \frac{A_0}{A_n}$$

Equation 4.5 Logarithmic decrement

In order to predict the logarithmic decrement the spacing of the strain gages on the Kolsky bar has to be equal. Therefore the first pair of gages mounted at the distance of 15.24 cm (6 inches) will be ignored. **Equation 4.5** is used to calculate the decrement for the gages mounted at the distances of 30.48 cm (12 inches), 60.96 cm (24 inches), 91.44 cm (36 inches), 121.92 cm (48 inches), 152.4 cm (60 inches), and 182.88 cm (72 inches). The results are plotted in **Figure 4.52**. A polynomial of 4th order is used in order to extrapolate the logarithmic decrement for the pressure peak at the bottom of the Kolsky bar. In this case the decrement (red cross) is predicted to be 0.98 at location n=1.

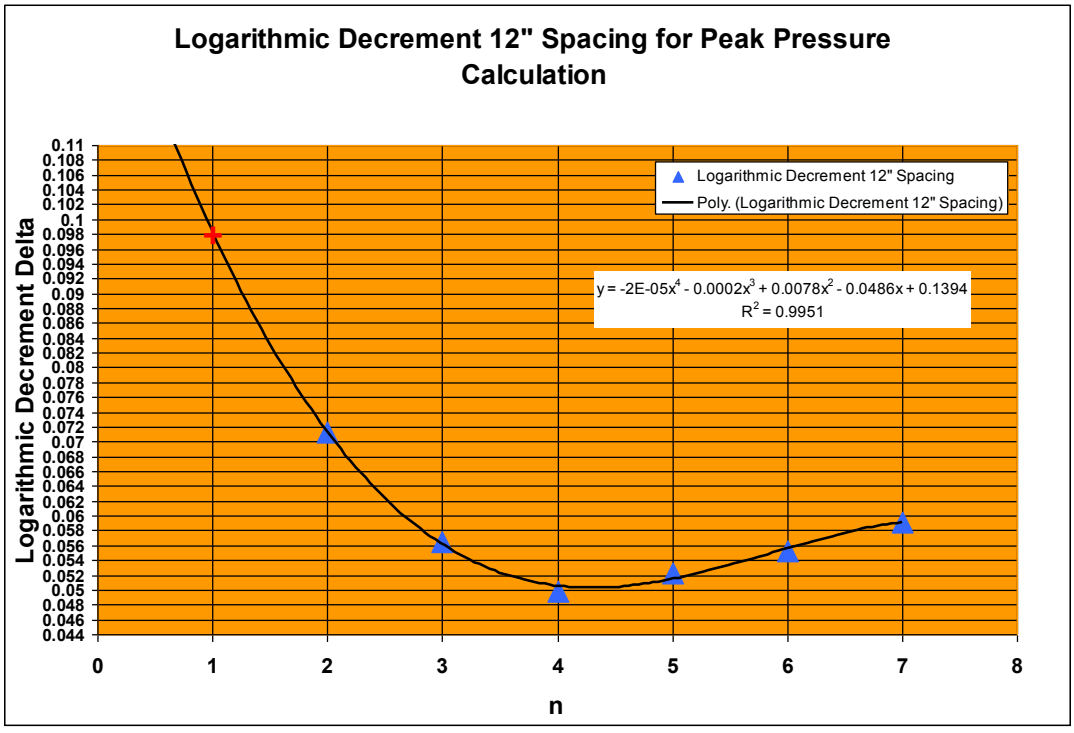

Figure 4.52 Logarithmic decrement δ for Gage Test 301

Using the predicted decrement from **Figure 4.52**, **Equation 4.5** can be rewritten as **Equation 4.6** in order to calculate the pressure – time profile for each measured value A_0 of the profile at the bottom of the Kolsky bar.

$$A_0 = 4_n + {}^{\delta *}$$

Equation 4.6 Pressure – time profile at the bottom of the Kolsky bar

The pressure – time profile including the calculated values for A_0 is shown in **Figure 4.53**. The peak pressure calculated for A_0 is about 300 mega Pascal (43,100 PSI) hence it exceeds the highest peak measured including the peak at the distance of 15.24 cm (6 inches) which was not considered for the calculation.

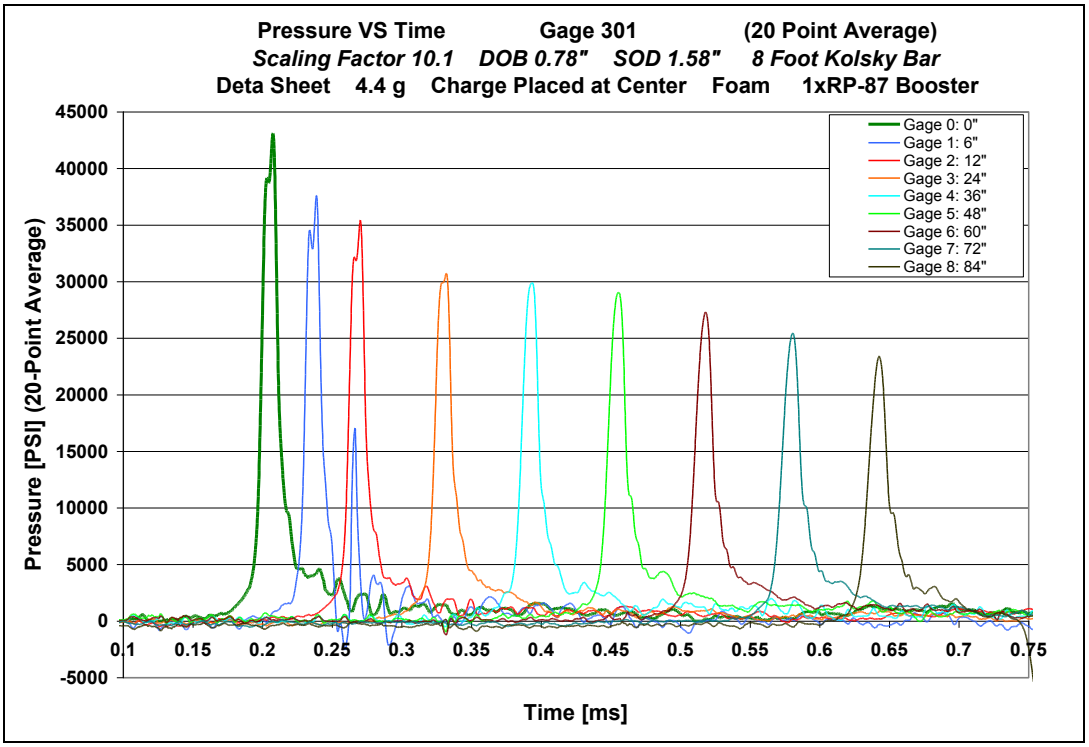

Figure 4.53 Pressure – time profile at the bottom of the Kolsky bar

Adding the calculated pressure – time profile to the shifted individual curves as described in section 2.13, proves the coherence with the measured profiles. The peak pressure of the calculated pressure – time profile is the highest as it should be. The signal characteristic is comparable to the pressure – time profile measured at the distances of 30.48 cm (12 inches) since it is calculated based on this signal. **Figure 4.54** contains the in time shifted individual curves.

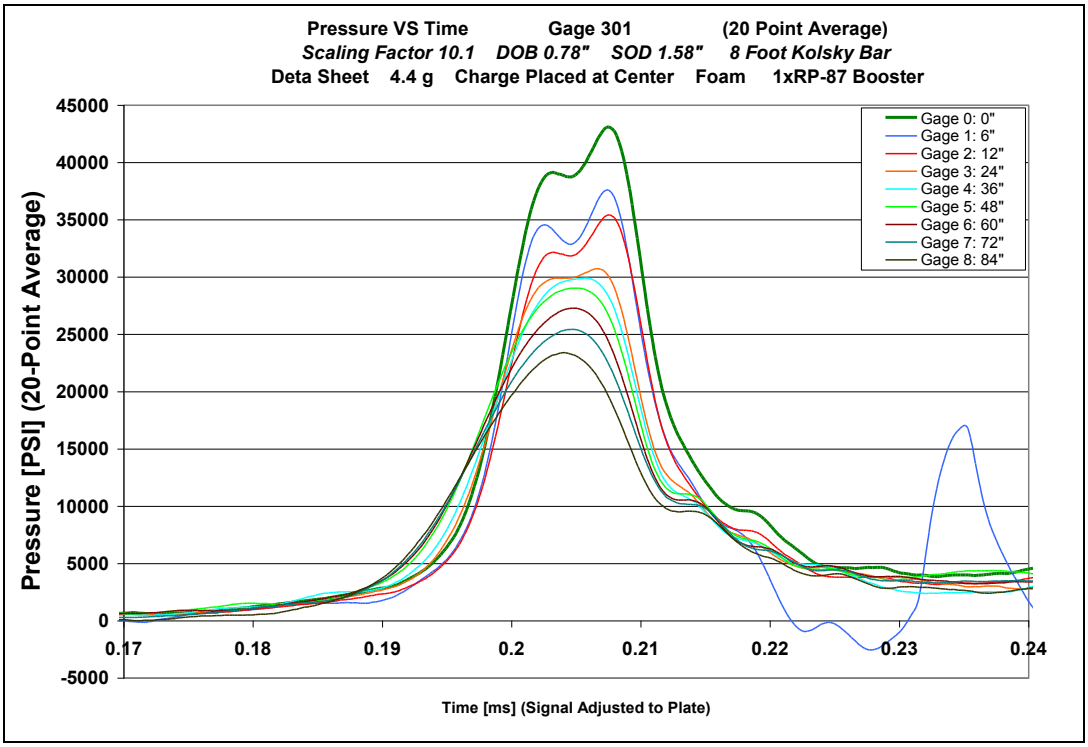

Figure 4.54 Shifted pressure-time profile for a Kolsky bar using multiple pairs of strain gages including the calculated profile (Gage 0)at the bottom of the Kolsky bar

In order to show how well the method works, a pressure – time profile recorded is predicted. Using the test data from the same test conducted, the pressure – time profile for Gage number 5 at the distance of 121.92 cm (48 inches) will be predicted using the data recorded from the very next location of Gage number 6 at

152.4 cm (60 inches). The logarithmic decrement for Gage number 5 is 0.0504 see blue cross in **Figure 4.55**. Using the logarithmic decrement, the recorded data from Gage number 6, and the **Equation 4.6**, the pressure – time profile of gage number 5 can be calculated. As can be seen in **Figure 4.56** the predicted pressure – time profile for Gage number 5 agrees pretty well with the measured pressure – time profile of Gage number 5.

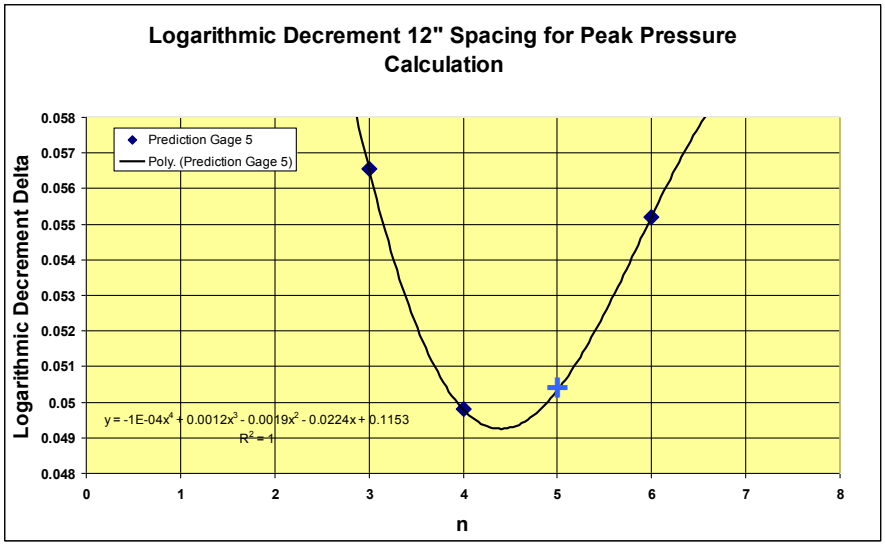

Figure 4.55 Logarithmic decrement δ for Gage Test 301 Gage 5

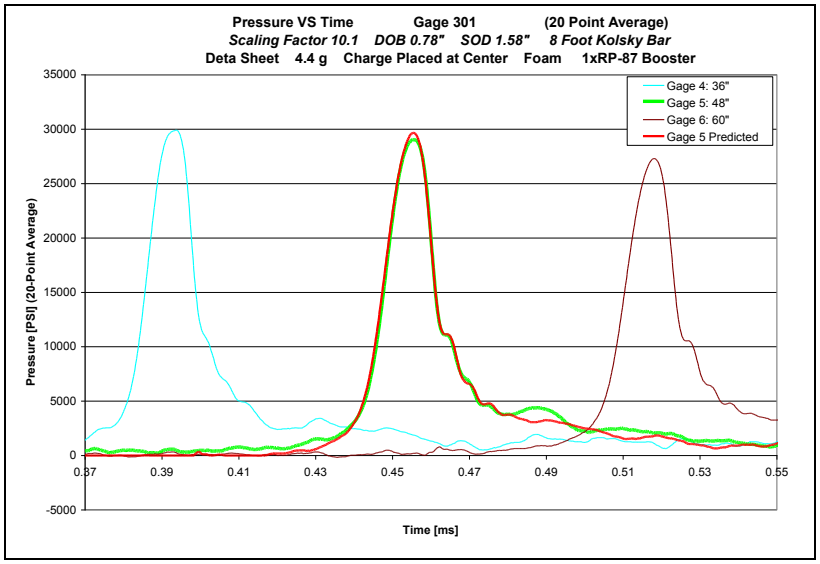

Figure 4.56 Pressure – time profile for Gage number 5 predicted and measured

The knowledge about the loading mechanisms and the set of tools provided in this chapter will be used in the next chapter in order to collect the pressure – time profile data in different test set-ups. Understanding the described technique of using the Kolsky bars is essential for this task

Chapter 5: Pressure – Time Profiles

This chapter describes the method used in order to obtain pressure distributions, specific and total impulses from the pressure – time profiles at various Stand-off Distances (SOD) and Depth of Burials (DOB) measured along the bottom of a target plate.

Mainly the test results will be obtained using the Kolsky bars. In some cases the pressure – time profiles are generated using PCB sensors due to the low pressures applied at greater distances to the detonating charge.

5.1 Pressure – Time Profiles at SOD 4 cm (1.58 inches) and DOB 1 cm (0.39 inches) in Saturated Sand

Most of the data collected was generated using a SOD of 4 cm (1.58 inches) and a DOB of 1 cm (0.39 inches). The Kolsky bar set-up used was shown in **Figure 4.23** and **Figure 4.25**. The explosive charges used were 4.4 g of Deta sheet. **Table 5.1** contains the results of 32 tests (192 recorded pressure – time profiles) conducted in saturated sand. The pressure – time profiles were recorded at the locations of 0 cm (0 inches), 1.01 cm (0.4 inches), 1.45 cm (0.57 inches), 2.54 cm (1 inch), 3.10 cm (1.22 inches), 3.91 cm (1.54 inches), 5.08 cm (2 inches), 6.35 cm (2.5 inches), 7.62 cm (3 inches). The table gives values for the maximum and minimum peak pressure measured at each location. The average peak pressure is calculated and so is the standard deviation based on the number of profiles recorded at each location. The standard deviations are increasing towards the center of the plate.

Location	Maximum Pressure	Minimum Pressure	Average Pressure	Number of Profiles	Standard Deviation
[Inch]	[PSI]	[PSI]	[PSI]		[PSI]
0	61,896	31,033	51,527	8	10,059
0.4	61,383	31,505	46,891	16	8,202
0.57	65,374	17,815	52,414	24	11,046
1	54,582	18,069	38,194	24	9,153
1.22	36,054	8,829	20,701	24	6,050
1.54	23,233	7,336	15,937	24	4,525
2	20,100	5,407	11,190	24	4,277
2.5	15,073	3,255	9,973	24	2,898
3	7,949	2,035	4,976	24	1,878

Table 5.1 Pressure - time results for saturated sand at SOD 4 cm (1.58 inches) and DOB 1 cm (0.39 inches)

Figure 5.1 shows the maximum and minimum pressure measured and the average pressure calculated at specific locations of the plate. Note that the maximum and average pressure rise at a distance of 1.45 cm (0.57 inches). Also the deviation is greatest at this location. With increasing distance from the center of the plate the peak pressure values decrease rapidly.

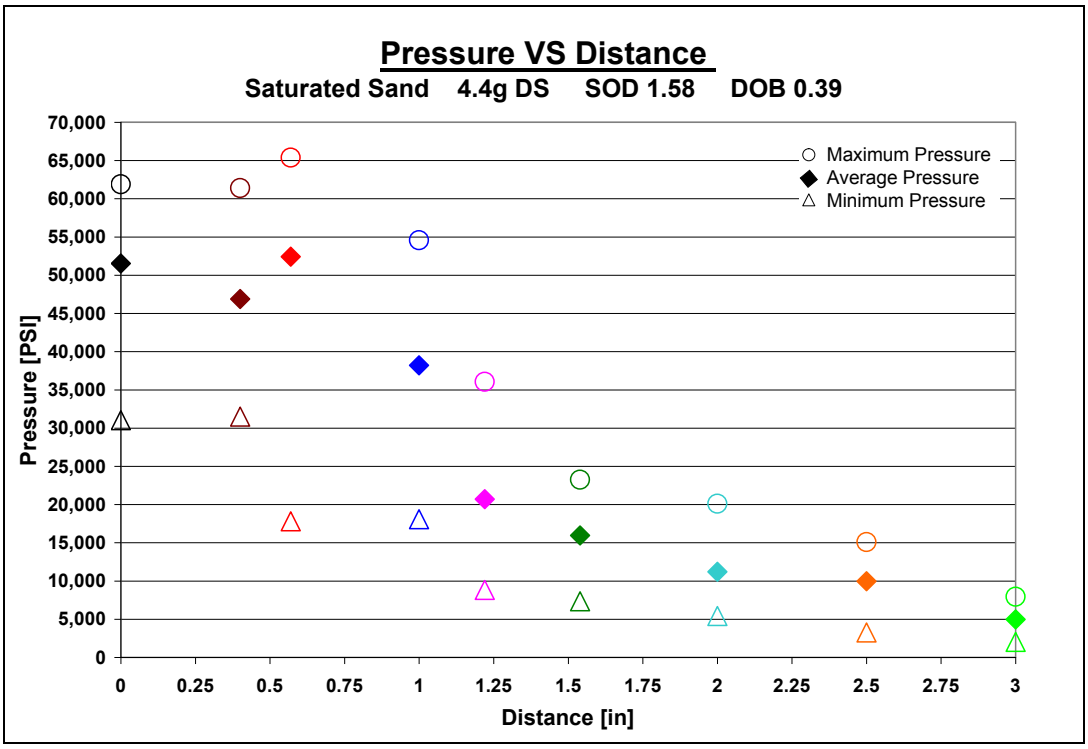

Figure 5.1 Peak pressure results for saturated sand at specific locations at SOD 4 cm (1.58 inches) and DOB 1 cm (0.39 inches)

In order to calculate the average pressure - time profile each single measured pressure - time profile has to be shifted in such a manner that the peak pressure values occur at the same time. The peak pressure alignment has to be conducted for each specific location where the pressure was measured. **Figure 5.2** shows the pressure - time profiles aligned at the locations of 0 cm (0 inches) and **Figure 5.3** at 1.01 cm (0.4 inches). It includes the average pressure - time profile. These profiles are later used for calculating the specific impulse at each location. **Figure 5.4** contains the pressure - time profile not aligned at the locations of 1.45 cm (0.57 inches) and **Figure 5.5** at 2.54 cm (1 inch). They show the variation in time of arrival for the peak pressures being measured. The figures include the average pressure - time profiles calculated from the aligned pressure - time profiles.

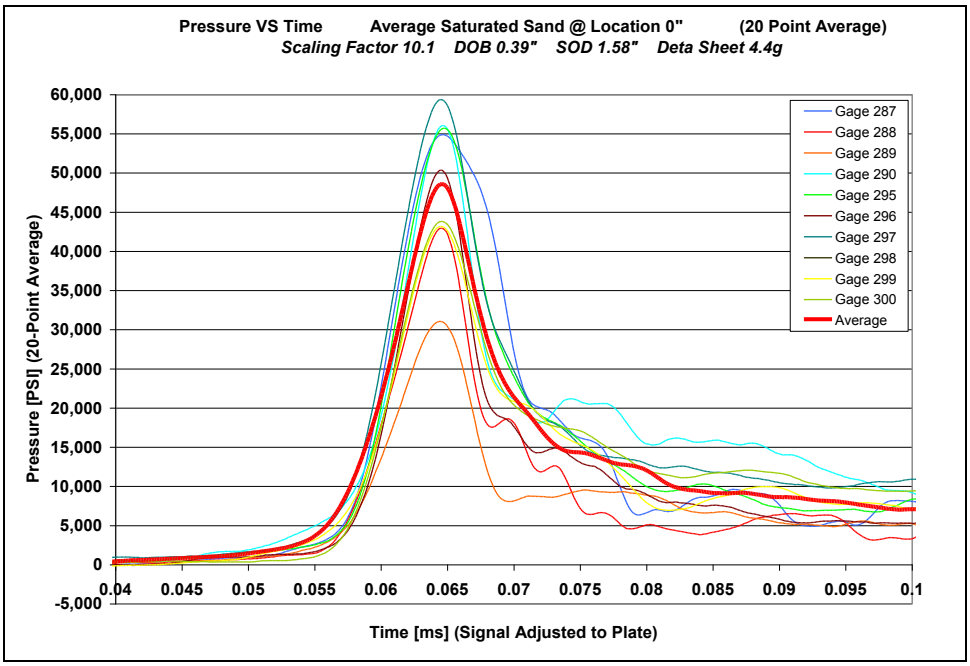

Figure 5.2 Peak pressure - time profiles aligned at location of 0 cm (0 inches) including average pressure - time profile

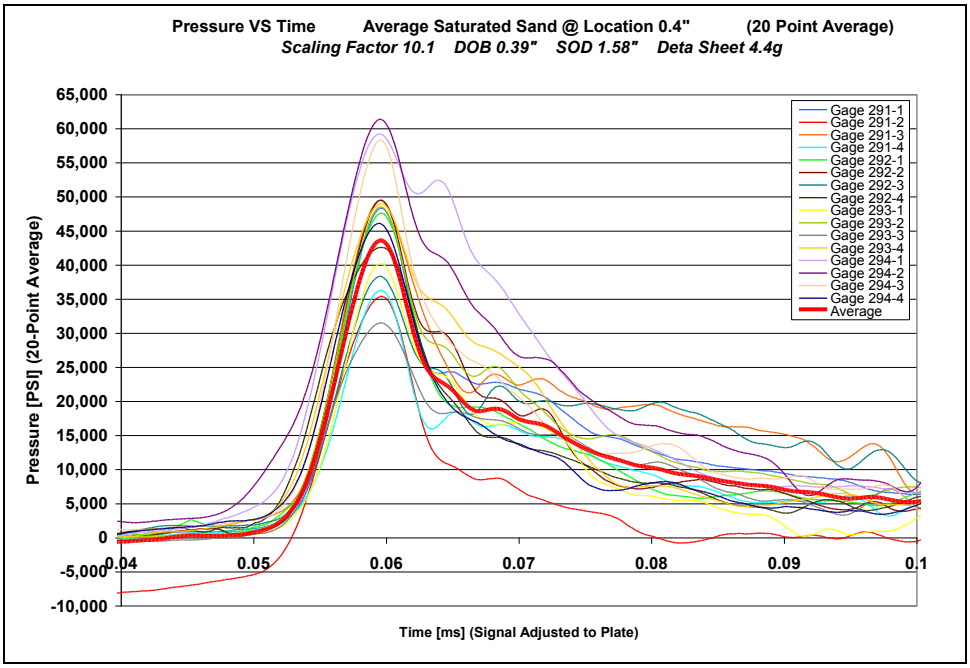

Figure 5.3 Peak pressure - time profiles aligned at location of 1.01 cm (0.4 inches) including average pressure - time profile

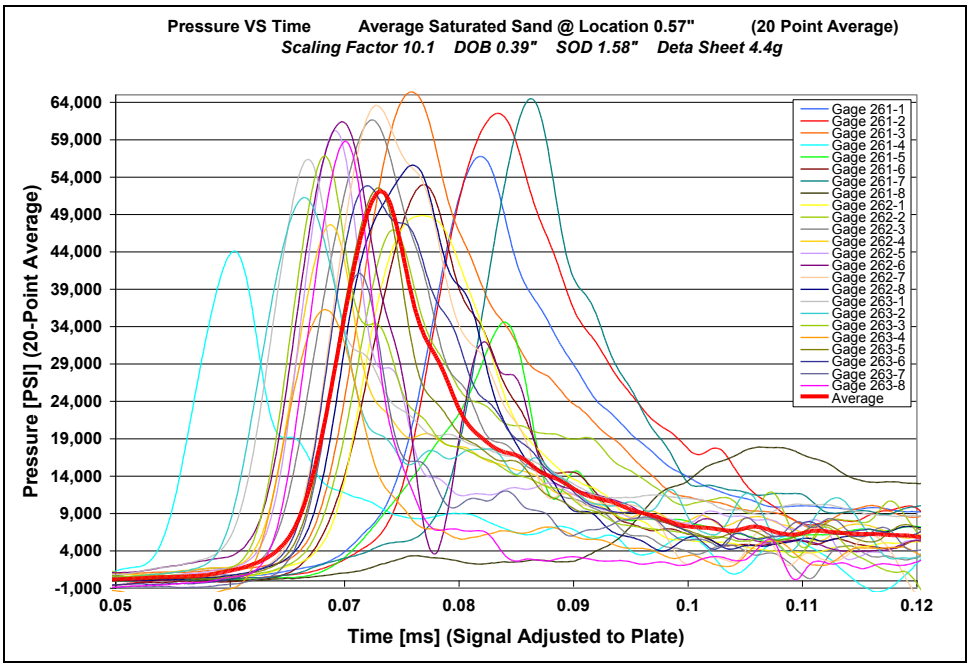

Figure 5.4 Peak pressure - time profiles not aligned at location of 1.45 cm (0.57 inches) including average pressure - time profile

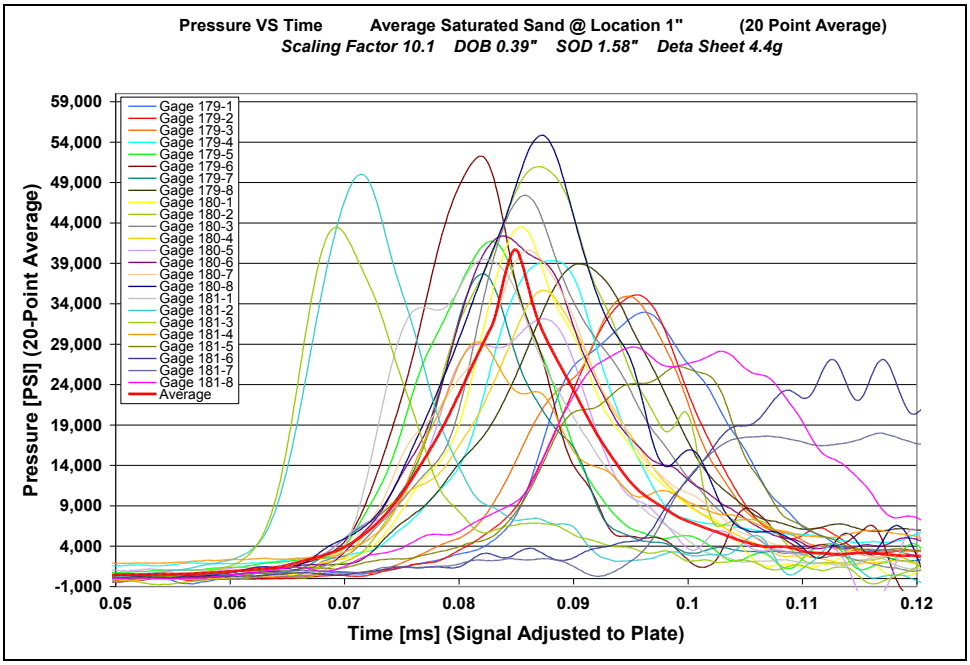

Figure 5.5 Peak pressure - time profiles not aligned at location of 2.54 cm (1 inch) including average pressure – time profiles

Figure 5.6 contains the pressure - time profiles not aligned at the locations of 3.10 cm (1.22 inches), 3.91 cm (1.54 inches), and 5.08 cm (2 inches). Like in **Figures 5.4 and 5.5** it shows the variation in time of arrival of the peak pressures being measured. The figure includes the average pressure - time profile calculated from the aligned pressure - time profiles.

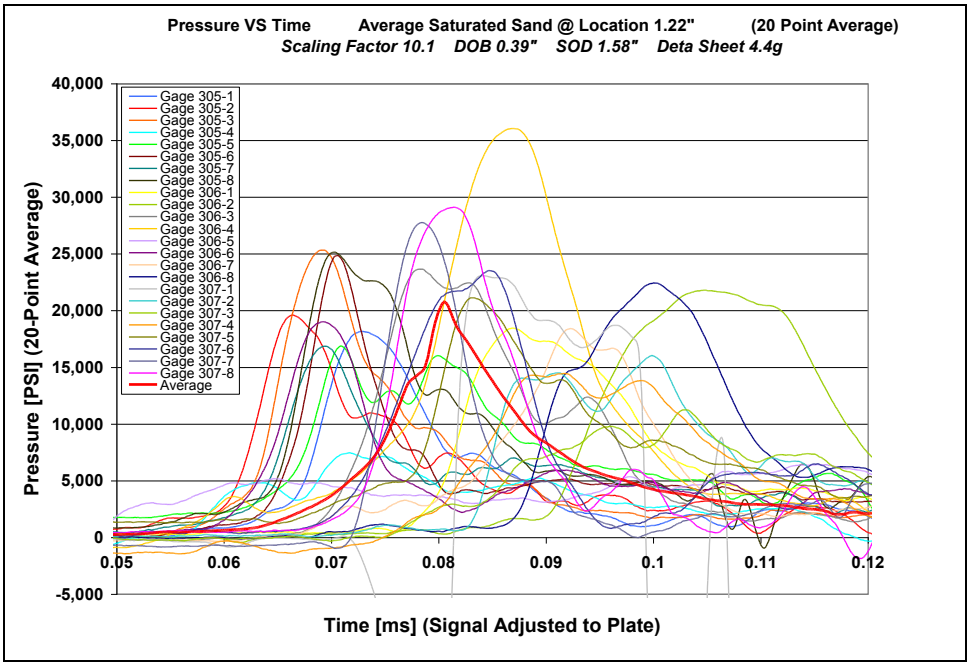

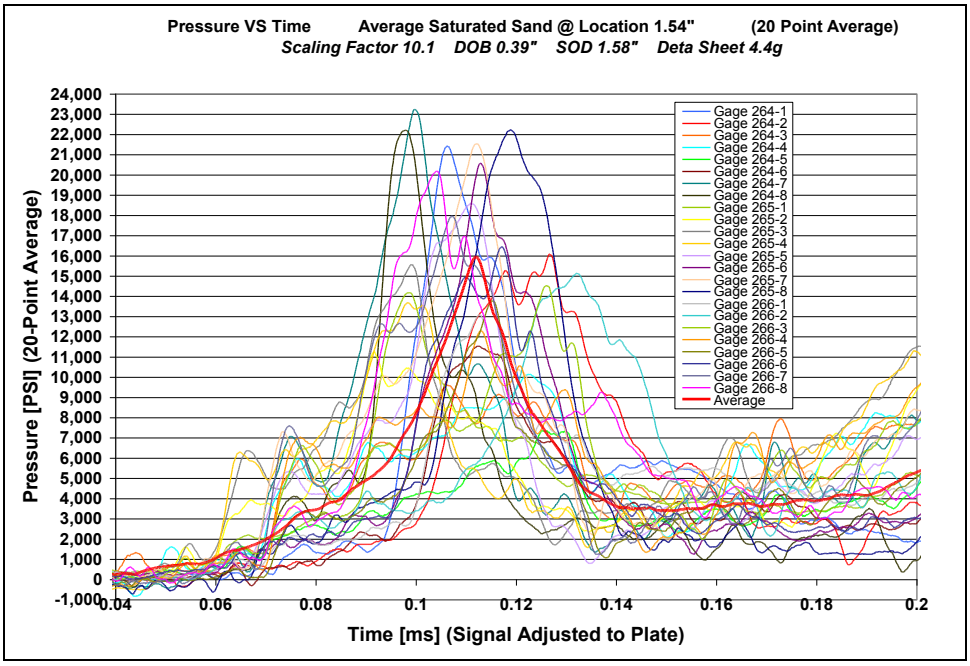

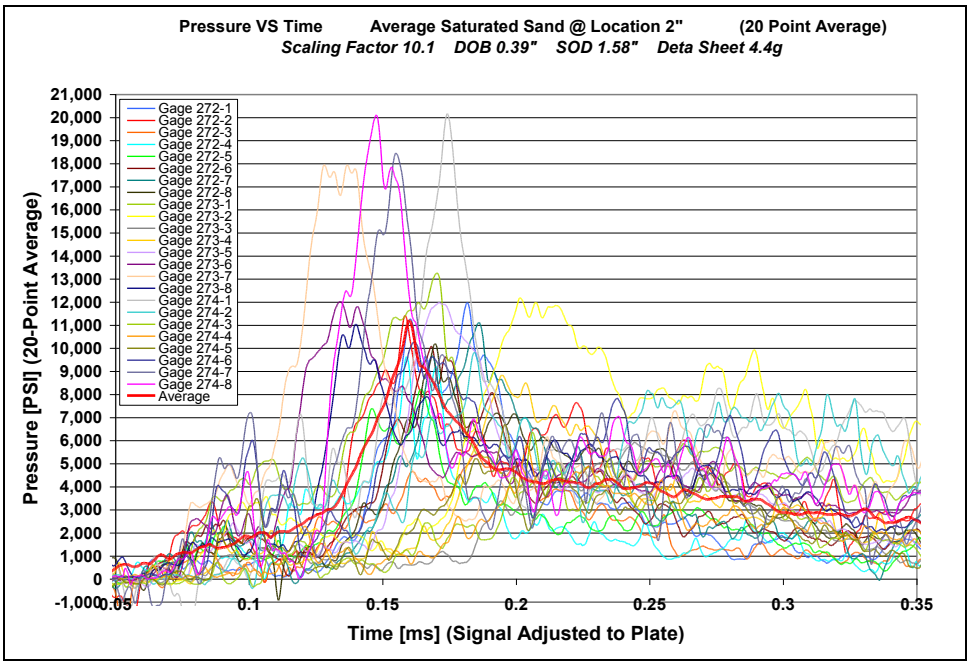

Figure 5.6 Peak pressure - time profiles not aligned at locations of 3.10 cm (1.22 inches), 3.91 cm (1.54 inches), and 5.08 cm (2 inches) including average pressure - time profiles

Figure 5.7 and **Figure 5.8** contain the pressure - time profiles not aligned at the locations of 6.35 cm (2.5 inches) and 7.62 cm (3 inches). These profiles can not be aligned since they do not show a distinctive peak pressure value. Therefore they have to be treated differently. The loading time lasts much longer and the peak pressure values are much lower than in the pressure - time profiles shown before. In these two cases the average pressure - time profiles shown in **Figure 5.**5 are calculated from the original not aligned measured pressure - time profiles.

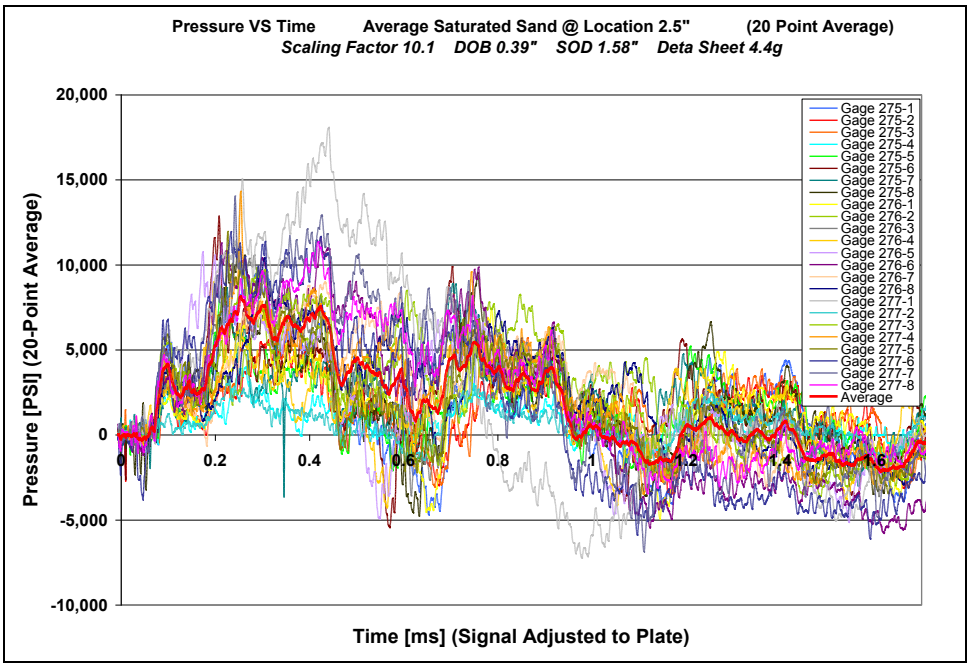

Figure 5.7 Peak pressure - time profiles not aligned at the location of 7,62 cm (3 inches) including average pressure – time profile

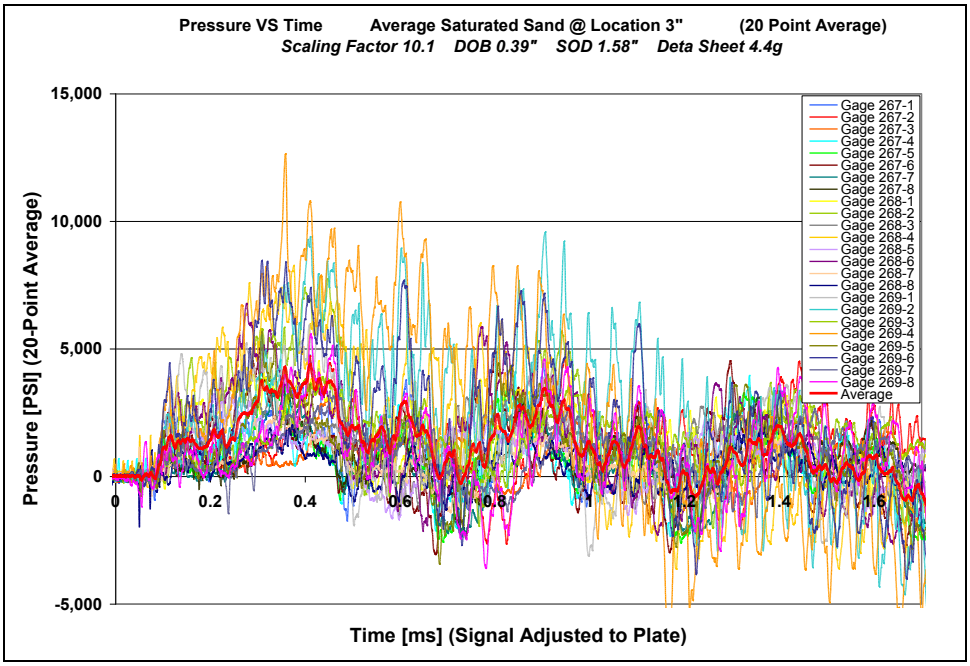

Figure 5.8 Peak pressure - time profiles not aligned at the location of 6.35 cm (2.5 inches) including average pressure – time profile

5.1.1 Average Pressure – Time Profiles at SOD 4 cm (1.58 inches) and DOB 1 cm (0.39 inches) in Saturated Sand

All of the 9 average pressure - time profiles are shown in **Figure 5.9**. This represents an average of all the usable data recorded. Other than averaging the data, no processing of the profiles has been involved yet. **Figure 5.10** shows the average peak pressure - time profiles at 0 cm (0 inches), 1.01 cm (0.4 inches), and 1.45 cm (0.57 inches) in more detail. All 3 profiles show an offset after the peak pressure was measured. The profiles do not intercept with the X-axis and keep a positive offset even though the pressure applied died off.

As in **Figure 5.11** can be seen in more detail, some of the pressure – time profiles have a precursor. This can be noticed very well in the pressure – time profile at 6.35 cm (2.5 inches) at the time of 0.1 milliseconds. This is caused by the shock waves generated in the plate reaching the bottom of the bars before the bars are impacted by the saturated sand.

All of the profiles have a positive offset after the peak pressure was measured. As shown in the previous chapter this offset is not related to any pressure applied which was proven comparing the images taken by a high speed camera.

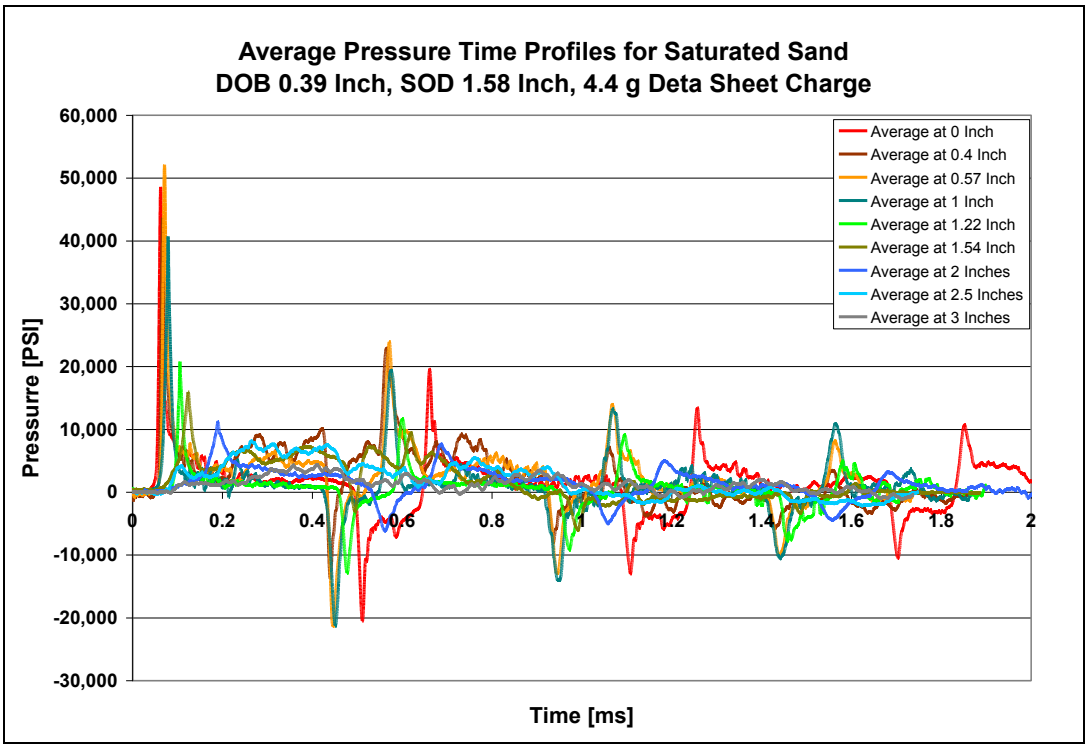

Figure 5.9 Average peak pressure - time profiles at all measured locations

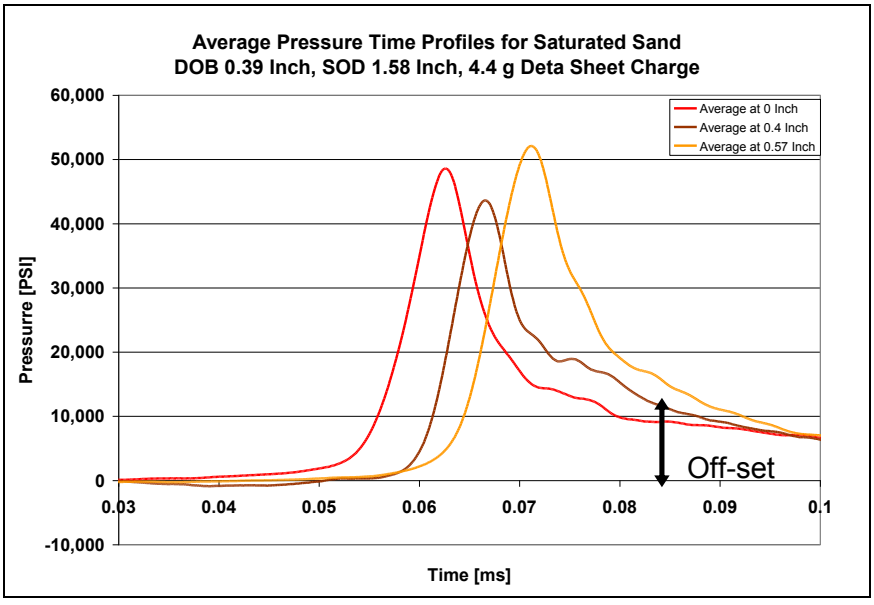

Figure 5.10 Detailed view of the average peak pressure - time profiles at 0 cm

(0 inches), 1.01 cm (0.4 inches), and 1.45 cm (0.57 inches)

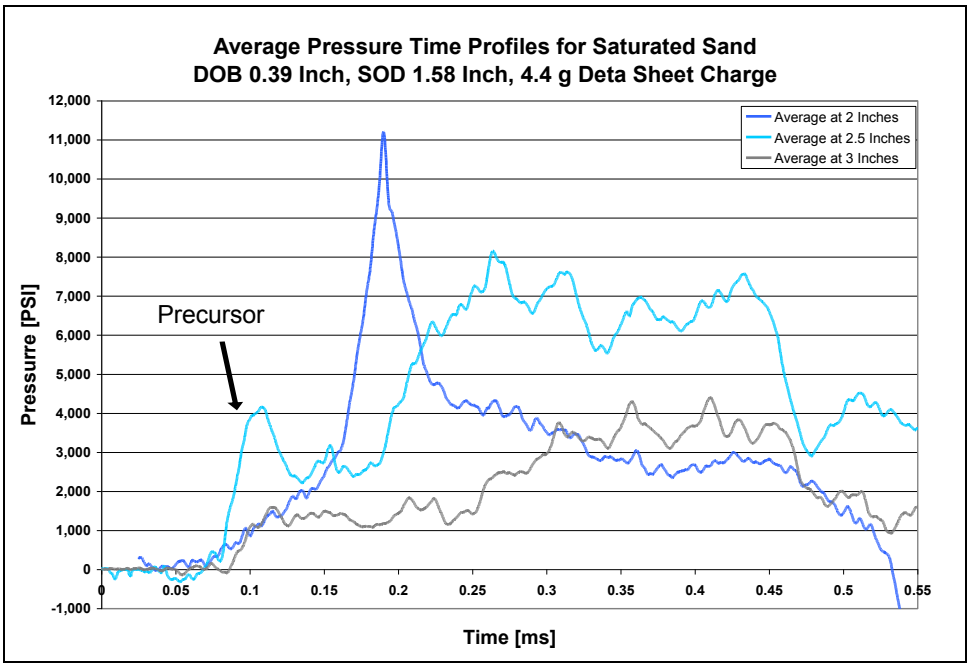

Figure 5.11 Detailed view of the average peak pressure - time profiles at 5.08 cm (2 inches), 6.35 cm (2.5 inches), and 7.62 cm (3 inches)

5.1.2 Processed Average Pressure – Time Profiles at SOD 4 cm (1.58 inches) and DOB 1 cm (0.39 inches) in Saturated Sand

All the average pressure – time profiles calculated have to be individually processed for validation. As an example the processing of 2 very different average pressure – time profiles at the location of 1.01 cm (0.4 inches) and 6.35 cm (2.5 inches) is shown in the following. **Figure 5.12** shows the peak pressure – time profile at the location of 1.01 cm (0.4 inches) in detail. In order to correct the positive offset between 0.04 and 0.05 milliseconds (blue arrow) the profile has to be shifted down in the order of 3.5 mega Pascal (500 PSI). The blue curve shows the original and the red one the shifted profile in **Figure 5.12**.

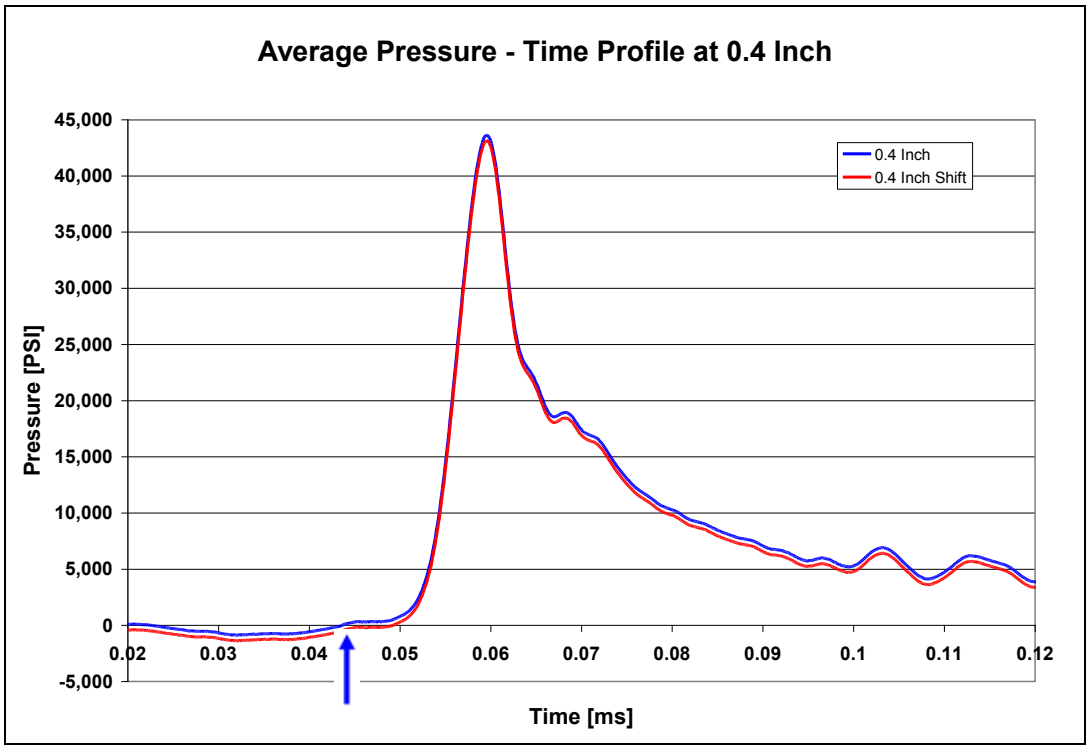

Figure 5.12 Detailed average peak pressure – time profile at the location of 1.01 cm (0.4 inches)

The average pressure – time profiles at locations further away from the center of the target plate have a precursor that generates an even larger offset. The high speed camera reveals that the loading has not yet reached the Kolsky bar even though the pressure – time recording shows already a positive peak. **Figure 5.13** shows a typical pressure – time profile at the location of 6.35 cm (2.5 inches). The high speed camera shows the beginning of the loading at 0.18 milliseconds. The precursor generated an offset of the average pressure – time profile of 18.6 mega Pascal (2,700 PSI). The blue curve in **Figure 5.13** represents the average pressure – time profile calculated and the red one the shifted profile. As described in chapter 2.12 the offset is caused by stress waves travelling very fast in the plate caused by the first impact at the center of the plate. Part of these stress waves are transmitted through the rubber seal between the Kolsky bar and the plate before any impact at the bottom of the bar is recorded.

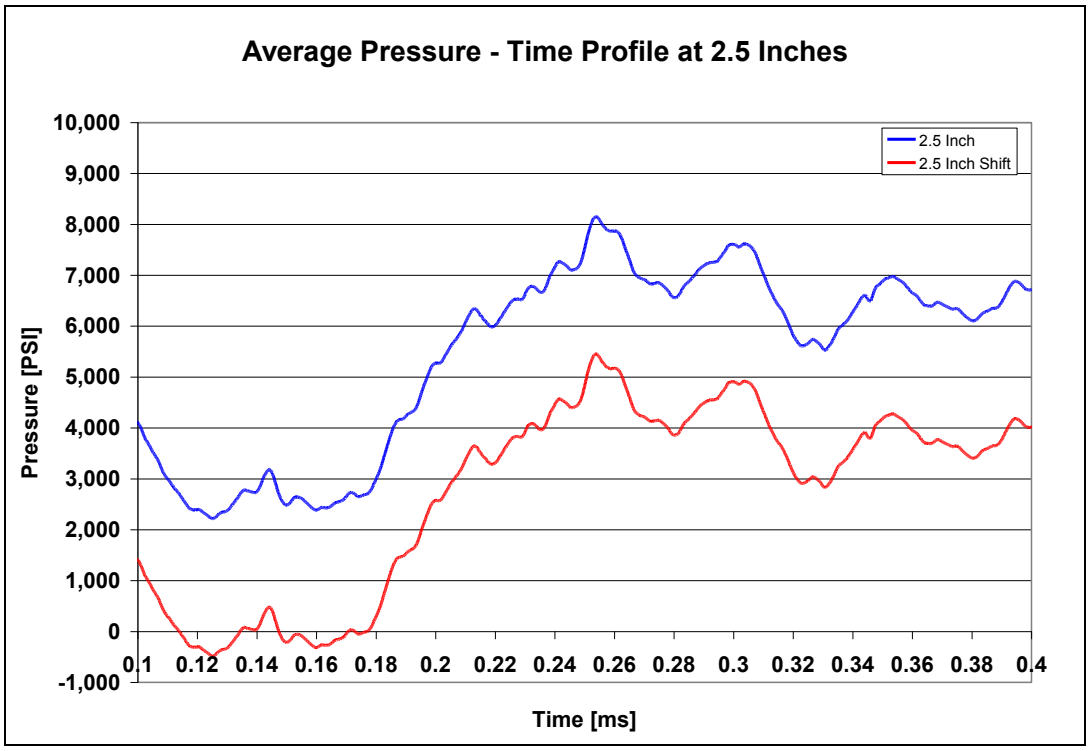

Figure 5.13 Detailed average peak pressure – time profile at the location of 6.35 cm (2.5 inches)

In order to calculate the pressure originally applied at the bottom of the Kolsky bar the logarithmic decrement has to be calculated as described in **section 4.3**. This processing has to be applied to each averaged pressure – time profile. **Figure 5.15** shows the logarithmic decrement calculated by using the 4 positive peak pressure values shown in **Figure 5.14** (note the arrows). The 3 red arrows in **Figure 5.14** show the reflected peak pressure values and the green arrow the original measured one. The Delta used for the calculation of the logarithmic decrement at this particular location has the value of 0.051 (compare **Figure 5.15**).

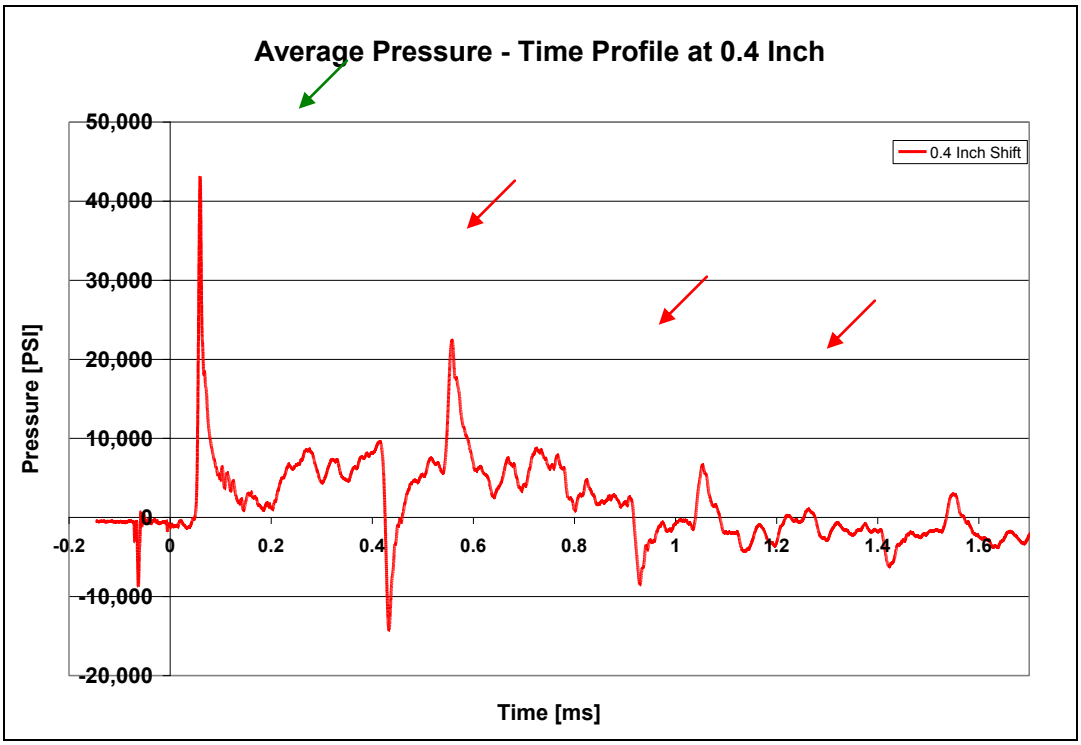

Figure 5.14 Average pressure – time profile at the location of 1.01 cm (0.4 inches)

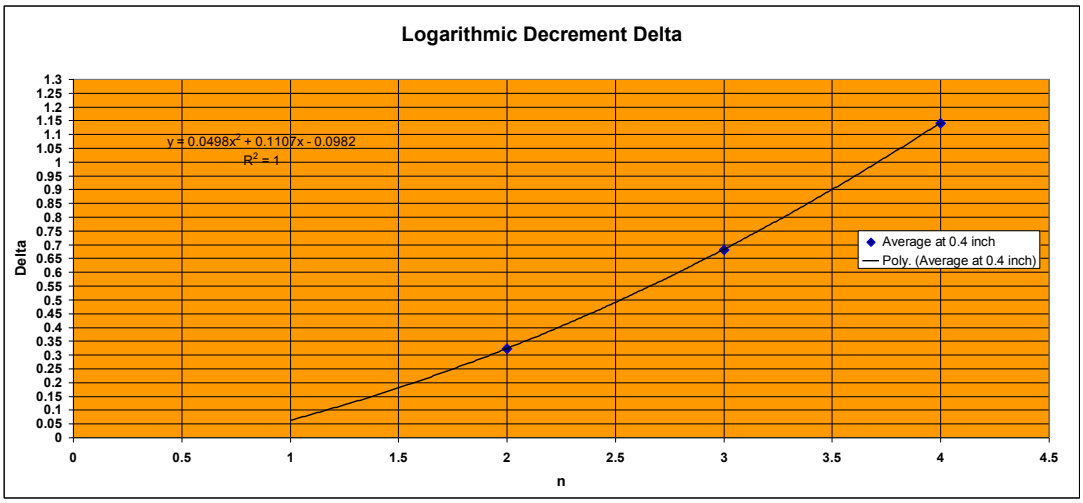

Figure 5.15 Logarithmic decrement at the location of 1.01 cm (0.4 inches)

In the second example at the location of 6.35 cm (2.5 inches) there are only 3 pressure values which are usable for calculating the logarithmic decrement. It is important to choose the values within equal spaced time intervals since the pressure – time recording does not show well expressed peak pressures any more, see **Figure 5.16**. The Delta used for the calculation of the logarithmic decrement at this particular location has the value of 0.05 (compare **Figure 5.17**).

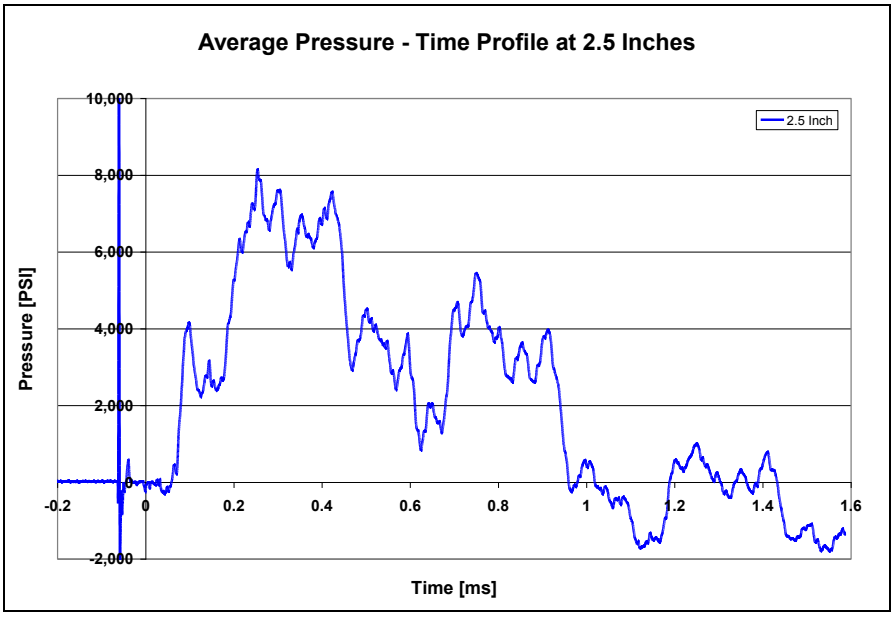

Figure 5.16 Average pressure – time profile at the location of 6.35 cm (2.5 inches)

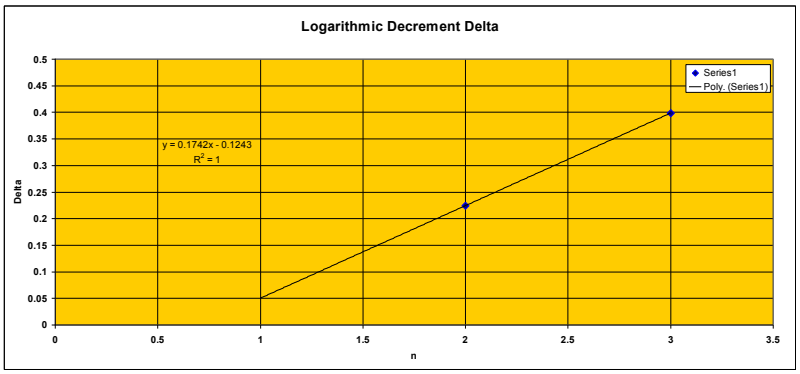

Figure 5.17 Logarithmic decrement at the location of 6.35 cm (2.5 inches)

Figure 5.18 shows the calculated pressure – time profile at the bottom of the Kolsky bar for the first example at the location of 1.01 cm (0.4 inches). The dark green curve shows the calculated and the light green one the shifted profile in **Figure 5.18**. Again the profile has to be shifted down on the order of 3.5 mega Pascal (500 PSI) as described earlier in order to compensate the offset between 0.04 and 0.05 milliseconds.

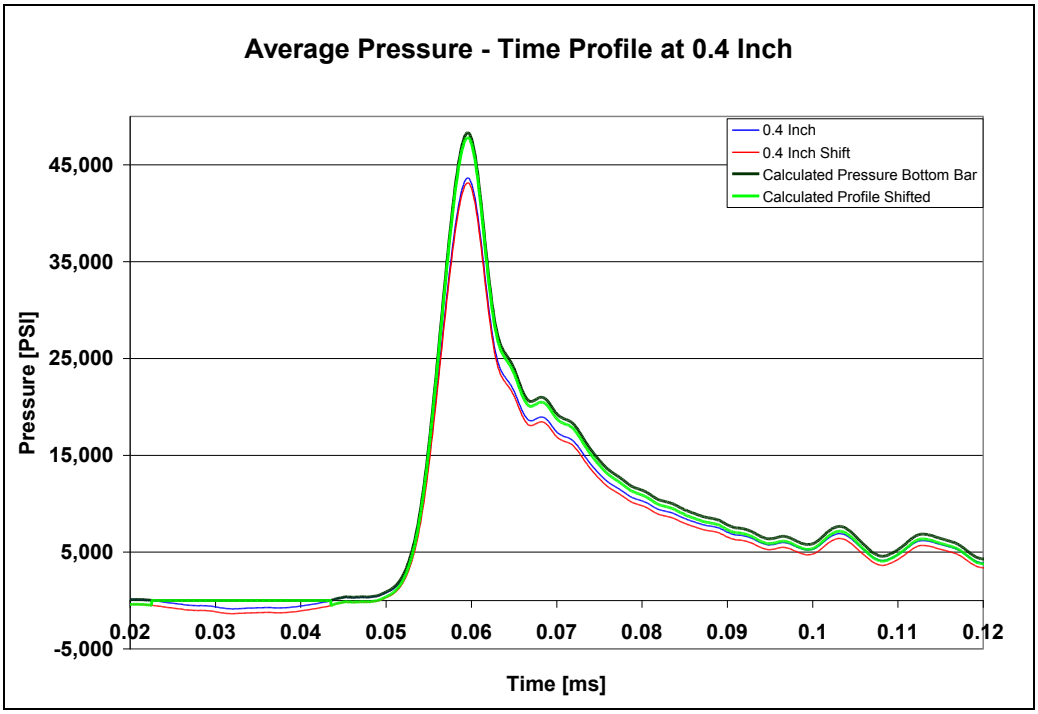

Figure 5.18 Average and calculated pressure – time profile at the location of 1.01 cm (0.4 inches)

Figure 5.19 shows the calculated pressure – time profile at the bottom of the Kolsky bar for the second example at the location of 6.35 cm (2.5 inches). The dark green curve shows the calculated and the light green one the shifted profile in **Figure 5.19**. Again the calculated profile (dark green curve) has to be shifted down in the order of 18.6 mega Pascal (2,700 PSI) to correct the offset between 0.12 and 0.18 milliseconds as described earlier.

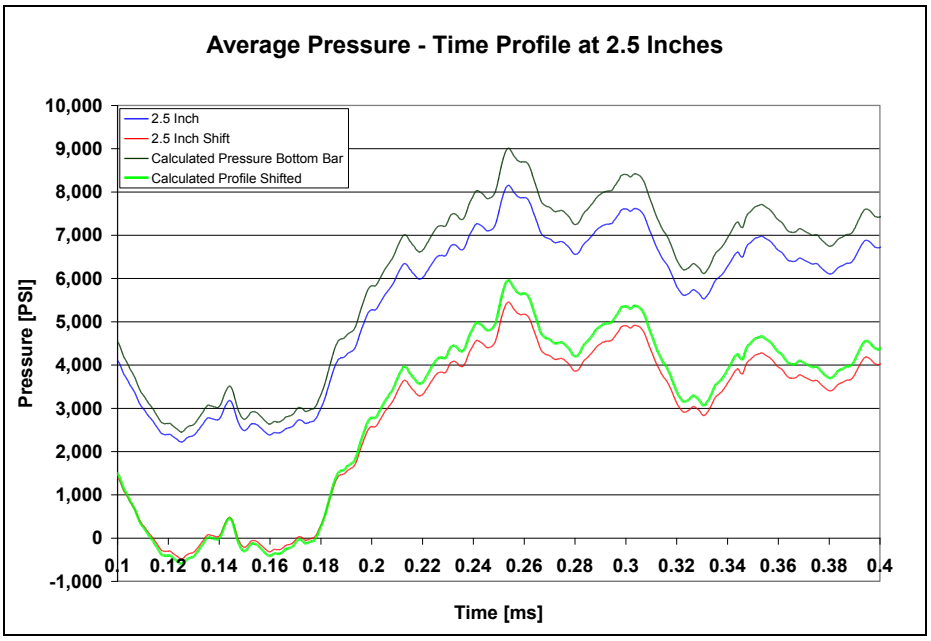

Figure 5.19 Average and calculated pressure – time profile at the location of 6.35 cm (2.5 inches)

The next step is to compensate for the drift, caused by the off-set, which appears in all of the signals. There exists always a positive offset after the peak pressure was recorded. The shifted calculated signal has to be drift compensated. Looking at the first example at the location of 1.01 cm (0.4 inches) the time of loading for the Kolsky bar appears to be around 22 microseconds. **Figure 5.20** shows the calculated and the drift compensated pressure – time profile. The drift compensation is done in such a manner that the profile is brought back to a pressure of 0 after reaching 22 microseconds of recording time. The compensation is done under the assumption the offset is linearly applied. Small decrements depending on the number of points measured in the pressure – time profile are subtracted from the original data so that the recording interval of 22 microseconds is validated.

For the second example at the location of 6.35 cm (2.5 inches) the time of loading for the Kolsky bar appears to be around 145 microseconds. **Figure 5.21** shows the calculated and the drift compensated pressure – time profile for the second

example. The procedure for compensation of all the calculated pressure – time profiles is done as described earlier.

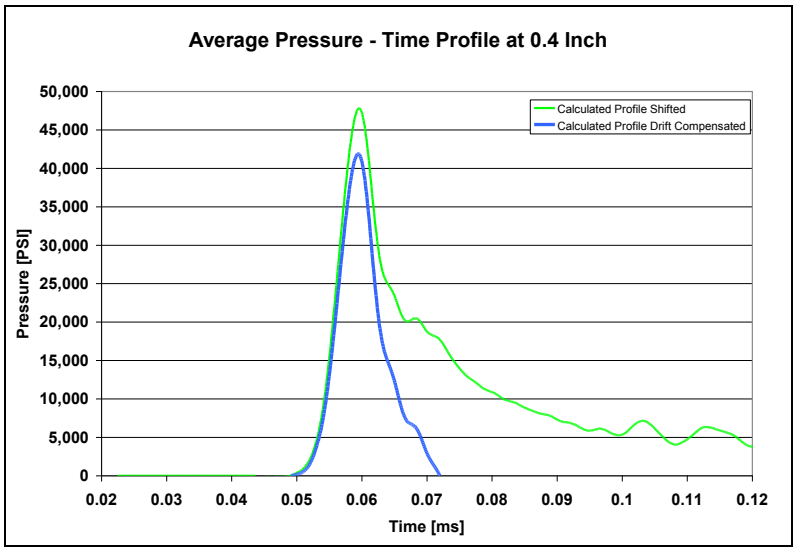

Figure 5.20 Calculated and drift compensated pressure – time profile at the location of 1.01 cm (0.4 inches)

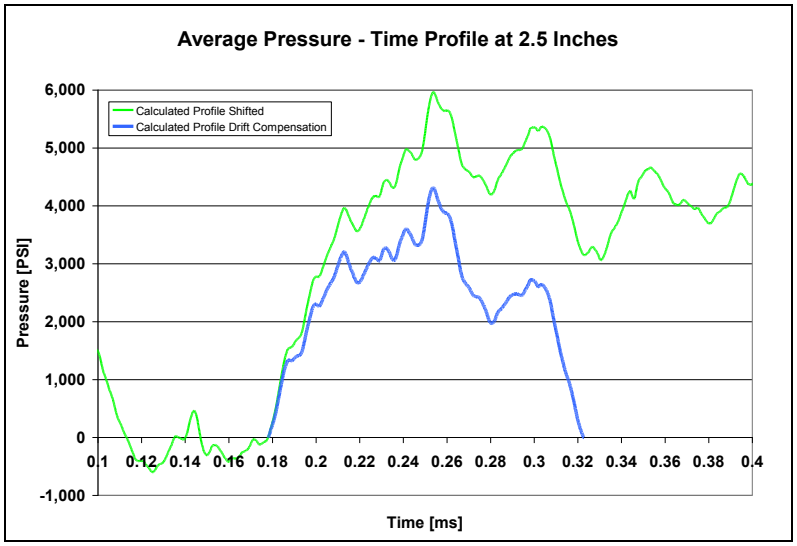

Figure 5.21 Calculated and drift compensated pressure – time profile at the location of 6.35 cm (2.5 inches)

Figure 5.22 contains all the processed pressure – time profiles which will be used for calculating the specific impulse at the specific locations of the plate. The figure shows the correct loading time intervals and the starting times of the loading for the saturated sand case using a plate at a SOD 4 cm (1.58 inches) and DOB 1 cm (0.39 inches) using a 4.4 g explosive charge. The pressure – time profiles of the locations of 0 cm (0 inches), 1.01 cm (0.4 inches), and 1.45 cm (0.57 inches) (**Figure 5.23**) show the same characteristic curve progression and almost the identical loading time interval. From then on at the locations further away from the center of the plate the loading times increase and the peak pressures drop very fast. **Table 5.2** contains the details about loading times, intervals, and peak pressure shifts for each processed average pressure –time profile.

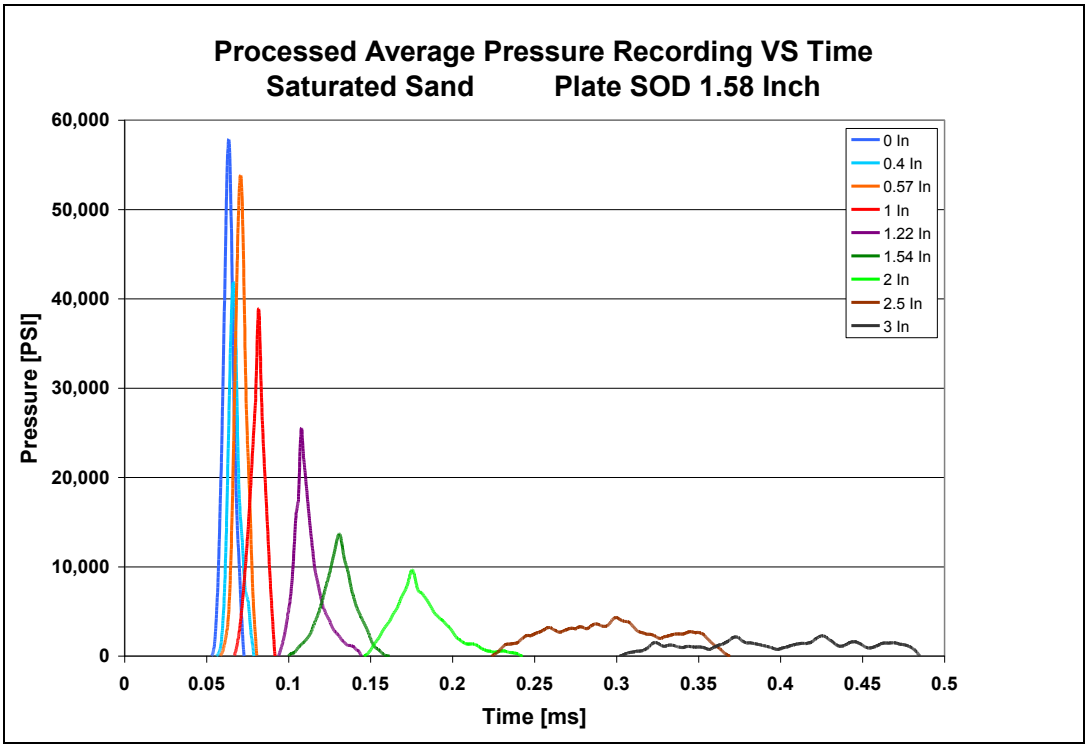

Figure 5.22 Processed pressure – time profiles at all locations

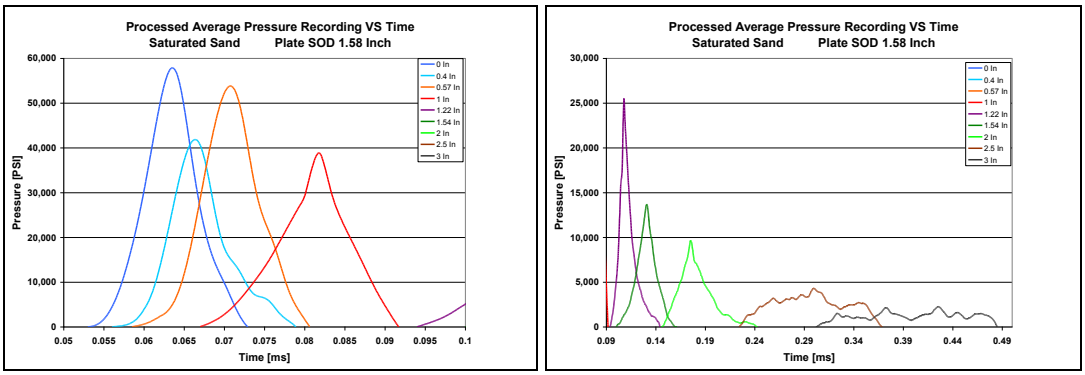

Figure 5.23 Details of the processed pressure – time profiles at all locations

Location	Loading Duration	Start Time	End Time	Pressure Off-set Correction	Peak Pressure
[in]	[µs]	[ms]	[ms]	[PSI]	[PSI]
0	20	0.053	0.073	4,000	57,875
0.4	22	0.056	0.078	500	41,868
0.57	22	0.058	0.080	2,000	53,827
1	25	0.067	0.092	4,800	38,880
1.22	50	0.094	0.144	2,800	25,536
1.54	61	0.1	0.161	3,930	13,699
2	96	0.146	0.242	3,700	9,650
2.5	145	0.224	0.369	2,700	4,315
3	183	0.302	0.485	2,900	2,265

Table 5.2 Loading time results for saturated sand at SOD 4 cm (1.58 inches) and DOB 1 cm (0.39 inches)

Figure 5.24 shows the peak pressure and the loading time interval distribution versus the location at the bottom of the target plate. The loading time interval stays

almost constant until it reaches the location of 2.54 cm (1 inch). After that it increases steadily with an almost constant slope. The peak pressure values decline fast and are lowest in the combination with the longest loading time interval.

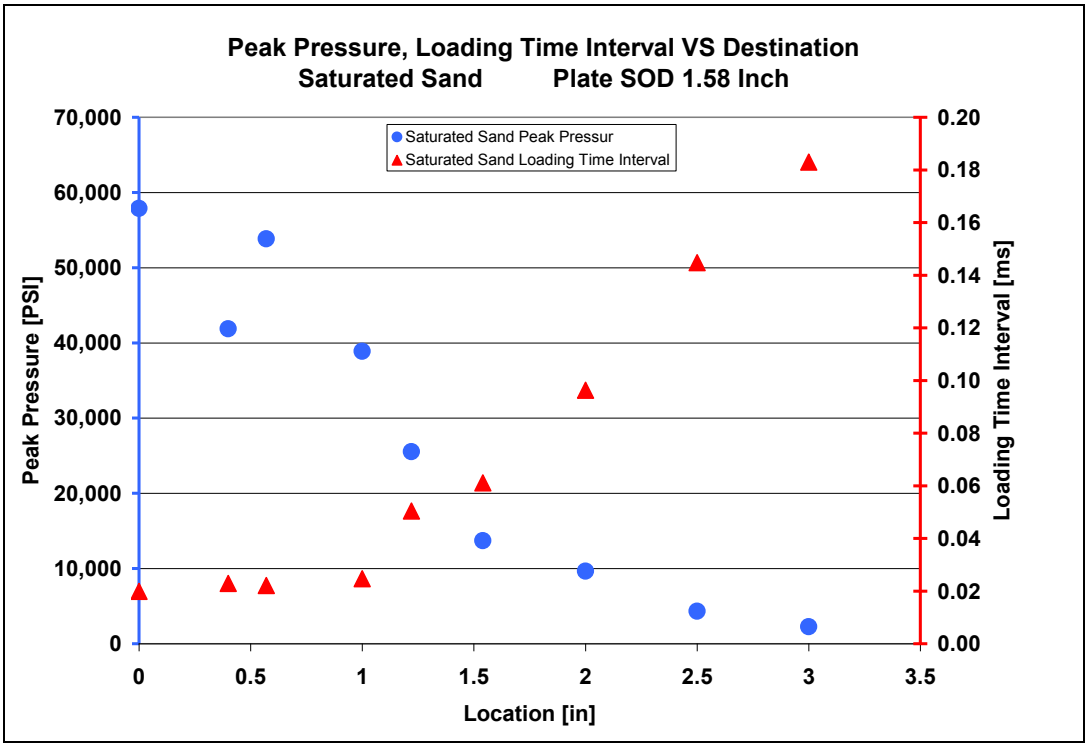

Figure 5.24 Peak pressure and loading time interval versus location

5.1.3 Specific Impulse Calculation at SOD 4 cm (1.58 inches) and DOB 1 cm (0.39 inches) in Saturated Sand

The impulse is defined as the integral of a force over time (**Equation 3.1**).

$$I = \int_{t_1}^{t_2} F dt$$

Equation 5.1 Impulse

Using a pressure – time profile for the calculation the force in **Equation 5.1** is replaced by pressure applied on the area at the bottom of the Kolsky bar (**Equation5.2**).

$$P = \frac{F}{A}$$

Equation 5.2 Pressure

In order to calculate the specific impulse of the average pressure – time profiles **Equation 5.3** is used where the time t_1 equals the beginning and t_2 the end of the loading interval.

$$\frac{I}{A} = \int_{t_1}^{t_2} P dt$$

Equation 5.3 Specific impulse

Using the calculated average pressure – time profiles shown in **Figure 5.22** the specific impulse at each location is calculated. Using **Equation 5.3** for each single profile generates the specific impulse shown in **Figure 5.25**. Keeping in mind that the pressure values are very low further away from the center of the plate, the specific impulse drops not as much as expected since the loading time intervals increase over distance. **Table 5.3** contains all results of the specific impulse calculation

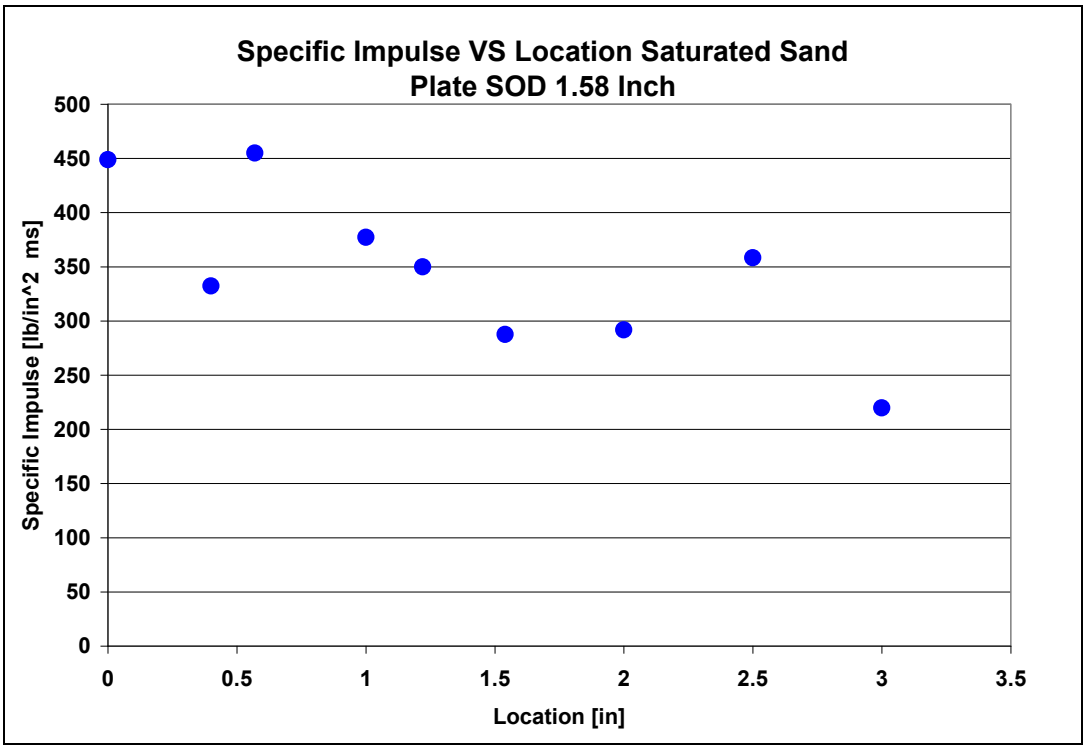

Figure 5.25 Specific impulse versus location

Specific Impulse [(lb / in^2) * ms]	Specific Impulse [(lb / in^2) * s]	Distance [in]
448.78	0.45	0.00
332.32	0.33	0.40
454.87	0.45	0.57
377.21	0.38	1.00
349.99	0.35	1.22
287.51	0.29	1.54
291.69	0.29	2.00
358.35	0.36	2.50
219.84	0.22	3.00

Table 5.3 Specific Impulse results for saturated sand at SOD 4 cm (1.58 inches) and DOB 1 cm (0.39 inches)

5.1.4 Total Impulse Calculation at SOD 4 cm (1.58 inches) and DOB 1 cm (0.39 inches) in Saturated Sand

Using the specific impulse the total impulse can be calculated using the following method. A trend line containing the specific impulse values has to be established see **Figure 5.26**. The total impulse is than defined as the volume of a solid obtained by rotating the given trend line around the Z – axis. **Figure 5.27** shows a three dimensional plot of the rotated trend line. The X - axis and the Y – axis in the plot represent the radius in inches and the Z – axis the specific impulse in lb ms/in^2.

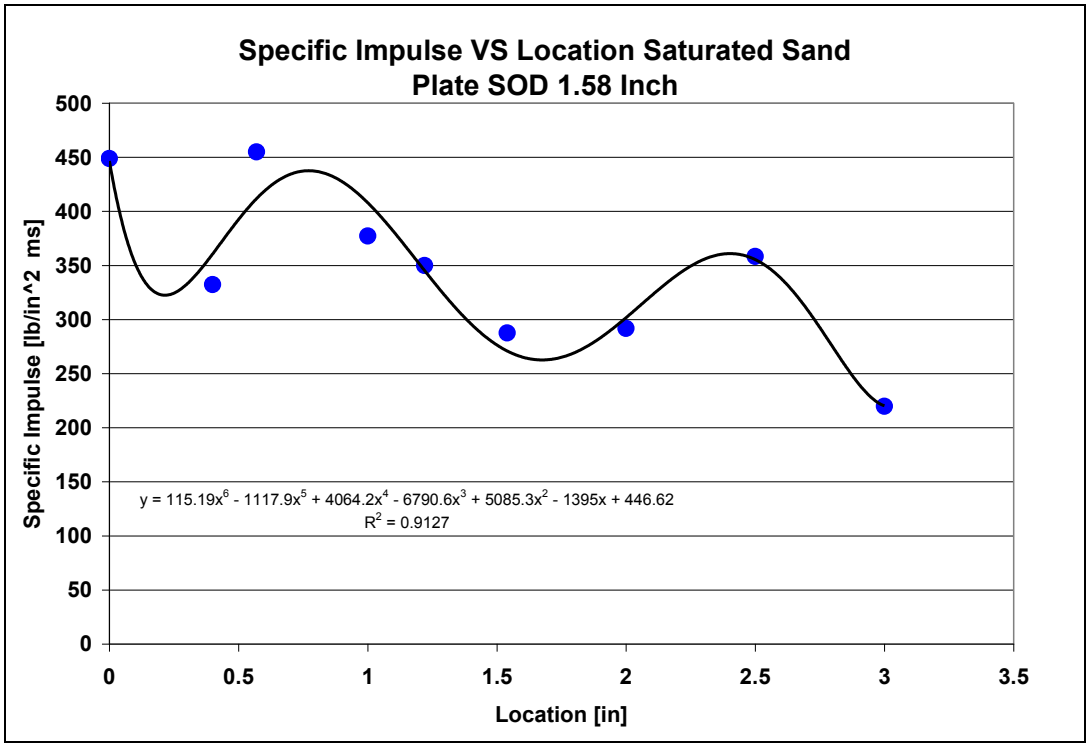

Figure 5.26 Specific impulse versus location including trend line

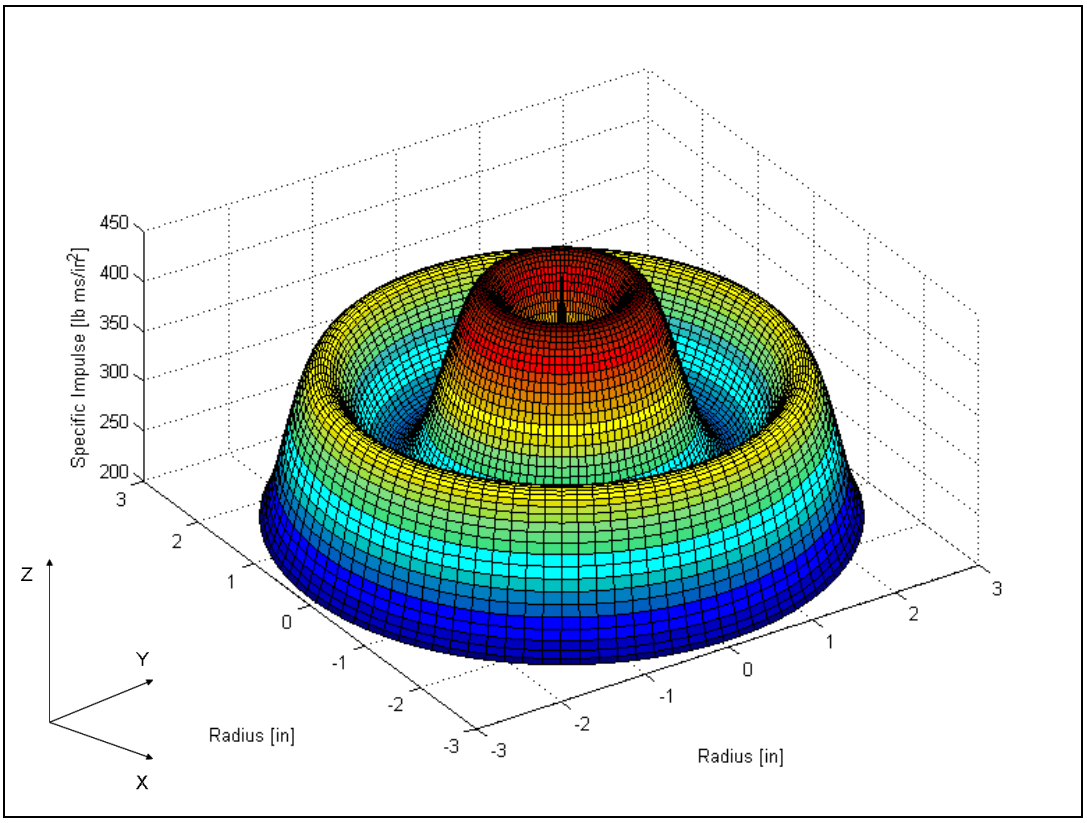

Figure 5.27 Solid obtained by rotating the given trend line

If the cross sections of the solid are taken parallel to the axis of revolution (Y-axis), then the cylindrical shell method **(13)**, **(14)** is used in order to calculate the volume of the solid, see **Figure 5.28**. Let the cylindrical shell have the radius x and the height y (f(x)), then its volume would be 2πxy times its thickness dx. 2πxy would be the area of the rectangle (red rectangle in **Figure 5.28**) formed by cutting the shell perpendicular to its radius and laying it out flat. In 3 dimensional space that rectangle forms a cylinder or shell. Integration, as an accumulative process, calculates then the volume of a family of shells. In this case the axis of revolution is the Y-axis. The variable y is represented by the function f(x) in the diagram (**Figure 5.28**). The variable x is the actual distance from the origin of the shell and dx is its thickness. The shell integration can be considered as a special case of evaluating a double integral and can be written as **Equation 5.4**.

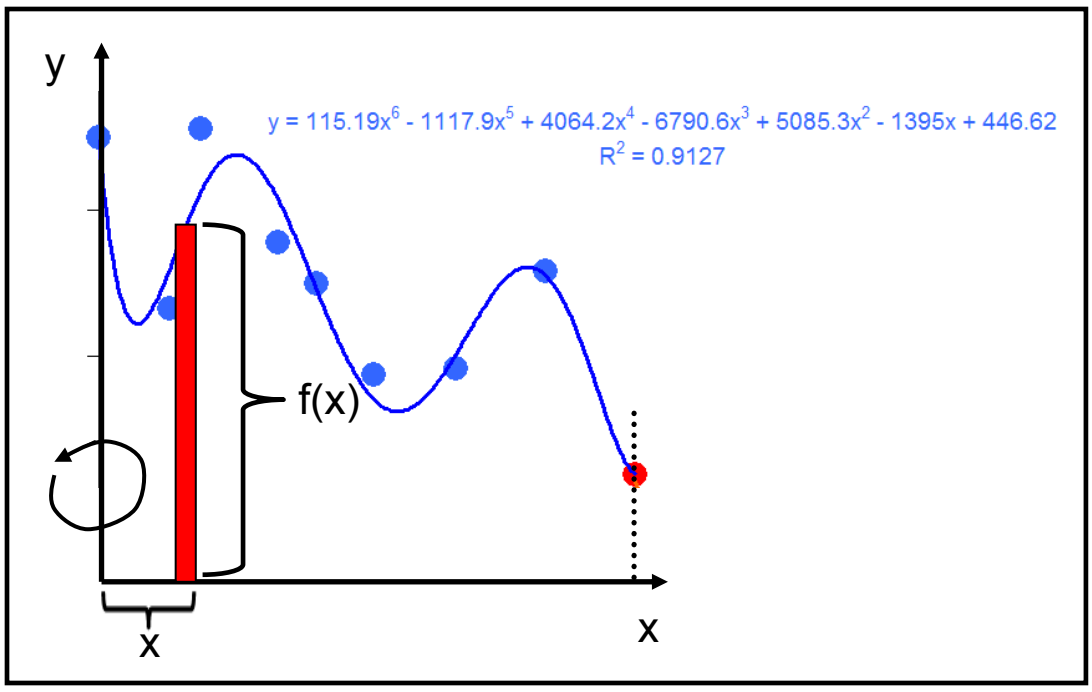

Figure 5.28 Diagram for shell method

Equation 5.4 is then used in order to calculate the total impulse according to its definition.

$$I_{Total} = V = 2\pi \int_{x_1}^{x_2} x * f(x)dx$$

Equation 5.4 Total impulse

Equation 5.5 is the equation of the trend line in **Figure 5.26** and being used for the integration.

$$f(x) = y = 115.19x^6 - 1117.9x^5 + 4064.2x^4 - 6790.6x^3 + 5085.3x^2 - 1395x + 446.62$$

Equation 5.5 Trend line for specific impulse values

The multiplication of the trend line function f(x) with x as per definition from **Equation 5.4** results in **Equation 5.6**.

$$x * \hat{}(x) = 15.19x^7 - 117.9x^6 + 1064.2x^5 - 5790.6x^4 + 5085.3x^3 - 1395x^2 + 146.62x$$

Equation 5.6 Equation used for integration

The integration of **Equation 5.6** using the limits $x_1 = 0$ and $x_2 = 3$ as interval is shown in **Equation 5.7**.

$$\int_{x_1=0}^{x_2=3} x * f(x) = \frac{15.19}{8}x^8 - \frac{117.9}{7}x^7 + \frac{1064.2}{6}x^6 - \frac{5790.6}{5}x^5 + \frac{5085.3}{4}x^4 - \frac{1395}{3}x^3 + \frac{146.62}{2}x^2 \Bigg|_0^3$$

Equation 5.7 Integral

Solving the integral and revolving it around the Z – axis results in the total impulse of 8.89 lbs (40 Ns) see **Equation 5.8**. This is the impulse a target plate of a diameter of 14.24 cm (6 inches) would absorb being exposed to the described test setup.

$$2\pi \int_{x_1=0}^{x_2=3} x * \hat{}(x) = 8.89[lbs]$$

Equation 5.8 Total Impulse

Using a second approach, impulse segments over the radius of the plate can be calculated using the same method. Instead of a trend line, a straight line connecting the specific impulse values has to be established see **Figure 5.29**. The total impulse is in this case defined as the accumulation of plate diameters obtained by revolving the given segments around the Z – axis. **Figure 5.30** shows a three dimensional plot of the revolved segments. The X - axis and the Y – axis in the plot represent the

radius in inches and the Z – axis the specific impulse in lb ms/in^2. This method results in obtaining total impulse values for target plates of smaller diameters.

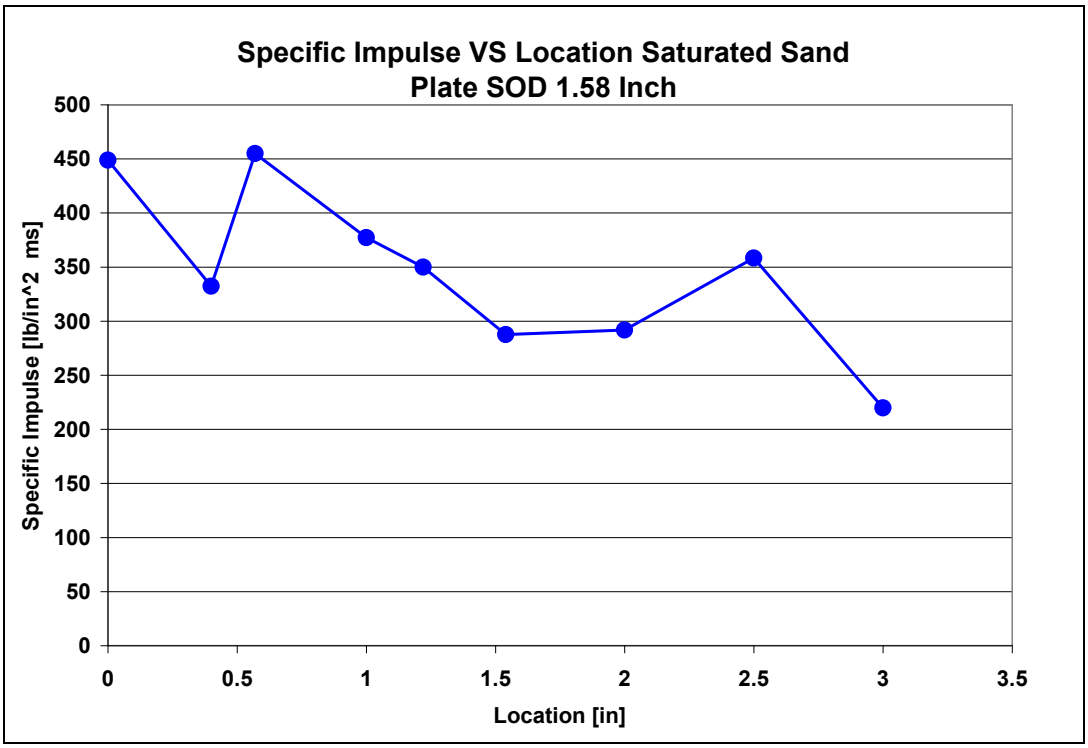

Figure 5.29 Specific impulse versus location

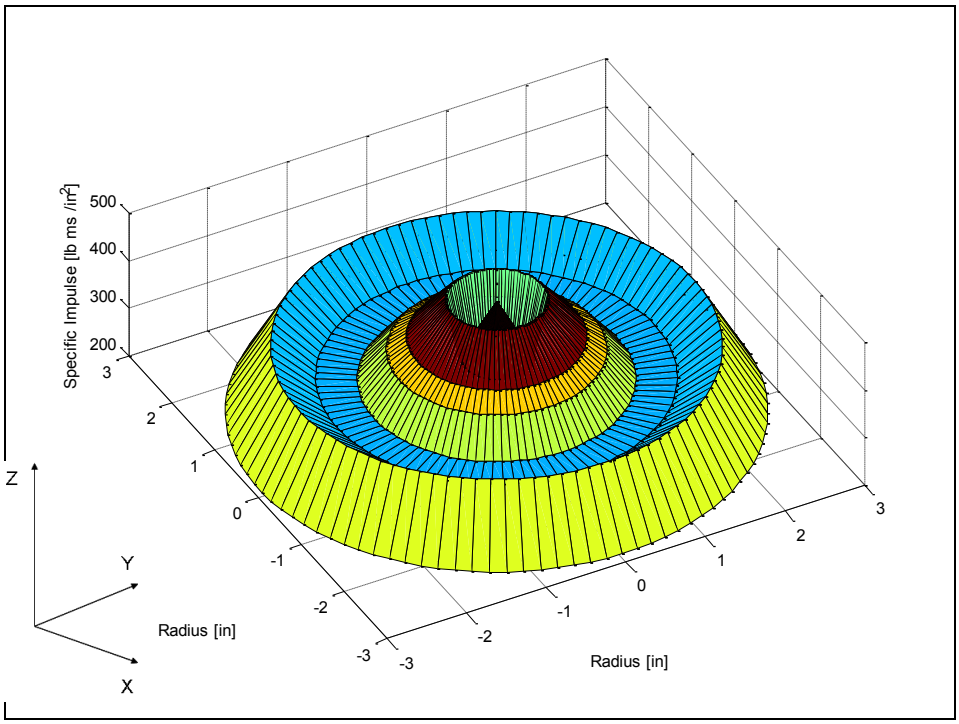

Figure 5.30 Solid obtained by rotating the given segments

Like described before, **Equation 5.4** is used in order to calculate the impulse in this case for certain segments according to the definition. In the following it will be demonstrated for the first segment from 0 to 1.02 cm (0.4 inches).

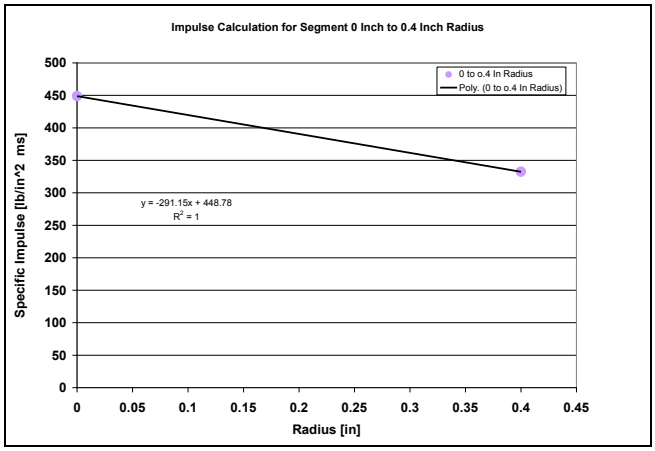

Figure 5.31 Specific impulse versus location of the first segment

Equation 5.9 is the equation of the trend line in **Figure 5.31** and is used for the integration.

$$f(x) = y = \text{?}91.15x + \text{¦}48.78$$

Equation 5.9 Trend line for specific impulse values

The multiplication of the trend line function f(x) with x as per definition from **Equation 5.4** results in **Equation 5.10**.

$$x * \text{ˆ}(x) = \text{?}91.15x^2 + \text{¦}48.78x$$

Equation 5.10 Equation used for integration

The integration of **Equation 5.10** using the limits $x_1 = 0$ and $x_2 = 0.4$ as interval is shown in **Equation 5.11**.

$$\int_{x_1=0}^{x_2=3} x * f(x) = \frac{291.15}{3}x^3 + \frac{448.78}{2}x^2$$

Equation 5.11 Integral for segment

Solving the integral and revolving it around the Z – axis results in the total impulse of 0.19 lbs (0.85 Ns) see **Equation 5.12**. This is the impulse a target plate of a diameter of 2.03 cm (0.8 inches) would absorb being exposed to the described test setup.

$$2\pi \int_{x_1=}^{x_2=} x * \text{ˆ}(x) = .19[lbs]$$

Equation 5.12 Total Impulse

Table 5.4 contains the results for calculating the impulse for each segment. The accumulated impulse for the diameter of 14.24 cm (6 inches) is 8.97 lbs (39.9 Ns) which is very close to the total impulse of 8.89 lbs (40 Ns) calculated using the trend line in **Figure 5.22**. All the impulse results are shown in **Figure 5.32**. It indicates how the impulse increases using larger size target plates.

Impulse Per Segment [lb s]	Total Impulse Accumulated [lb s]	Diameter [in]
0.19	0.19	0.8
0.21	0.39	1.14
0.87	1.27	2
0.56	1.82	2.44
0.88	2.71	3.08
1.48	4.19	4
2.31	6.49	5
2.48	8.97	6

Table 5.4 Impulse results for saturated sand at SOD 4 cm (1.58 inches) and DOB 1 cm (0.39 inches) for single segments and accumulated over diameter

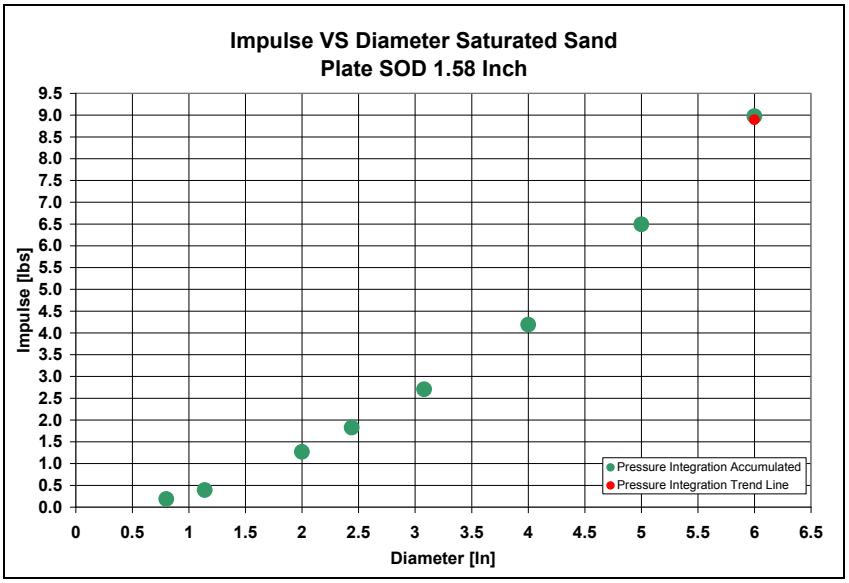

Figure 5.32 Impulse versus diameter of target plates based on the integration of the processed pressure – time profiles

5.1.5 Impulse Measurement at SOD 4 cm (1.58 inches) and DOB 1 cm (0.39 inches) in Saturated Sand

A test series using a variety of plates of different diameters (**Figure 5.33**) keeping the weight constant (10.3 kg) was conducted in the Dynamic Effects Laboratory. The test setup was the same as being used for the pressure measurement series. The weight of 10.3 kg was chosen according to a test series conducted before in order to determine the maximum impulse delivered to a target plate. Obviously if a target plate is too heavy it will not move upon impact of the saturated sand being ejected from the crater. If it is too light it will move with respect to the ejecta coming up later in time and therefore not absorb the maximum impulse. **Figure 5.34** contains some of the test results of the impulse versus plate mass / explosive mass ratio. The measured impulse being indicated in **Figure 5.34** suggests that the plate mass / explosive mass ratio has to be in the vicinity of 2300 in order to absorb the maximum impulse. Increasing or decreasing the ratio lowers the impulse values.

The round plates used for the impulse testing were suspended above the test bed using a wire rope and 4 hooks mounted on the top of the plates, see **Figure 5.35**. Several diameters were used in order to determine the impulse distribution over the diameter of a plate. By increasing the diameter, eventually a plate size is achieved in which the maximum impulse is delivered. The diameters used were 5.08 cm (2 inches), 10.16 cm (4 inches), 15.24 cm (6 inches), 20.32 cm (8 inches), 25.4 cm (10 inches), 36.32 cm (14.3 inches), and 48.26 cm (19 inches). The plates of the diameter of 5.08 cm (2 inches) and 10.16 cm (4 inches) were made of steel and the others made of aluminum. The initial velocity of the plate was measured using 2.54 cm (1 inch) of travel distance of the plates. In case of the plate of the diameter of 5.08 cm (2 inches) the travel distance was less since the small area of impact did not displace the plate that far.

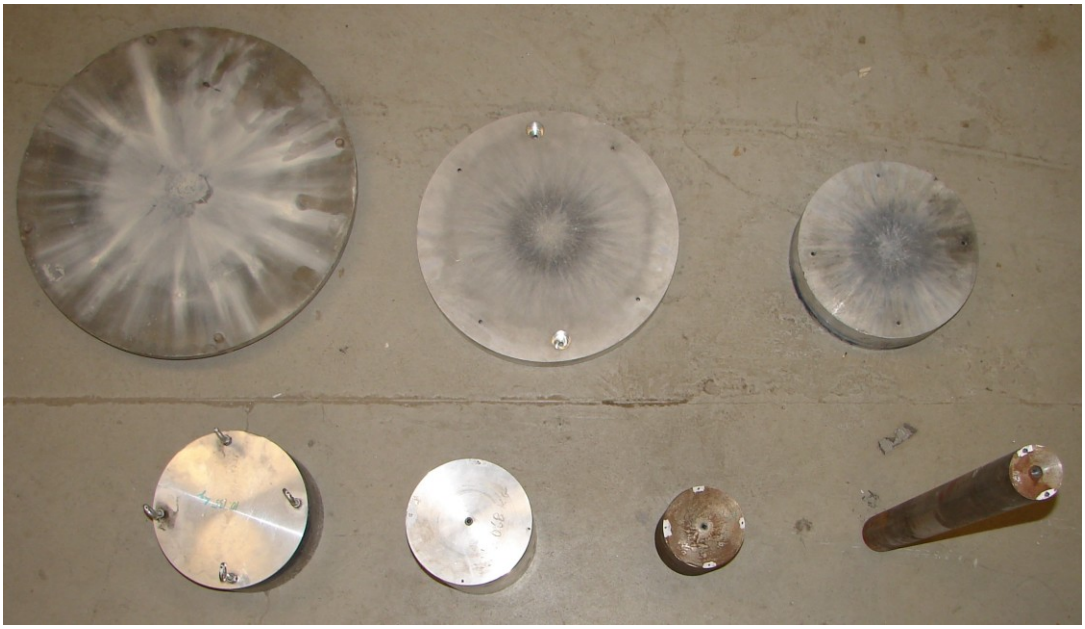

Figure 5.33 Round plates of different diameters and constant weight

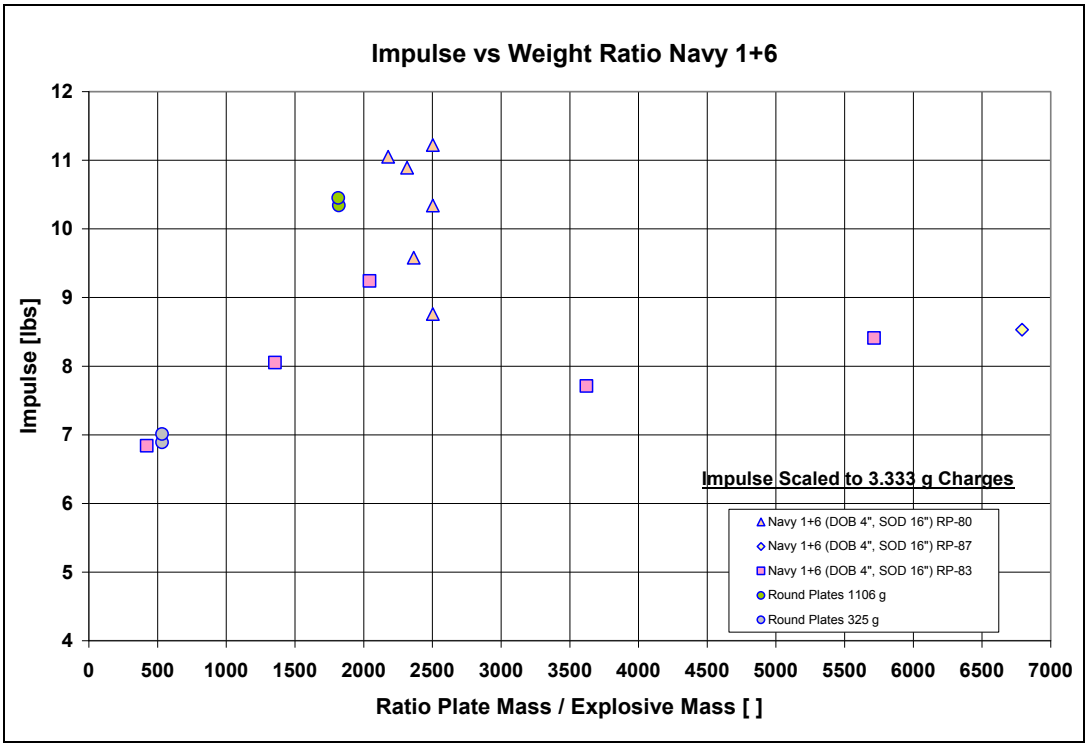

Figure 5.34 Plate mass / explosive mass ratios

Figure 5.35 20.32 cm (8 inches) diameter round plate test setup

The test results are shown in **Figure 5.36**. The impulse increases steadily until the maximum is reached at a plate diameter of 25.4 cm (10 inches). The largest plate (diameter 48.26 cm (19 inches)) shows a decreasing impulse value. At this time we do not know why this occurs.

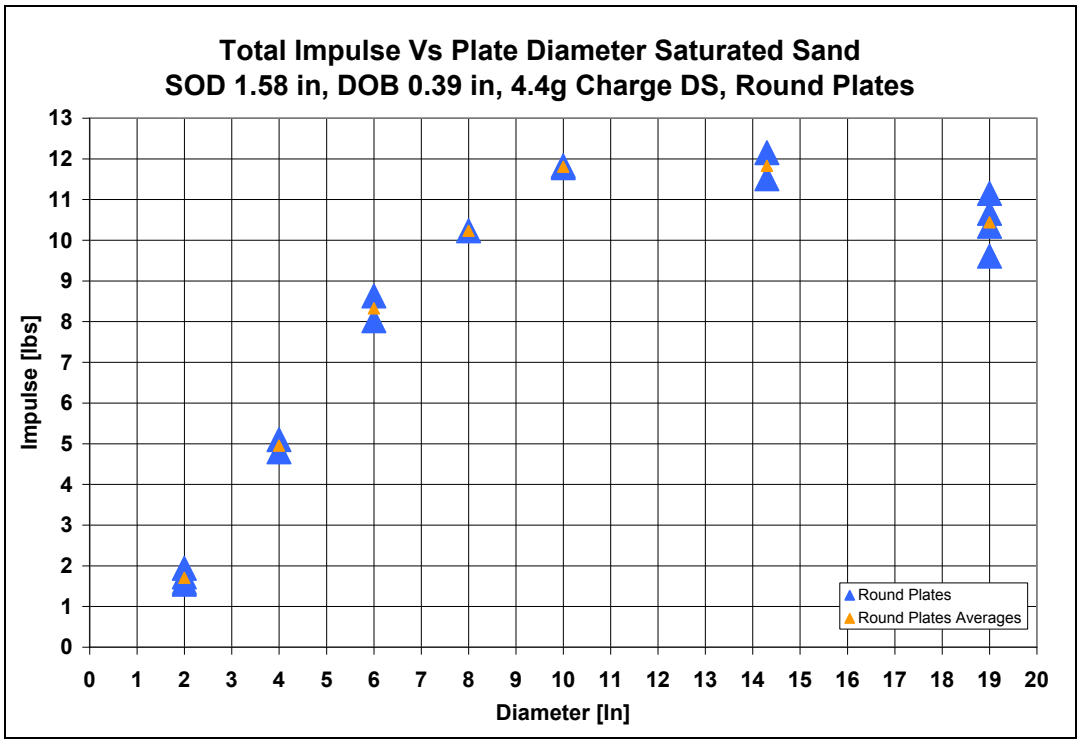

Figure 5.36 Impulse results round plates

5.1.6 Verification of Pressure Test Results at SOD 4 cm (1.58 inches) and DOB 1 cm (0.39 inches) in Saturated Sand Using Impulse Results from Round Plates

Plotting the test results obtained by the integration of the pressure measurements (**Figure 5.27**) and the results of impulse measured using the round plates on the same plot, shows that both data sets agree pretty well (**Figure 5.37**), which indicates that the processing of the pressure – time profiles was done correctly. At the diameter of 5.08 cm (2 inches) and 10.16 cm (4 inches) the impulse of the integrated pressures is slightly lower. A reason for the data not agreeing at the location of 5.08 cm (2 inches) can be that it is difficult to measure the displacement exactly of the 10.3 kg plate since it is only displaced a few millimeters. At the location of 10.16 cm (4 inches) the impulse measured using the plates is higher and at 15.24 cm (6 inches) is slightly lower. Data scatter is always involved in the test results since the preparation of the soil bed is very crucial and a small difference in the status of compaction or saturation level of the test bed has an influence of the outcome of the test results.

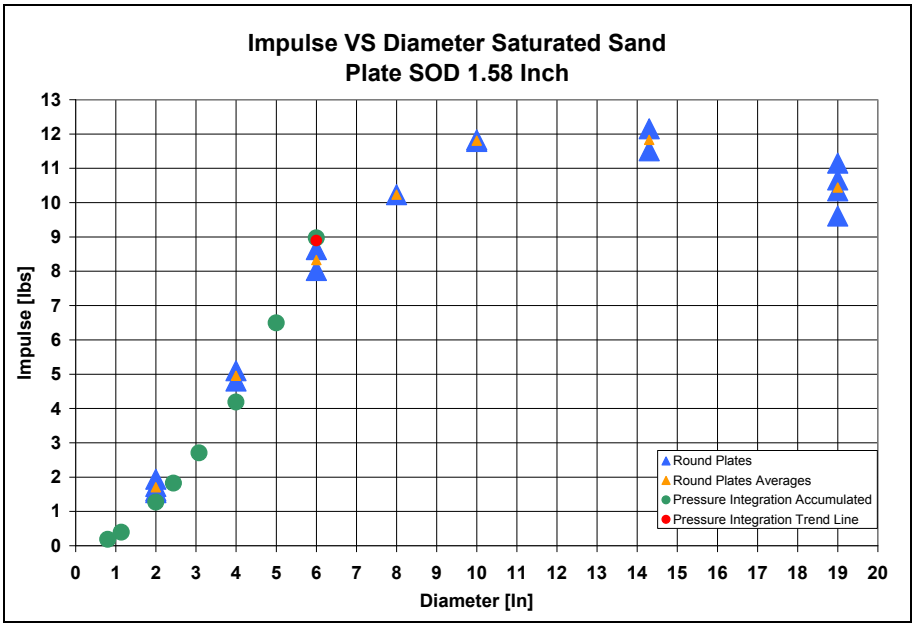

Figure 5.37 Impulse results round plates and pressure integration

Taking the impulse results from the series of plate tests between the diameter of 15.24 cm (6 inches) and 36.32 cm (14.3 inches), the specific impulse can be estimated based on the total impulse measured. Including this results in **Figure 5.28**, the specific impulse distribution over the whole target plate can be plotted (**Figure 5.38**).

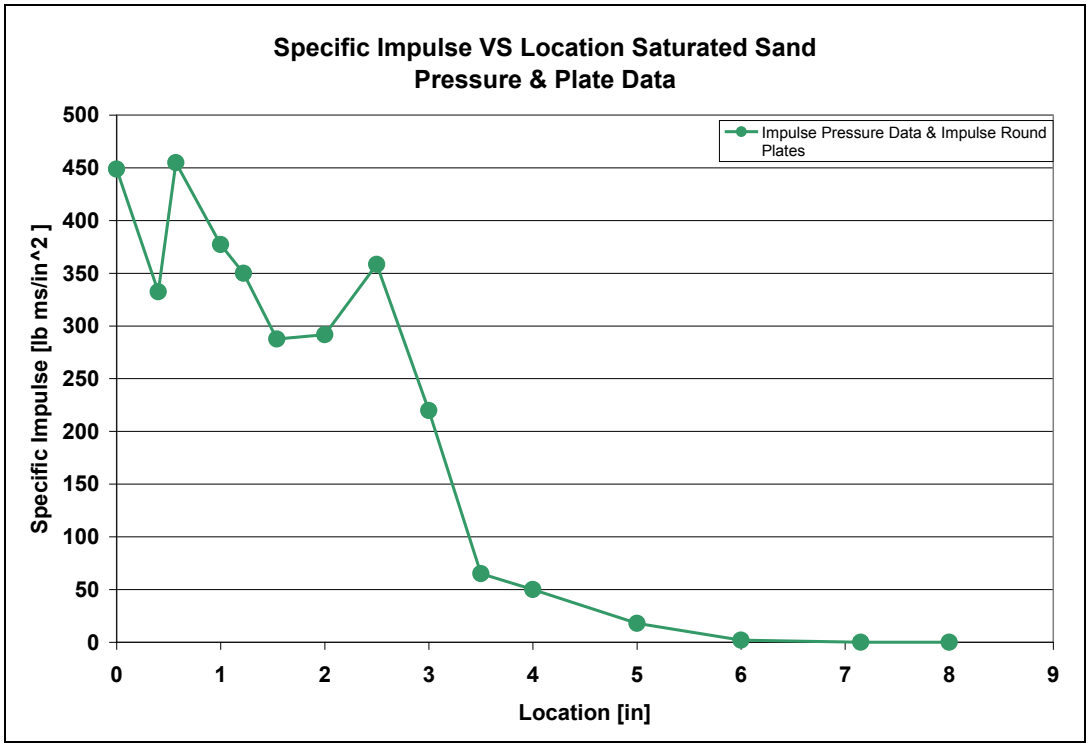

Figure 5.38 Specific impulse distribution on the target plate

As described in **Section 5.14** the total impulse is obtained by rotating the given segments around the Y – axis. **Figure 5.39** shows a three dimensional plot of the rotated segments from **Figure 5.38** forming a solid. The horizontal axis in the plot represent the radii in inches and the Z – axis the specific impulse in lb ms/in^2.

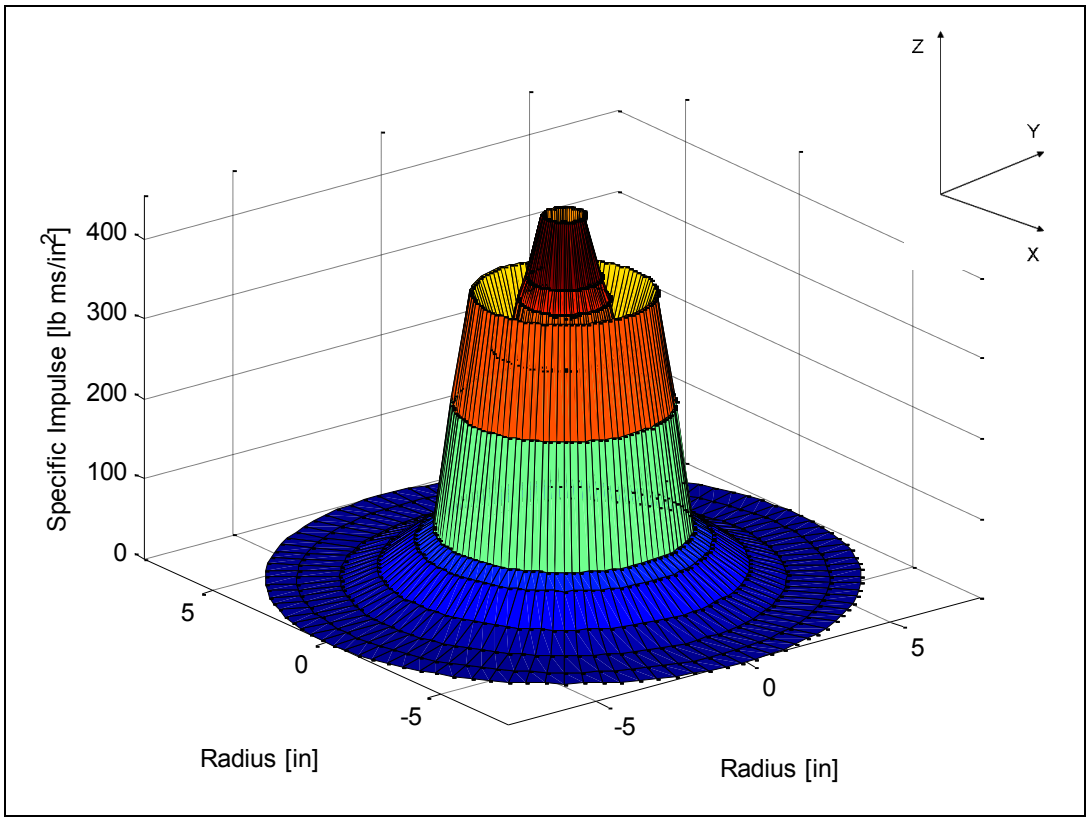

Figure 5.39 Solid obtained by rotating the given segments

Taking the same impulse results as shown in **Figure 5.38** and splitting the set of data into two parts for the integrated pressure results and the plate test results, two trend lines can be established (**Figure 5.40**). Using both trend lines the total impulse is then defined as the volume of a solid obtained by rotating the given trend lines like shown before around the Y – axis. **Figure 5.41** shows a three dimensional plot of the rotated trend lines. The volume of the solid represents the total impulse absorbed by a target plate tested under described conditions and characterizes the impulse distribution best.

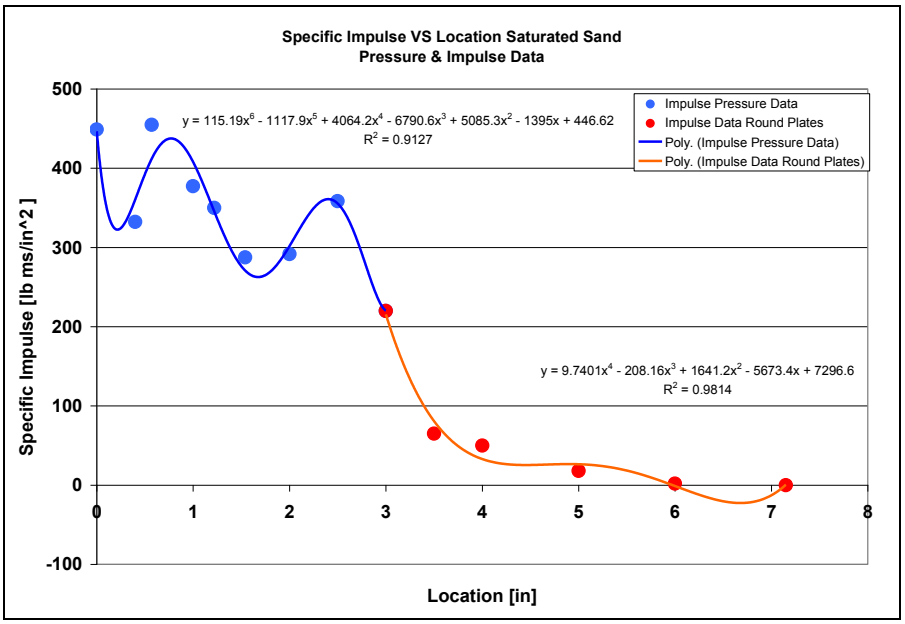

Figure 5.40 Specific impulse distribution on the target plate characterized by trend lines

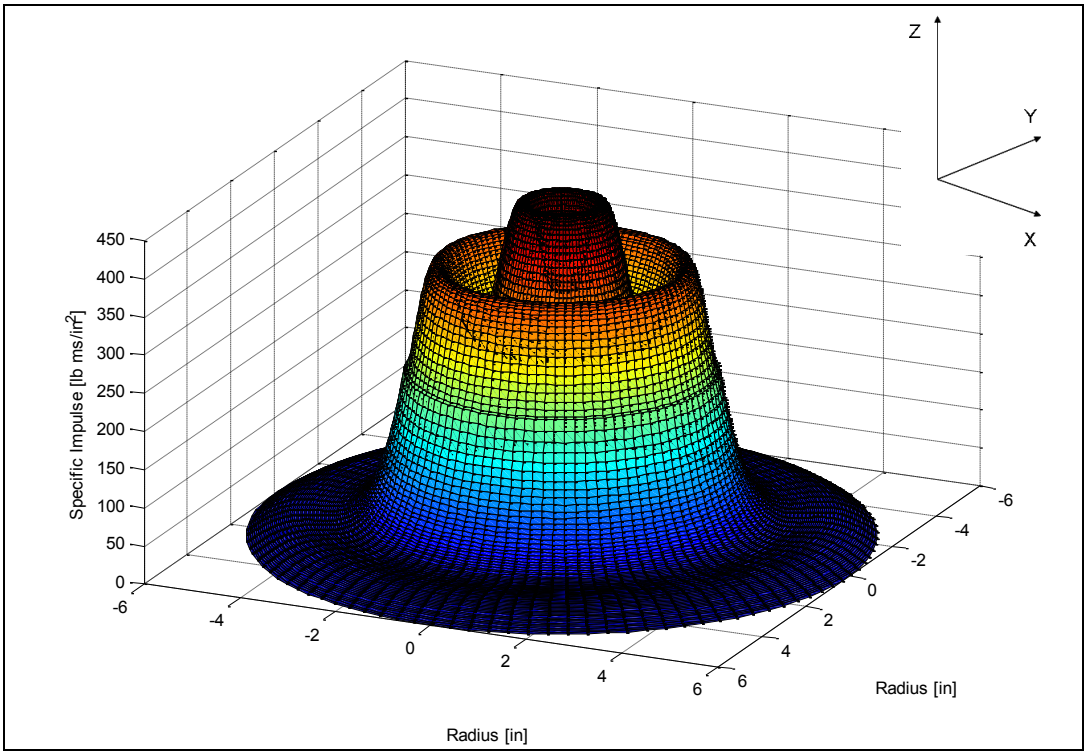

Figure 5.41 Solid obtained by rotating the given trend lines

5.1.7 Verification of Pressure Test Results at SOD 4 cm (1.58 inches) and DOB 1 cm (0.39 inches) in Saturated Sand Using Punch Gage Results

A total of 5 punch gage tests were conducted in order to verify results obtained by the pressure tests. As a target plate a steel plate was designed containing holes at the same locations where the pressure was measured before. The locations were at 0 cm (0 inches), 1.45 cm (0.57 inches), 2.54 cm (1 inch), 3.91 cm (1.54 inches), 5.08 cm (2 inches), 6.35 cm (2.5 inches), 7.62 cm (3 inches). The punch gage consisted of round brass specimens which were designed to rupture at the average pressure measured at a certain location. In order to test this setup successfully it is absolutely essential to test the brass material used in the punch gage testing in a tensile test in order to determine the tensile strength. It is not recommended to use values published in the literature for brass material since material properties vary greatly depending on the alloy used in the manufacturing process. It is absolutely crucial to design the thickness of the brass specimen according to the test results of the tensile testing. In the following the design of the punch gage test is described.

5.1.7.1 Tensile Strength Test Results

In total 4 brass specimens were tested in a tensile test in order to determine the tensile strength of the brass material used for the punch gages in the punch gage test setup. The specimens were tested under tension applying an increasing force and measuring the displacement until failure occurred. **Figure 5.42** shows two of the specimens after being tested and **Figure 5.43** shows a typical force versus displacement test result for brass.

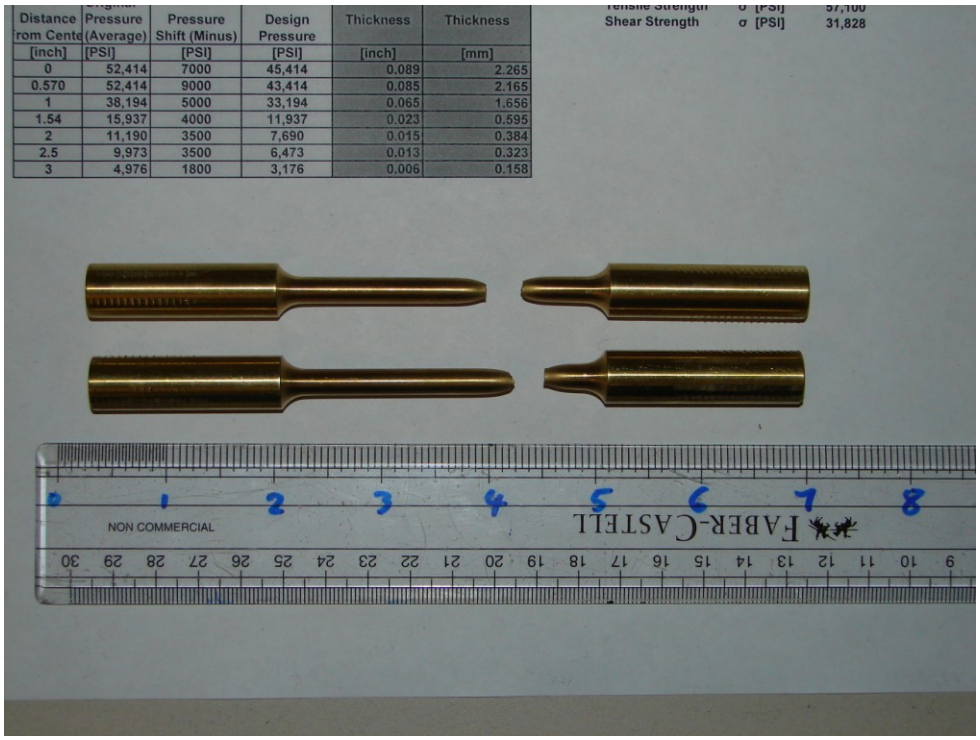

Figure 5.42 Specimens tested in the tensile test

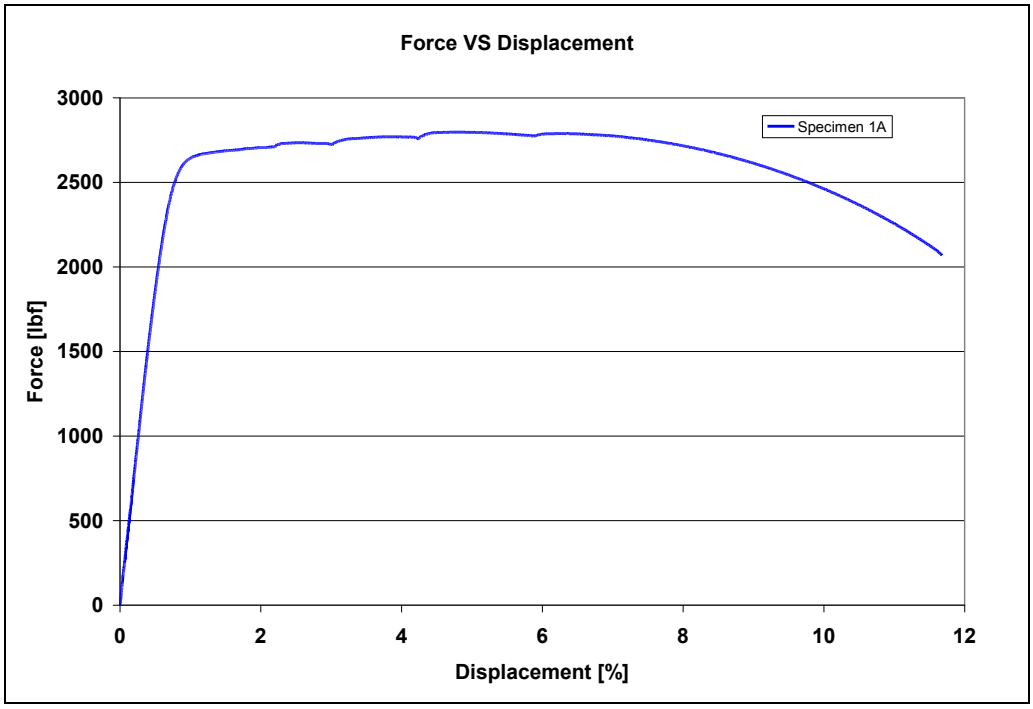

Figure 5.43 Typical test result for a tensile test for brass

In order to calculate the shear strength of the brass specimen the failure stress was calculated using the applied force F over the area A tested (**Equation 5.13)**.

$$P = \frac{F}{A}$$

Equation 5.13 Stress P

Figure 5.44 contains the calculated results. The stress versus the strain in micro strain is shown. The failure stress for specimen A1 was calculated to be 393 mega Pascal (57,000 PSI).

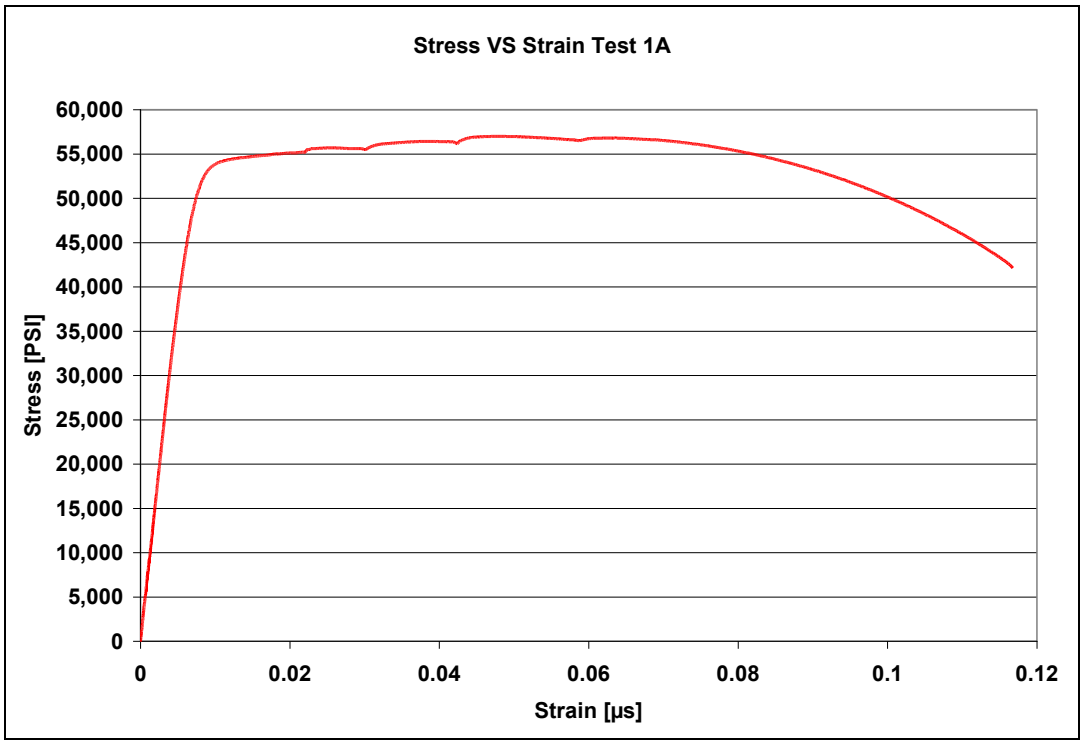

Figure 5.44 Failure stress calculated from tensile test for brass for specimen A1

A common practice is to consider either the yield or tensile strength of a material and multiply that value by $\sqrt{3}/3 = 0.5774$ to estimate the shear strength

(15). The tensile strength σ for specimen A1 equals the failure stress calculated. The shear strength τ is than calculated using **Equation 5.14**.

$$\tau = 0.5574 * \text{ r}$$

Equation 5.14 Shear strength τ

In order to calculate the thickness t of the specimens in which failure occurs, the surface area A_s and the shear face A_f have to be determined. **Figure 5.45** shows a schematic of a brass specimen.

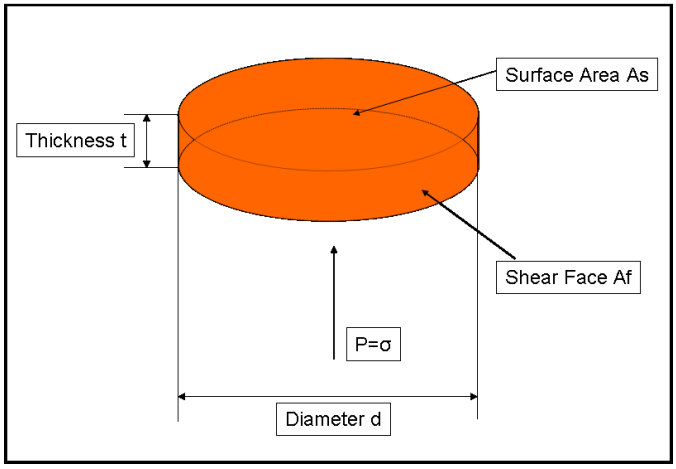

Figure 5.45 Schematic of brass specimen

The characteristic **Equation 5.15** is used to determine the failure thickness t of the brass specimen at a certain failure pressures P applied. The variables r and d are the radius and diameter of the specimen. The variables Af and As are the area of the shear face and the surface.

$$P = \frac{A_f}{A_s} * \quad = \frac{2 * \ : * r * t}{\pi * r^2} * \quad = \frac{2 * t}{r} * \quad = \frac{4 * t}{d} *$$

Equation 5.15 Characteristic equation for failure pressure

Equation 5.15 can be rewritten for calculating the thickness t (**Equation 5.16**). The pressure P where the specimen should fail is known from the pressure – time profiles, the diameter d of the bras specimens is determined by the test setup of the target plate of the punch gage testing. The shear diameter used is 0.635 cm (0.25 inches). The shear strength τ is calculated using **Equation 5.14**.

$$t = \frac{P * d}{4 *}$$

Equation 5.16 Calculation of specimen thickness

5.1.7.2 Punch Gage Test Preparation

The steel plate tested had 83 holes drilled at a diameter of 0.635 cm (0.25 inches). **Figure 5.46** shows the bottom of the target plate. Note the plate had a lip according to the specimen's thickness machined around the hole in order to allow a flush fit of the brass specimens to the bottom of the plate. **Table 5.5** contains the distribution of the holes over the radius of the plate.

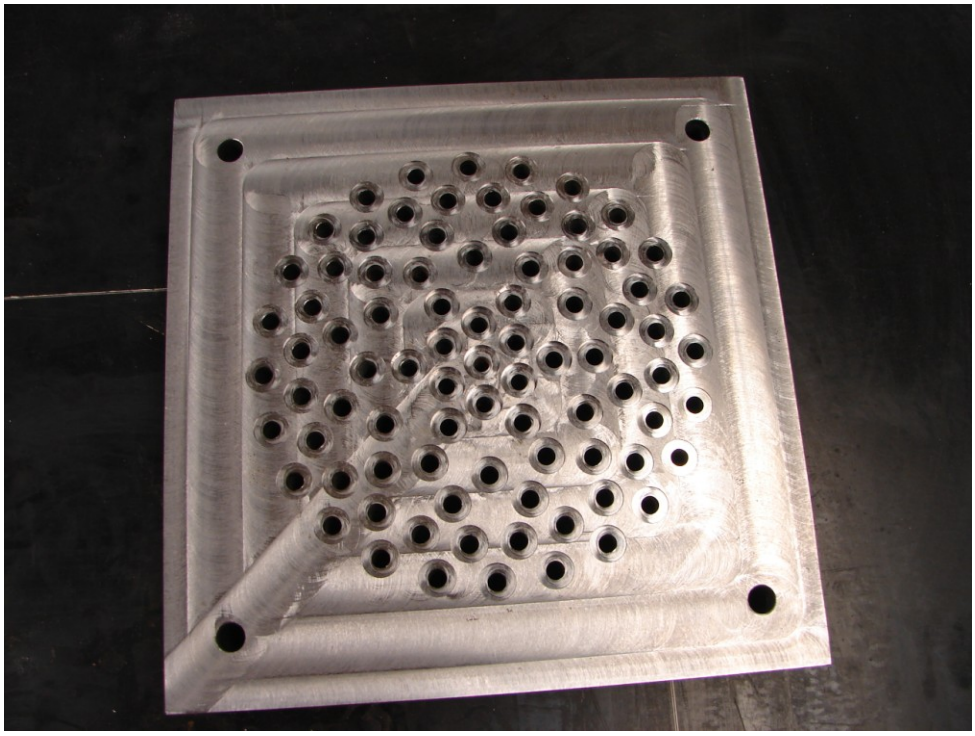

Figure 5.46 Bottom of target plate without brass specimens

Hole Location [in]	0	0.57	1	1.54	2	2.5	3
Number Of Specimen	1	6	6	12	12	24	24

Table 5.5 Hole distribution of the target plate

The specifics of the last successfully conducted test are described in the following. The average pressure values the brass specimens were designed for are listed in the **Table 5.6**. The average shear strength τ of 219.4 mega Pascal (31,828 PSI) was determined from 2 specimen tested as described in a tensile strength test. The equations shown above were used to calculate the thickness of the brass specimens as shown before testing in **Figure 5.47**.

Distance From Center	Average Pressure	Average Pressure	Thickness	Thickness
[inch]	[PSI]	[Mega Pascal]	[inch]	[mm]
0	45,414	313.1	0.089	2.265
0.570	43,414	299.3	0.085	2.165
1	33,194	228.9	0.065	1.656
1.54	11,937	82.3	0.023	0.595
2	7,690	53.0	0.015	0.384
2.5	6,473	44.6	0.013	0.323
3	3,176	21.9	0.006	0.158

Table 5.6 Average pressures and designed thickness of brass specimens

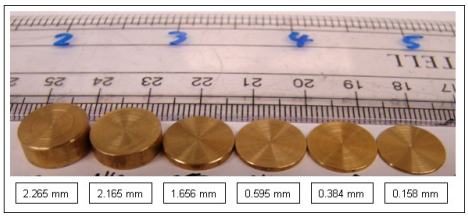

Figure 5.47 Designed brass specimens before testing

The specimens were mounted in the target plate as shown in **Figure 5.48**. Note the tight fit and the flush mount of the specimens. The plate was then mounted on a frame (**Figure 5.49**) and tested using the test conditions as described.

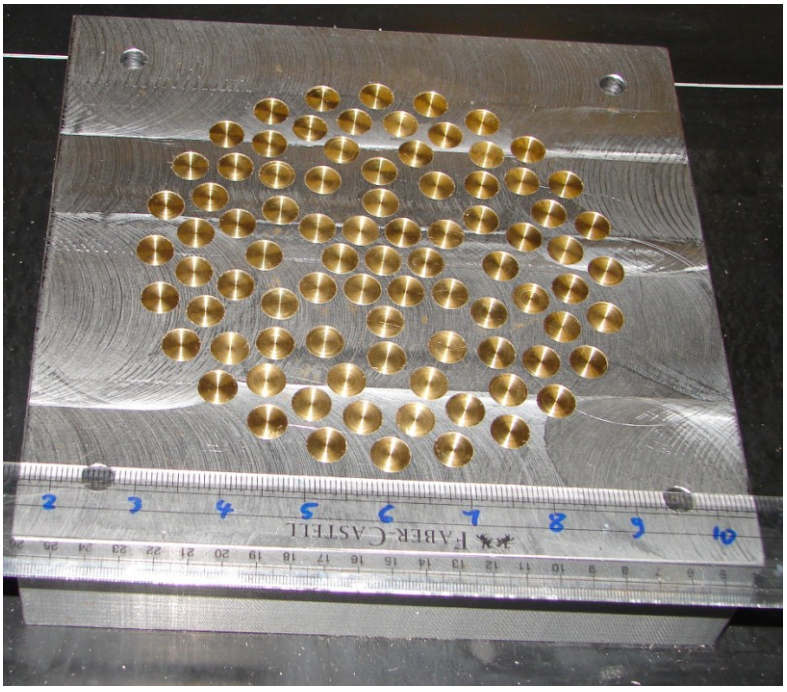

Figure 5.48 Bottom of target plate before testing

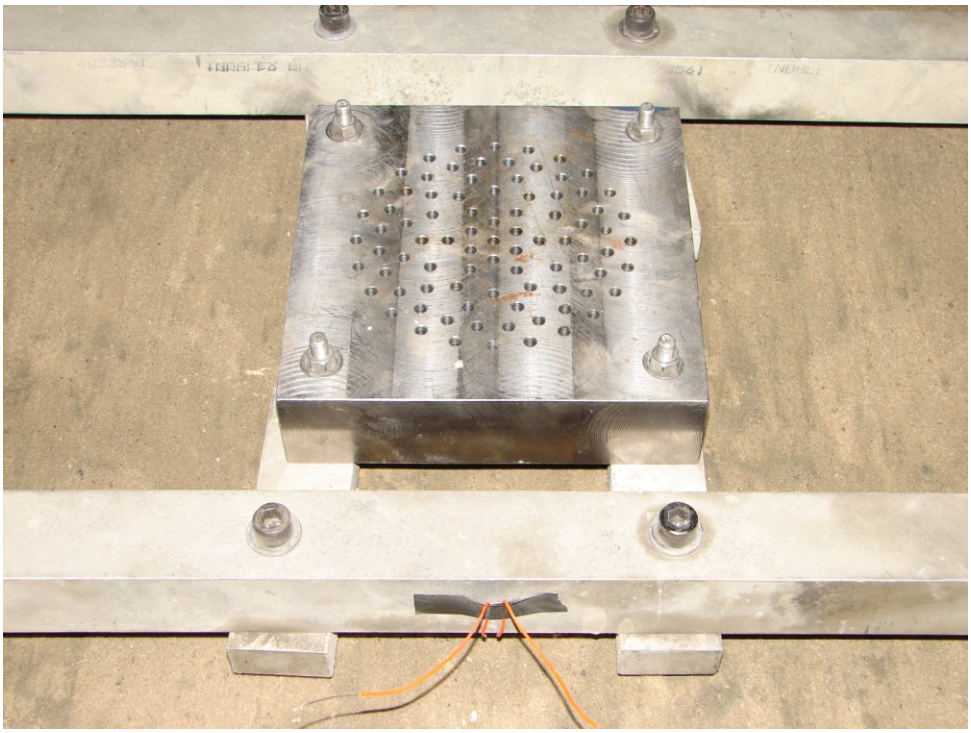

Figure 5.49 Test setup for punch gage target plate

5.1.7.3 Punch Gage Test Results

As shown in **Figure 5.50** during testing some of the brass specimens failed due to the exceeded design pressures applied, a result expected since the average pressure values were used for the design of the brass specimens.

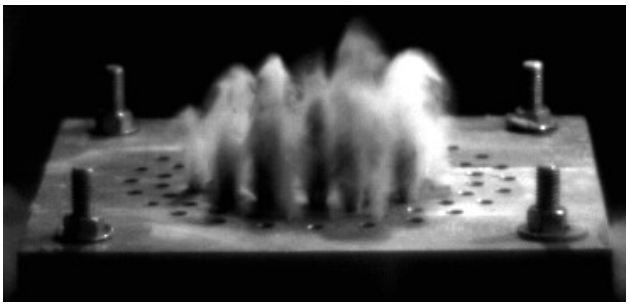

Figure 5.50 Target plate during testing

An examination of the bottom of the target plate after testing revealed that at the locations of 0 cm (0 inches), 1.45 cm (0.57 inches), and 2.54 cm (1 inch) none of the specimens sheared (**Figure 5.51**). At the other locations further away from the center of the plate the specimens started to shear. Specifically at the location of 3.91 cm (1.54 inches) 9 of the 12 specimens sheared and 3 were dented. At the location of 5.08 cm (2 inches) 10 of the 12 specimens sheared and 2 were dented. At the location of 6.35 cm (2.5 inches) 8 of the 24 specimens sheared and the others were dented. And finally at the location of 7.62 cm (3 inches) 17 of the 24 specimens were sheared off and the other 5 dented, compare **Figure 5.51**.

Removing the specimens at the locations of 0 cm (0 inches), 1.45 cm (0.57 inches), and 2.54 cm (1 inch) from the target plate revealed that they partially sheared, compare **Figure 5.52**. A reason why they did not shear completely can be that the loading times at these locations last between 20 to 25 microseconds. This might not be enough time to cause complete failure. Further out from the center at the location of 3.91 cm (1.54 inches) the loading time lasts 61 and at 7.62 cm (3 inches) 183 microseconds.

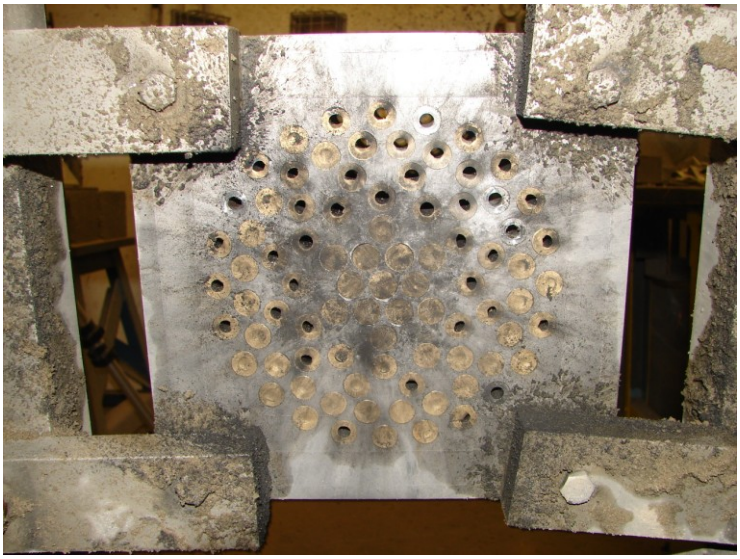

Figure 5.51 Target plate after testing

Figure 5.52 Partially sheared specimens

5.2 Pressure – Time Profiles at SOD 2 cm (0.79 inches) and DOB 1 cm (0.39 inches) in Saturated Sand

A test series was conducted reducing the SOD of the target plate to 2 cm (0.79 inches). The DOB of 1 cm (0.39 inches) was kept the same as described in **Section 5.1**. The explosive charges used were 4.4 g of Deta Sheet. **Table 5.7** contains the results of 14 tests (100 recorded pressure – time profiles) conducted in saturated sand. The pressure – time profiles were recorded at the locations of 0 cm (0 inches), 1.45 cm (0.57 inches), 2.54 cm (1 inch), 3.10 cm (1.22 inches), 3.91 cm (1.54 inches), 5.08 cm (2 inches), and 6.35 cm (2.5 inches). The table contains values for the maximum and minimum peak pressure measured at each location. The average peak pressure is calculated and so is the standard deviation based on the number of profiles recorded at each location. The standard deviations are increasing towards the center of the plate.

Location	**Maximum Pressure**	**Minimum Pressure**	**Average Pressure**	**Number of Profiles**	**Standard Deviation**
[Inch]	**[PSI]**	**[PSI]**	**[PSI]**		**[PSI]**
0	79,281	46,756	57,547	14	9,517
0.57	76,465	45,574	61,323	13	9,018
1	53,178	24,705	38,194	14	7,939
1.22	40,089	14,426	20,701	14	9,457
1.54	26,845	8,048	15,937	17	5,164
2	8,364	4,162	11,190	14	1,261
2.5	4,701	1,820	9,973	14	804

Table 5.7 Pressure - time results for saturated sand at SOD 2 cm (0.79 inches) and DOB 1 cm (0.39 inches)

Figure 5.53 shows the maximum and minimum pressure measured and the average pressure calculated at specific locations of the plate. Note that the average pressure rises at a distance of 1.45 cm (0.57 inches) like it did in **Figure 5.1**. With increasing distance from the center of the plate the peak pressure values decrease more rapidly than in **Figure 5.1** shown for twice the SOD (4 cm (1.58 inches)). This fact did not allow measurement of the pressure at the location of 7.62 cm (of 3 inches) since the pressure values were too low for the Kolsky bars at this location.

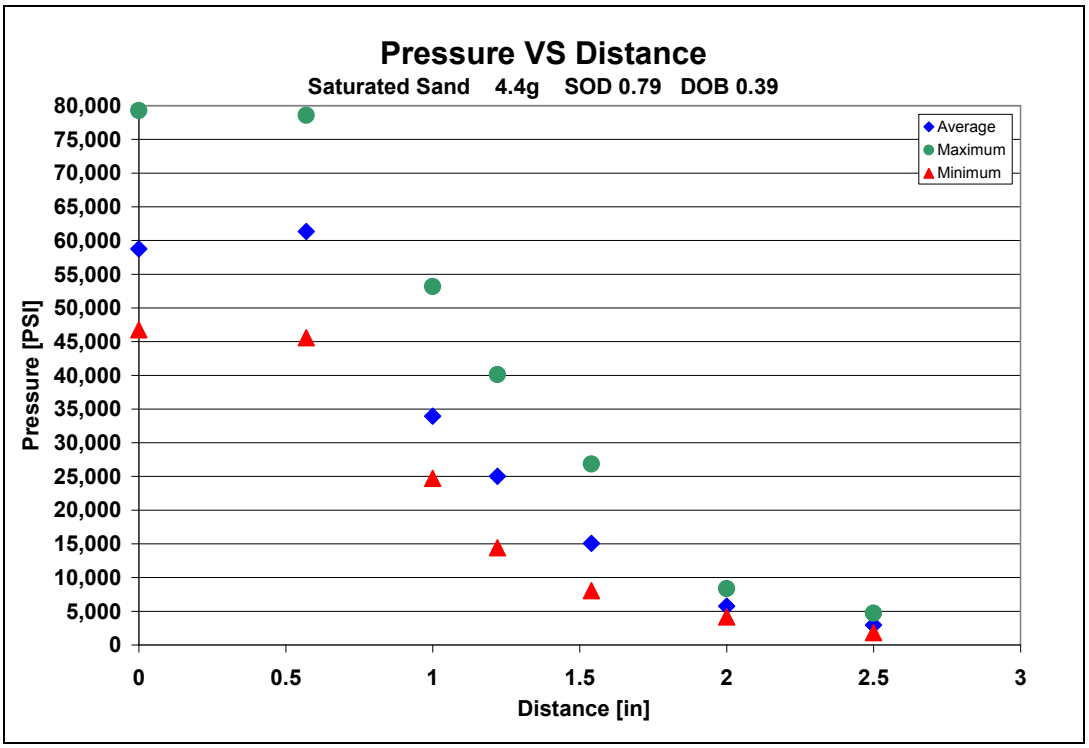

Figure 5.53 Peak pressure results for saturated sand at specific locations at SOD 2 cm (0.79 inches) and DOB 1 cm (0.39 inches)

In order to calculate the average pressure - time profile each single measured pressure - time profile has to be shifted in such a manner that the peak pressure values are occurring at the same time like described before in **Section 5.1**. The processing of the pressure – time profiles includes alignment of the peak pressures at each single

location and calculation of the average pressure – time profile. The logarithmic decrement of each average profile is then calculated, shifted and drift compensated.

Figure 5.54 contains all the processed average pressure – time profiles which are subsequently used for calculating the specific impulse at the specific locations of the plate. The figure shows the correct loading time intervals and the starting times of the loading for the saturated sand case using a plate at a SOD of 2 cm (0.79 inches) and DOB of 1 cm (0.39 inches) using a 4.4 g explosive charge.

The pressure – time profile at the locations of 0 cm (0 inches) shows a longer loading time than the profiles at 1.45 cm (0.57 inches) and 2.54 cm (1 inch) (**Figure 5.55**). The profile at the location of 1.45 cm (0.57 inches) contains the highest peak pressure. From then on at the locations further away from the center of the plate the loading times increase and the peak pressure drop faster than shown in the pressure – time profiles at a SOD of 4 cm (1.58 inches). **Table 5.8** contains the details about loading times, intervals, and peak pressure shifts for each processed average pressure –time profile.

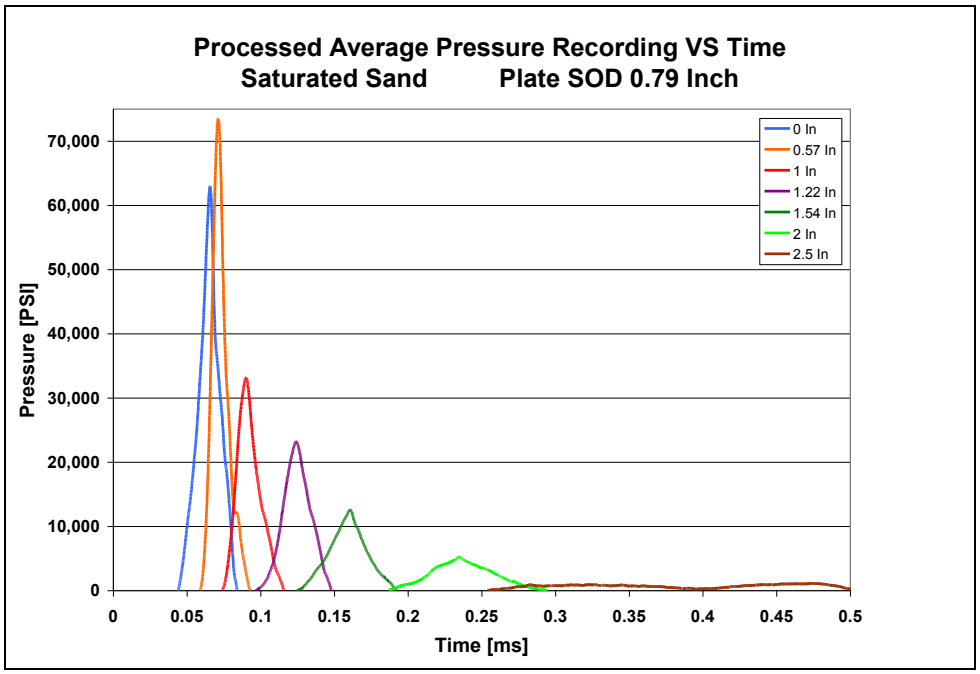

Figure 5.54 Processed pressure – time profiles at all locations at SOD 2 cm (0.79 inches)

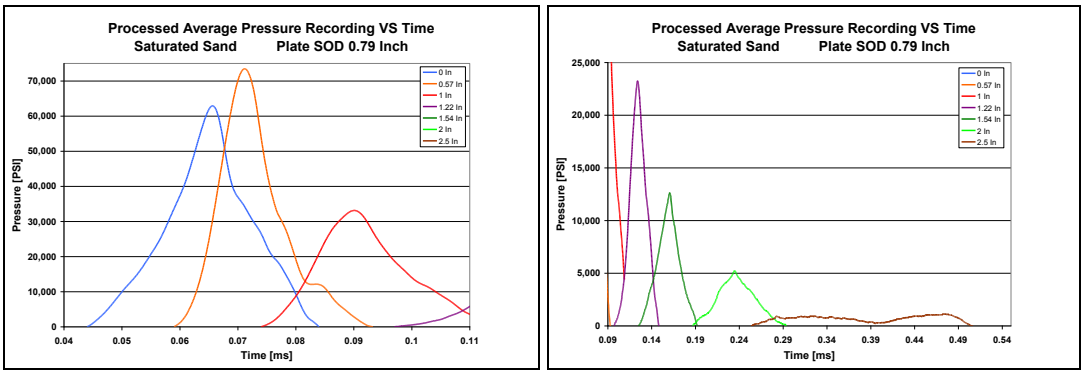

Figure 5.55 Details of the processed pressure – time profiles at all locations

Location	Loading Duration	Start Time	End Time	Pressure Off-set Correction	Peak Pressure
[in]	[µs]	[ms]	[ms]	[PSI]	[PSI]
0	40	0.044	0.084	5,000	62,924
0.57	34	0.059	0.093	5,000	73,502
1	42	0.074	0.116	3,000	33,141
1.22	51	0.097	0.148	2,300	23,256
1.54	67	0.125	0.192	1,400	12,641
2	106	0.187	0.293	1,150	5,234
2.5	251	0.254	0.505	1,106	1,630

Table 5.8 Loading time results for saturated sand at SOD 2 cm (0.79 inches) and DOB 1 cm (0.39 inches)

Figure 5.56 shows the peak pressure and the loading time interval distribution versus the location at the bottom of the target plate. The loading time interval drops a little from the center out and then starts to increase constantly until it reaches the location of 2.54 cm (1 inch). At the location of 3.10 cm (1.22 inches) it increases more rapidly. The peak pressure values peak at the location of 1.45 cm (0.57 inches)

and decline quickly from then on and are lowest in the combination with the longest loading time interval.

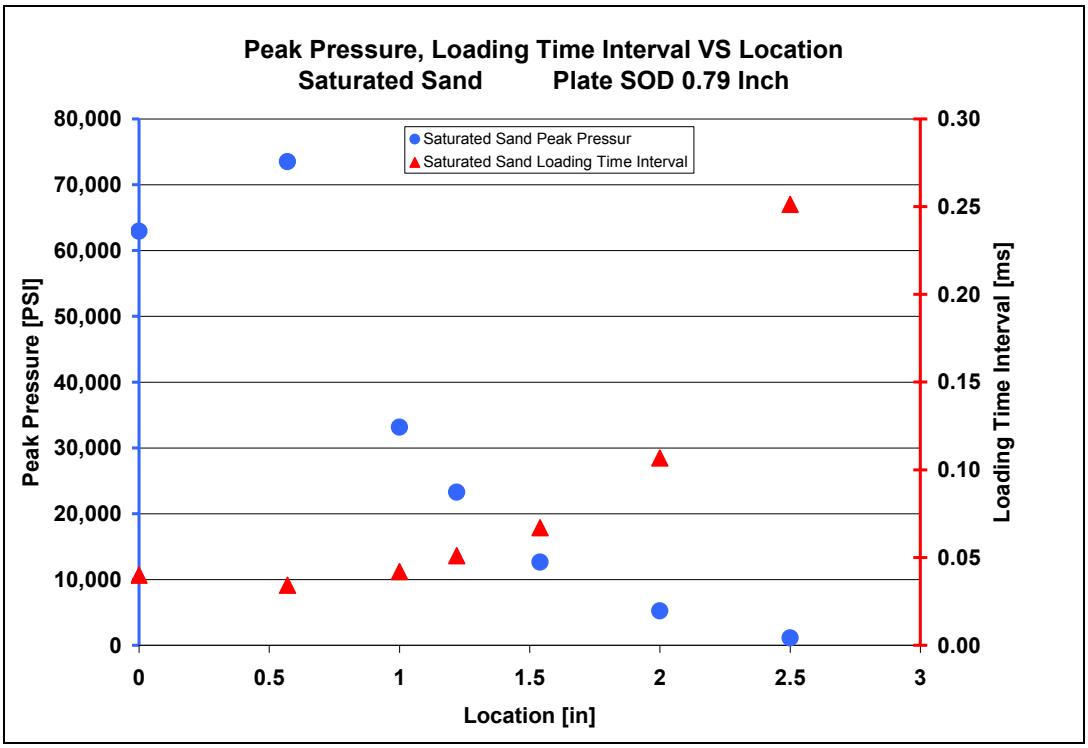

Figure 5.56 Peak pressure and loading time interval versus location at SOD 2 cm (0.79 inches)

5.2.1 Specific Impulse Calculation at SOD 2 cm (0.79 inches) and DOB 1 cm (0.39 inches) in Saturated Sand

Using the calculated average pressure – time profiles shown in **Figure 5.54** the specific impulse at each location is calculated. The specific impulses are shown in **Figure 5.57**. The specific impulse is highest at the center location at 0 cm (0 inches) and drops from then on consistently to a very low value at the location of 6.35 cm (2.5 inches). Note the difference in the specific impulse distribution compared to

the SOD of 4 cm (1.58 inches), see **Figure 5.25**. **Table 5.9** contains all results of the specific impulse calculation for the SOD of 2 cm (0.79 inches).

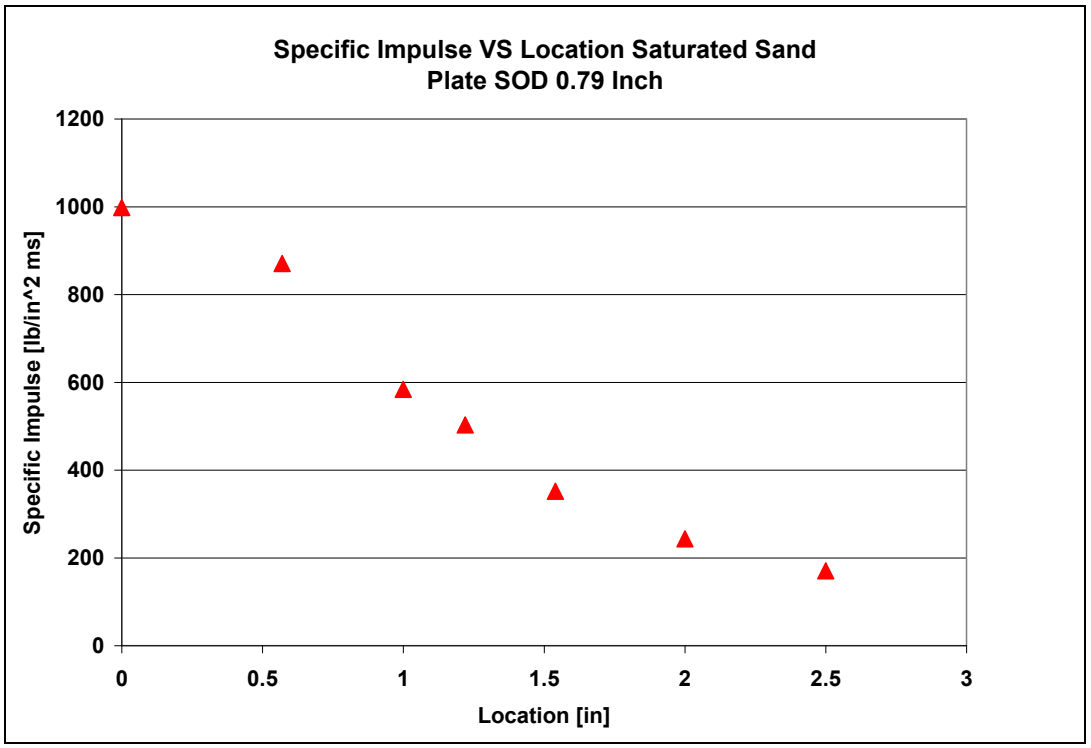

Figure 5.57 Specific impulse versus location at SOD 2 cm (0.79 inches)

Specific Impulse [(lb / in^2) * ms]	Specific Impulse [(lb / in^2) * s]	Distance [in]
998.01	0.998	0
870.45	0.870	0.57
584.00	0.584	1
503.00	0.503	1.22
351.85	0.352	1.54
243.49	0.243	2
170.71	0.171	2.5

Table 5.9 Specific Impulse results for saturated sand at SOD 2 cm (0.79 inches) and DOB 1 cm (0.39 inches)

5.2.2 Total Impulse Calculation at SOD 2 cm (0.79 inches) and DOB 1 cm (0.39 inches) in Saturated Sand

Using the specific impulse the total impulse can be calculated as shown in **Section 5.1.4**. A trend line based on the specific impulse values has to be established see **Figure 5.58**. The total impulse is than defined as the volume of a solid obtained by rotating the given trend line around the vertical axis. **Figure 5.59** shows a three dimensional plot of the rotated trend line. Note the difference compared to the larger SOD of 4 cm (1.58 in) shown in **Figure 5.27**.

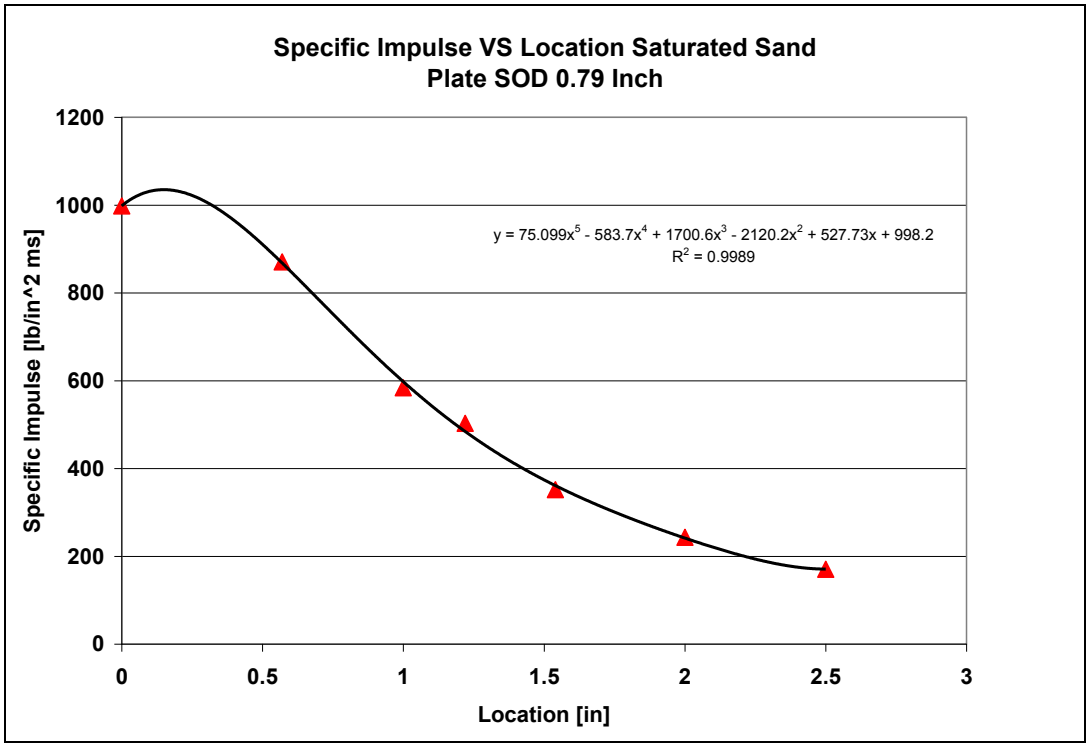

Figure 5.58 Specific impulse versus location including trend line for SOD 2 cm (0.79 inches)

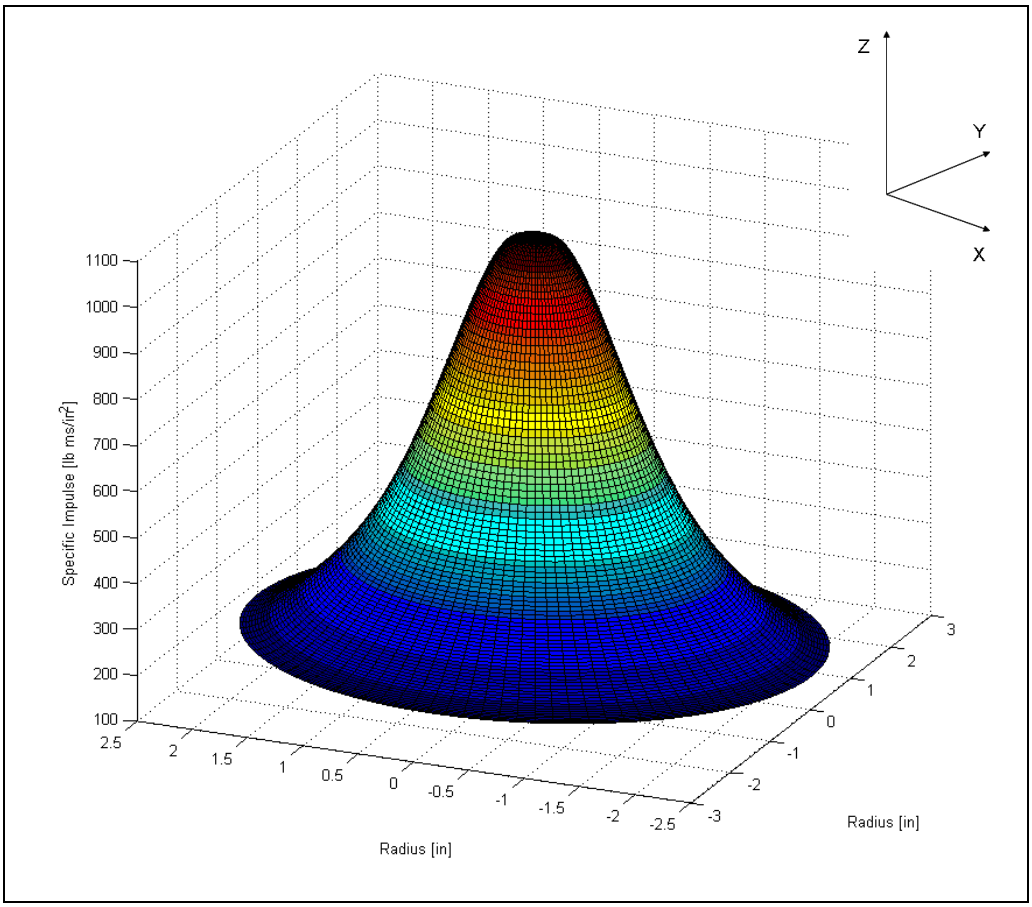

Figure 5.59 Solid obtained by rotating the given trend line at SOD 2 cm (0.79 inches)

Using a second approach, impulse segments over the radius of the plate can be calculated using the same method as before. Again instead of a trend line a straight line connecting the specific impulse values has to be established see **Figure 5.60**. The total impulse is obtained by rotating the given segments around the vertical axis. **Figure 5.61** shows a three dimensional plot of the rotated segments. The results of both methods are very similar for the SOD of 2 cm (0.79 inches).

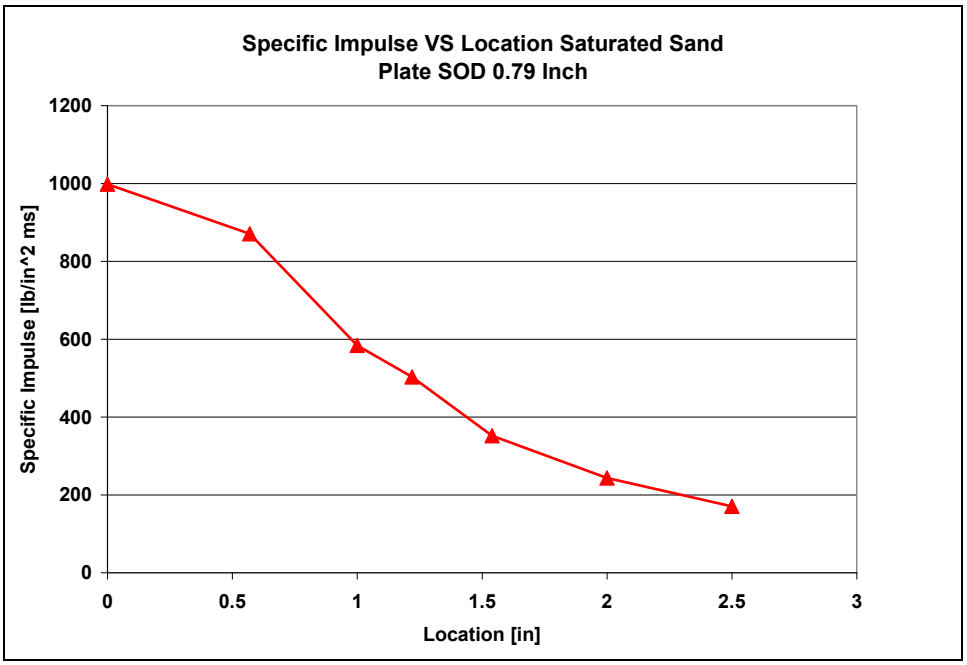

Figure 5.60 Specific impulse versus location at SOD 2 cm (0.79 inches)

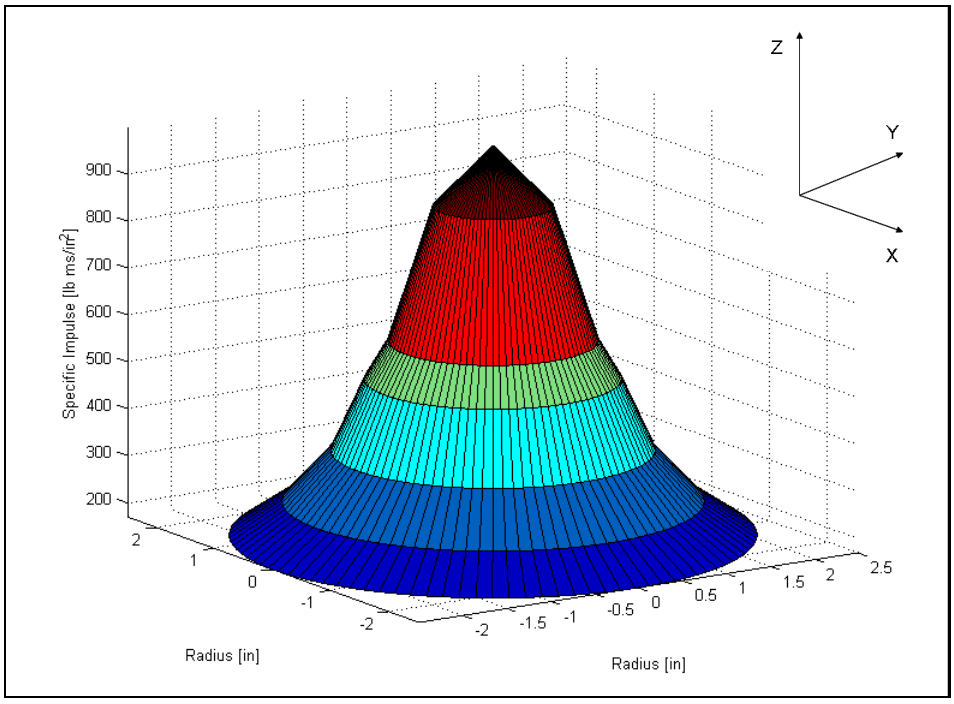

Figure 5.61 Solid obtained by rotating the given segments for SOD 2 cm (0.79 inches)

As described in **Section 5.14 Equations 5.4** to **5.12** are used in order to calculate the total impulse in this case for certain segments according to the definition. Depending on target plate size this allows an evaluation of the total impulse absorbed by the target.

Table 5.10 contains the results for calculating the impulse for each segment and the trend line. The accumulated impulse for the diameter of 12.7 cm (5 inches) is 33 Ns (7.42 lbs) which is very close to the total impulse of 32.8 Ns (7.38 lbs) calculated using the trend line in **Figure 5.58**. All the calculated impulse results are shown in **Figure 5.62**. It indicates how the impulse increases using larger size target plates.

Impulse Per Segment [lb s]	Total Impulse Accumulated [lb s]	Diameter [in]	Radius [in]
0.93	0.93	1.14	0.57
1.51	2.45	2	1
0.83	3.28	2.44	1.22
1.18	4.46	3.08	1.54
1.51	5.97	4	2
1.45	7.42	5	2.5
Trend Line			
7.38	7.38	5	2.5

Table 5.10 Impulse results for saturated sand at SOD 2 cm (0.79 inches) and DOB 1 cm (0.39 inches) for single segments and accumulated over diameter

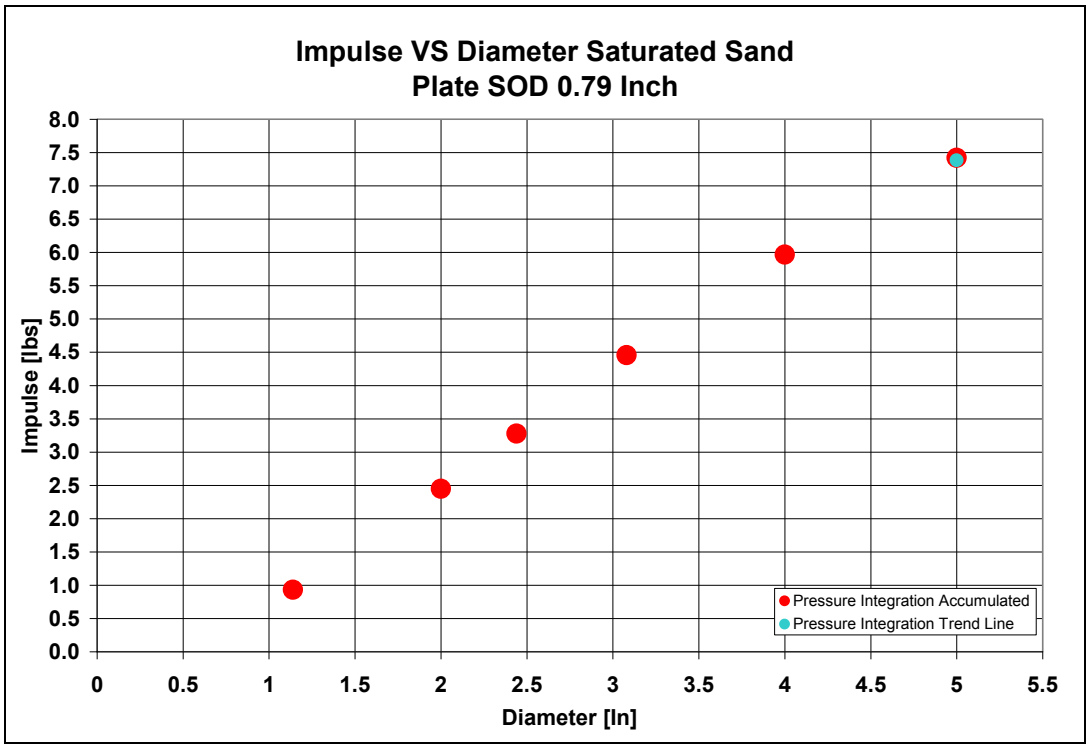

Figure 5.62 Impulse versus diameter of target plates for SOD 2 cm (0.79 inches)

5.3 Pressure – Time Profiles at SOD 6 cm (2.38 inches) and DOB 1 cm (0.39 inches) in Saturated Sand

A test series was conducted enlarging the SOD of the target plate to 6 cm (2.38 inches). The DOB of 1 cm (0.39 inches) was kept the same as described in **Section 5.1** and **5.2**. The explosive charges used were 4.4 g of Deta Sheet. **Table 5.11** contains the results of 15 tests (112 recorded pressure – time profiles) conducted in saturated sand. The pressure – time profiles were recorded at the locations of 0 cm (0 inches), 1.45 cm (0.57 inches), 2.54 cm (1 inch), 3.10 cm (1.22 inches), 3.91 cm (1.54 inches), 5.08 cm (2 inches), 6.35 cm (2.5 inches), and 7.62 cm (3 inches). The table contains values for the maximum and minimum peak pressure measured at each location. The average peak pressure is calculated and so is the standard deviation based on the number of profiles recorded at each location. The average peak pressure is highest at the location of 1.45 cm (0.57 inches) as in the other set-ups using a lower SOD.

Location	**Maximum Pressure**	**Minimum Pressure**	**Average Pressure**	**Number of Profiles**	**Standard Deviation**
[Inch]	**[PSI]**	**[PSI]**	**[PSI]**		**[PSI]**
0	51,394	17,659	29,404	15	9,706
0.57	43,568	18,149	32,329	15	7,488
1	30,145	10,033	21,791	12	5,866
1.22	30,123	7,692	18,668	14	6,510
1.54	24,504	2,742	13,206	14	10,306
2	13,750	3,024	8,357	14	3,445
2.5	6,814	3,299	5,056	14	1,472
3	5,886	1,661	3,206	14	995

Table 5.11 Pressure - time results for saturated sand at SOD 6 cm (2.38 inches) and DOB 1 cm (0.39 inches)

Figure 5.63 shows the maximum and minimum pressure measured and the average pressure calculated at specific locations of the plate. Note that the average pressure rises at a distance of 1.45 cm (0.57 inches) like it did in **Figure 5.1** and **5.53**. With increasing distance from the center of the plate the peak pressure values drop but not as rapidly as in the case of SOD (2 cm (0.39 inches). Therefore it was possible to measure the pressure at the location of 7.62 cm (3 inches).

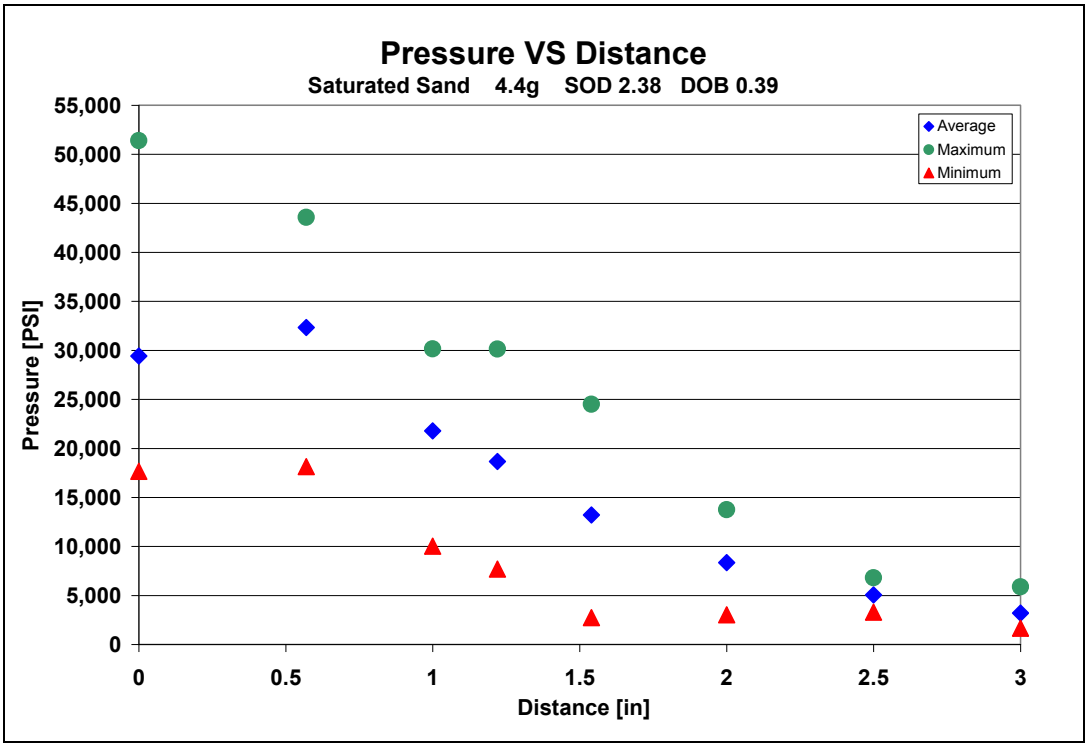

Figure 5.63 Peak pressure results for saturated sand at specific locations at SOD 6 cm (2.38 inches) and DOB 1 cm (0.39 inches)

Again each single measured pressure - time profile has to be shifted as described before in **Section 5.1**. The processing of the pressure – time profiles includes alignment of the peak pressures at each single location and calculation of the average pressure – time profile. The logarithmic decrement of each average profile is then calculated, shifted and drift compensated.

Figure 5.64 contains all the processed average pressure – time profiles which are subsequently used for calculating the specific impulse at the specific locations of the plate for the SOD of 6 cm (2.38 inches). The figure shows the correct loading time intervals and the starting times of the loading for the saturated sand case using a plate at a SOD of 6 cm (2.38 inches) and DOB of 1 cm (0.39 inches) using a 4.4 g explosive charge.

The pressure – time profile at the locations of 0 cm (0 inches) shows a longer loading time than the profiles at 1.45 cm (0.57 inches) and 2.54 cm (1 inch) (**Figure 5.65**). The profile at the location of 1.45 cm (0.57 inches) contains the highest peak pressure. From then on at locations further away from the center of the plate the loading times increase and the peak pressure drop faster than shown in the pressure – time profiles at a SOD of 4 cm (1.58 inches). **Table 5.12** contains the details about loading times, intervals, and peak pressure shifts for each processed average pressure –time profile.

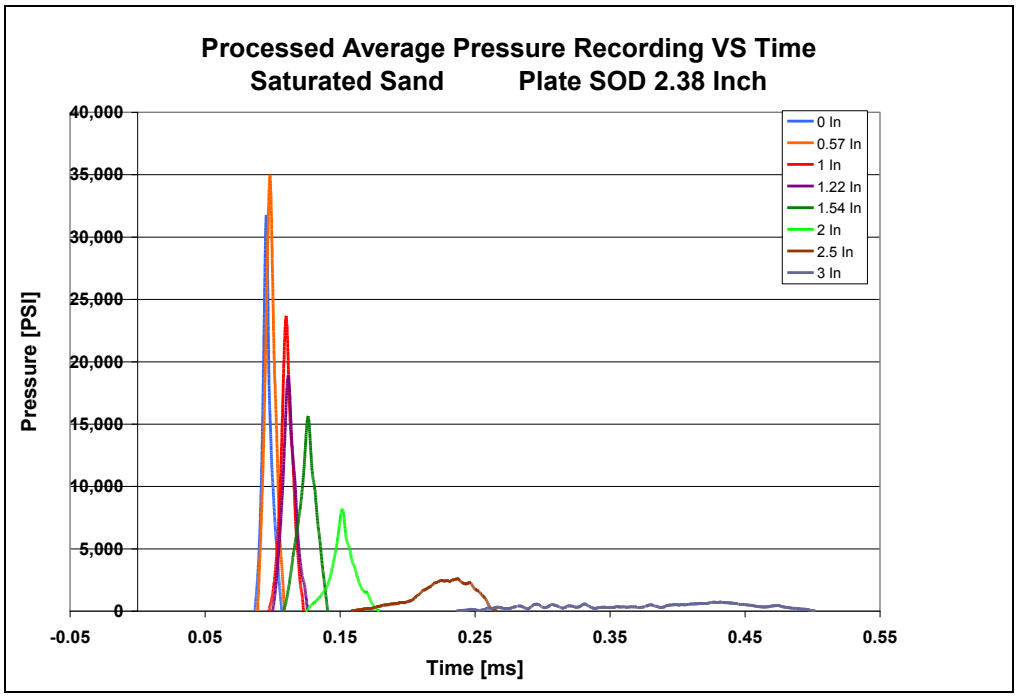

Figure 5.64 Processed pressure – time profiles at all locations at SOD 6 cm (2.38 inches)

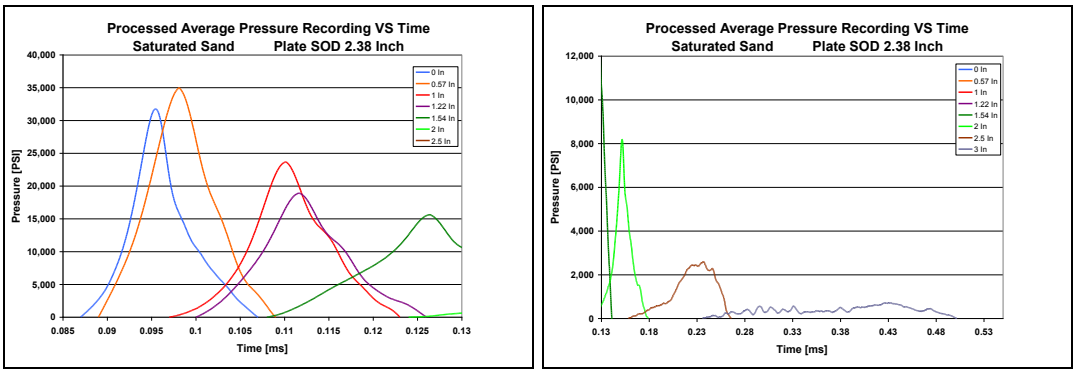

Figure 5.65 Details of the processed pressure – time profiles at all locations

Location	Loading Duration	Start Time	End Time	Pressure Off-set Correction	Peak Pressure
[in]	[µs]	[ms]	[ms]	[PSI]	[PSI]
0	20	0.087	0.107	5,000	31,750
0.57	20	0.089	0.109	2,000	34,990
1	26	0.097	0.123	1,000	23,660
1.22	26	0.100	0.126	900	18,920
1.54	33	0.108	0.141	500	15,640
2	55	0.124	0.179	900	8,200
2.5	108	0.158	0.266	920	2,600
3	266	0.236	0.502	1,410	720

Table 5.12 Loading time results for saturated sand at SOD 6 cm (2.38 inches) and DOB 1 cm (0.39 inches)

Figure 5.66 shows the peak pressure and the loading time interval distribution versus the location at the bottom of the target plate. The loading time interval stays pretty much constant from the center out until it reaches the location of 3.10 cm (1.22 inches) and then starts to increase exponentially. The peak pressure values peak

again at the location of 1.45 cm (0.57 inches) and decline quickly from then on and are lowest in the combination with the longest loading time interval.

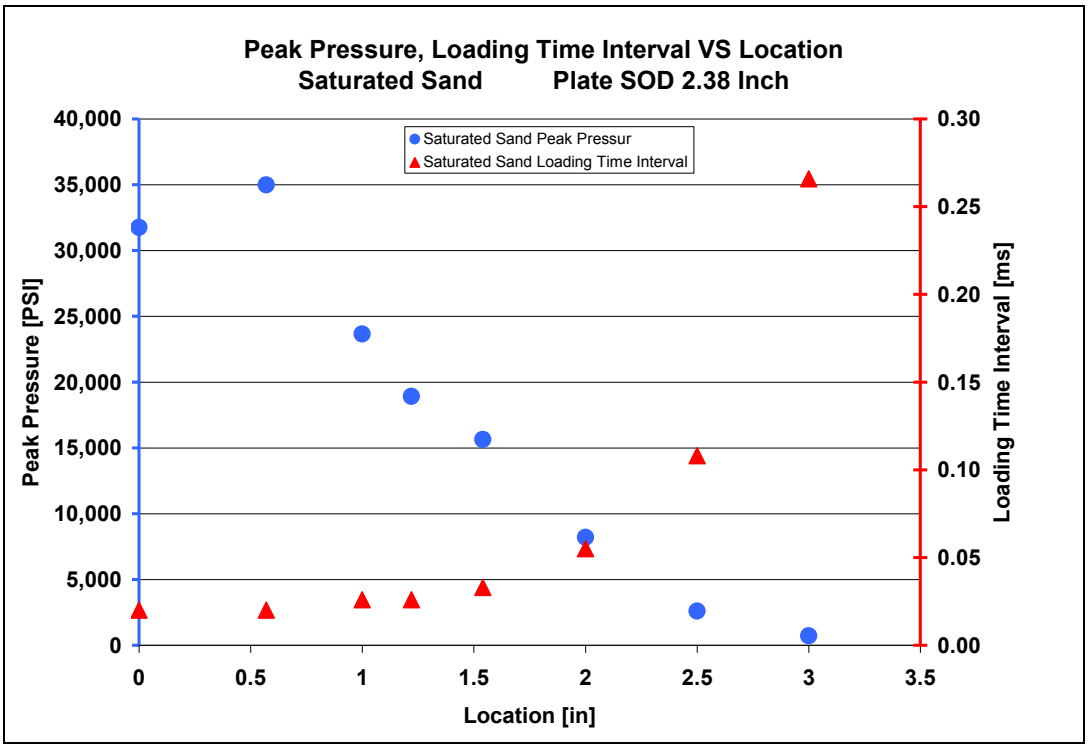

Figure 5.66 Peak pressure and loading time interval versus location at SOD 6 cm (2.38 inches)

5.3.1 Specific Impulse Calculation at SOD 6 cm (2.38 inches) and DOB 1 cm (0.39 inches) in Saturated Sand

Using the calculated average pressure – time profiles shown in **Figure 5.64** the specific impulse at each location is calculated. The specific impulses are shown in **Figure 5.67**. The specific impulse is highest at the location of 1.45 cm (0.57 inches) and drops from then on to the low value of 0.43 Ns (0.097 lbs) at the location of 7.62 cm (3 inches). Note that the highest specific impulse value compared to the SOD of 4 cm (1.58 inches) appears to be at the same location of 1.45 cm (0.57

inches), see **Figure 5.25**. **Table 5.13** contains all results of the specific impulse calculation for the SOD of 6 cm (2.38 inches).

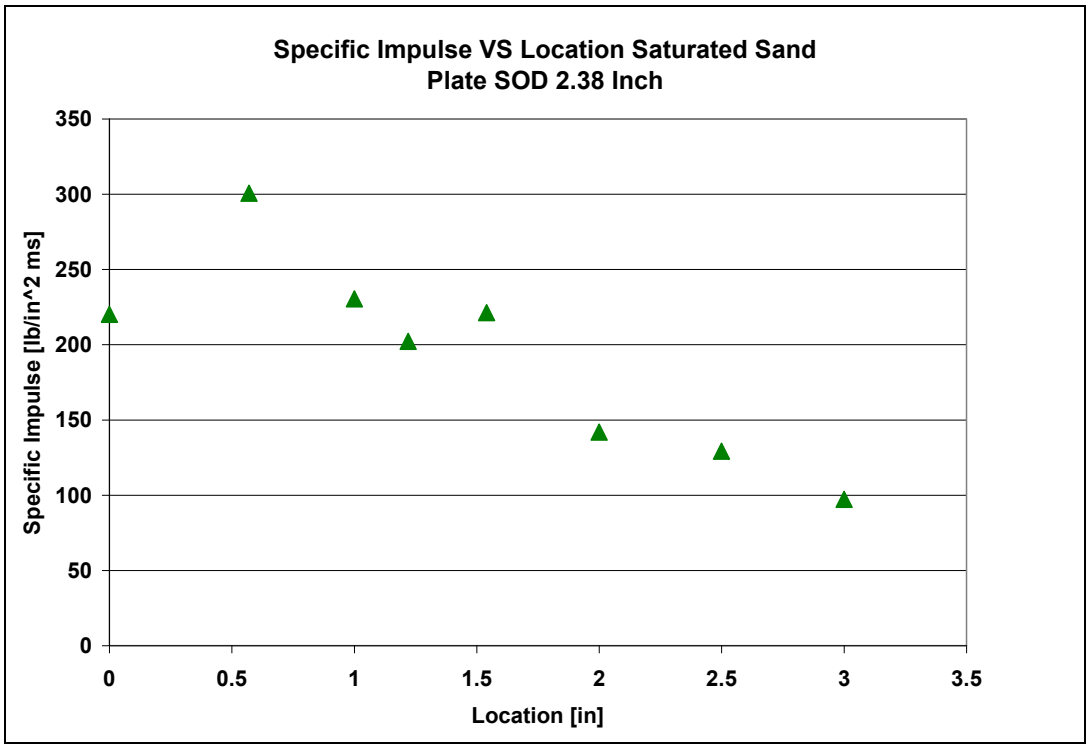

Figure 5.67 Specific impulse versus location at SOD 6 cm (2.38 inches)

Specific Impulse [(lb / in^2) * ms]	Specific Impulse [(lb / in^2) * s]	Distance [in]
220.208	0.220	0
300.661	0.301	0.57
230.464	0.230	1
202.232	0.202	1.22
221.335	0.221	1.54
141.938	0.142	2
129.247	0.129	2.5
97.188	0.097	3

Table 5.13 Specific Impulse results for saturated sand at SOD 6 cm (2.38 inches) and DOB 1 cm (0.39 inches)

5.3.2 Total Impulse Calculation at SOD 6 cm (2.38 inches) and DOB 1 cm (0.39 inches) in Saturated Sand

Using the specific impulse the total impulse can be calculated as shown in **Section 5.1.4**. A trend line based on the specific impulse values has to be established as in the other cases shown, see **Figure 5.68**. The total impulse is then defined as the volume of a solid obtained by rotating the given trend line around the vertical axis. **Figure 3.69** shows a three dimensional plot of the rotated trend line.

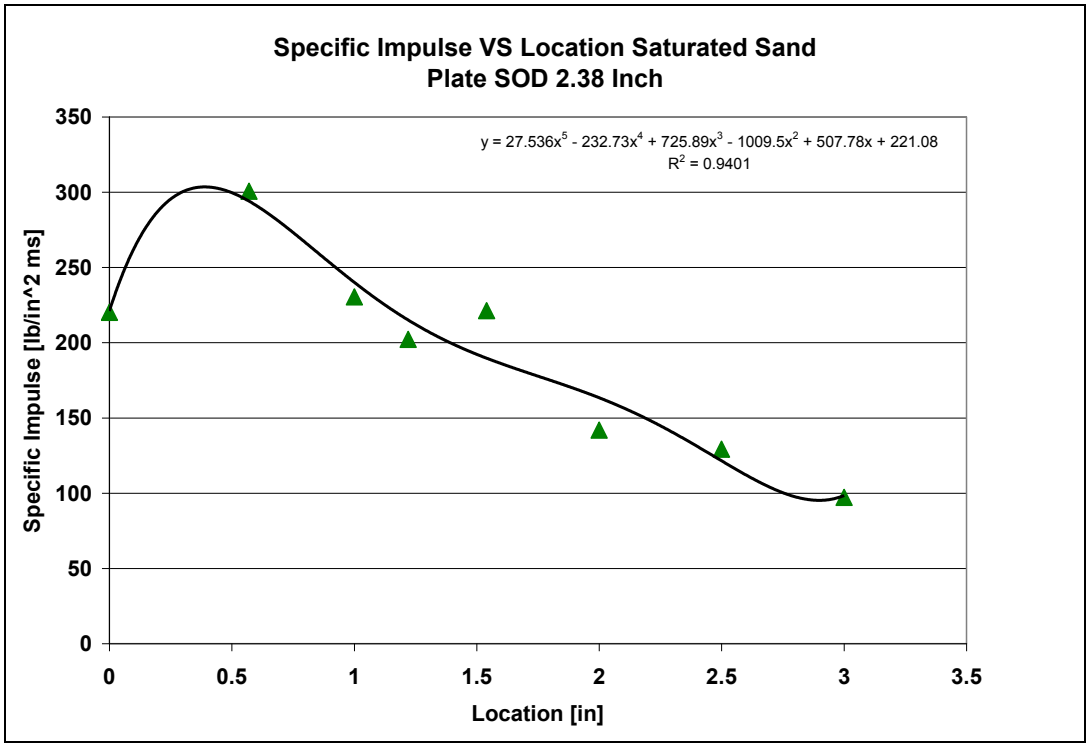

Figure 5.68 Specific impulse versus location including trend line for SOD 6 cm (2.38 inches)

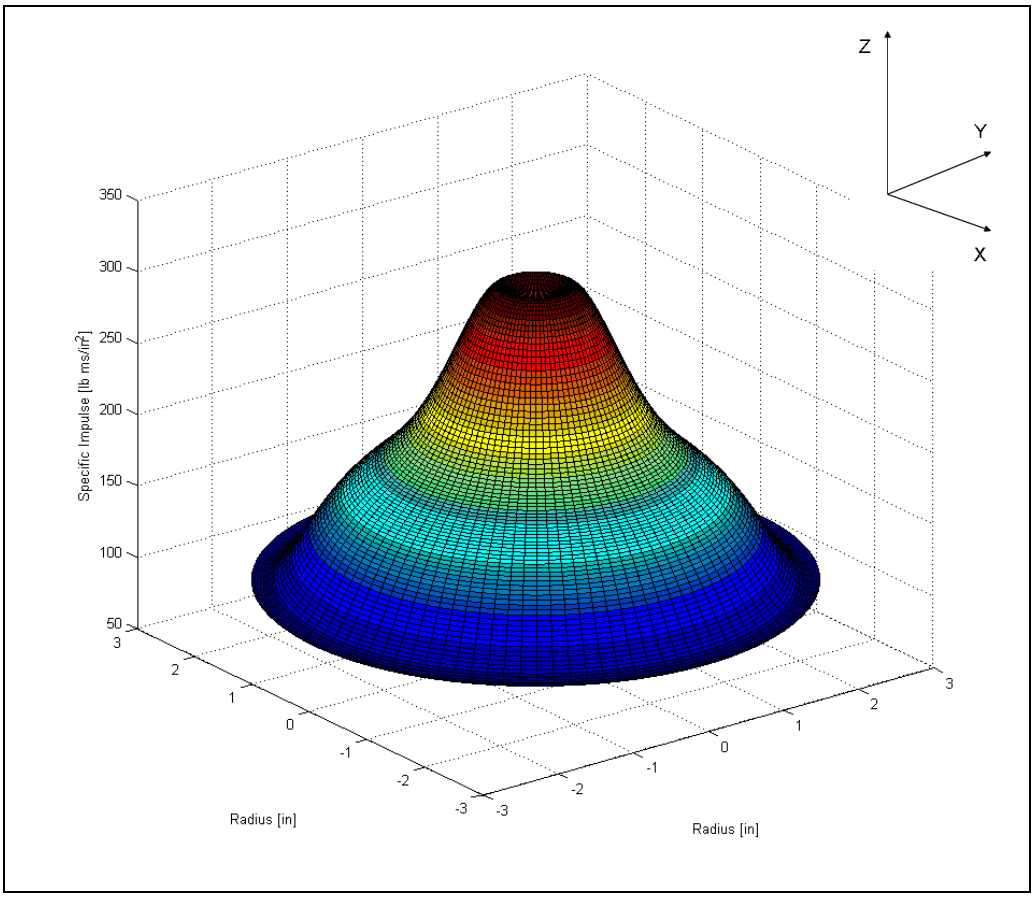

Figure 5.69 Solid obtained by rotating the given trend line at SOD 6 cm (2.38 inches)

Using the second approach as before, impulse segments over the radius of the plate can be calculated using the same method. Again instead of a trend line a straight line connecting the specific impulse values has to be established see **Figure 5.70**. The total impulse is obtained by rotating the given segments around the vertical axis. **Figure 5.71** shows a three dimensional plot of the rotated segments. The plot showing the segments emphasizes the step at the location of 3.91 cm (1.54 inches) more compared to the trend line shown in **Figure 5.67**.

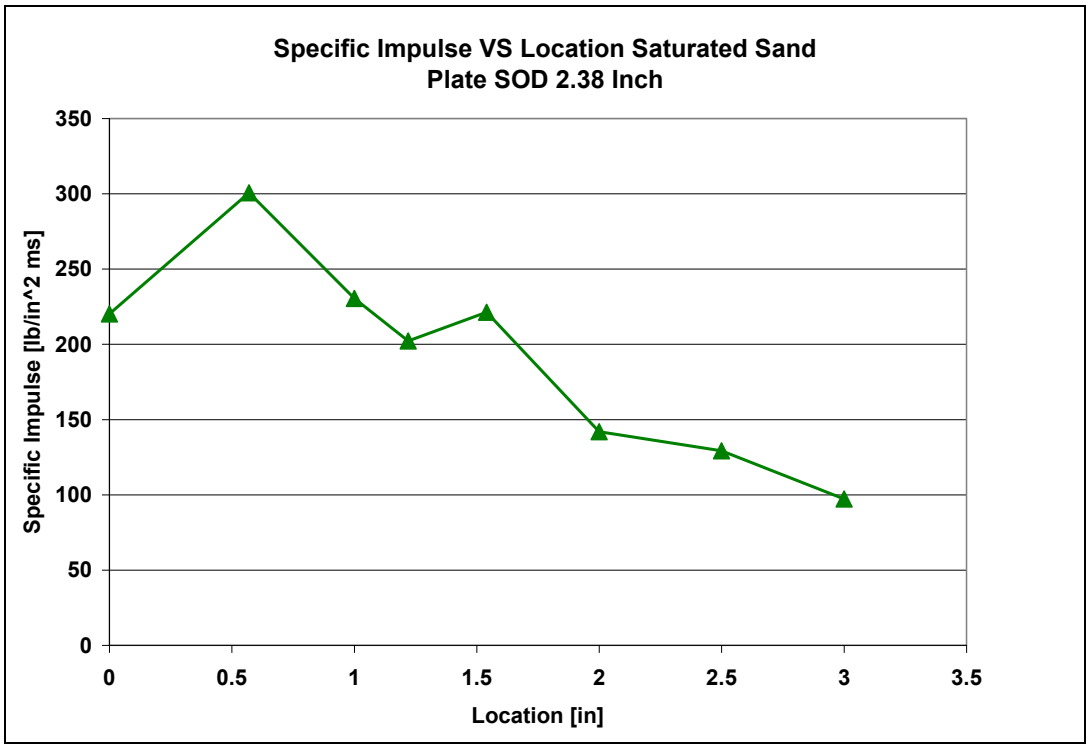

Figure 5.70 Specific impulse versus location at SOD 6 cm (2.38 inches)

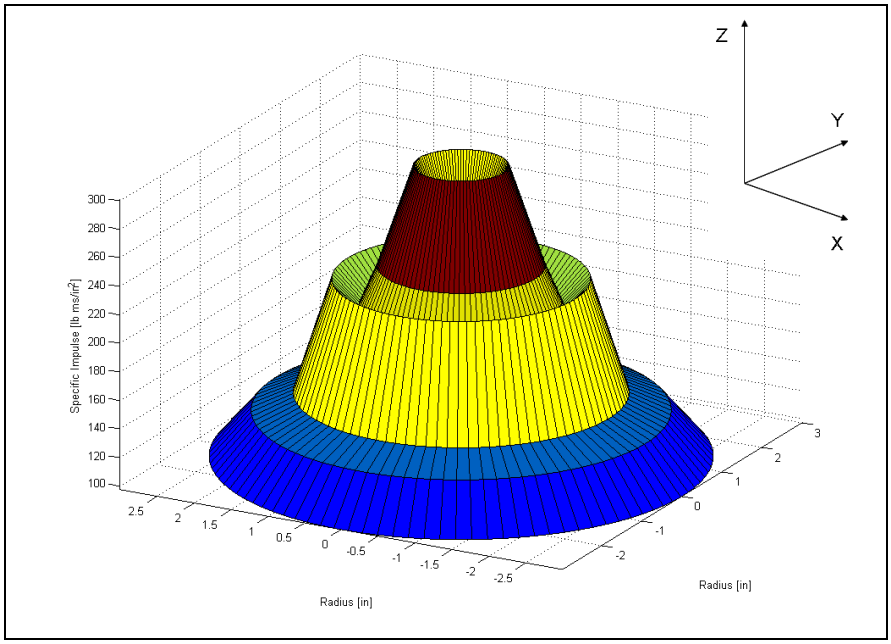

Figure 5.71 Solid obtained by rotating the given segments for SOD 6 cm (2.38 inches)

As described in **Section 5.14 Equations 5.4** to **5.12** are used in order to calculate the total impulse for this case for certain segments according to the definition. Depending on target plate size this allows evaluation of the total impulse absorbed by various target sizes at the SOD of 6 cm (2.38 inches).

Table 5.14 contains the results for calculating the impulse for each segment and the trend line. The accumulated impulse for the diameter of 15.24 cm (6 inches) is 20.51 Ns (4.61 lbs) which is almost the same as the total impulse of 20.37 Ns (4.58 lbs) calculated using the trend line in **Figure 5.68**. All the calculated impulse results are shown in **Figure 5.72**. It indicates how the impulse increases using larger size target plates.

Impulse Per Segment [lb s]	Total Impulse Accumulated [lb s]	Diameter [in]	Radius [in]
0.28	0.28	1.14	0.57
0.56	0.84	2	1
0.33	1.17	2.44	1.22
0.59	1.76	3.08	1.54
0.92	2.68	4	2
0.96	3.63	5	2.5
0.97	4.61	6	3
Trend Line			
4.58	4.58	6	3

Table 5.14 Impulse results for saturated sand at SOD 6 cm (2.38 inches) and DOB 1 cm (0.39 inches) for single segments and accumulated over diameter

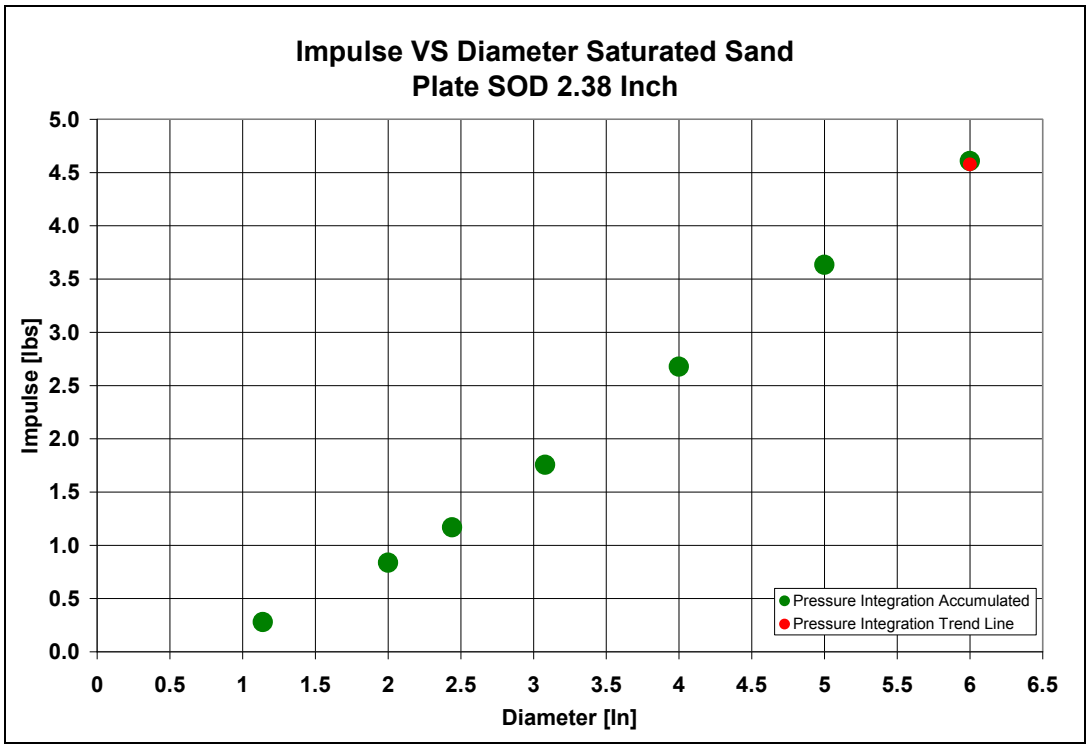

Figure 5.72 Impulse versus diameter of target plates for SOD 6 cm (2.38 inches)

5.4 Pressure – Time Profiles at SOD 4 cm (1.58 inches) and DOB 1 cm (0.39 inches) in Dry Sand

A test series was conducted duplicating the SOD of the target plate to 4 cm (1.58 inches) in dry sand. The DOB of 1 cm (0.39 inches) was kept the same as described in **Section 5.1** and **5.2**. The explosive charges used were 4.4 g of Deta Sheet. As explained in chapter 2 the loading mechanism for dry sand is very different compared to saturated sand. **Figure 4.30** in chapter 4 shows the top view of the dome development over time in dry sand using the same test set-up as described in this section. **Figure 4.30** shows the charge at 24 microseconds completely detonated and there appears to be a ring in the dry sand showing ionization. Apparently this causes a high level of noise which disables the Kolsky bars. The bars function like antennas and therefore record the noise. In order to use the Kolsky bars in the dry sand environment the bars and the target plate have to be shielded and connected to common ground. Each bar and the bars as a unit were shielded using aluminum foil. **Figure 5.73** shows the modified setup.

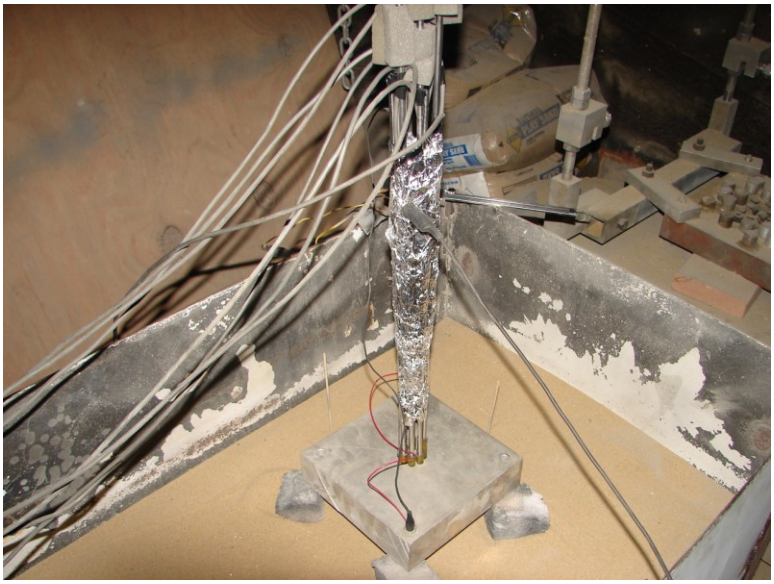

Figure 5.73 Shielded Kolsky bar setup in dry sand testing

Table 5.15 contains the results of 15 tests (184 recorded pressure – time profiles) conducted in dry sand. The pressure – time profiles were recorded using Kolsky bars at the locations of 0 cm (0 inches), 1.45 cm (0.57 inches), 2.54 cm (1 inch), 3.10 cm (1.22 inches), 3.91 cm (1.54 inches), 5.08 cm (2 inches), and 6.35 cm (2.5 inches). Since the peak pressure drops very fast further away from the center of impact, dynamic pressure sensors from PCB were used at the locations of 7.62 cm (3 inches), 8.89 cm (3.5 inches), 10.16 cm (4 inches), 11.43 cm (4.5 inches), and 12.70 cm (5 inches). At each mentioned location a total of 5 pressure sensors were used in a circular arrangement mounted flush to the bottom of the target plate. In total 2 pressure sensors of the type 113B24 (sensitivity 5.0 mV/PSI) and 3 sensors of the type S102B (sensitivity 1.0 mV/PSI) were used. The recorded pressure – time profiles were filtered using a low pass filter between 10 and 25 MHz according to the results of the Fourier spectra of each recorded profile.

The table contains values for the maximum and minimum peak pressure measured at each location. The average peak pressure is calculated and so is the standard deviation based on the number of profiles recorded at each location. The standard deviations are larger compared to the saturated sand case due to the change in loading mechanism. The loading applied to the target plate has a non-uniform character and the peak pressures and their impact times measured at certain locations are therefore more randomly distributed.

From 8.89 cm (3.5 inches) on to 12.70 cm (5 inches) the maximum, minimum and average pressure values stay pretty constantly low.

Location	Maximum Pressure	Minimum Pressure	Average Pressure	Number of Profiles	Standard Deviation
[Inch]	[PSI]	[PSI]	[PSI]		[PSI]
0	51,438	9,900	38,265	15	12,898
0.57	67,514	21,226	36,405	13	12,561
1	39,963	5,343	21,582	21	9,780
1.22	34,227	7,150	17,821	14	8,173
1.54	28,741	2,483	9,281	18	5,720
2	11,293	1,764	4,084	20	2,228
2.5	759	305	582	8	147
3	382	57	170	15	80
3.5	51	31	42	15	7
4	64	33	47	15	10
4.5	57	33	45	15	7
5	60	29	44	15	8

Table 5.15 Pressure - time results for dry sand at SOD 4 cm (1.58 inches) and DOB 1 cm (0.39 inches)

Figure 5.74 shows the maximum and minimum pressure measured and the average pressure calculated at specific locations of the plate. At the center of the plate the range of the pressure measured is largest but note that the average pressure is closer to the maximum pressure measured. Due to the loading mechanism it is possible that sometimes the center does absorb very low pressure. Even though the peak pressure rises at a distance of 1.45 cm (0.57 inches) the average pressure drops. With increasing distance from the center of the plate the peak pressure values drop very fast until they reach the location of 7.62 cm (3 inches). As mentioned pressure values stay constantly low from there on, see **Figure 5.75**.

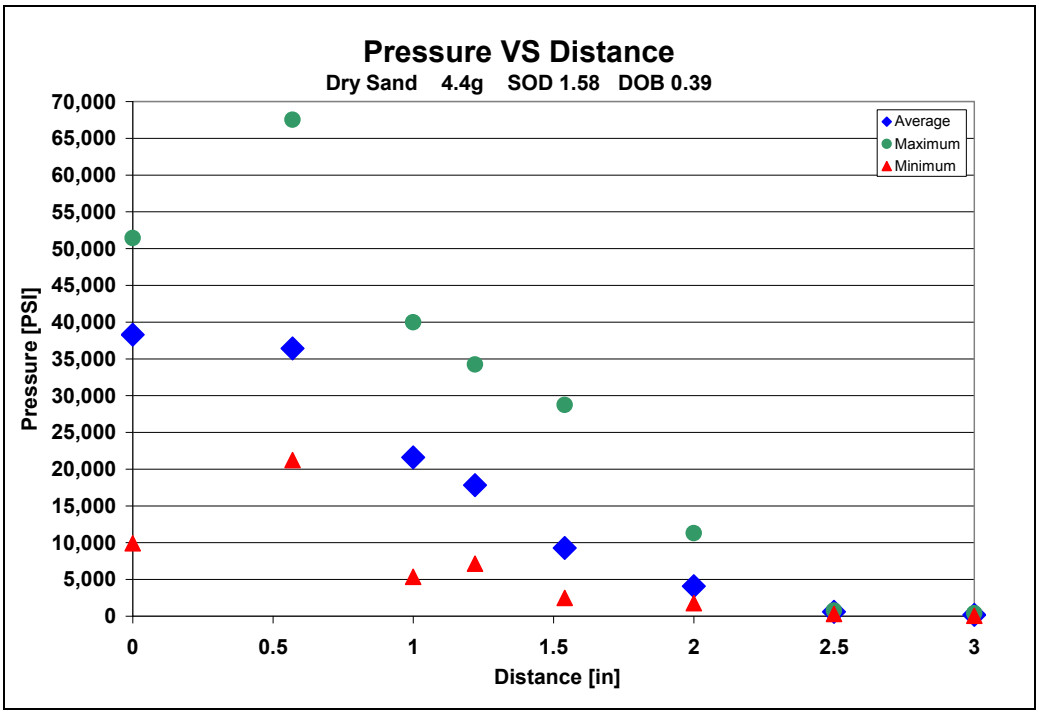

Figure 5.74 Pressure results for dry sand between 0 and 7.62 cm (3 inches) for SOD 4 cm (1.58 inches) and DOB 1 cm (0.39 inches)

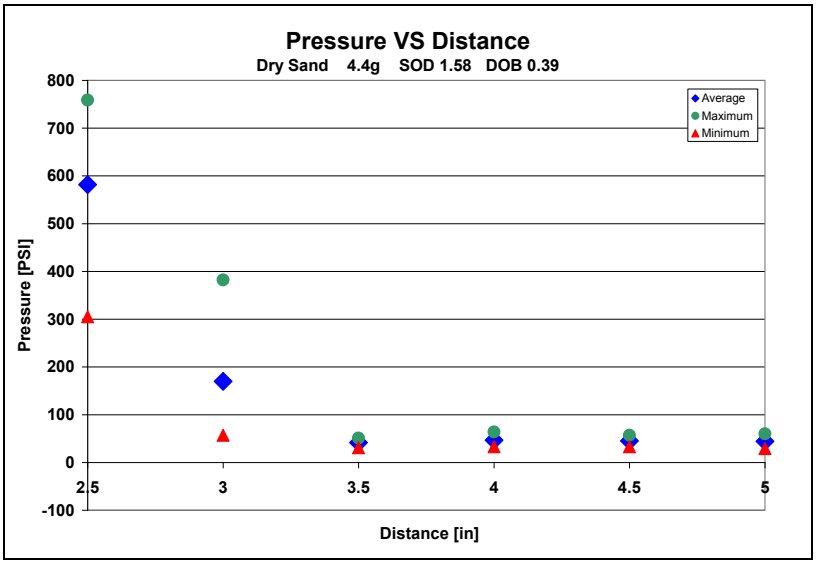

Figure 5.75 Pressure results for dry sand between 6.35 cm (2.5 inches) and 12.70 cm (5 inches) for SOD 4 cm (1.58 inches) and DOB 1 cm (0.39 inches)

As in the saturated sand cases each single measured pressure - time profile has to be shifted as described before in **Section 5.1**. Here the processing of the pressure – time profiles includes alignment of the peak pressures at each single location and calculation of the average pressure – time profile. The logarithmic decrement of each average profile is then calculated, shifted and drift compensated for the measurements taken using the pressure transducers.

Figure 5.76 contains all the processed average pressure – time profiles for dry sand which are subsequently used for calculating the specific impulse at the specific locations of the plate for the SOD of 4 cm (1.58 inches). The figure shows the correct average loading time intervals and the starting times of the loading for the dry sand case using a plate at a SOD of 4 cm (1.58 inches) and DOB of 1 cm (0.39 inches) and using a 4.4 g explosive charge. For a more detailed view compare **Figure 5.77**.

The pressure – time profile at the locations of 0 cm (0 inches) shows the shortest loading time. The loading times increase with increasing distance from the center of the plate. The profile at the location of 0 cm (0 inches) contains the highest peak pressure. From then on at the locations further away from the center of the plate the peak pressure drop and stay almost constant between 8.89 cm (3.5 inches) and 12.70 cm (5 inches). **Table 5.16** contains the specifics about loading times, intervals, and peak pressure shifts for each processed average pressure –time profile.

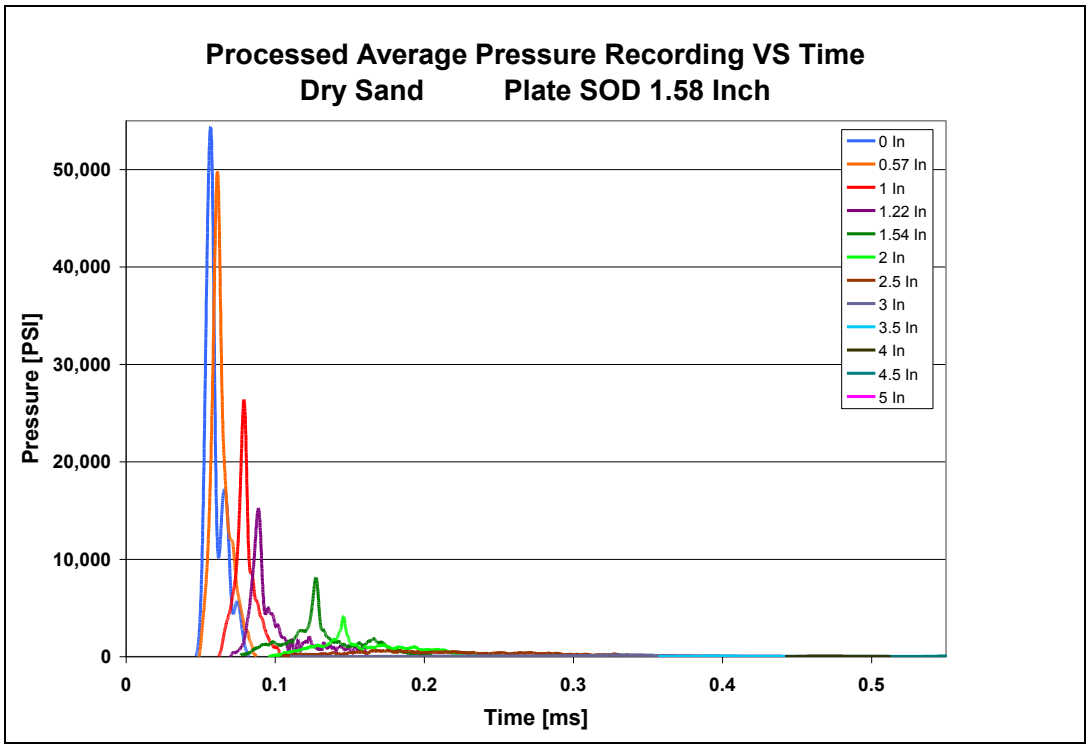

Figure 5.76 Processed pressure – time profiles at all locations at SOD 4 cm (1.58 inches) for dry sand

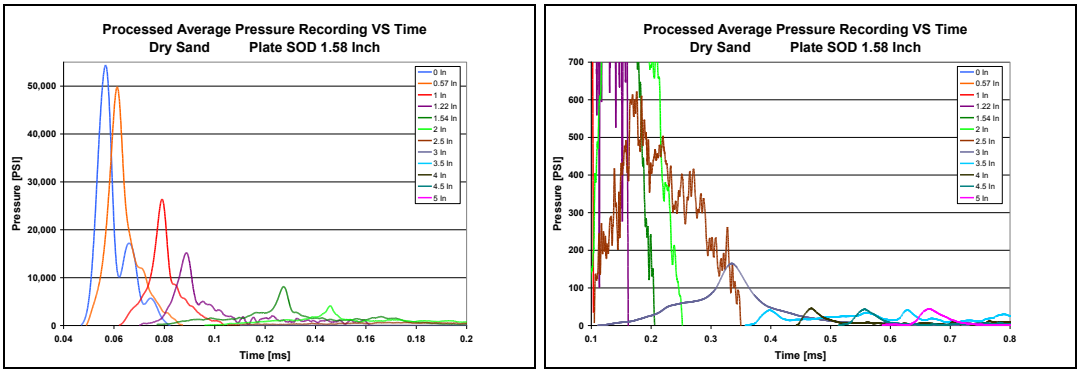

Figure 5.77 Details of the processed pressure – time profiles at all locations for dry sand

Location	Loading Duration	Start Time	End Time	Pressure Off-set Correction	Peak Pressure
[in]	[μs]	[ms]	[ms]	[PSI]	[PSI]
0	35	0.047	0.82	750	54,377
0.57	38	0.049	0.87	1,000	49,803
1	42	0.062	0.104	1,000	26,384
1.22	92	0.070	0.162	350	15,207
1.54	129	0.077	0.206	35	8,124
2	156	0.096	0.252	410	4,113
2.5	245	0.105	0.350	440	622
3	786	0.110	0.896	4	165
3.5	903	0.132	1.200	0.7	41
4	1180	0.193	1.373	0	46
4.5	1620	0.250	1.870	1.7	43
5	1630	0.370	2.000	0	44

Table 5.16 Loading time results for dry sand at SOD 4 cm (1.58 inches) and DOB 1 cm (0.39 inches)

Figure 5.78 shows the peak pressure and the loading time interval distribution versus the location at the bottom of the target plate for dry sand. The loading time interval shows a jump between 6.35 cm (2.5 inches) and 7.62 cm (3 inches). The peak pressure values peak at the center location of 0 cm (0 inches) and decline from then on and are lowest in the combination with the longest loading time intervals.

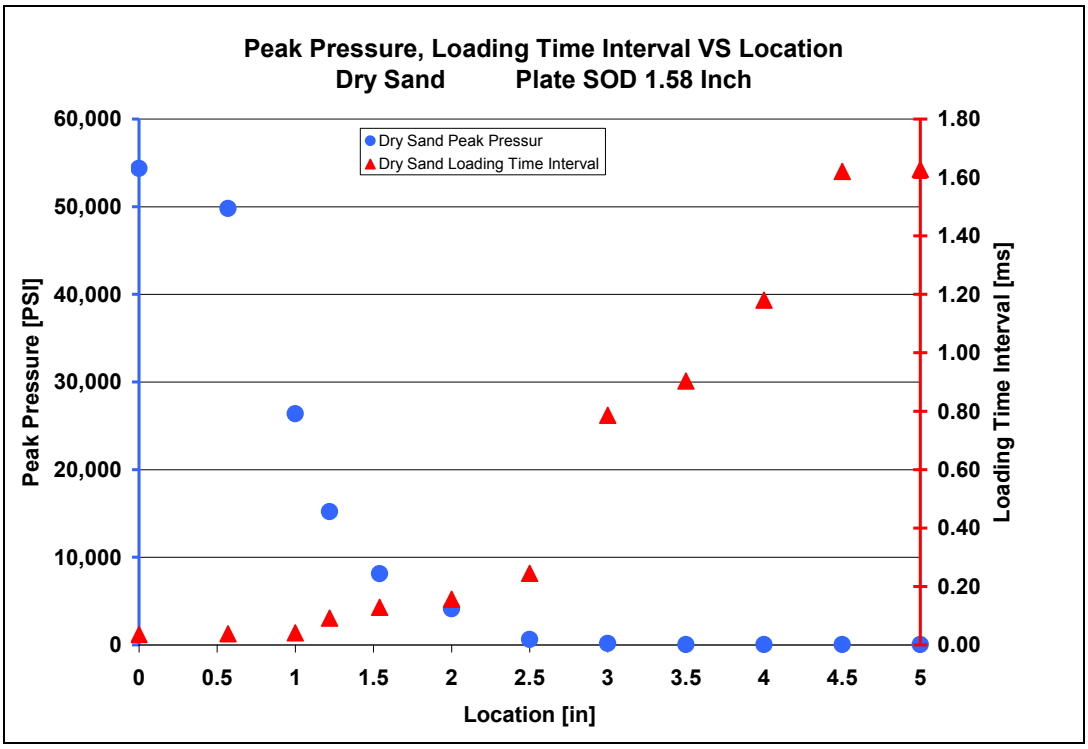

Figure 5.78 Peak pressure and loading time interval versus location at SOD 4 cm (1.58 inches) for dry sand

5.4.1 Specific Impulse Calculation at SOD 4 cm (1.58 inches) and DOB 1 cm (0.39 inches) in Dry Sand

Using the calculated average pressure – time profiles shown in **Figure 5.76** the specific impulse at each location is calculated. The specific impulses are shown in **Figure 5.79**. The specific impulse is highest at the center of the plate and at the location of 1.45 cm (0.57 inches) forming a plateau. Between 1.45 cm (0.57 inches) and 2.54 cm (1 inch) the specific impulse drops 50 %. From 2.54 cm (1 inch) to 7.62 cm (3 inches) the specific impulse decreases gradually keeping the slope almost constant. Between 7.62 cm (3 inches) and 12.70 cm (5 inches) the specific impulse stays almost constant and adds very little to the total impulse. **Table 5.17** contains all

results of the specific impulse calculation for the SOD of 4 cm (1.58 inches) for dry sand.

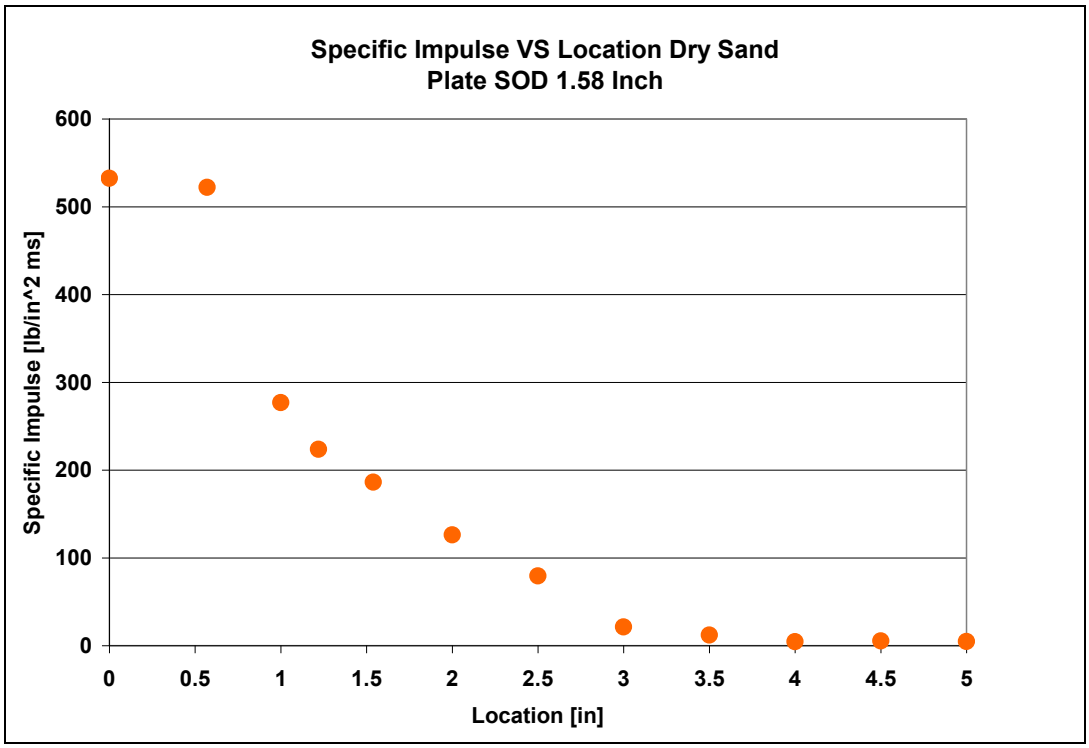

Figure 5.79 Specific impulse versus location at SOD 4cm (1,58 inches) for dry sand

Specific Impulse [(lb / in^2) * ms]	Specific Impulse [(lb / in^2) * s]	Distance [in]
532.336	0.532	0
522.123	0.522	0.57
276.787	0.277	1
223.739	0.224	1.22
186.303	0.186	1.54
126.228	0.126	2
79.452	0.079	2.5
21.233	0.021	3
12.095	0.012	3.5
4.497	0.004	4
5.295	0.005	4.5
4.841	0.005	5

Table 5.17 Specific Impulse results for dry sand at SOD 4 cm (1.38 inches) and DOB 1 cm (0.39 inches)

5.4.2 Total Impulse Calculation at SOD 4 cm (1.58 inches) and DOB 1 cm (0.39 inches) in Dry Sand

Using the specific impulse for dry sand the total impulse can be calculated as shown in **Section 5.1.4**. A trend line based on the specific impulse values has to be established as in the other cases shown, see **Figure 5.80**. The total impulse is then defined as the volume of a solid obtained by rotating the given trend line around the vertical axis. In the dry sand case two trend lines are established in order to better match the shape of the specific impulse distribution. **Figure 5.81** shows a three dimensional plot of the rotated trend line.

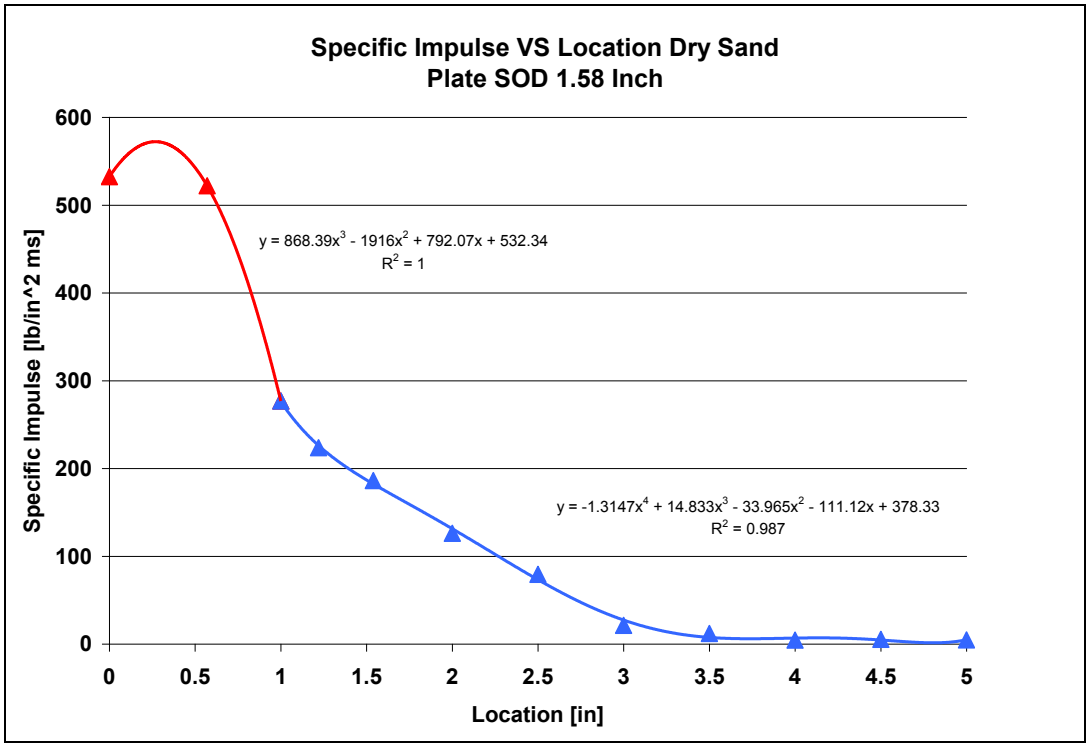

Figure 5.80 Specific impulse versus location including trend line for SOD 4 cm (1.58 inches) for dry sand

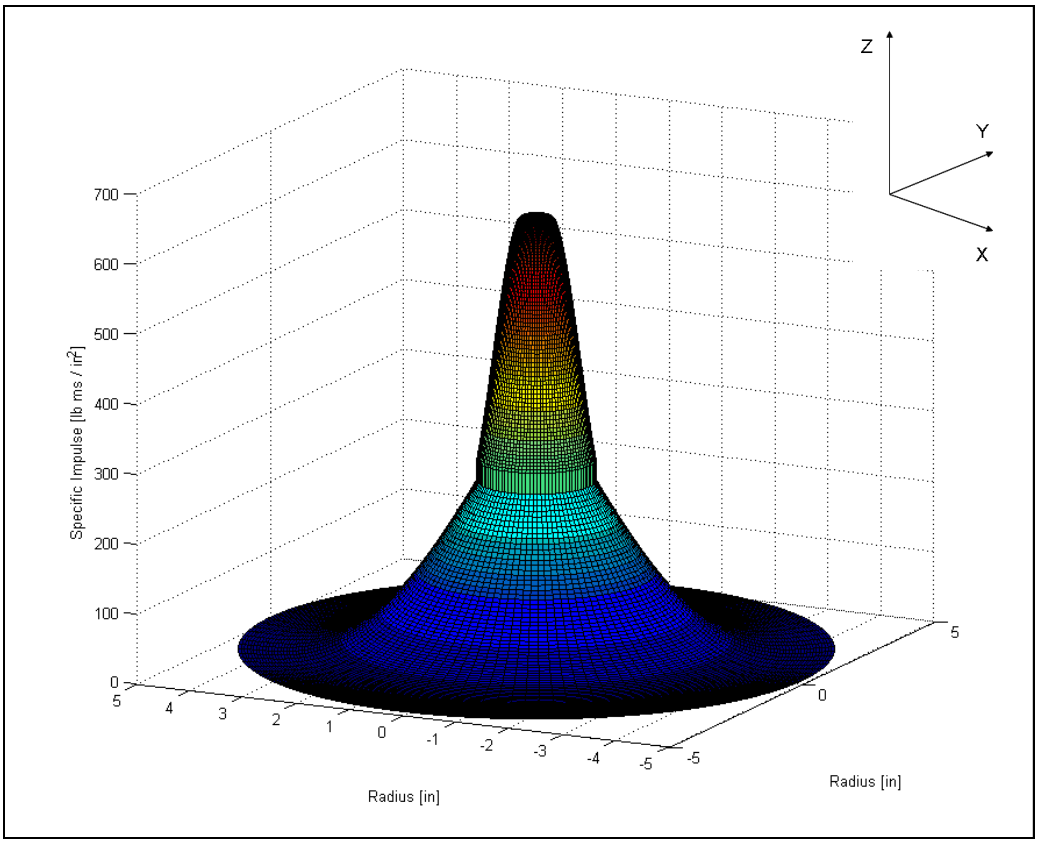

Figure 5.81 Solid obtained by rotating two given trend lines at SOD 4 cm (1.58 inches) for dry sand

Using the second approach as before, impulse segments over the radius of the plate can be calculated using the same method. Again instead of a trend line a straight line connecting the specific impulse values has to be established see **Figure 5.82**. The total impulse is obtained by rotating the given segments around the vertical axis. **Figure 5.83** shows a three dimensional plot of the rotated segments. The plot showing the segments emphasizes the plateau between 0 and 1.45 cm (0.57 inches).

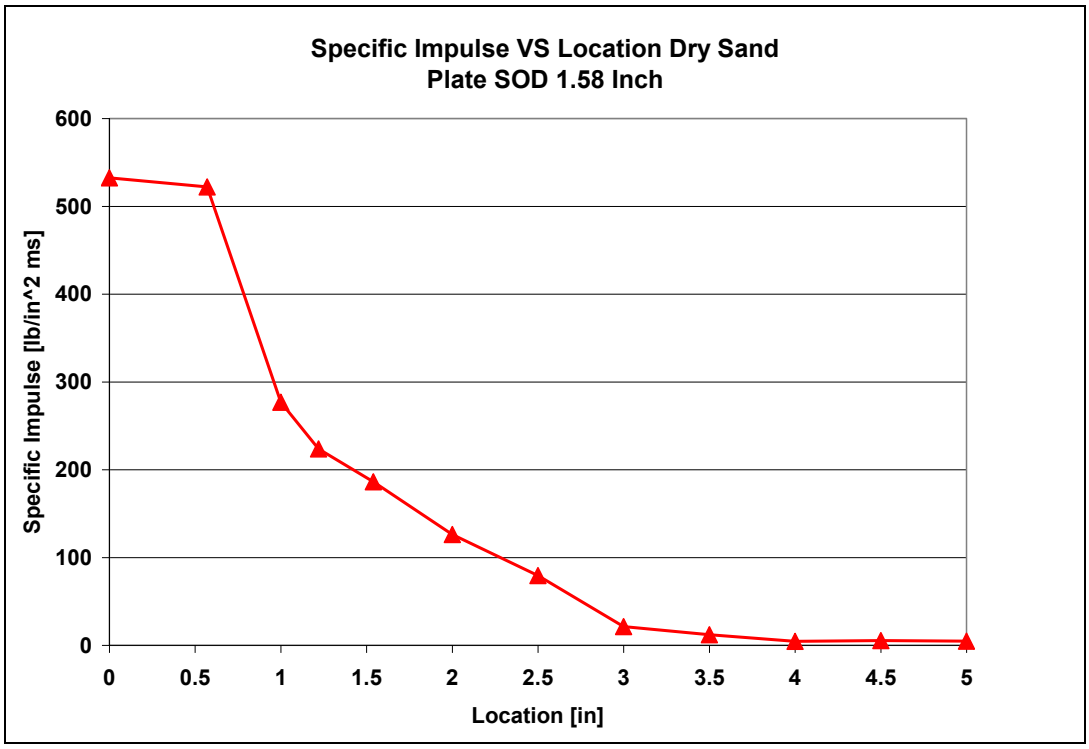

Figure 5.82 Specific impulse versus location at SOD 4 cm (1.58 inches) for dry sand

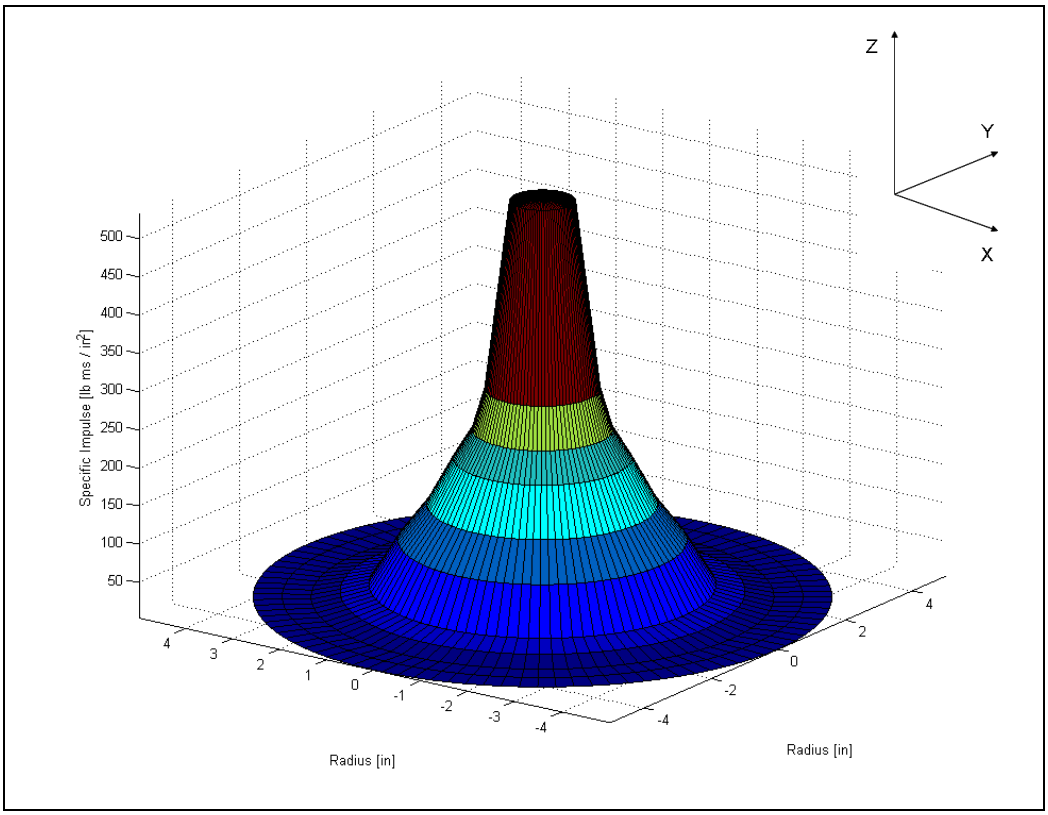

Figure 5.83 Solid obtained by rotating the given segments for SOD 4 cm (1.58 inches) for dry sand

Equations 5.4 to **5.12** are used in order to calculate the total impulse for the dry sand case for certain segments according to the definition. Depending on target plate size this allows evaluation of the total impulse absorbed by the target at the SOD of 4 cm (1.58 inches) under dry sand conditions.

Table 5.18 contains the results for calculating the impulse for each segment and the 2 trend lines. The accumulated impulse for the diameter of 25.40 cm (10 inches) is 20.73 Ns (4.66 lbs) which is almost the same as the total impulse of 20.06 Ns (4.51 lbs) calculated using the 2 trend lines in **Figure 5.80**. All the calculated impulse results are shown in **Figure 5.84**. It indicates how the impulse increases using larger size target plates.

Impulse Per Segment [lb s]	Total Impulse Accumulated [lb s]	Diameter [in]	Radius [in]
0.54	0.54	1.14	0.57
0.82	1.36	2	1
0.38	1.74	2.44	1.22
0.57	2.31	3.08	1.54
0.79	3.10	4	2
0.72	3.82	5	2.5
0.43	4.25	6	3
0.17	4.42	7	3.5
0.10	4.52	8	4
0.07	4.58	9	4.5
0.08	4.66	10	5
2 Trend Lines			
1.41	1.41	2	1
3.10	3.10	10	5
	4.51	10	5

Table 5.18 Impulse results for dry sand at SOD 4 cm (1.58 inches) and DOB 1 cm (0.39 inches) for single segments and accumulated over diameter

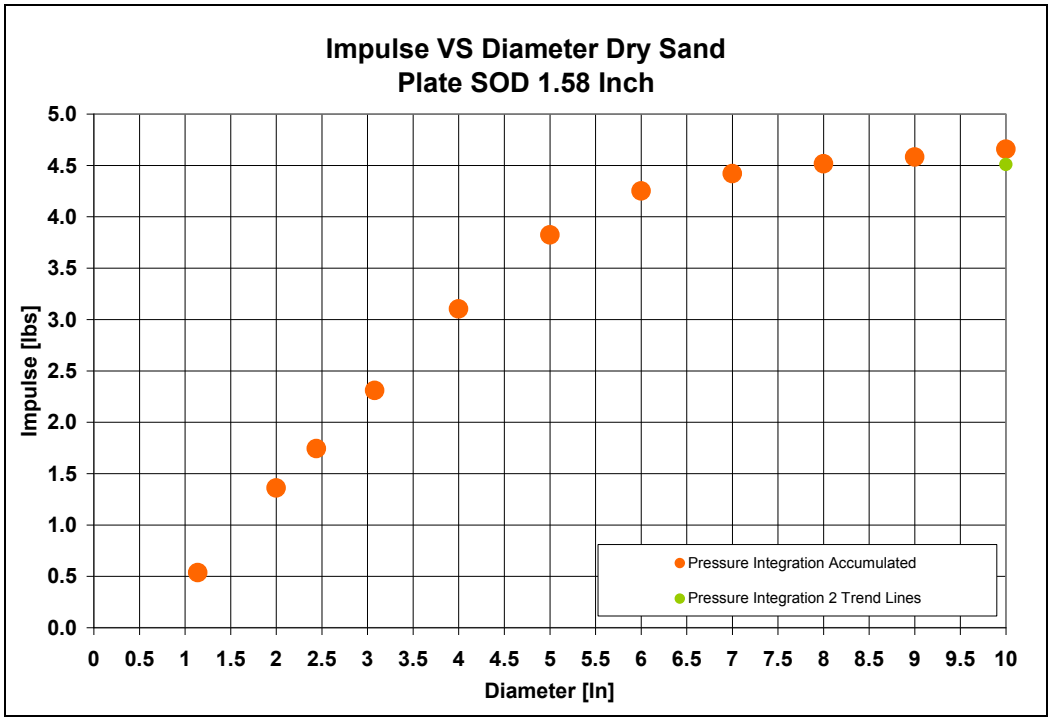

Figure 5.84 Impulse versus diameter of target plates for SOD 4 cm (1.58 inches) for dry sand

5.4.3 Impulse Measurement at SOD 4 cm (1.58 inches) and DOB 1 cm (0.39 inches) in Dry Sand

A test series for dry sand using a variety of plates of different diameters (**Figure 5.33**) keeping the weight constant (10.3 kg) was conducted in the Dynamic Effects Laboratory. The test setup was the same as being used for the pressure measurement series in dry sand. Several diameters were used in order to determine the impulse distribution over the diameter of a plate. By increasing the diameter eventually a plate size is achieved in which the maximum impulse is delivered. The diameters used were the same as for saturated sand test series [5.08 cm (2 inches), 10.16 cm (4 inches), 15.24 cm (6 inches), 20.32 cm (8 inches), 25.4 cm (10 inches), 36.32 cm (14.3 inches), and 48.26 cm (19 inches)].

The test results are shown in **Figure 5.85**. The impulse increases steadily over the first 20.32 cm (8 inches) of diameter. With further increasing diameter the impulse increases very little. The largest plate diameter of 48.26 cm (19 inches) shows a slightly higher impulse value which is questionable.

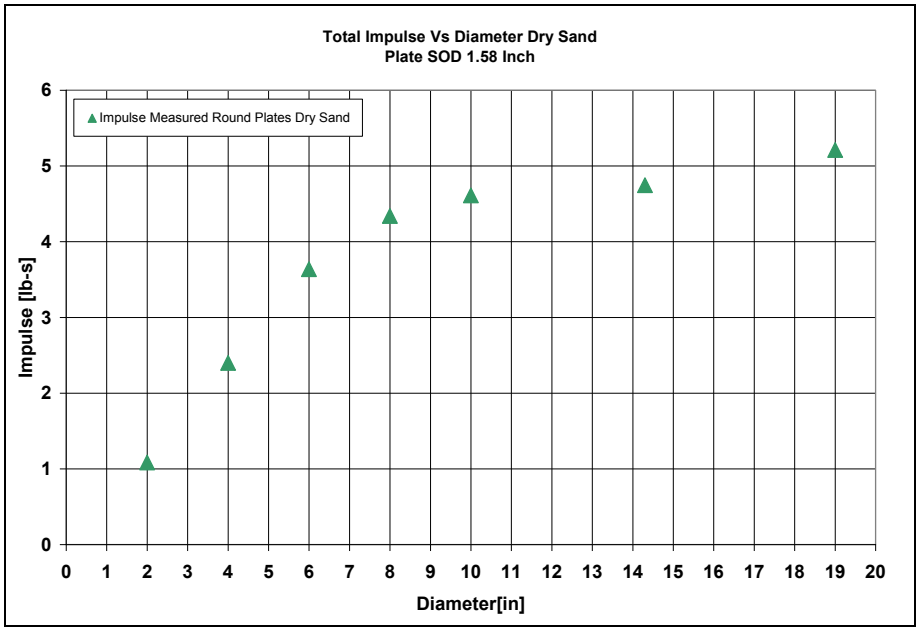

Figure 5.85 Impulse results round plates for dry sand

5.4.4 Verification of Pressure Test Results at SOD 4 cm (1.58 inches) and DOB 1 cm (0.39 inches) in Dry Sand Using Impulse Results Round Plates

Plotting the test results gained by the integration of the pressure measurements (**Figure 5.84**) and the results of impulse measured using the round plates on the same plot, shows that both data sets agree pretty well (**Figure 5.86**) at the diameter of 25.40 cm (10 inches). However the slope for the pressure tests has a steeper rise compared to the integrated pressure values. A reason for the differences in the slopes can be that it is uncertain if the plate mass / explosive mass ratio for dry sand should be the same as for saturated sand. The weight of 10.3 kg for the target plates was chosen according to a test series conducted before in saturated sand in order to determine the maximum impulse delivered to a target plate, see **Figure 5.34**. This ratio might be different for impulse testing using dry sand.

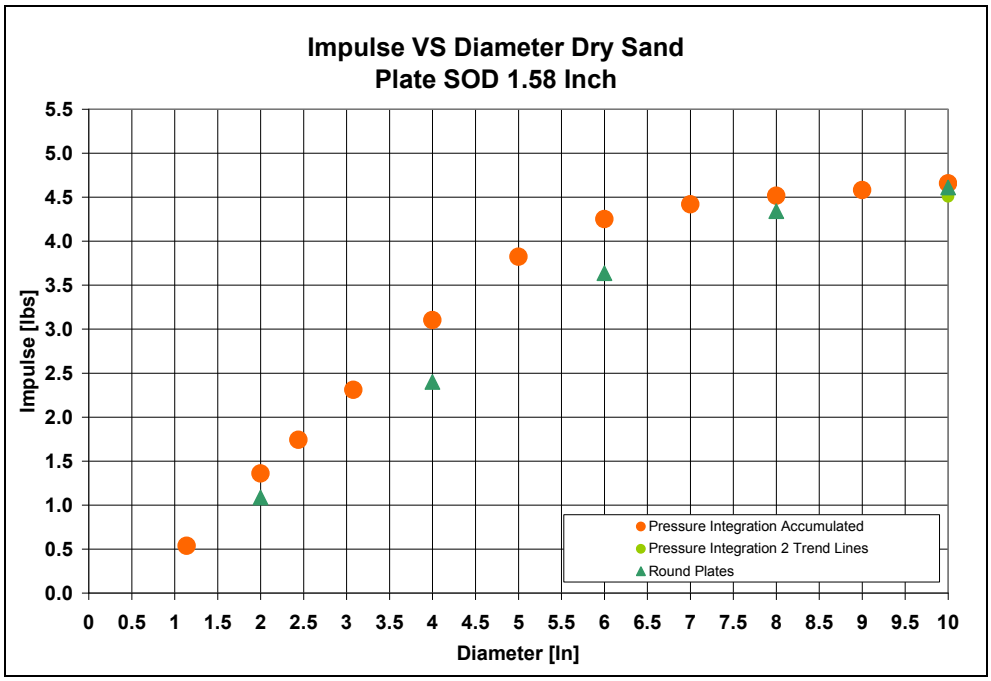

Figure 5.86 Impulse results round plates and pressure integration for dry sand

5.5 Pressure – Time Profiles at SOD 4 cm (1.58 inches) and DOB 1 cm (0.39 inches) in Water

An additional test series was conducted using water matching the SOD of the target plate of 4 cm (1.58 inches) in dry sand and saturated sand. The DOB of 1 cm (0.39 inches) was kept the same as described in **Section 5.1** and **5.2**. The explosive charges used were 4.4 g of Deta Sheet. Again as shown in chapter 2 the loading mechanism for water is very different compared to saturated and dry sand. **Figure 4.32** in chapter 2 shows the top view of the dome development over time in water using the same test set-up as described in this section. **Figure 5.87** shows the modified test setup using a frame in order to keep the charge centered under the test plate. The charge is held at the exact SOD by using a wooden stick. This allows detonating the charge in water without any interference of a close boundary effect. **Figure 5.88** shows the setup from the top before the water level is adjusted to the required SOD of 4 cm (1.58 inches).

Figure 5.87 Test setup for water testing using a frame and a wooden stick

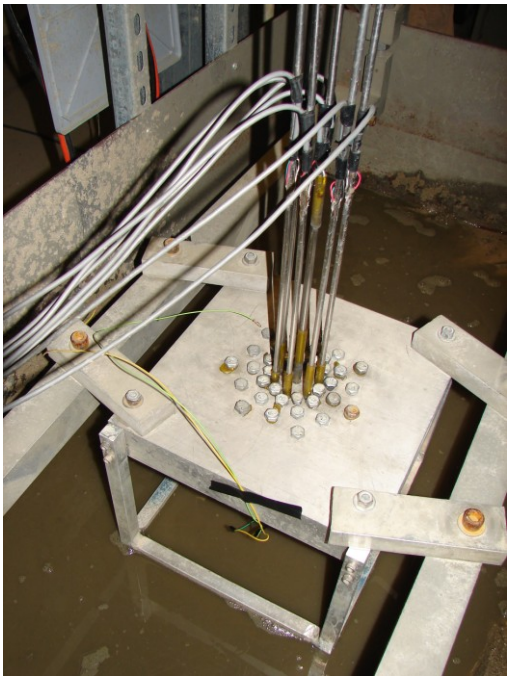

Figure 5.88 Test setup for water testing using a frame and a wooden

Table 5.19 contains the results of 22 tests (156 recorded pressure – time profiles) conducted in water. The pressure – time profiles were recorded using Kolsky bars at the locations of 0 cm (0 inches), 1.45 cm (0.57 inches), 2.54 cm (1 inch), 3.91 cm (1.54 inches), 5.08 cm (2 inches), 6.35 cm (2.5 inches), and 7.62 cm (3.0 inches). The table contains values for the maximum and minimum peak pressure measured at each location. The average peak pressure is calculated and so is the standard deviation based on the number of profiles recorded at each location. The standard deviation values are lower at the locations of 0 cm (0 inches), 1.45 cm (0.57 inches), and 2.54 cm (1 inch) compared to all saturated sand and dry sand cases due to the change in loading mechanism for water. The loading applied to the target plate has a very uniform character and the peak pressures and their impact times measured at certain locations are therefore more uniformly distributed. But at the location of 3.91 cm (1.54 inches) the standard deviation is very high due to the large range between low and high pressures measured.

Location	Maximum Pressure	Minimum Pressure	Average Pressure	Number of Profiles	Standard Deviation
[Inch]	[PSI]	[PSI]	[PSI]		[PSI]
0	51,907	31,126	43,718	19	5,643
0.57	36,789	21,806	28,804	12	5,048
1	41,516	26,288	32,176	25	4,224
1.54	49,454	9,989	22,935	46	10,787
2	19,353	6,009	12,423	27	2,960
2.5	9,710	4,136	6,572	13	1,661
3	5,518	2,821	4,320	14	750

Table 5.19 Pressure - time results water at SOD 4 cm (1.58 inches) and DOB 1 cm (0.39 inches)

Figure 5.89 shows the maximum and minimum pressure measured and the average pressure calculated at specific locations of the plate. At the location of 3.91 cm (1.54 inches) of the plate the range of the pressure measured is largest but note that the average pressure is closer to the minimum pressure measured. The largest average pressure is measured at the center of the plate and drops at the location of 1.45 cm (0.57 inches) but rises again at the location of 2.54 cm (1 inch). Between the location of 2.54 cm (1 inch) and 7.62 cm (3 inches) the average pressure drops consistently.

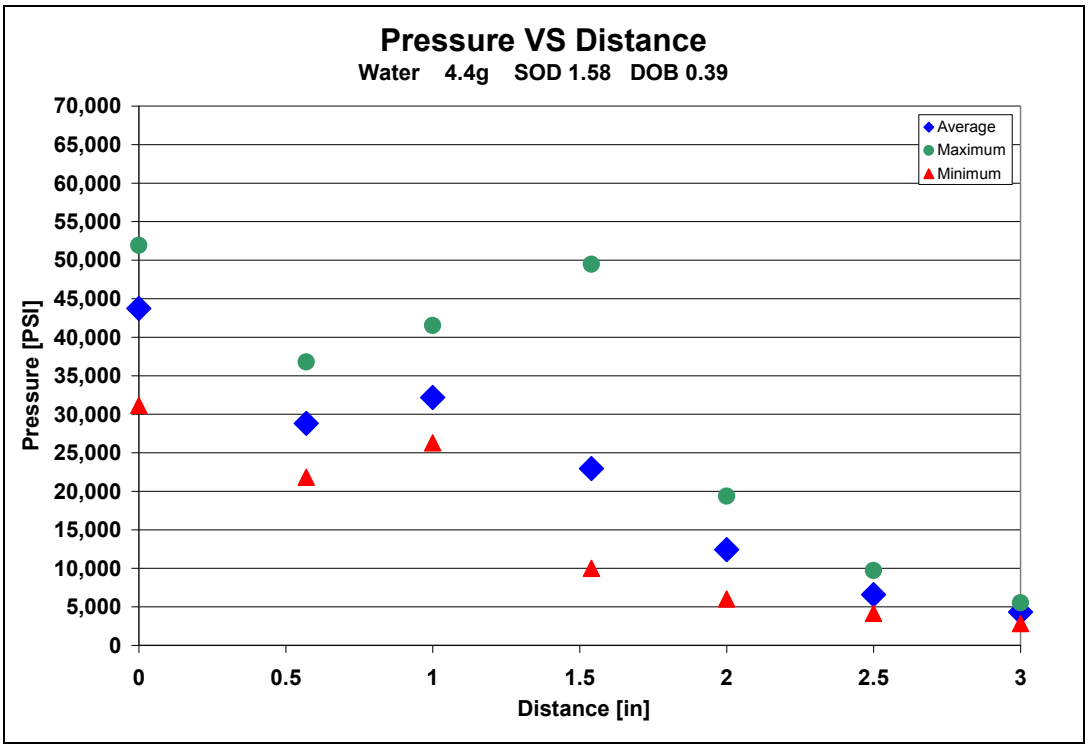

Figure 5.89 Pressure results for water

As in the saturated sand and dry sand cases each single measured pressure - time profile has to be shifted as described before in **Section 5.1**. Here the processing of the pressure – time profiles includes alignment of the peak pressures at each single location and calculation of the average pressure – time profile. The logarithmic decrement of each average profile is then calculated, shifted and drift compensated for the measurements taken using Kolsky bars.

Figure 5.90 contains all the processed average pressure – time profiles for water which are subsequently used for calculating the specific impulse at the specific locations of the plate for the SOD of 4 cm (1.58 inches). The figure shows the correct average loading time intervals and the starting times of the loading for the water case using a plate at a SOD of 4 cm (1.58 inches) and DOB of 1 cm (0.39 inches) and using a 4.4 g explosive charge.

The pressure – time profile at the locations of 0 cm (0 inches) shows the shortest loading time. The loading times increase with increasing distance from the

center of the plate. The profile at the location of 0 cm (0 inches) contains the highest peak pressure. At the location of 1.45 cm (0.57 inches) the peak pressure drops to almost the same level as at the location of 3.91 cm (1.54 inches). **Table 5.20** contains the specifics about loading times, intervals, and peak pressure shifts for each processed average pressure –time profile.

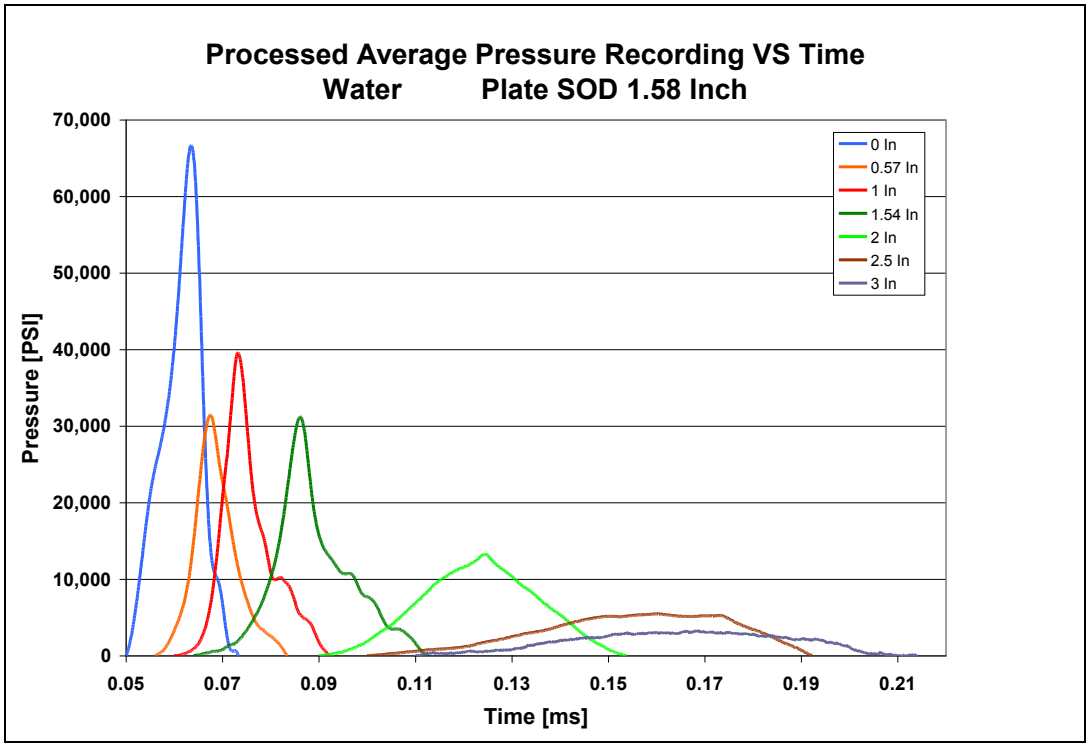

Figure 5.90 Processed pressure – time profiles at all locations at SOD 4 cm (1.58 inches) for water

Location	Loading Duration	Start Time	End Time	Pressure Off-set Correction	Peak Pressure
[in]	[µs]	[ms]	[ms]	[PSI]	[PSI]
0	23	0.050	0.073	3000	66,675
0.57	27	0.056	0.083	2,000	31,463
1	32	0.060	0.092	2,000	39,554
1.54	48	0.064	0.112	650	31,207
2	64	0.090	0.154	1,000	13,259
2.5	92	0.100	0.192	670	5,476
3	104	0.110	0.214	1,000	3,313

Table 5.20 Loading time results for water at SOD 4 cm (1.58 inches) and DOB 1 cm (0.39 inches)

Figure 5.91 shows the peak pressure and the loading time interval distribution versus the location at the bottom of the target plate for water. The loading time interval increases exponential with increasing distance from the center of the target plate. The peak pressure values peak at the center location of 0 cm (0 inches) and at the location of 1.45 cm (0.57 inches) the peak pressure shows a drop. At 2.54 cm (1 inch) the peak pressure rises again and declines from then on and is lowest in the combination with the longest loading time interval.

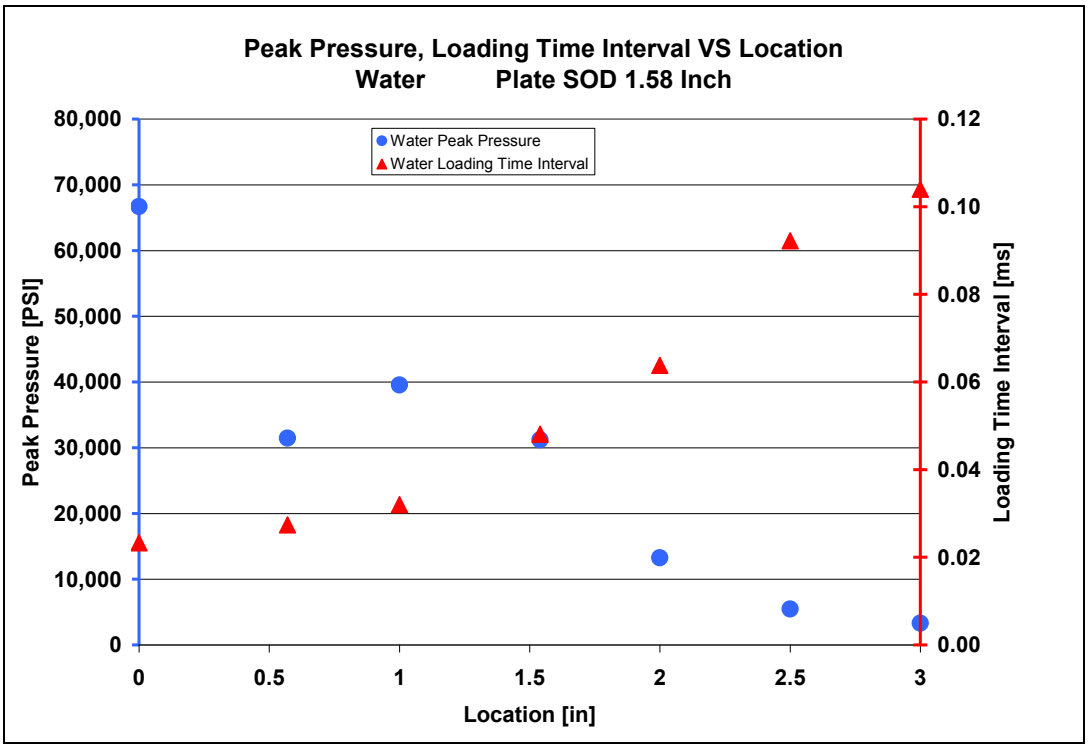

Figure 5.91 Peak pressure and loading time interval versus location at SOD 4 cm (1.58 inches) for water

5.5.1 Specific Impulse Calculation at SOD 4 cm (1.58 inches) and DOB 1 cm (0.39 inches) in Water

Using the calculated average pressure – time profiles shown in **Figure 5.90** the specific impulse at each location is calculated. The specific impulses are shown in **Figure 5.92**. The specific impulse is highest at the center of the plate and dips at the location of 1.45 cm (0.57 inches). The specific impulse forms an arc between the location of 1.45 cm (0.57 inches) and 7.62 cm (3 inches), showing the maximum at the location of 3.91 cm (1.54 inches).

Table 5.21 contains all results of the specific impulse calculation for the SOD of 4 cm (1.58 inches) for water.

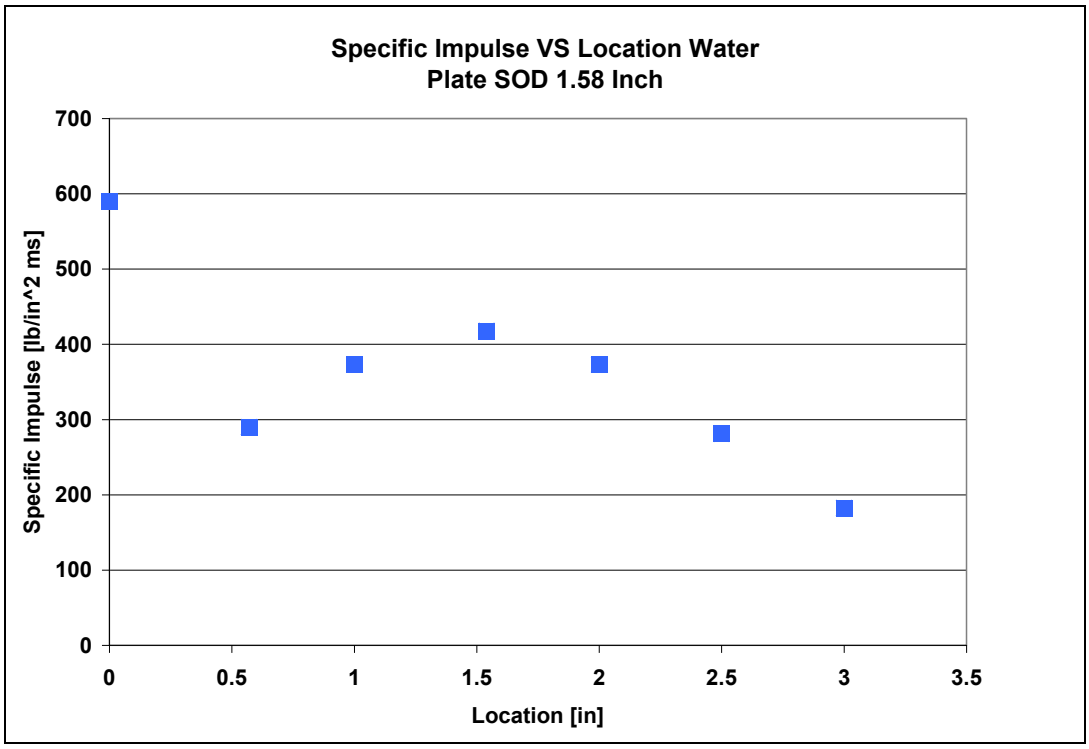

Figure 5.92 Specific impulse versus location at SOD 4 cm (1.58 inches) for water

Specific Impulse [(lb / in^2) * ms]	Specific Impulse [(lb / in^2) * s]	Distance [in]
589.838	0.590	0
289.935	0.290	0.57
372.874	0.373	1
417.569	0.418	1.54
373.000	0.373	2
281.107	0.281	2.5
182.368	0.182	3

Table 5.21 Specific Impulse results for water at SOD 4 cm (1.58 inches) and DOB 1 cm (0.39 inches)

5.5.2 Total Impulse Calculation at SOD 4 cm (1.58 inches) and DOB 1 cm (0.39 inches) in Water

Using the specific impulse for water the total impulse can be calculated as in **Section 5.1.4**. A trend line based on the specific impulse values has to be established as in the other cases shown, see **Figure 5.93**. The total impulse is then defined as the volume of a solid obtained by rotating the given trend line around the vertical axis. **Figure 5.94** shows a three dimensional plot of the rotated trend line.

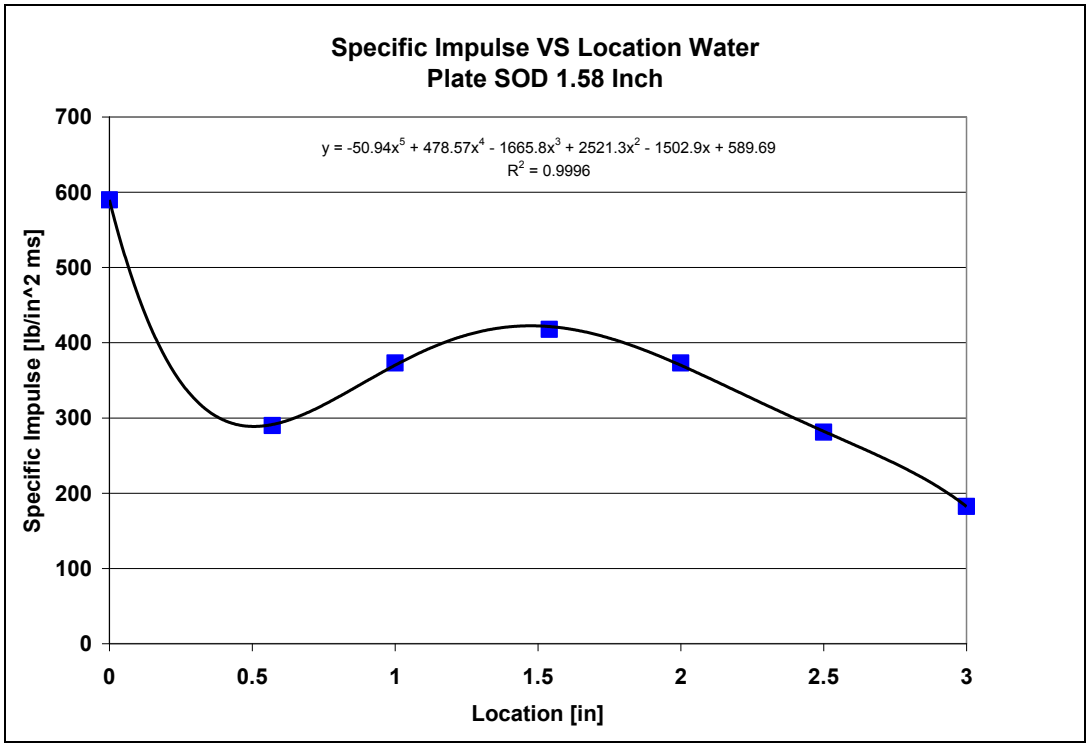

Figure 5.93 Specific impulse versus location including trend line for SOD 4 cm (1.58 inches) for water

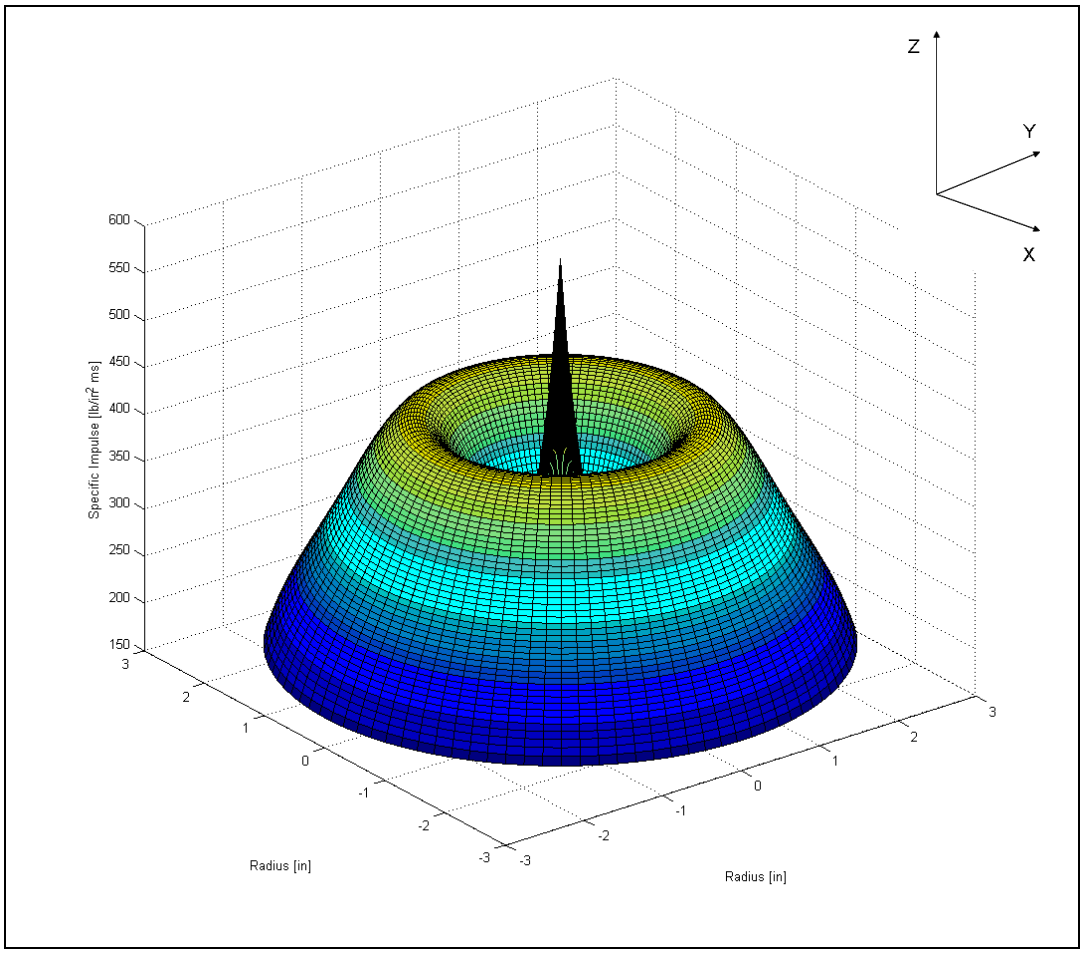

Figure 5.94 Solid obtained by rotating the trend line at SOD 4 cm (1.58 inches) for water

Using the second approach, impulse segments over the radius of the plate can be calculated using the same method. Again instead of a trend line a straight line connecting the specific impulse values has to be established see **Figure 5.95**. The total impulse is obtained by rotating the given segments around the Z – axis. **Figure 5.96** shows a three dimensional plot of the rotated segments. The plot showing the segments emphasizes the plateau between 0 and 1.45 cm (0.57 inches).

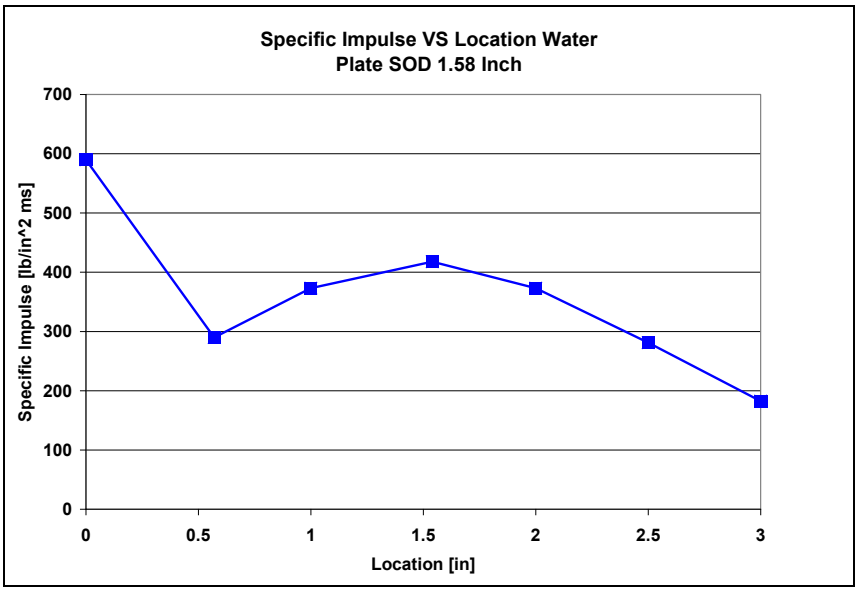

Figure 5.95 Specific impulse versus location at SOD 4 cm (1.58 inches) for water

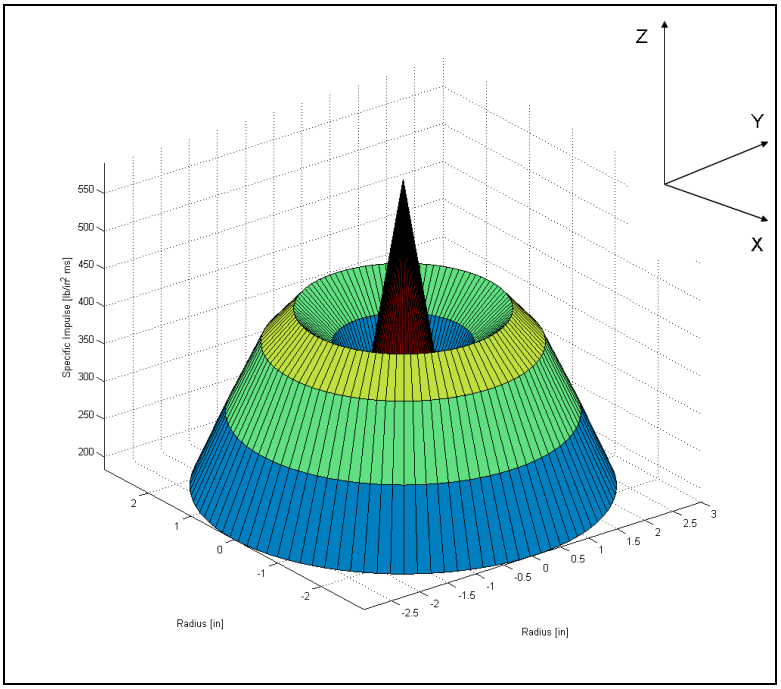

Figure 5.96 Solid obtained by rotating the given segments for SOD 4 cm (1.58 inches) for water

Equations 5.4 to **5.12** are used in order to calculate the total impulse for the water case for certain segments according to the definition. Depending on target plate size this allows evaluation of the total impulse absorbed by a target of given size at the SOD of 4 cm (1.58 inches) under water conditions.

Table 5.22 contains the results for calculating the impulse for each segment and the trend line. The accumulated impulse for the diameter of 15.24 cm (6 inches) is 40.57 Ns (9.12 lbs) which is almost the same as the total impulse of 40.75 Ns (9.16 lbs) calculated using the trend line in **Figure 5.93**. All the calculated impulse results are shown in **Figure 5.97**. It indicates how the impulse increases using larger size target plates.

Impulse Per Segment [lb s]	Total Impulse Accumulated [lb s]	Diameter [in]	Radius [in]
0.40	0.40	1.14	0.57
0.71	1.11	2	1
1.71	2.82	3.08	1.54
2.02	4.84	4	2
2.30	7.14	5	2.5
1.99	9.12	6	3
Trend Line			
9.16	9.16	6	3

Table 5.22 Impulse results for water at SOD 4 cm (1.58 inches) and DOB 1 cm (0.39 inches) for single segments and accumulated over diameter

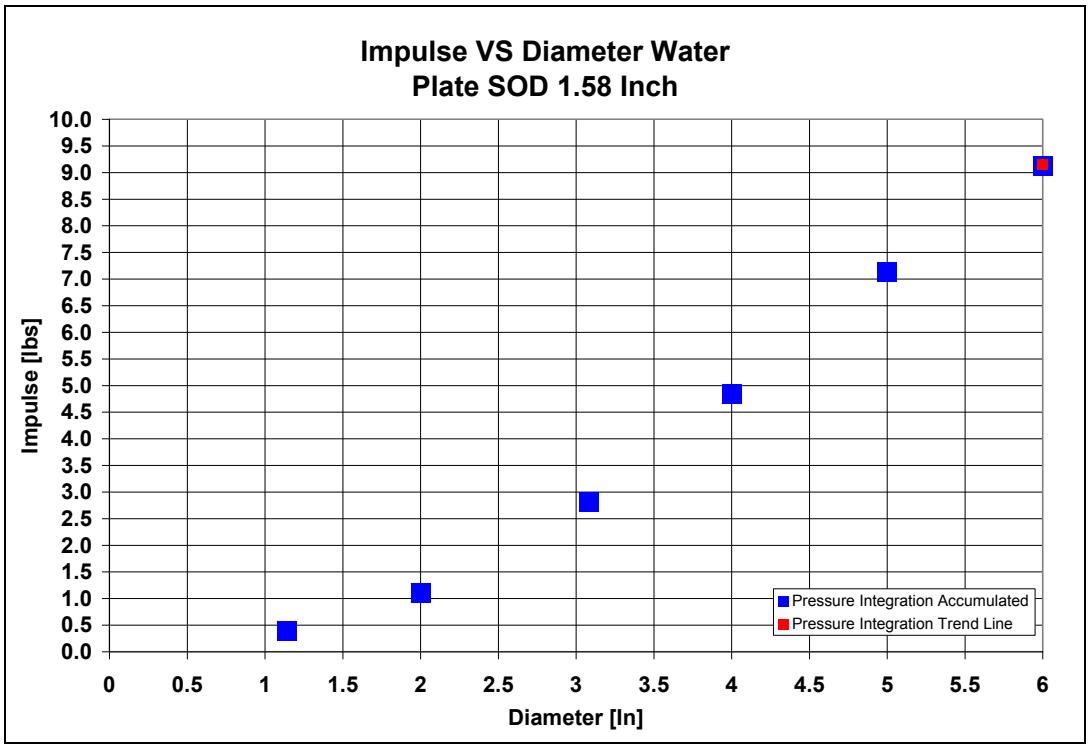

Figure 5.97 Impulse versus diameter of target plates for SOD 4 cm (1.58 inches) for water impact

5.5.3 Impulse Measurement at SOD 4 cm (1.58 inches) and DOB 1 cm (0.39 inches) in Water

A test series for water using a variety of plates of different diameters (**Figure 5.33**) keeping the weight constant (10.3 kg) was conducted in the Dynamic Effects Laboratory. The test setup was the same as being used for the pressure measurement series in water. Several diameters were used in order to determine the impulse distribution over the diameter of a plate. By increasing the diameter eventually a plate size is achieved in which the maximum impulse is delivered. The diameters used were the same as for saturated sand test series [5.08 cm (2 inches), 10.16 cm (4 inches), 15.24 cm (6 inches), 20.32 cm (8 inches), 25.4 cm (10 inches), 36.32 cm

(14.3 inches), and 48.26 cm (19 inches)]. Additionally a plate of the diameter of 30.48 cm (12 inches) was tested.

The test results are shown in **Figure 5.98**. The impulse increases steadily over the first 35.56 cm (14 inches) of diameter. With further increasing diameter the impulse decreases a little using the largest plate diameter of 48.26 cm (19 inches). The reason for the decrease is still under investigation.

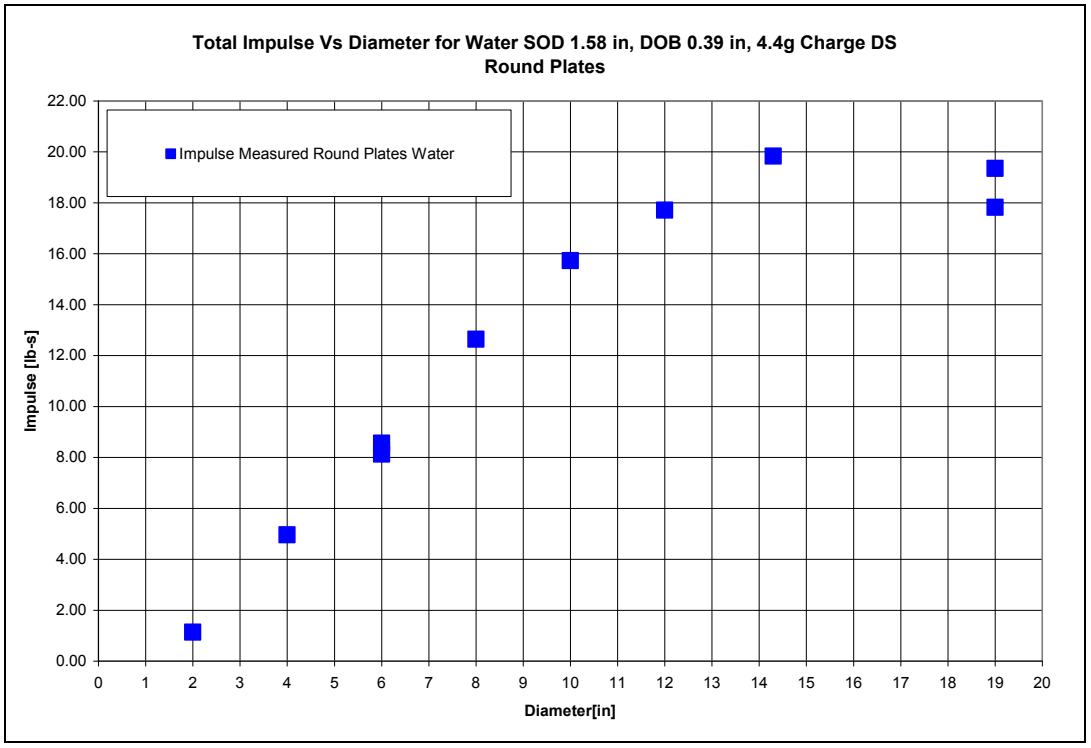

Figure 5.98 Impulse results round plates for water

5.5.4 Verification of Pressure Test Results at SOD 4 cm (1.58 inches) and DOB 1 cm (0.39 inches) in Water Using Impulse Results Round Plates

Plotting the test results obtained by the integration of the pressure measurements (**Figure 5.97**) and the results of impulse measured using the round plates on the same plot, shows that both data sets agree pretty well at all locations (**Figure 5.99**).

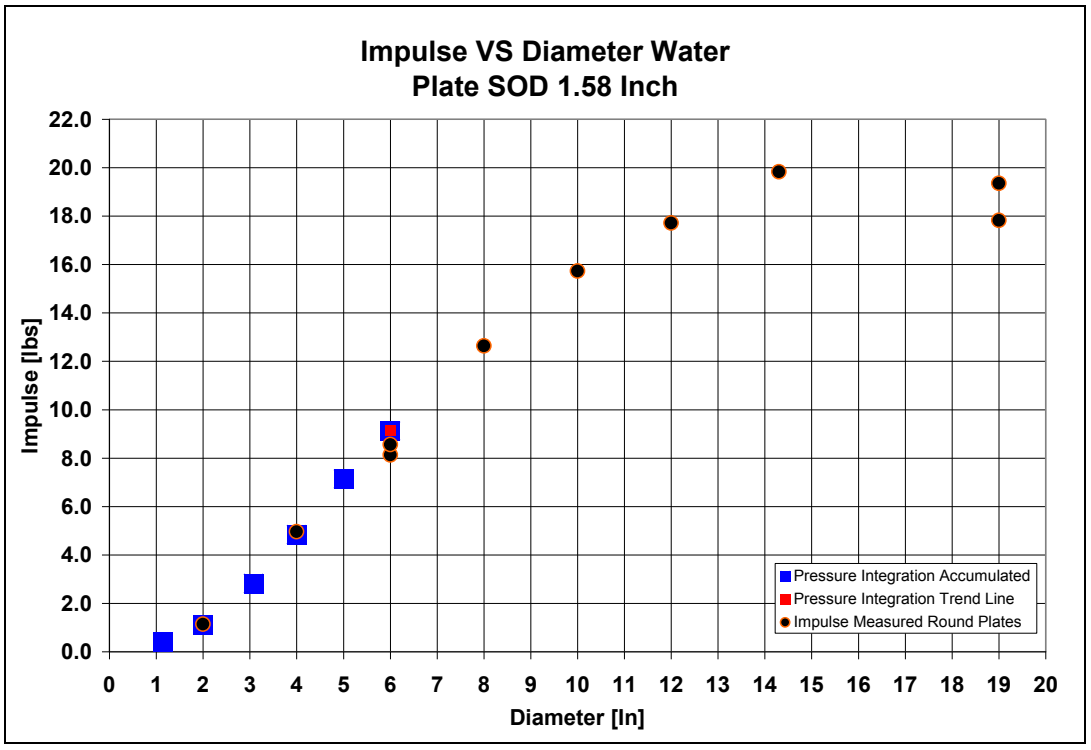

Figure 5.99 Impulse results round plates and pressure integration for water

In the following section the obtained results will be summarized. Various test setups will be compared and differences will be pointed out.

Chapter 6: Results and Discussion

This section presents the results obtained in the different test series conducted. The test series will be compared and differences in loading mechanisms, pulse widths, and average peak pressures will be pointed out.

First pressure distributions over the flat bottom of a vehicle at 3 different SODs and the same DOB for tests conducted in saturated sand and then impulse results for tests conducted at the same conditions will be discussed. The peak pressure results for the same test series will be highlighted.

Second pressure distributions over the bottom of a vehicle and impulse results for tests conducted using 3 different materials (saturated sand, dry sand, water) at the same SOD and DOB will be compared. Peak pressure results for the same set of tests will be conveyed.

Additionally first results obtained by using the computer code DYSMAS (Dynamic System Mechanics Advanced Simulation) will be briefly reported.

6.1 Pressure Distribution over the Bottom of a Vehicle for Saturated Sand at 3 Different SODs and DOB 1 cm (0.39 inches)

The loading applied to a target plate is considered as most severe using saturated sand compared to any other mixture of soil containing a variety of moisture content. In the following the pressure distribution on the bottom of a vehicle is shown for 3 different SODs and the same DOB.

6.1.1 Pressure Distribution over the Bottom of a Vehicle for Saturated Sand at Standard *(Intermediate SOD)* Conditions

The standard conditions are considered to be a SOD of 4 cm (1.58 inches) and a DOB of 1 cm (0.39 inches) which scales to full scale to a SOD of 40.6 cm (16 inches) and a DOB of 10.2 cm (4 inches). The results of 192 measured pressure – time profiles are shown in **Figure 6.1**. The figure includes the maximum and minimum pressures measured and the calculated average pressure at locations of 0 cm (0 inches), 1.01 cm (0.4 inches), 1.45 cm (0.57 inches), 2.54 cm (1 inch), 3.10 cm (1.22 inches), 3.91 cm (1.54 inches), 5.08 cm (2 inches), 6.35 cm (2.5 inches), and 7.62 cm (3 inches). The average pressure values have to be processed in order to calculate the average pressure value at the bottom of the target plate as shown in **Section 4.3.** The processed average pressure values are shown in **Figure 6.2**. Two polynomial trend lines are used to characterize the pressure profile according to the location on the target plate.

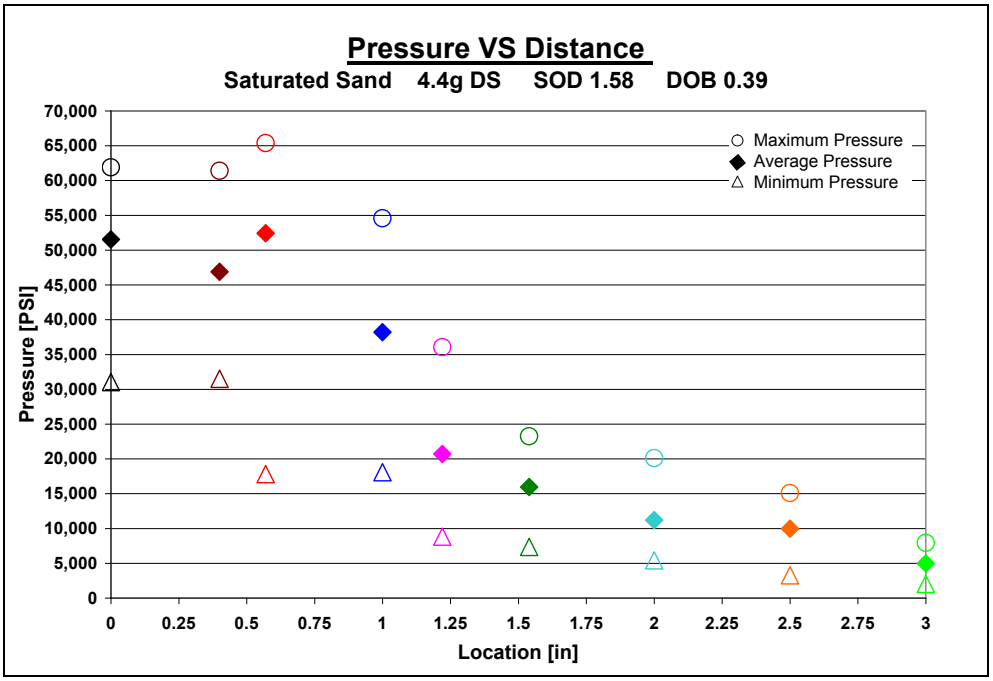

Figure 6.1 Measured pressures for saturated sand at SOD 4 cm (1.58 inches)

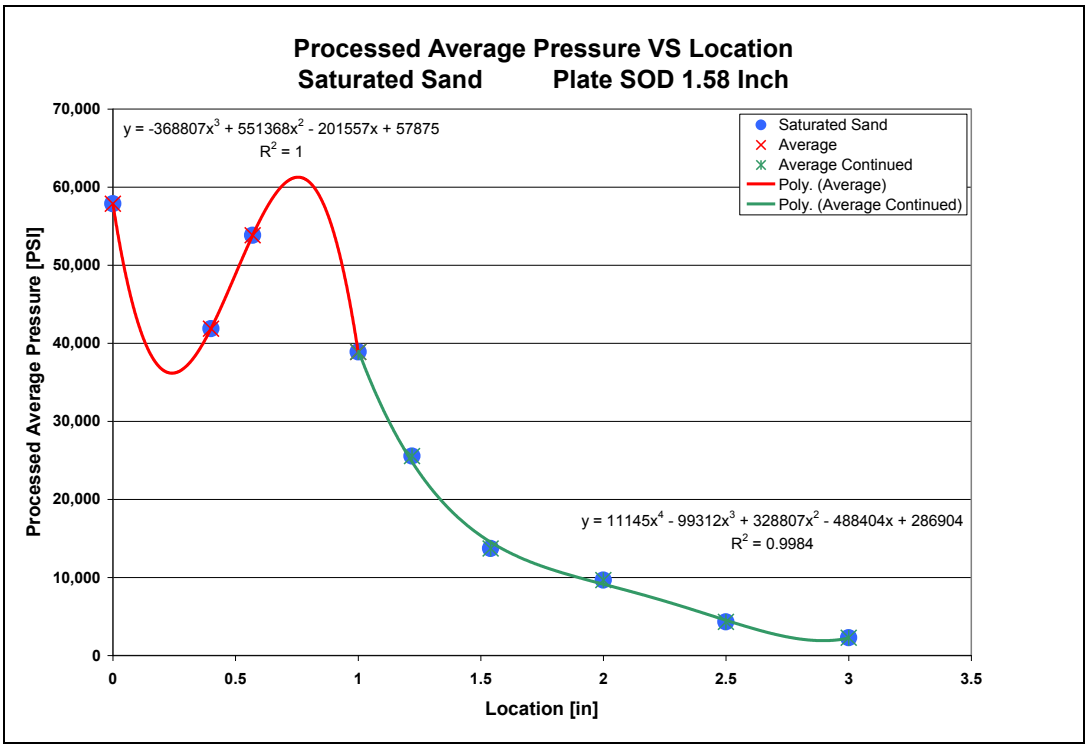

Figure 6.2 Processed average pressures for saturated sand at SOD of 4 cm (1.58 inches)

The two trend lines and the related equations shown in **Figure 6.2** can be used in order to process a three dimensional plot, shown in **Figure 6.3**, of the pressure distribution on the bottom of a vehicle with a flat bottom. **Figure 6.4** gives a more detailed view of the center of impact. The shown distribution covers a radius of 7.6 cm (3 inches) with respect to full scale of 77 cm (30.3 inches).

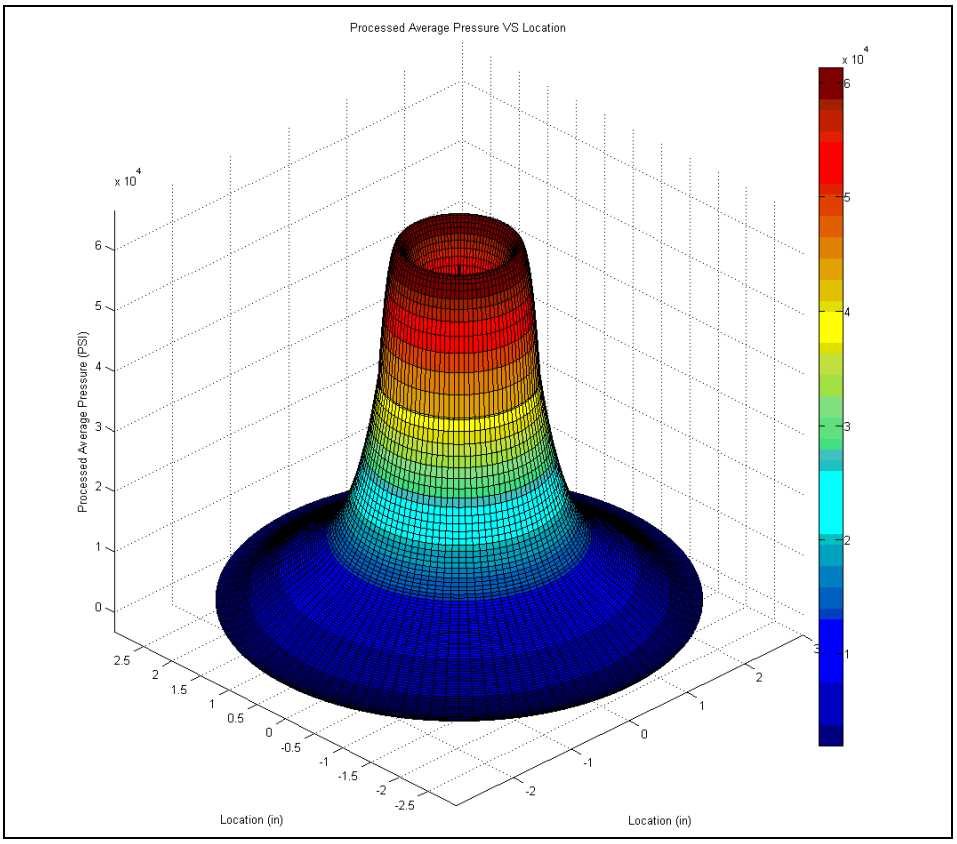

Figure 6.3 Three dimensional plot of processed average pressure distribution for *intermediate* SOD in saturated sand

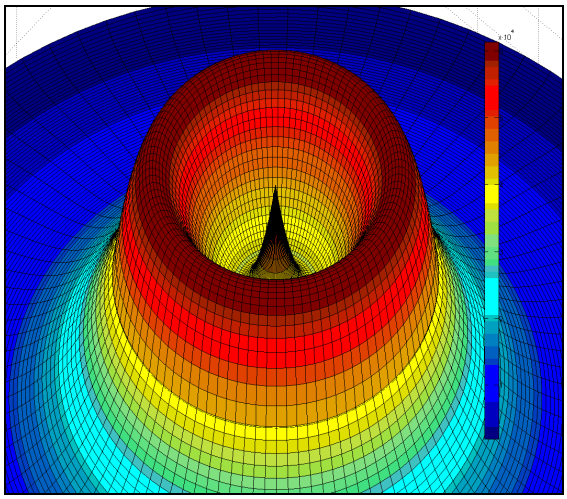

Figure 6.4 Detailed view of center of impact for *intermediate* SOD

6.1.2 Pressure Distribution over the Bottom of a Vehicle for Saturated Sand at *Closest* Stand-off Distance

The *closest* SOD was chosen to be a SOD of 2 cm (0.79 inches) at the same DOB of 1 cm (0.39 inches) which scales to full scale to a SOD of 20.3 cm (8 inches) and a DOB of 10.2 cm (4 inches). The results of 100 measured pressure – time profiles are shown in **Figure 6.5**. The figure includes the maximum and minimum pressures measured and the calculated average pressure at locations of 0 cm (0 inches), 1.45 cm (0.57 inches), 2.54 cm (1 inch), 3.10 cm (1.22 inches), 3.91 cm (1.54 inches), 5.08 cm (2 inches), and 6.35 cm (2.5 inches). Again the average pressure values have to be processed in order to calculate the average pressure value at the bottom of the target plate as shown in **Section 4.3.** The processed average pressure values are shown in **Figure 6.6**. Two polynomial trend lines are used to characterize the pressure profile according to the location on the target plate.

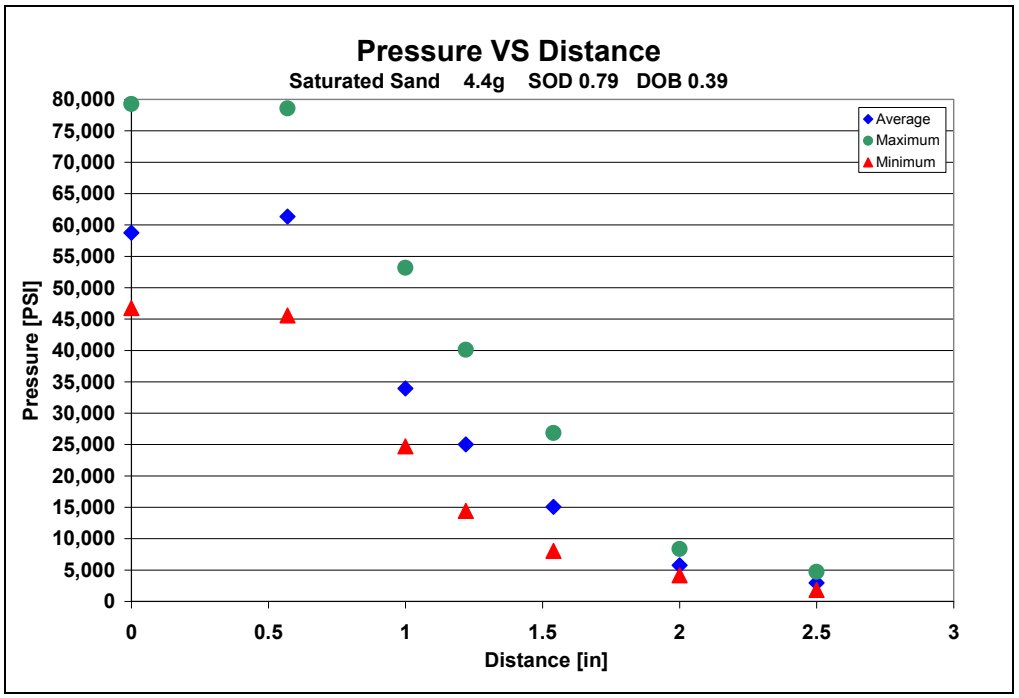

Figure 6.5 Measured pressures for saturated sand at SOD 2 cm (0.79 inches)

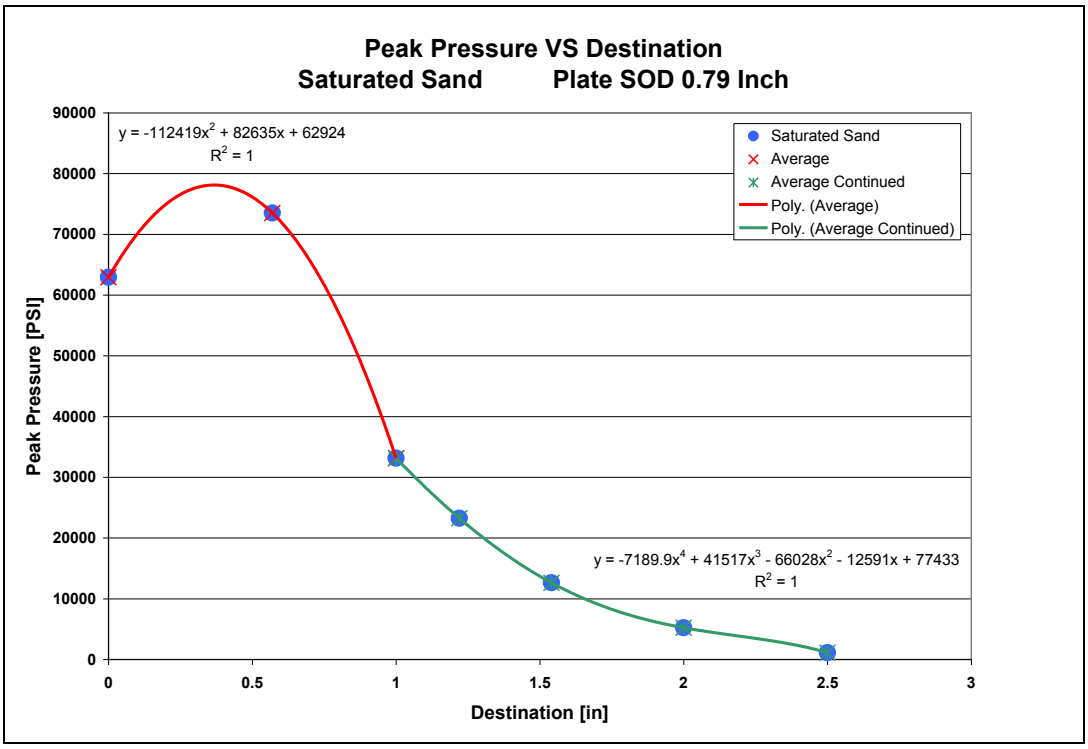

Figure 6.6 Processed average pressures for saturated sand at SOD of 2 cm (0.79 inches)

The two trend lines and the related equations shown in **Figure 6.6** can be used in order to process a three dimensional plot, shown in **Figure 6.7**, of the pressure distribution on the bottom of a vehicle with a flat bottom at a SOD of 2 cm (0.79 inches). **Figure 6.8** gives a more detailed view of the center of impact. The shown distribution in this case covers a radius of 6.4 cm (2.5 inches) with respect to full scale of 64 cm (25.25 inches). The detailed view does not show a needlepoint at the center of impact as seen in **Figure 6.4** for the *intermediate* SOD. A reason could be that there was no pressure measurement recorded at the location of 1.01 cm (0.4 inches) and therefore the trend line shows a different characteristic.

The peak average pressures from the center to the location of about 2.54 cm (1 inch) are higher at the *closest* SOD. With increasing distance from the location of 2.54 cm (1 inch) on the average pressures for the *closest* SOD are lower than for the *intermediate* SOD.

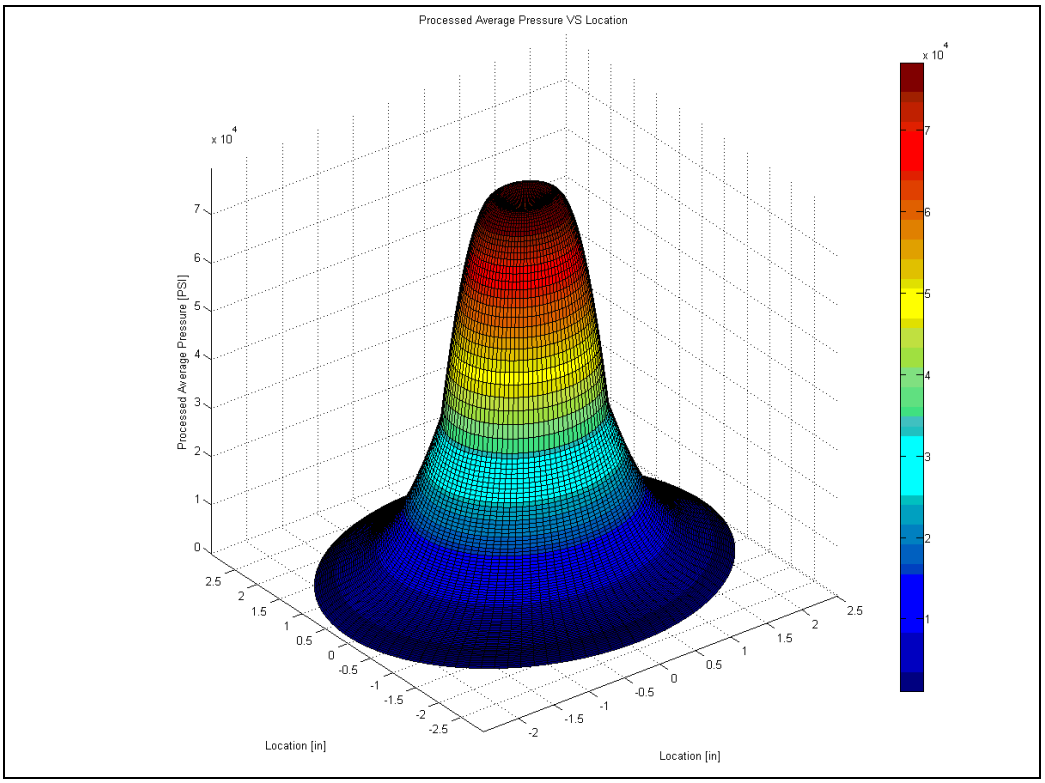

Figure 6.7 Three dimensional plot of processed average pressure distribution for *closest* SOD in saturated sand

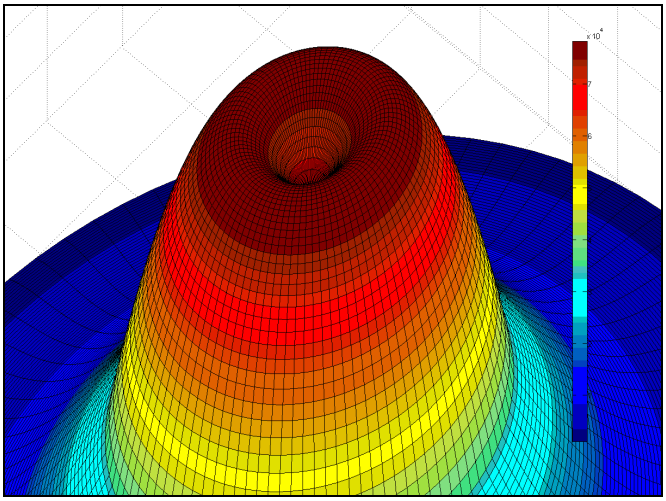

Figure 6.8 Detailed view of center of impact for *closest* SOD

6.1.3 Pressure Distribution over the Bottom of a Vehicle for Saturated Sand at *Largest* Stand-off Distance

The *largest* SOD was chosen to be a SOD of 6 cm (2.38 inches) at the same DOB of 1 cm (0.39 inches) which scales to full scale to a SOD of 60.6 cm (24 inches) and a DOB of 10.2 cm (4 inches). The results of 112 measured pressure – time profiles are shown in **Figure 6.9**. The figure includes the maximum and minimum pressures measured and the calculated average pressure at locations of 0 cm (0 inches), 1.45 cm (0.57 inches), 2.54 cm (1 inch), 3.10 cm (1.22 inches), 3.91 cm (1.54 inches), 5.08 cm (2 inches), 6.35 cm (2.5 inches), and 7.62 cm (3 inches). Like for the other test results described before, the average pressure values have to be processed in order to calculate the average pressure value at the bottom of the target plate as shown in **Section 4.3.** The processed average pressure values are shown in **Figure 6.10**. Two polynomial trend lines are used to characterize the pressure profile according to the location on the target plate.

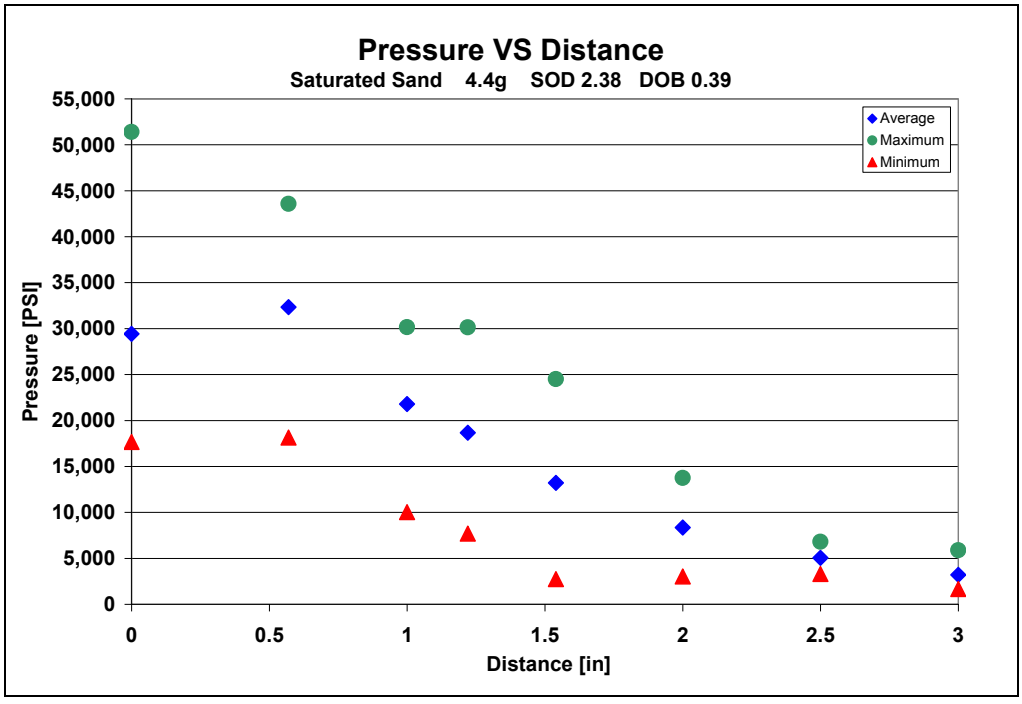

Figure 6.9 Measured pressures for saturated sand at SOD 6 cm (2.38 inches)

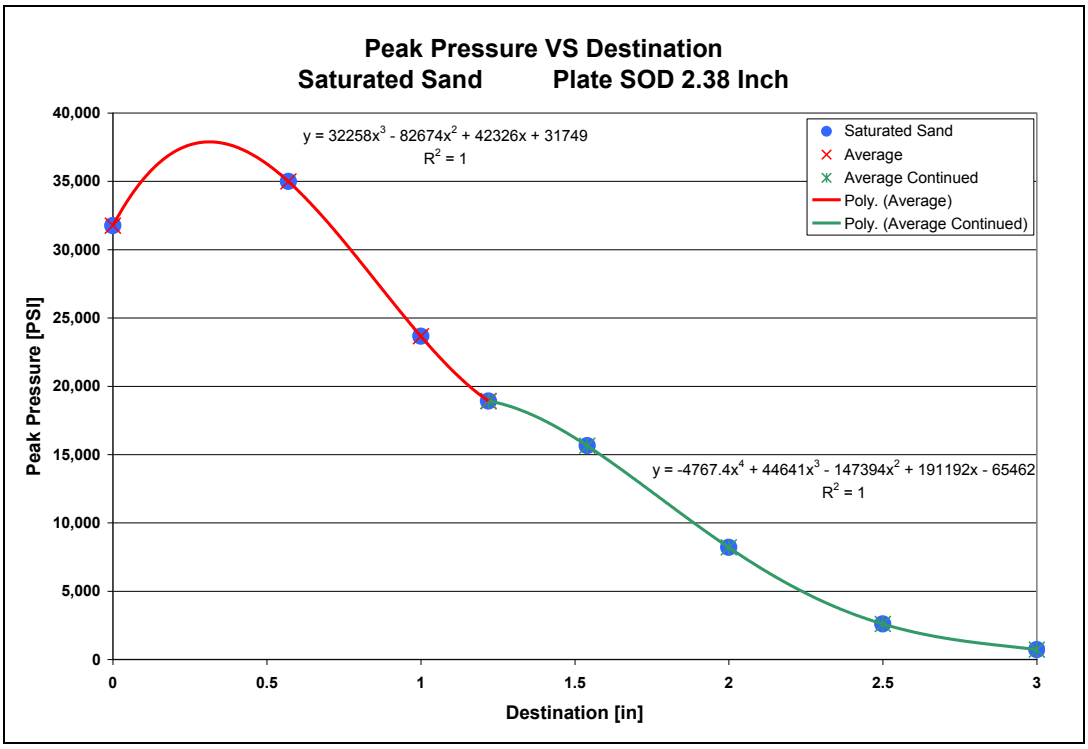

Figure 6.10 Processed average pressures for saturated sand at SOD of 6 cm (2.38 inches)

The two trend lines and the related equations shown in **Figure 6.10** are used in order to process a three dimensional plot, shown in **Figure 6.11**, of the pressure distribution on the bottom of a vehicle with a flat bottom at a SOD of 6 cm (2.38 inches). **Figure 6.12** gives a more detailed view of the center of impact. The shown distribution using the *largest* SOD covers a radius of 7.6 cm (3 inches) with respect to full scale of 77 cm (30.3 inches). The detailed view does not show a needlepoint at the center of impact as seen in **Figure 6.4** for the *intermediate* SOD. As mentioned, the reason could be that there was no pressure measurement recorded at the location of 1.01 cm (0.4 inches) and therefore the trend line has a different characteristic.

The peak average pressure values at all locations are lower than in the cases of the *intermediate* and *closest* SOD as expected.

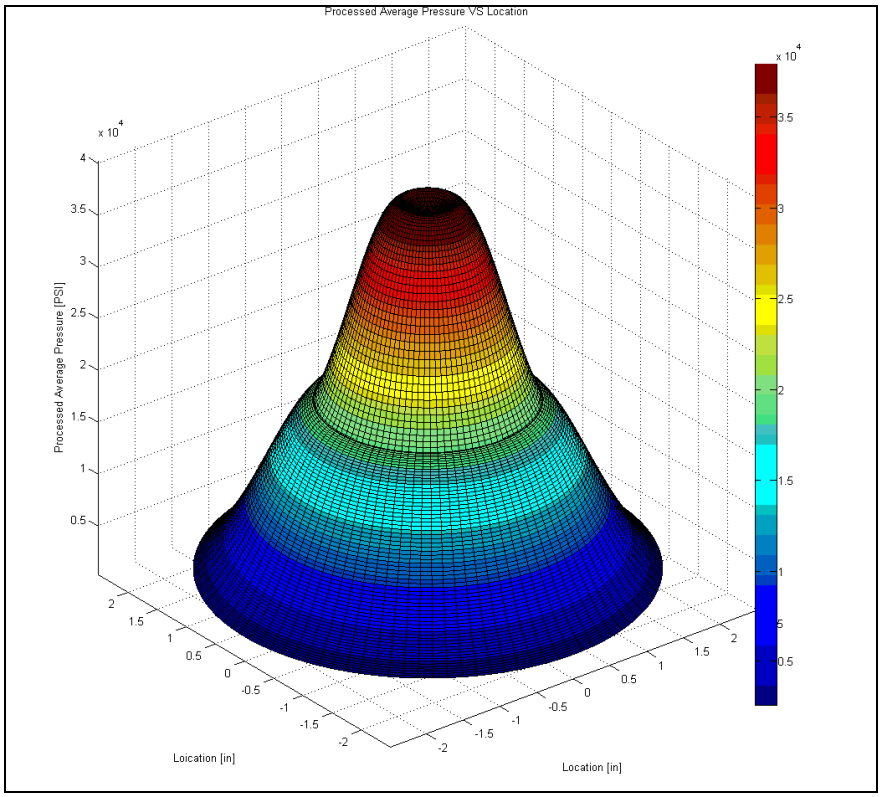

Figure 6.11 Three dimensional plot of processed average pressure distribution for *largest* SOD in saturated sand

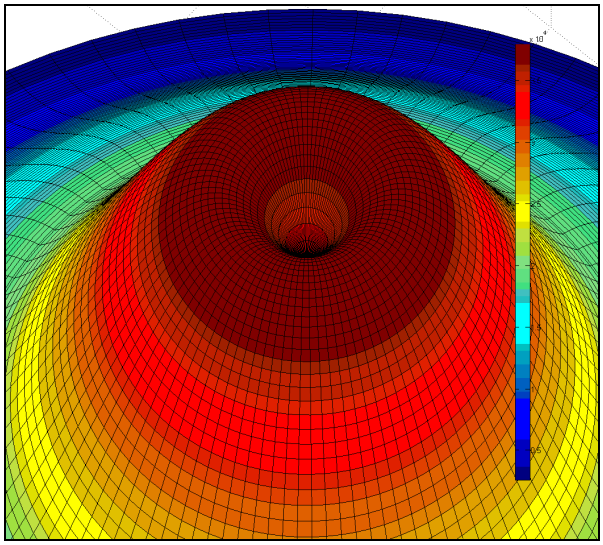

Figure 6.12 Detailed view of center of impact for *largest* SOD

6.1.4 Comparison of the Pressure Distribution over the Bottom of a Vehicle for Saturated Sand

Comparing the results of the saturated sand tests conducted (**Figure 6.13**), it is obvious that a larger SOD lowers the peak pressure values immensely between the center of impact (0 cm) and the location of 3.9 cm (1.54 inches), respectively 39.5 cm (15.6 inches) full scale. As mentioned before, a pressure measurement at the location of 1 cm (0.4 inches) for the *closest* SOD and the *largest* is needed in order to compare the results to the *intermediate* SOD. For the *intermediate* SOD the pressure decreases between the center of impact and the location of 1.37 cm (0.54 inches) and it is unknown if the *closest* and the *largest* SOD show the same characteristics.

Comparing the pressure values for the *closest* and the *largest* SOD between the center and 2.54 cm (1 inch), increasing the SOD by 4 cm (1.58 inches), respectively 40.4 cm (16 inches) in full scale, reduces the average peak pressure by 50 percent.

From the location of 3.9 cm (1.54 inches) to 7.62 cm (3 inches), respectively 39.5 cm (15.6 inches) to 77 cm (30.3 inches) full scale, the average peak pressure values for all 3 cases are very similar. Surprisingly the *closest* SOD shows consistently the lowest peak pressure. At the location of 3.9 cm (1.54 inches) the *lowest* average peak pressure value comes with the *closest* SOD, followed by the *intermediate* average peak pressure value and the *intermediate* SOD. The *largest* average peak pressure value comes with the *largest* SOD. From 5.1 cm (2 inches) on, the average peak pressure value for the *closest* SOD crosses over and stays in between the *largest* and the *intermediate* SOD.

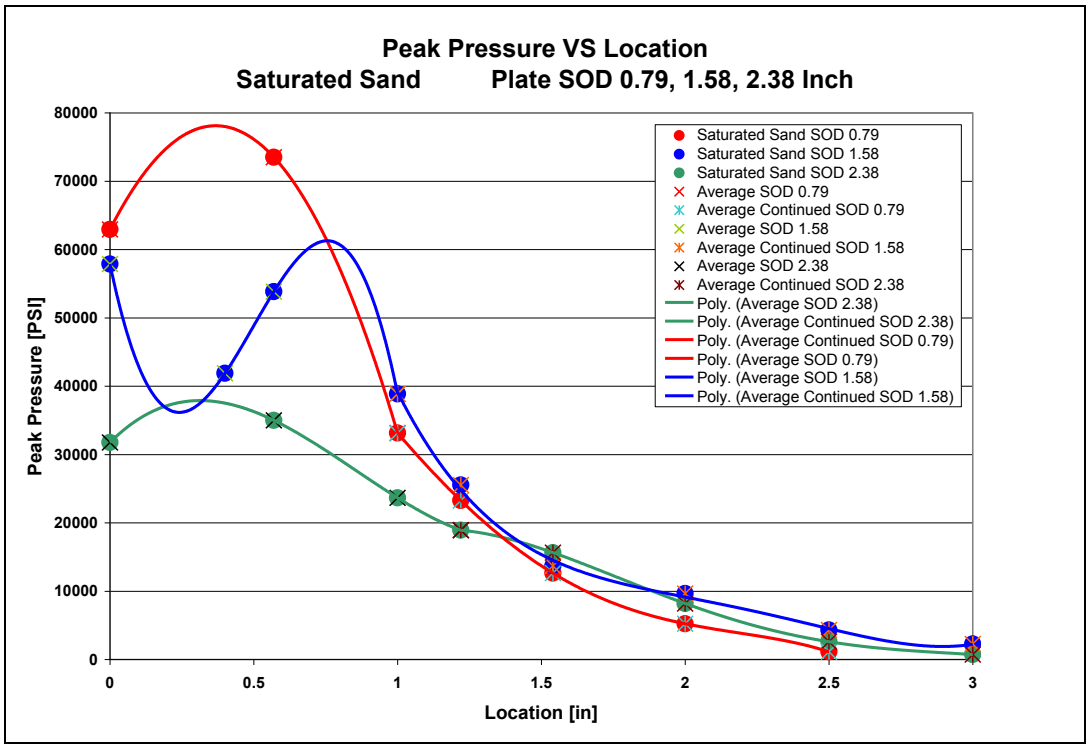

Figure 6.13 Processed average pressures for saturated sand at all SODs

6.2 Impulse Distribution over the Bottom of a Vehicle for Saturated Sand at 3 Different SODs and DOB 1 cm (0.39 inches)

The specific impulse calculated from the average pressure values at each location of the plate for the 3 different stand-off distances is shown in **Figure 6.14**. The trend lines show the distribution of the specific impulse versus the location on the target plate and highlight the influence of the change in SOD.

The specific impulse values for the *closest* SOD of 2 cm (0.79 inches) are largest from the center of the plate up to the location of 3.91 cm (1.54 inches). The larger specific impulse values are mainly due to the larger loading pulse widths and

not because of the higher peak pressure values. The only significantly higher pressure value for the closest SOD appears to be at the location of 1.45 cm (0.57 inches) and is paired with a large loading interval, too. At the location of 5.08 cm (2 inches) and 6.35 cm (2.5 inches) the specific impulse for the SOD of 2 cm (0.79 inches) drops below the specific impulse values for the medium SOD of 4 cm (1.58 inches) even though the loading pulse width is larger. The reason for that is the fast declining peak pressure values.

The specific impulse values for the *largest* SOD of 6 cm (2.38 inches) are the lowest of all 3 cases as expected since the average peak pressure values are low and the loading pulse widths are shorter.

In the case of the *intermediate* SOD of 4 cm (1.58 inches) the specific impulse values are in between the values of the higher and lower SOD cases except for the 2 locations mentioned earlier in which the values drop very fast for the closer SOD.

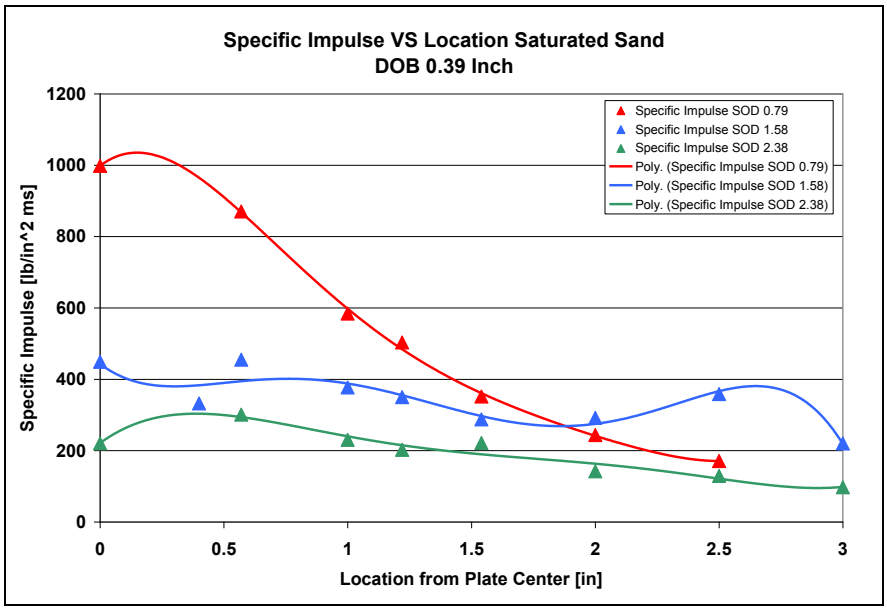

Figure 6.14 Specific Impulse in saturated sand for SOD of
2 cm (0.79 inches), *closest* SOD;
4 cm (1.58 inches), *intermediate* SOD;
6 cm (2.38 inches), *largest* SOD

Using the specific impulse values the total impulse for all 3 stand-off distances can be calculated, see **Figure 6.15**. As expected the *closest* SOD of 2 cm (0.79 inches) shows the highest accumulated impulse values and the *largest* SOD of 6 cm (2.38 inches) the lowest accumulated impulse over the diameter of the target plate. The curve for the *intermediate* SOD of 4 cm (1.58 inches) falls in between.

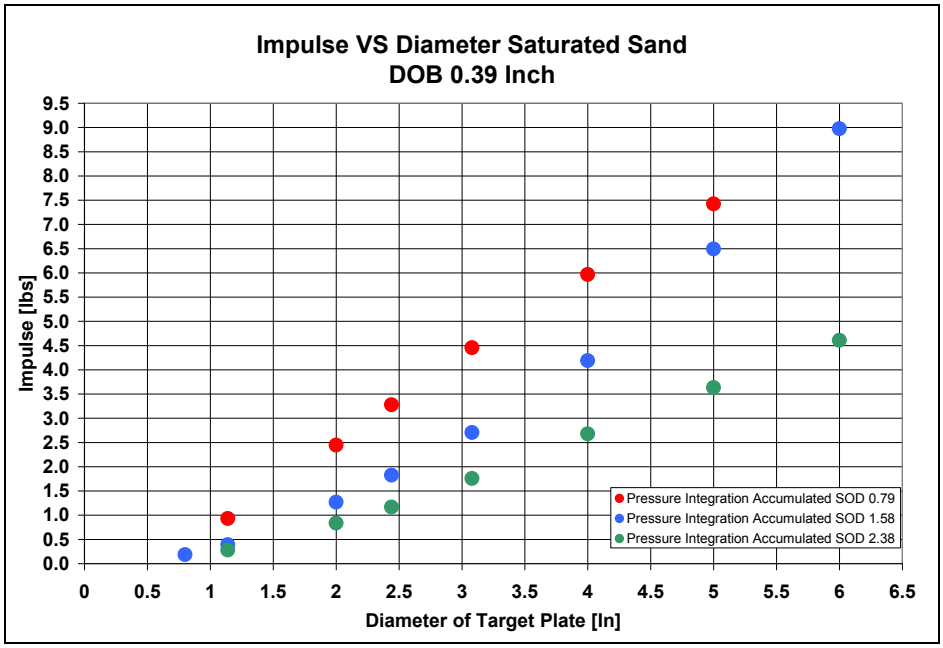

Figure 6.15 Total Impulse accumulated in saturated sand for SOD of
2 cm (0.79 inches), *closest* SOD;
4 cm (1.58 inches), *intermediate* SOD;
6 cm (2.38 inches), *largest* SOD

Comparing the 3-D plots for the 3 different Stand-off distances, **Figure 6.17** for the *intermediate* SOD of 4 cm (1.58 inches) represents a different characteristic compared to **Figure 6.16** and **6.18**. **Figure 6.17** shows 2 rims which the other cases do not show. The first rim closer to the center can be explained because an average pressure value was determined at the location of 1.02 cm (0.4 inches) from the target plate which was not done for the other 2 stand-off distances. It could very well be that the other stand-off distances show the same characteristic at this location. The

second rim at the location of 6.35 cm (2.5 inches) is definitely not apparent in the other two Figures. In **Figure 6.18** there is a bulging visible close to the location of 5.08 cm (2 inches) which could be remains of a transition in loading forming the second rim in **Figure 6.17**. Definitely more testing is required in order to determine more details about the transition.

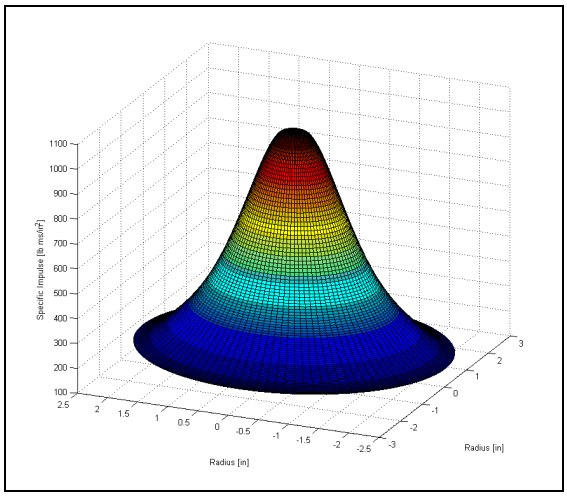

Figure 6.16 3-D plot for total impulse *closest* SOD 2 cm (0.79 inches)

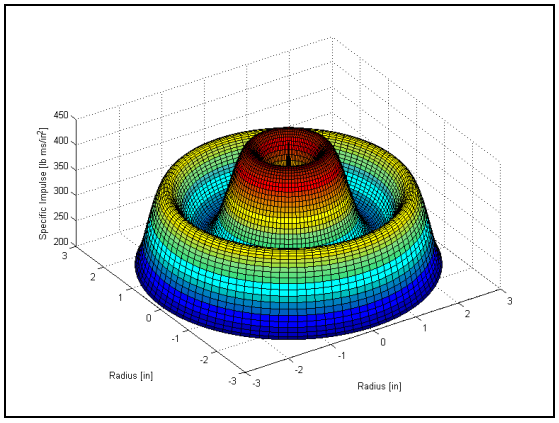

Figure 6.17 3-D plot for total impulse *intermediate* SOD 4 cm (1.58 in.)

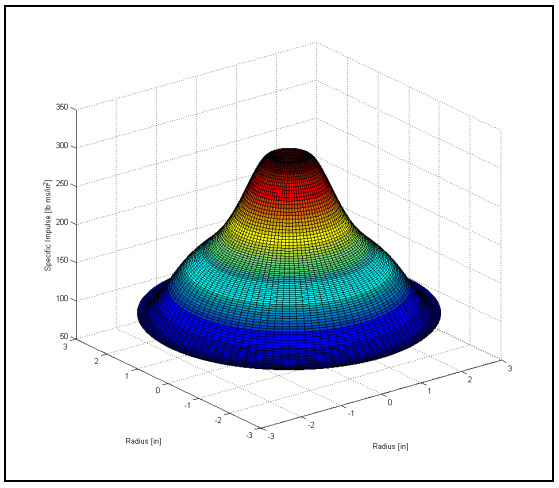

Figure 6.18 3-D plot for total impulse *largest* SOD 6 cm (2.38 inches)

Taking into account not having generated the average peak pressure value and therefore the specific impulse for the *intermediate* SOD of 4 cm (1.58 inches) at the location of 1.02 cm (0.4 inches) from the target plate the first rim does not exist, see **Figure 6.19**. Compare **Figure 6.19** to **Figure 6.17**. Hence the impact zone close to the center of the plate looks similar to the other two cases, compare **Figure 6.16** and **6.18**. This implies that the pressure-time profiles should be spaced in smaller steps in order to get a more detailed view of the loading applied to the target plate.

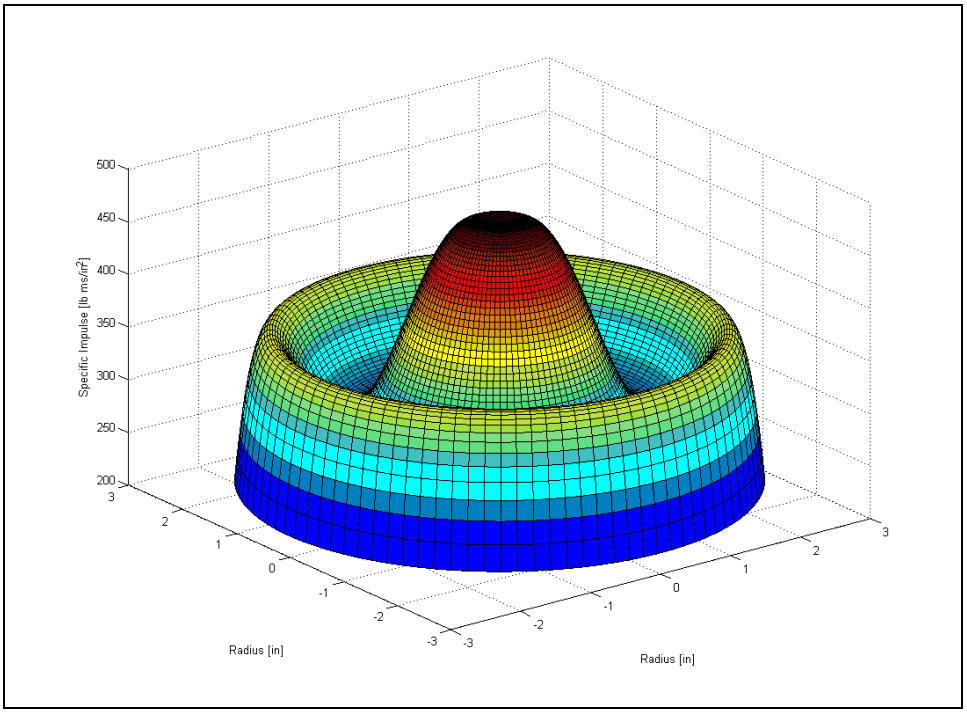

Figure 6.19 Modified 3-D plot for total impulse for the *intermediate* SOD 4 cm (1.58 inches)

6.3 Peak Pressure Results for Saturated Sand at 3 Different SODs and at DOB 1 cm (0.39 inch)

The stand-off distance SOD of a vehicle plays a major role in the survivability of the impact. As a rule of thumb, the larger the SOD the lower is the risk of severe injury. In the following 3 different cases of SOD for saturated sand are compared. The stand-off distances are 2 cm (0.79 inches, *close*), 4 cm (1.58 inches, *intermediate*), and 6 cm (2.38 inches, *large*). Scaled up to full size field test, the *closest* SOD would be 20.2 cm (8 inches), *intermediate* SOD 40.4 cm (16 inches), and largest SOD 60.6 cm (24 inches).

The SOD is an important factor in how the loading is applied to the bottom of a target plate. **Figure 6.20** shows the loading for the 3 cases of saturated sand at comparable times using the high speed camera and Plexiglas witness plates as described in **Section 4**. At 54 μs for the closest SOD the target plate has been already impacted while in the two cases of larger SOD the dome still rises.

At 68 μs the expanding ring of the loading at the *intermediate* SOD is clearly visible. The *closest* SOD shows fracturing in the Plexiglas. In the case of the *largest* SOD the dome has still not impacted.

At 82 μs at the *closest* SOD the expanding ring of loading is obscured by the cracking in the Plexiglas sheet. At the *intermediate* the expanding ring of the loading is very visible. At the *largest* SOD the dome has not impacted.

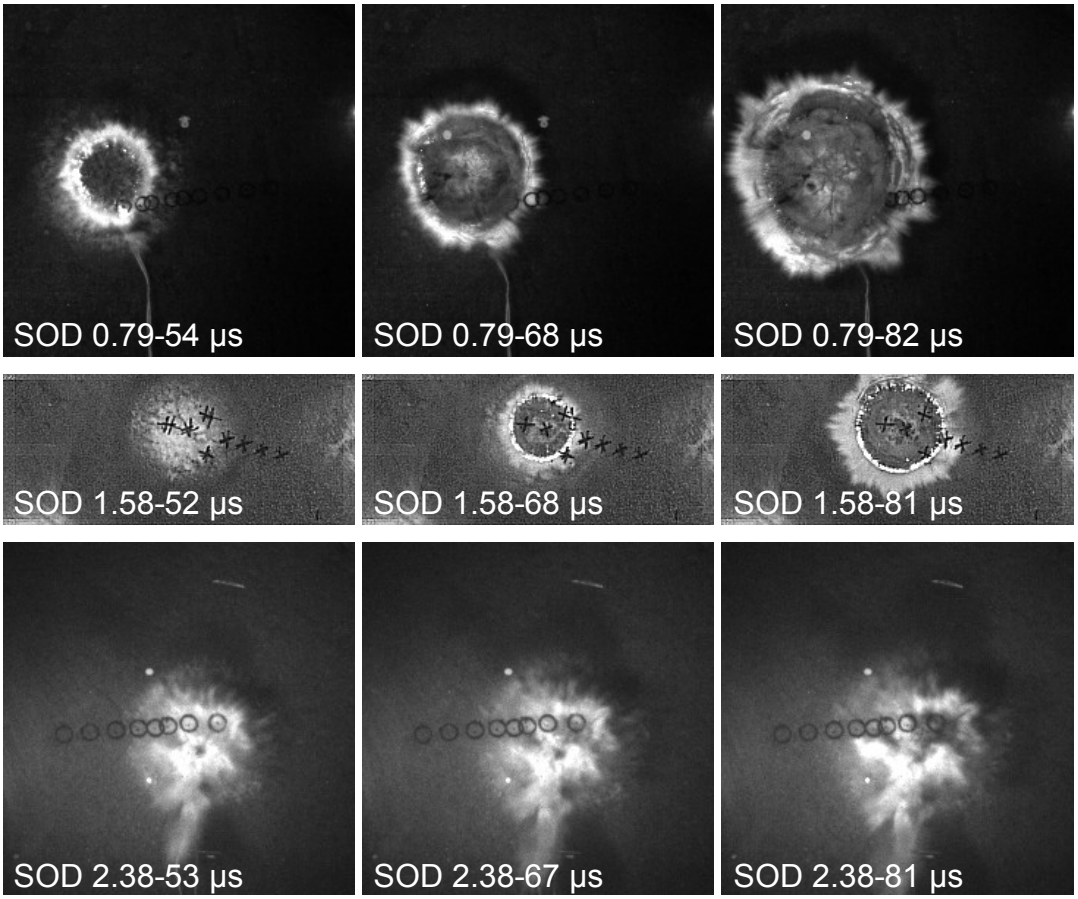

Figure 6.20 Loading on acrylic sheets at 3 different SODs using saturated Sand at earlier time frames

At 97 µs the expanding ring for the *closest* SOD of 2 cm (0.79 inches) is clearly visible, compare **Figure 6.21**. It is much broader than at the same time for the *intermediate* SOD of 4 cm (1.58 inches). At this time the dome starts hitting the bottom of the acrylic plate for the *largest* SOD of 6 cm (2.38 inches).

At 140 µs the expanding ring again is much broader for the *closest* SOD compared to the other SODs. For the *largest* SOD the ring seems to be less uniformly pronounced compared to the *intermediate* SOD. This fact accounts for a higher standard deviation in the peak pressure measurement for the larger SOD. At the time frame of 211 µs the expanding ring starts fading in all 3 cases. Note that the fracture left after the loading was applied in the case of the *closest* SOD is most severe. And note that the ring in the case of the *largest* SOD has caught up in total size of expansion. It

seems that the ring at the *largest* SOD expands faster compared to the other cases. This will be noticeable looking at the single pressure-time profiles which will be shown below.

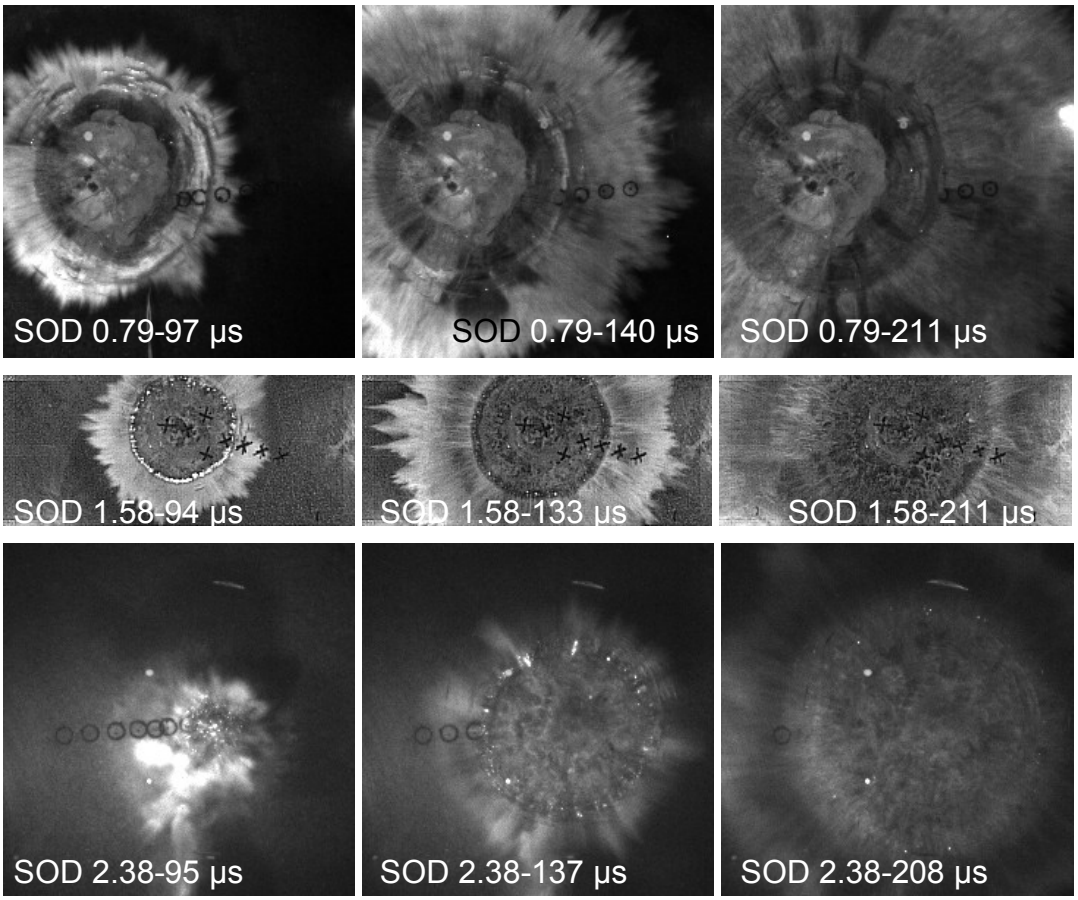

Figure 6.21 Loading on acrylic sheets at 3 different SODs using saturated Sand at later time frames

Finally looking at **Figure 6.22** for the case of the *largest* SOD at 109 μs there is clearly no ring of loading yet developed. The loading is applied in a more randomly distributed manner.

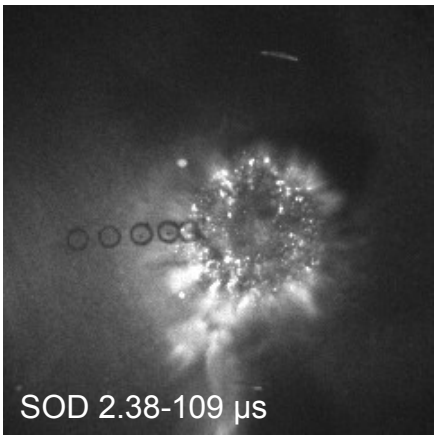

Figure 6.22 Loading on an acrylic sheet at *largest* SOD of 6 cm (2.38inches) at the time frame of 109 µs

Looking at the 3 cases of the different SOD for saturated sand and plotting the corresponding pressure-time profiles reveals the differences between the cases. **Figure 6.23** contains the average pressure-time profiles at the distance of 0 cm and 1.45 cm (0.57 inches) from the center of the plate for all 3 cases.

At the location of 0 cm (0 inches), at the center of the impact, the pressure-time profile of the *closest* SOD starts earliest and is the broadest. The peak pressure is not much higher compared to the *intermediate* SOD. At the *largest* SOD the peak pressure is much lower but the pressure-time profile has the same pulse width as the one at the *intermediate* SOD.

At the location of 1.45 cm (0.57 inches) the pulse width for the pressure-time profile for the *closest* and *intermediate* SOD start almost at the same time, but again for the *closest* SOD the profile is much broader. Also the peak pressure is significant higher for the *closest* SOD compared to the *intermediate* SOD. For the *largest* SOD the profile looks almost the same as at the location of 0 cm and the starting time of the loading pulse width starts almost at the same time, too. With larger SOD of the target the rising dome spreads out further before impact and therefore covers at impact time a broader area.

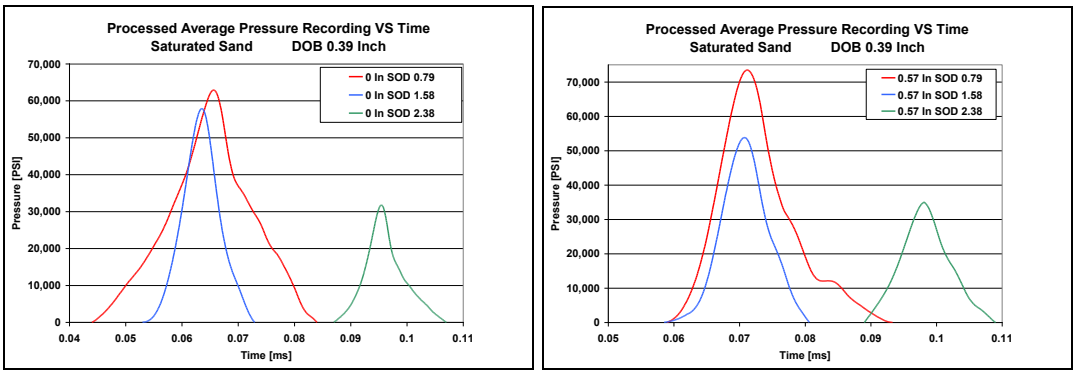

Figure 6.23 Average pressure-time profiles at 0 cm and 1.45 cm (0.57 inches) from the center of the plate

Figure 6.24 shows the average pressure-time profiles at the distance of 2.54 cm (1 inch) and 3.1 cm (1.22 inches) from the plate center. Surprisingly the peak pressure drops at both locations for the *closest* SOD below the peak pressure for the case of the *intermediate* SOD and the starting time of the loading applied starts later. But still the loading interval is much broader than for the other two cases with increased SOD which results in a larger impulse delivered to the target plate. Another interesting result is that at the location of 3.1 cm (1.22 inches) in the case of the *largest* SOD the loading time starts almost at the same time as for the *closest* SOD.

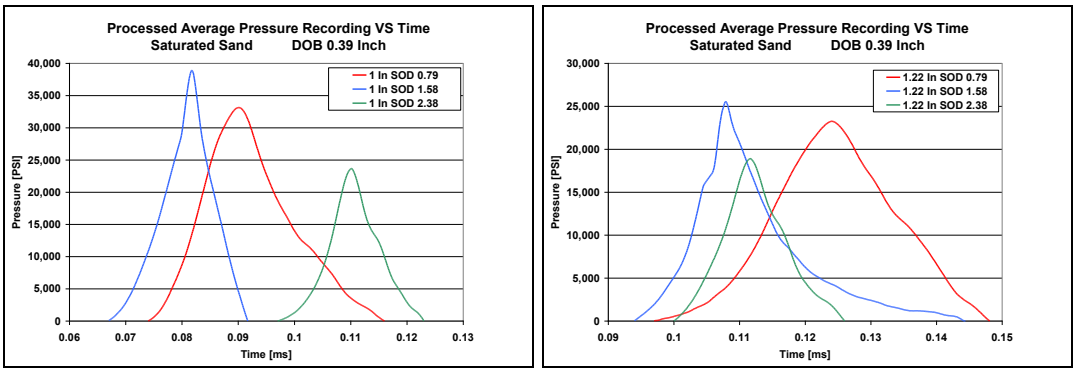

Figure 6.24 Average pressure-time profiles at 2.54 cm (1 inch) and 3.1 cm (1.22 inches) from the center of the plate

At the location of 3.91 cm (1.54 inches) from the plate center the maximum average peak pressure comes from the *largest* SOD. The broadest pressure-time profile shown in **Figure 6.25** still belongs to the *closest* SOD.

At the location of 5.08 cm (2 inches) from the center of impact the earliest average pressure-time profile recorded is for the *largest* SOD. The largest peak pressure calculated belongs to the *intermediate* SOD. The broadest pressure-time profile still is represented by the *closest* SOD. At this location the time at which the loading starts, increases for all cases with the *largest* SOD starting first, followed by the *intermediate* SOD and last by the *closest* SOD.

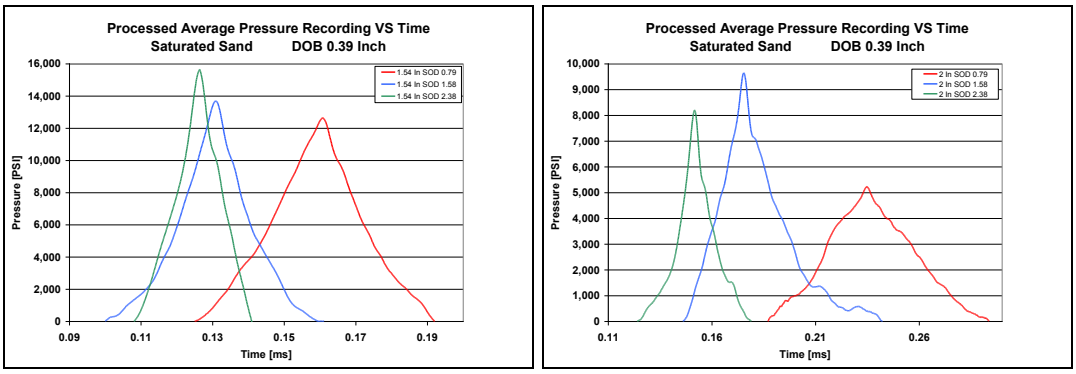

Figure 6.25 Average pressure-time profiles at 3.91 cm (1.54 inches) and 5.08 cm (2 inches) from the center of the plate

At the location of 6.35 cm (2.5 inches) from the center of the plate the earliest average pressure-time profile recorded is for the *largest* SOD, compare **Figure 6.26**. The largest peak pressure calculated belongs to the *intermediate* SOD. The broadest pressure-time profile and the lowest maximum pressure still are represented by the *closest* SOD. This represents the same trend as seen at the location of 5.08 cm (2 inches). The loading interval still has the same order as at the location of 3.91 cm (1.54 inches), the *largest* SOD leading, followed by the *intermediate* SOD and last by the *closest* SOD.

At the location of 7.62 cm (3 inches) the pressure for the *closest* SOD could not be measured any more using Kolsky bars. Still the loading interval for the *largest*

SOD starts earlier in time than for the *intermediate* SOD. Overall the peak pressures drop very low.

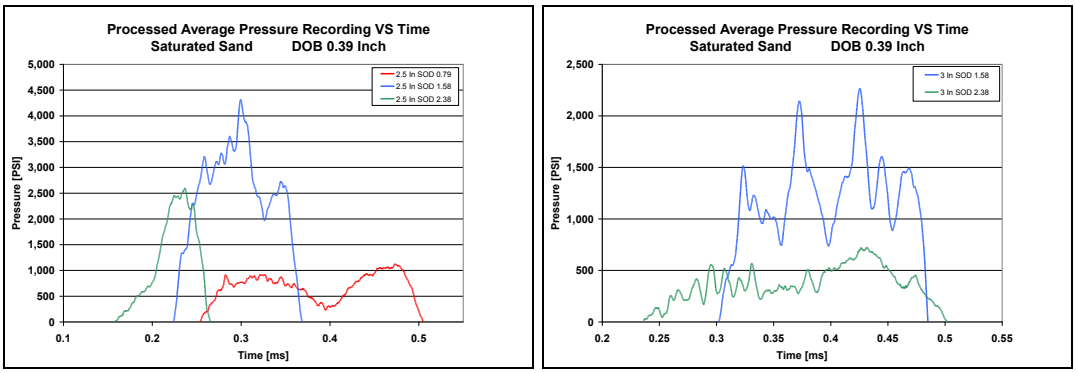

Figure 6.26 Average pressure-time profiles at 6.35 cm (2.5 inches) and 7.62 cm (3 inches) from the center of the plate

Figure 6.27 shows the calculated average peak pressure values as a function of location on the plate for the 3 cases where saturated sand was used. It shows the above described peak pressure distribution at each location calculated based on the measured values on the target plate.

In the following the differences between the measured average peak pressure values and the processed ones will be discussed. Note that the processing of the pressure-time profiles is described in **Section 4.3**. Comparing the measured average peak pressure values with the processed ones for the *closest* SOD reveals the differences at each location, see **Figure 6.28**. The measured values are larger at the location of 0 cm and 1.45 cm (0.57 inches) due to the processing of the pressure-time values. The calculated values need to be shifted significantly down since the higher level of the stress transmitted into the Kolsky bars closer to the center of the impact causes a high off-set. From the location of 2.54 cm (1 inch) on the down shift is much less and results in a higher peak pressure value for the processed average peak pressure, compare **Figure 6.28**.

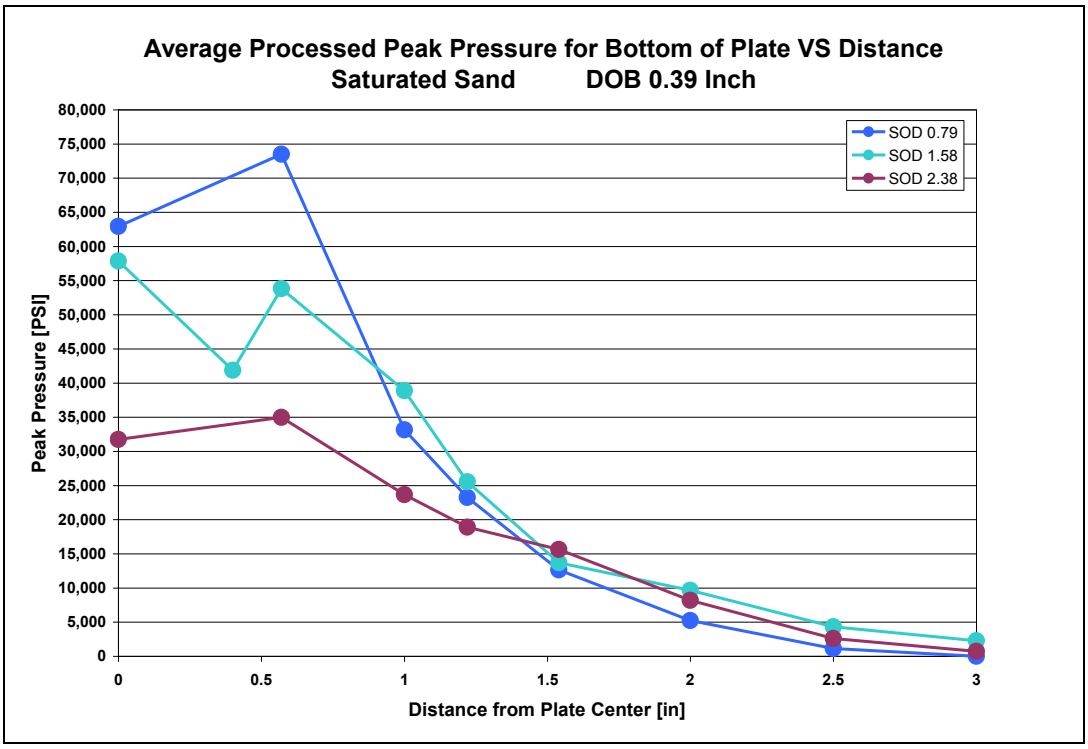

Figure 6.27 Processed average pressure values for the bottom of the target plate for saturated sand

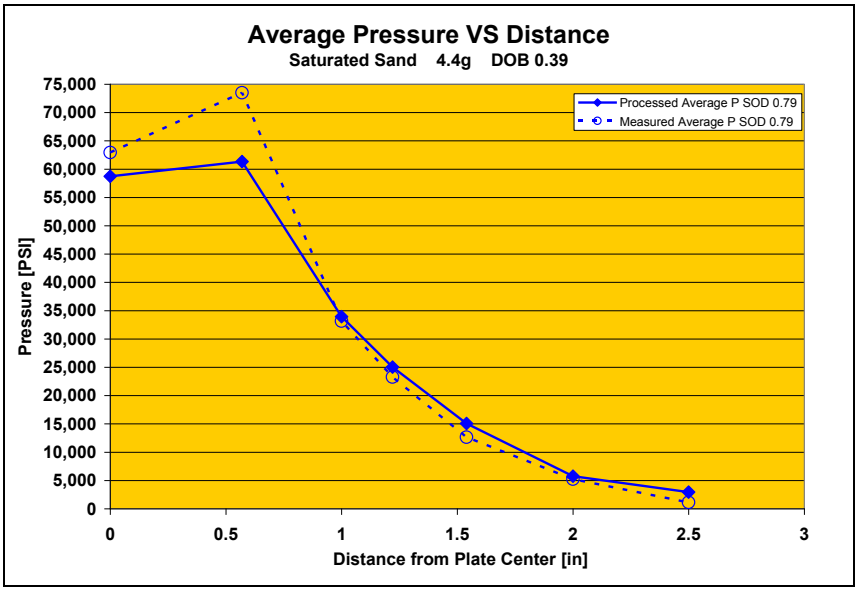

Figure 6.28 Processed versus measured average pressure values for the *closest* SOD of 2 cm (0.79 inches)

Comparing the measured average peak pressure values with the processed ones for the *intermediate* SOD show the same trends as seen in **Figure 6.28** with one exception at the location of 1.02 cm (0.4 inches), see **Figure 6.29**.

The measured values are again larger at the location of 0 cm and 1.45 cm (0.57 inches) due to the processing of the pressure-time values. But at the location of 1.02 cm (0.4 inches) the processed value is located above the measured value. Due to the lack of data from the other two cases at this location a final conclusion is difficult to make.

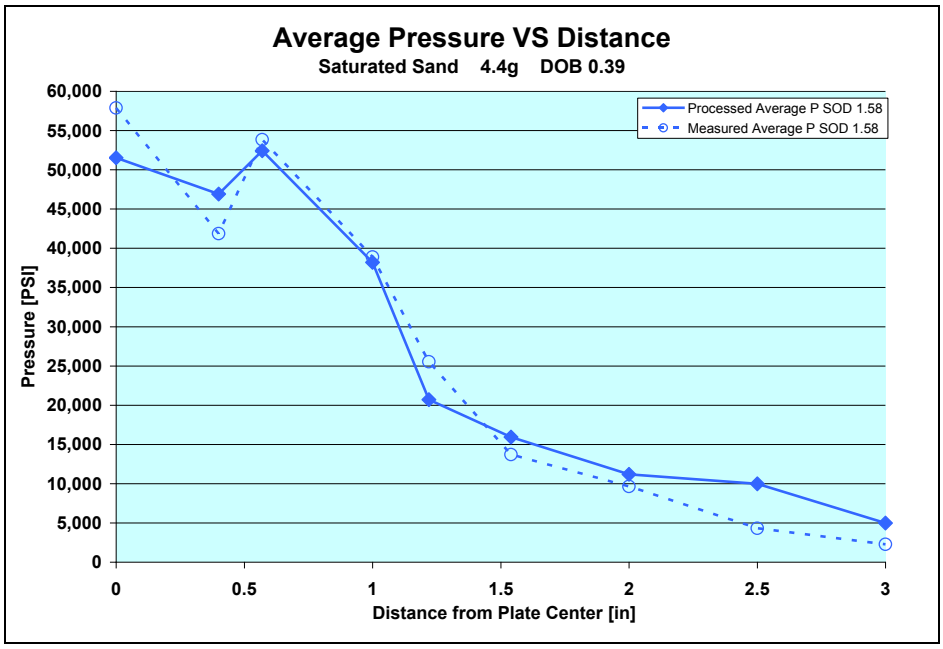

Figure 6.29 Processed versus measured average pressure values for the *intermediate* SOD of 4 cm (1.58 inches)

Comparing the measured average peak pressure values with the processed ones for the *largest* SOD show that the processed peak pressures stay below the measured ones up to the location of 5.08 cm (2 inches), see **Figure 6.30**.

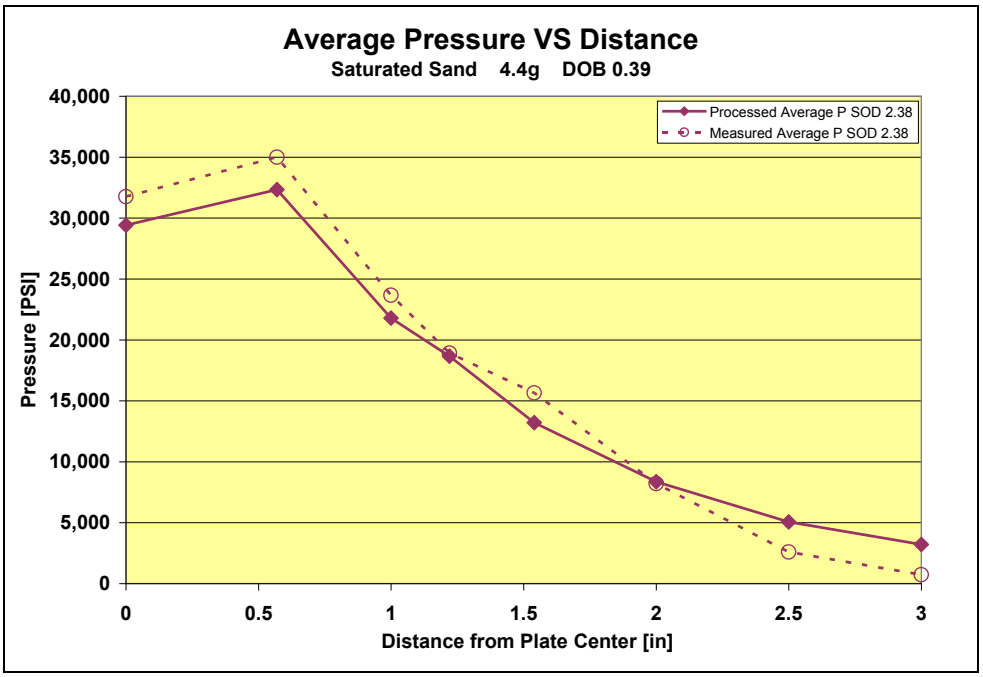

Figure 6.30 Processed versus measured average pressure values for the *largest* SOD of 6 cm (2.38 inches)

As shown earlier comparing the single average pressure-time profiles at certain locations for different stand-off distances, the pulse width for the loading applied on the bottom of the target plate is different (see **Figure 6.31**). The *closest* SOD features the longest pulse widths. For the *intermediate* and the *largest* SOD the loading pulse widths are identical for the locations of 0 cm to 2.54 cm (1 inch). The loading pulse width increases from there on for the *intermediate* SOD and stays in between the curves for the *largest* and *closest* SOD. After passing the location of 6.35 cm (2.5 inches) it decreases and falls below the *largest* SOD. A reason can be that for *larger* SODs the loading time at a fixed location further out on the plate increases significantly. The loading pulse width for the *closest* SOD is always greater than the pulse width for the *largest* SOD at all locations.

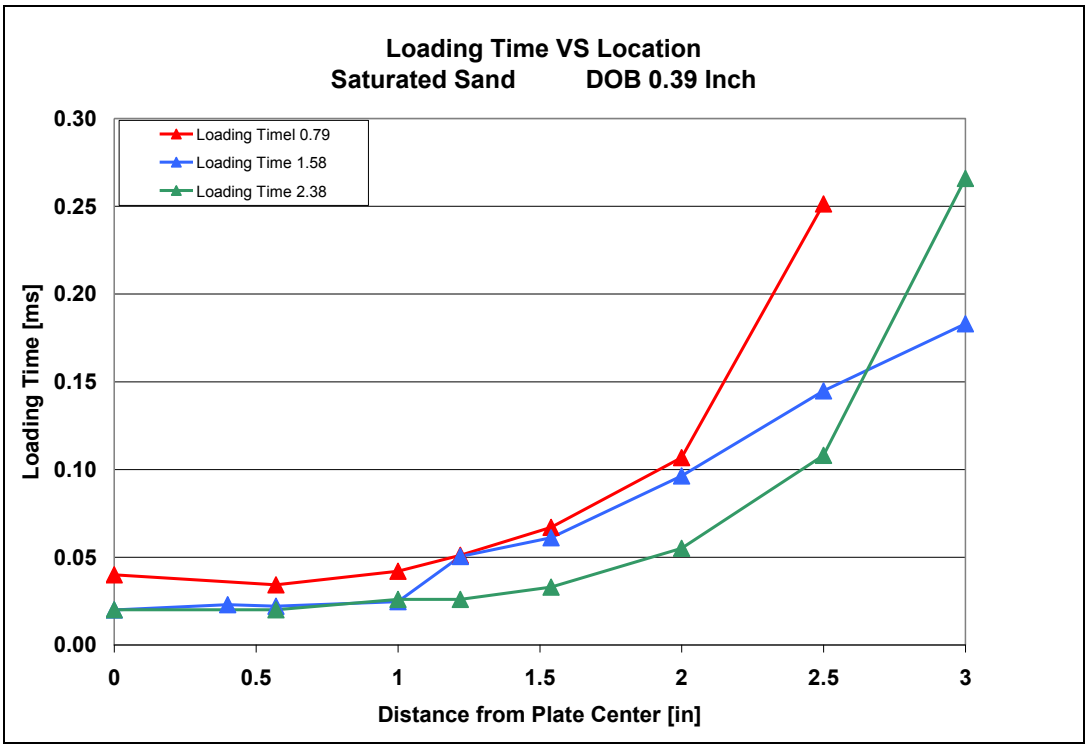

Figure 6.31 Loading pulse widths for different stand-off distances in saturated sand

6.4 Pressure Distribution over the Bottom of a Vehicle for 3 Different Impacting Materials (Saturated Sand, Dry Sand, Water) at the same SOD and DOB

As mentioned before, the loading applied to a target plate is considered as most severe using saturated sand. In the following the pressure distribution on the bottom of a vehicle is shown for 3 different materials (saturated sand, dry sand, water) at the same SOD and same DOB. The results for saturated sand at *intermediate* SOD were already reported in **Section 6.1.1**.

6.4.1 Pressure Distribution over the Bottom of a Vehicle for Dry Sand

The dry sand was tested at standard conditions which are SOD of 4 cm (1.58 inches) and a DOB of 1 cm (0.39 inches) which scales to full scale to a SOD of 40.6 cm (16 inches) and a DOB of 10.2 cm (4 inches). The results of 184 measured pressure – time profiles are shown in **Figure 6.32**. The figure includes the maximum and minimum pressures measured and the calculated average pressure at locations of 0 cm (0 inches), 1.45 cm (0.57 inches), 2.54 cm (1 inch), 3.10 cm (1.22 inches), 3.91 cm (1.54 inches), 5.08 cm (2 inches), 6.35 cm (2.5 inches), and 7.62 cm (3 inches). The average pressure values have to be processed in order to calculate the average pressure value at the bottom of the target plate as shown in **Section 4.3.** The processed average pressure values are shown in **Figure 6.33**. Two polynomial trend lines are used to characterize the pressure profile according to the location on the target plate.

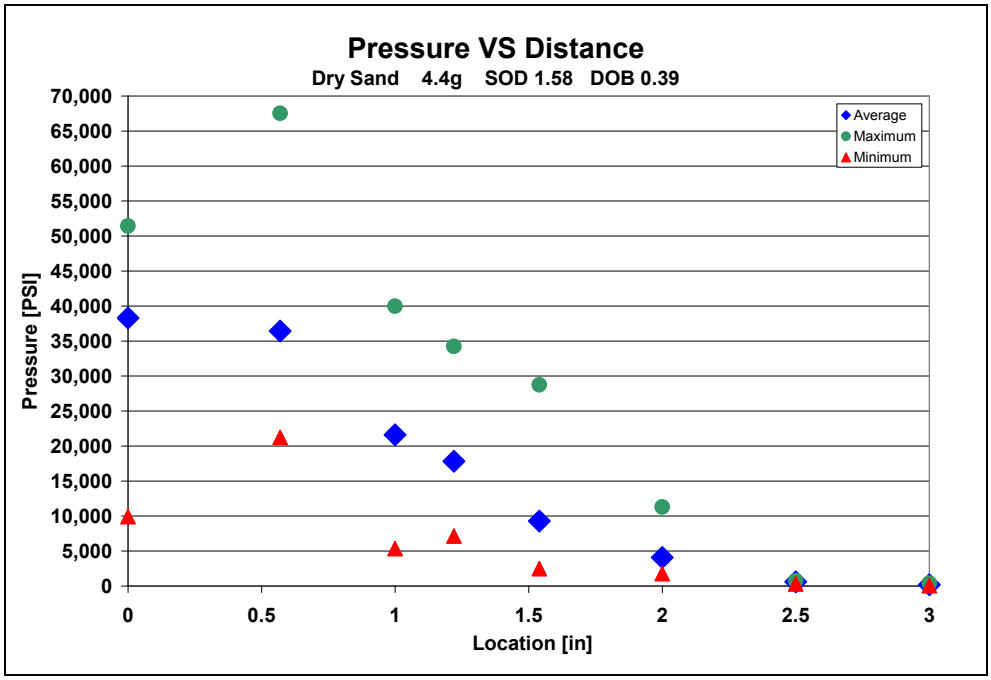

Figure 6.32 Measured pressures for dry sand at SOD 4 cm (1.58 inches)

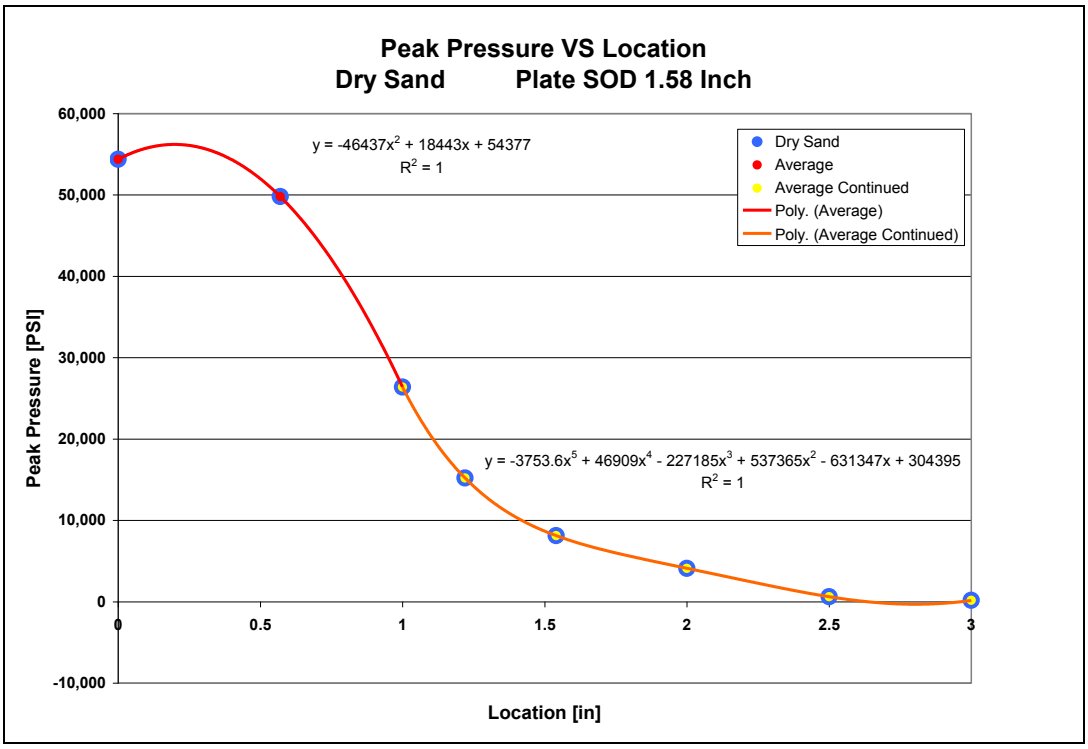

Figure 6.33 Processed average pressures for dry sand at SOD of 4 cm (1.58 inches)

The two trend lines and the related equations shown in **Figure 6.33** can be used in order to process a three dimensional plot, shown in **Figure 6.34**, of the pressure distribution on the bottom of a vehicle with a flat bottom. **Figure 6.35** gives a more detailed view of the center of impact. The shown distribution covers a radius of 7.6 cm (3 inches) with respect to full scale of 77 cm (30.3 inches).

For dry sand the pressure distribution was measured until the radius of 12.7 cm (5 inches), respectively of 1.28 m (4.2 feet) full scale. Kolky bars were used from the center of impact to a radius of 6.35 cm (2.5 inches) and further out pressure sensors from PCB. The results are shown in **Section 5.4**.

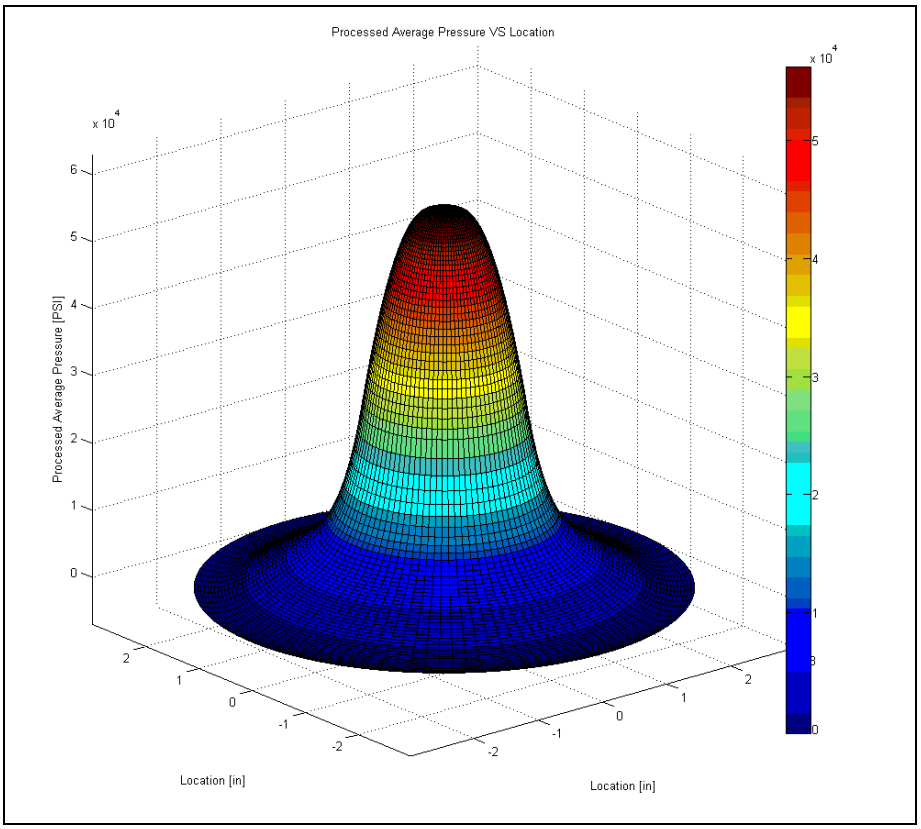

Figure 6.34 Three dimensional plot of processed average pressure distribution for *intermediate* SOD in dry sand

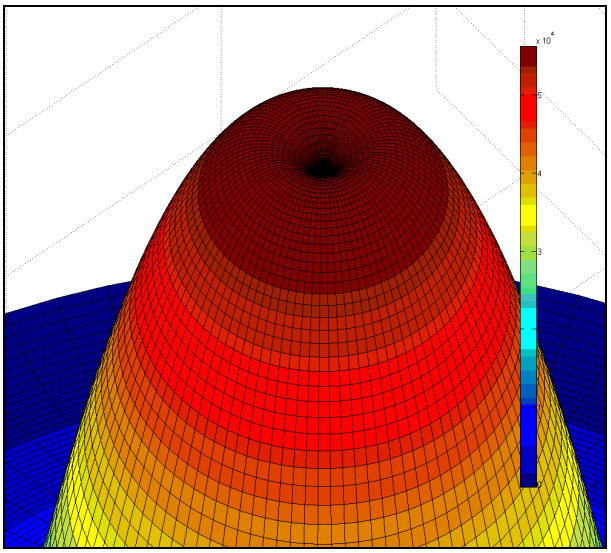

Figure 6.35 Detailed view of center of impact for *intermediate* SOD in dry sand

6.4.2 Pressure Distribution over the Bottom of a Vehicle for Water

The water was tested at the same standard conditions which are SOD of 4 cm (1.58 inches) and a DOB of 1 cm (0.39 inches) respectively scales to full scale to a SOD of 40.6 cm (16 inches) and a DOB of 10.2 cm (4 inches). The results of 156 measured pressure – time profiles are shown in **Figure 6.36**. The figure includes the maximum and minimum pressures measured and the calculated average pressure at locations of 0 cm (0 inches), 1.45 cm (0.57 inches), 2.54 cm (1 inch), 3.91 cm (1.54 inches), 5.08 cm (2 inches), 6.35 cm (2.5 inches), and 7.62 cm (3 inches). Note the increased deviation at the location of 3.91 cm (1.54 inches) (**Figure 6.36**). The processed average pressure values are shown in **Figure 6.37**. One polynomial trend line is used to characterize the pressure profile according to the location on the target plate.

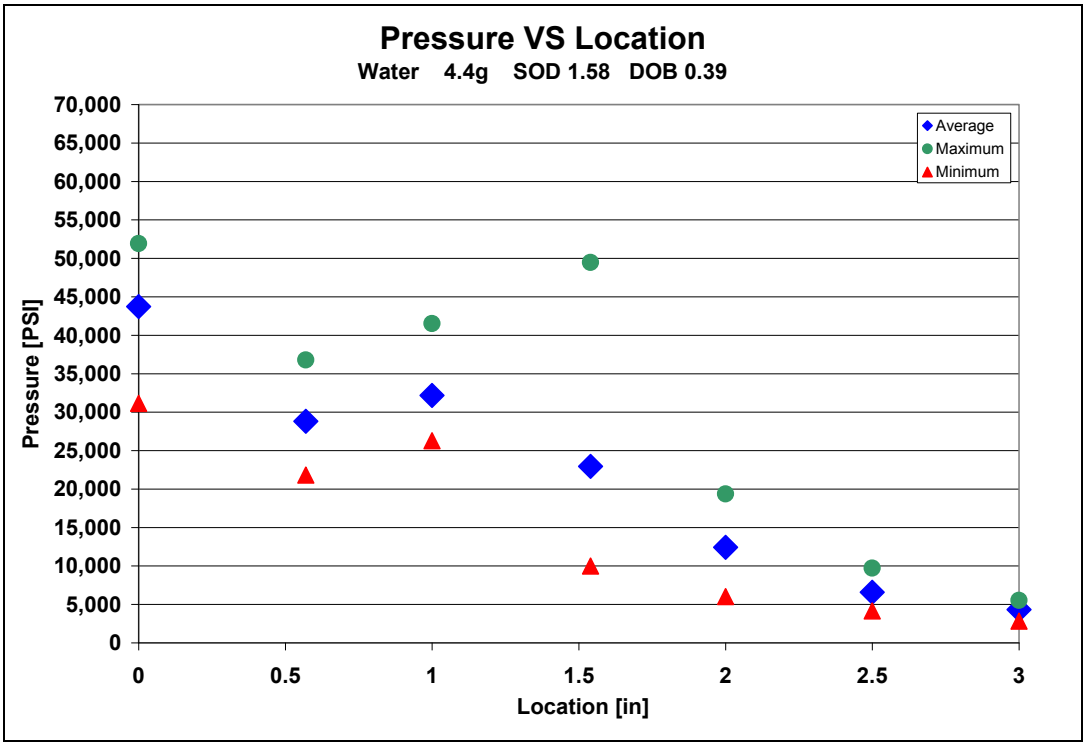

Figure 6.36 Measured pressures for water at SOD 4 cm (1.58 inches)

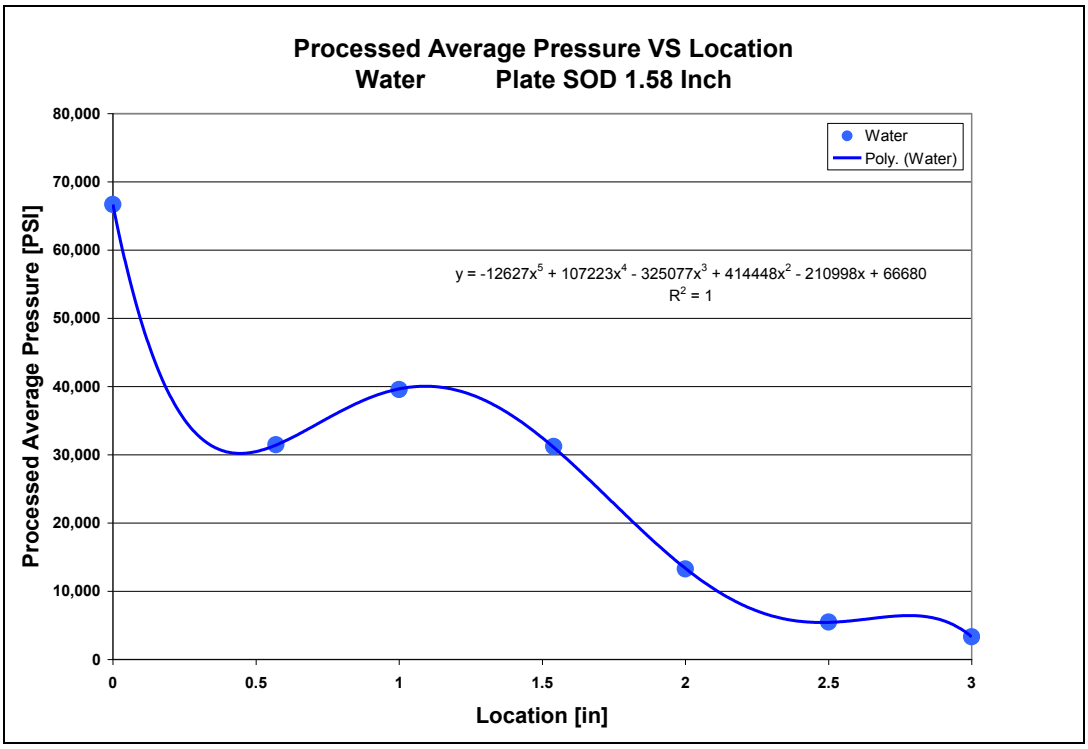

Figure 6.37 Processed average pressures for water at SOD of 4 cm (1.58 inches)

The trend line and the related equation shown in **Figure 6.37** is used in order to process a three dimensional plot, shown in **Figure 6.38**, of the pressure distribution on the bottom of a vehicle with a flat bottom. **Figure 6.39** gives a more detailed view of the center of impact. The shown distribution covers a radius of 7.6 cm (3 inches) with respect to full scale of 77 cm (30.3 inches). The water shows a needle point at the center of impact which represents the peak pressure value on the bottom of the target plate.

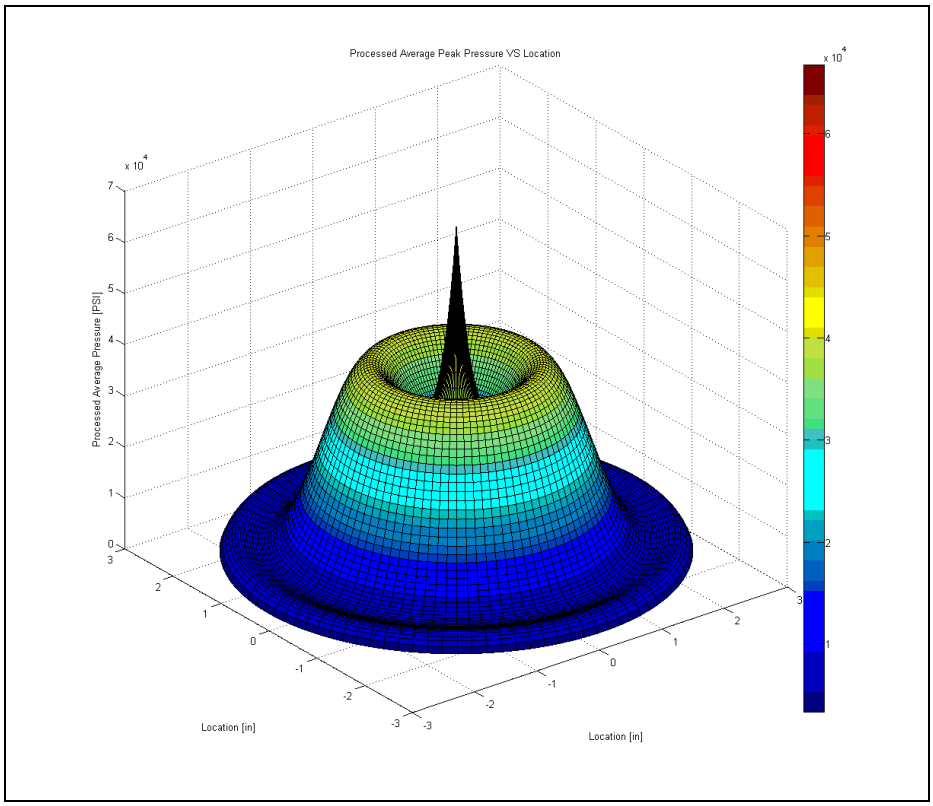

Figure 6.38 Three dimensional plot of processed average pressure distribution for *intermediate* SOD in water

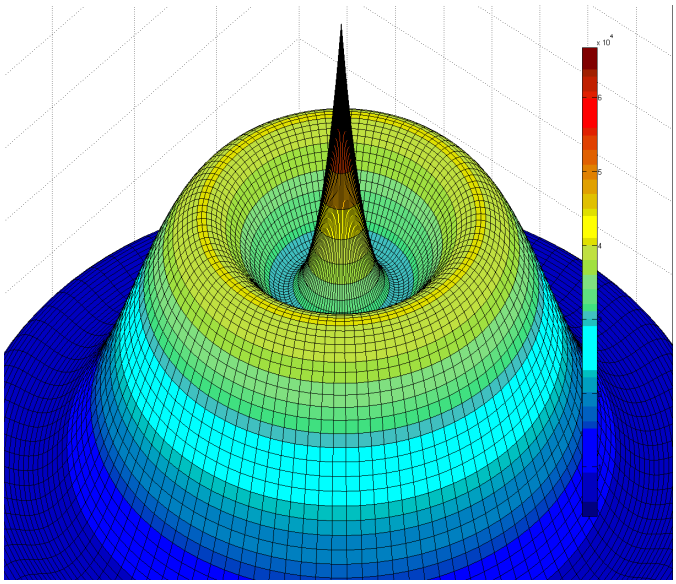

Figure 6.39 Detailed view of center of impact for *intermediate* SOD in water

6.4.3 Comparison of the Pressure Distribution over the Bottom of a Vehicle for 3 Different Impacting Materials (Saturated Sand, Dry Sand, Water) at the same SOD and DOB

Comparing the results of the *saturated sand, dry sand*, and *water* tests conducted (**Figure 6.40**), it is obvious that *dry sand* results are the lowest at almost all locations. Surprisingly the test results for *water* show the lowest average peak pressure at the location of 1.45 cm (0.57 inches) which is significantly lower compared to the other test results at that location. At all the other locations the test results for *water* show the highest peak pressure values. As mentioned before in the saturated test series, a pressure measurement at the location of 1 cm (0.4 inches) for the *water* test and the *dry sand* test is needed in order to compare the results to the *saturated sand* test at this location.

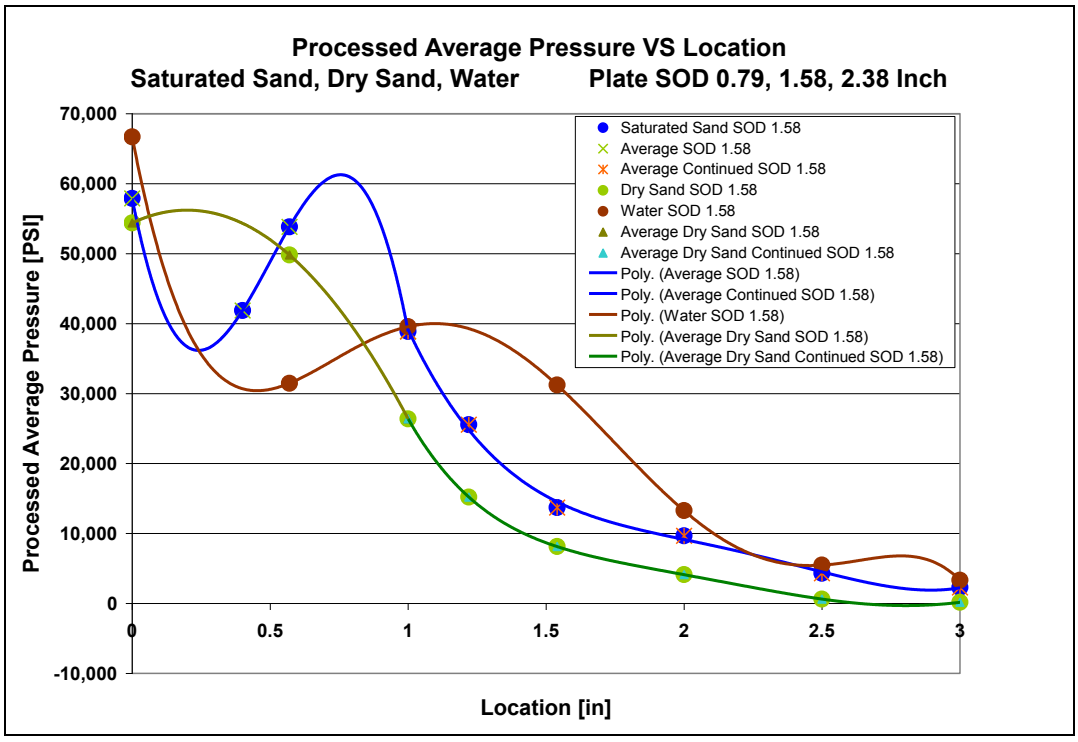

Figure 6.40 Processed average pressures for *saturated sand, dry sand, water*

6.5 Impulse Results for Saturated Sand, Dry Sand and Water at the same SOD and DOB

The test results compared in the following were gained using the same test set-up for *saturated sand, dry sand*, and *water*. The difference between the test series is the change in material used for the loading. The DOB used was 1 cm (0.39 inches) and the SOD 4 cm (1.58 inches).

The specific impulse generated from the processed average pressure values at each location of the plate for the 3 different types of loadings is shown in **Figure 6.41**.

The specific impulse values for *water* are largest from the center of the plate and drop rapidly to a low at the location of 1.45 cm (0.57 inches). With increasing distance from the center of the plate the specific impulse increases to a maximum at the location of 3.92 cm (1.54 inches). With further increasing distance the specific impulse decreases constantly.

For the *dry sand* the specific impulse is largest at the center of the plate. It has decreased slightly at the location of 1.45 cm (0.57 inches). The specific impulse drops vastly at the location 2.54 cm (1 inch) and is the lowest at this location for all 3 cases. With increasing distance from the center of the plate the impulse decreases constantly in a linear manner and stays below saturated sand and water until it reaches the location of 7.62 cm (3 inches). Between 7.62 cm (3 inches) and 12.7 cm (5 inches) the specific impulse stays very low, see **Figure 6.42**.

For the *saturated sand* the specific impulse is lowest at the center of the plate. It drops further at the location of 1.02 cm (0.4 inches), has its maximum at the next location of 1.45 cm (0.57 inches), decreases from there on and stays in between the values for water and dry sand until it increases at the location of 6.35 cm (2.5 inches).

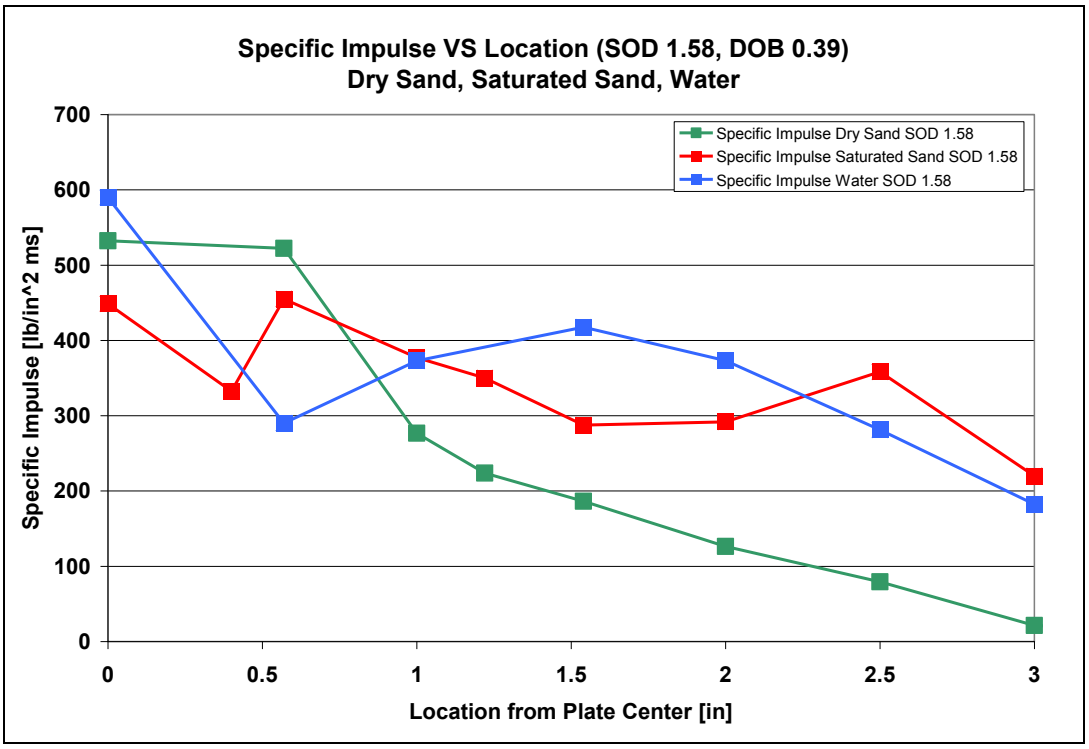

Figure 6.41 Specific impulse for the same stand-off distance using *saturated sand, dry sand, water*

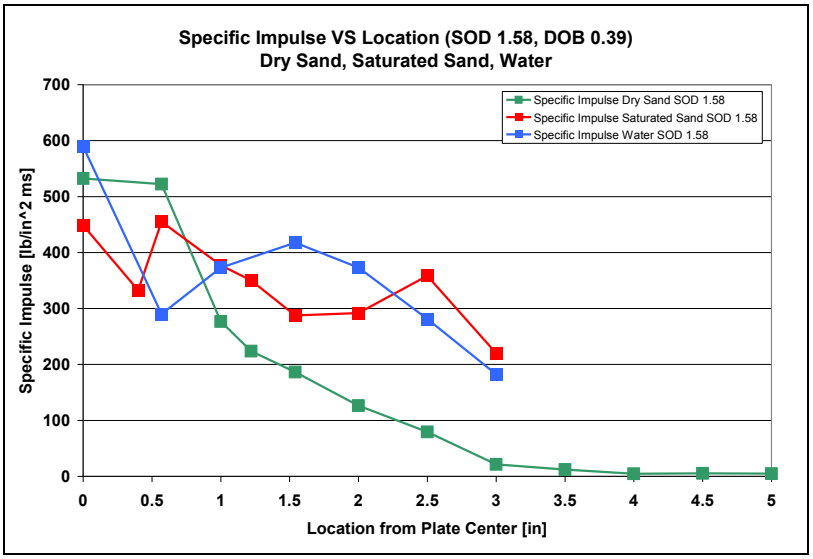

Figure 6.42 Specific impulse for the same stand-off distance using *saturated sand, water, dry sand* details

Comparing the 3-D plots for the 3 different loading conditions reveals the differences between the cases.

Figure 6.43 shows the impulse for the *dry sand* loading. As shown in the plot the impulse forms a plateau at the center of the plate followed by a steep decline. The decline eases off about half way down and forms a cone shape. The shape of the plot creates the least volume of the 3 cases and has therefore the smallest total impulse.

Figure 6.44 shows the impulse for the *saturated sand*. As described before the impulse is very high at the center of the plate and declines fast and increases again forming the first rim. Further away from the center the impulse declines again and increases shortly after forming the second rim. The shape of the plot for saturated sand creates the second largest volume of the 3 cases and has therefore the second largest impulse.

Figure 6.45 shows the impulse for *water*. The impulse is very high at the center of plate forming a needle shape. It declines fast and increases again forming a rim. From the top of the rim it declines constantly forming a bell shape. The shape of the plot for water creates by far largest volume of the 3 cases and has therefore the largest total impulse.

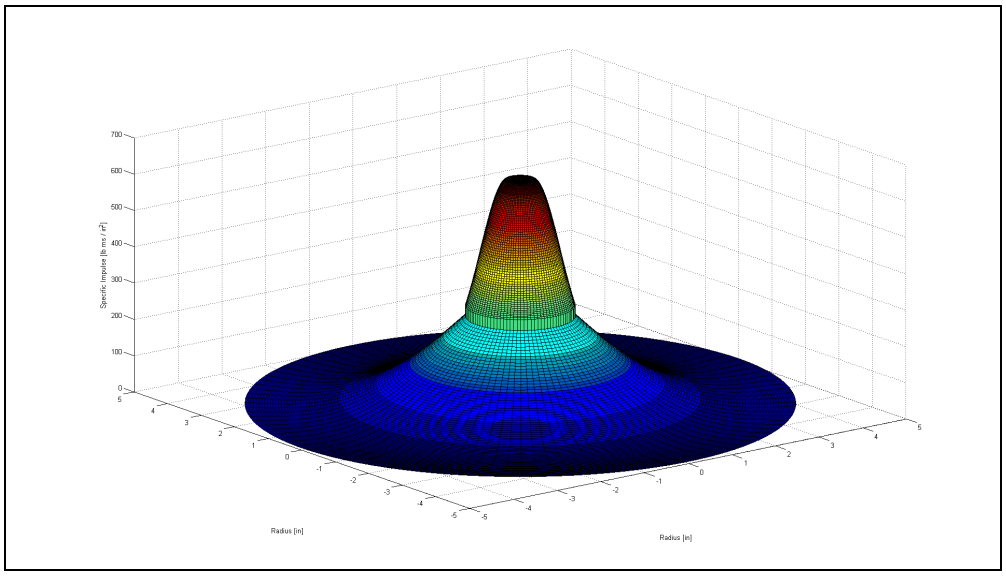

Figure 6.43 3-D plot for impulse for *dry sand*

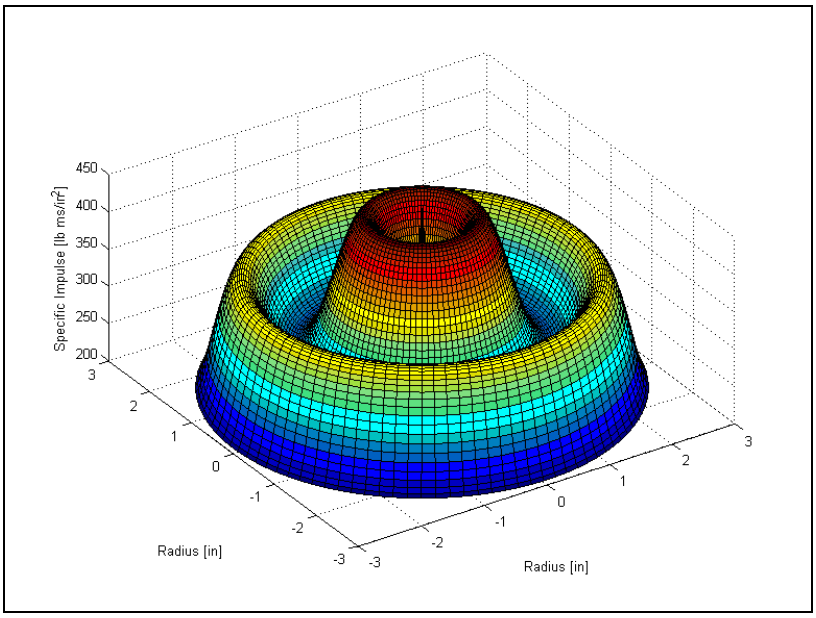

Figure 6.44 3-D plot for impulse for *saturated sand*

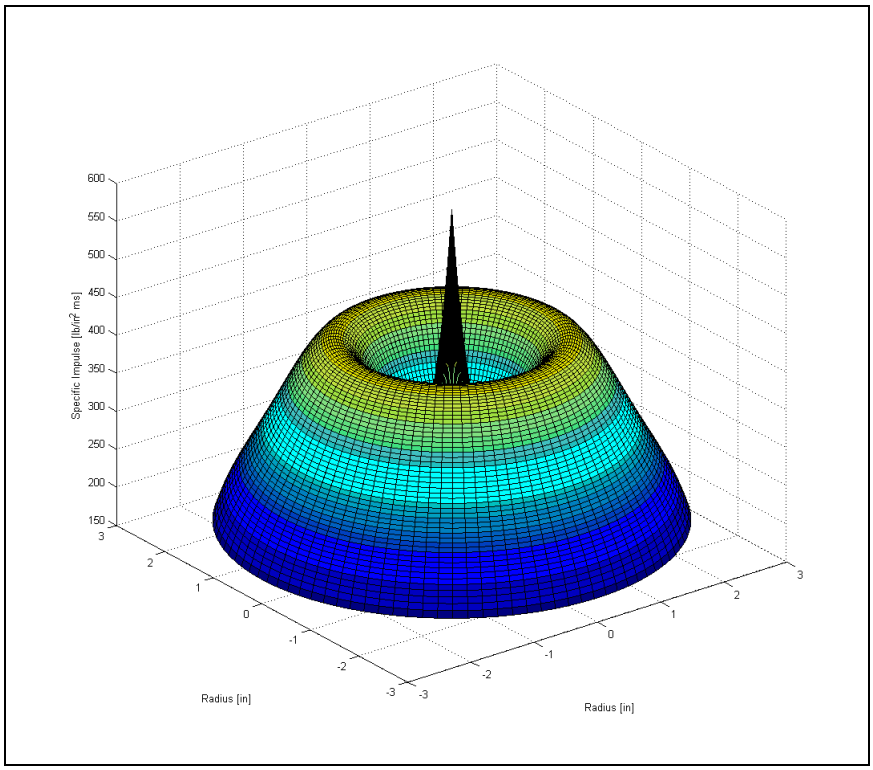

Figure 6.45 3-D plot for impulse for *water*

The impulse results for all cases are shown in **Figure 6.46**. The plot shows the accumulated impulse over the diameter of a circular target plate. There is not much difference between the 3 different types of loading applied until the target size reaches 7.62 cm (3 inches). The impulse delivered is almost the same. At the diameter of 10.16 cm (4 inches) it starts to make a difference what type of loading is applied to the bottom of the target. *Water* delivers the most impulse followed by *saturated sand* and *dry sand*. At the diameter of 12.7 cm (5 inches) for *water* and *saturated sand* the delivered impulse is about 40% higher compared to *dry sand*. At the diameter of 15.24 cm (6 inches) the impulse delivered by *water* and *saturated sand* compared to *dry sand* increases by 50%. The impulse for *dry sand* starts leveling off at this diameter and increases only very little until the diameter of 25.4 cm (10 inches) is reached.

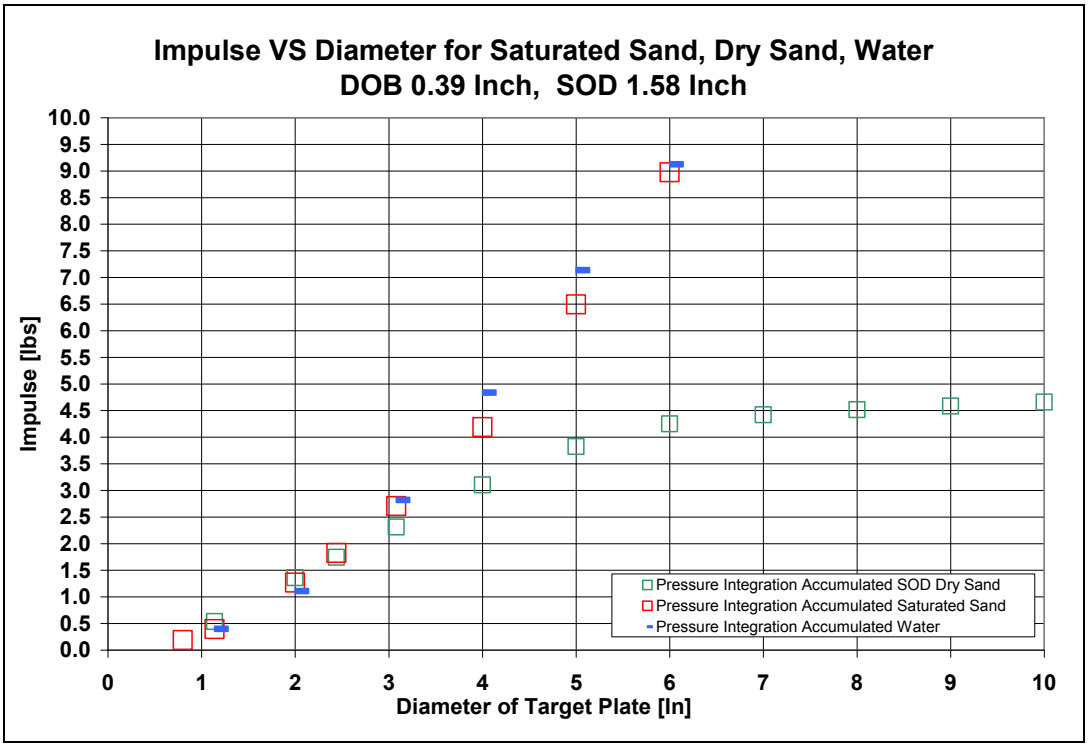

Figure 6.46 Impulse for the same stand-off distance using *saturated sand, dry sand, water*

Figure 6.47 combines both types of tests conducted, impulse measurement tests using the round target plates and the accumulated impulse using the processed average pressure-time profiles from the pressure test series. As earlier shown both types of tests for each type of loading agree very well. At the plate diameter of 36.32 cm (14.3 inches) *water* has delivered the largest impulse almost 50% more than *saturated sand*. The impulse for *dry sand* has leveled off and reaches only 25% of the impulse caused by *water*. Increasing the diameter of the plate does not further contribute to increase the impulse delivered.

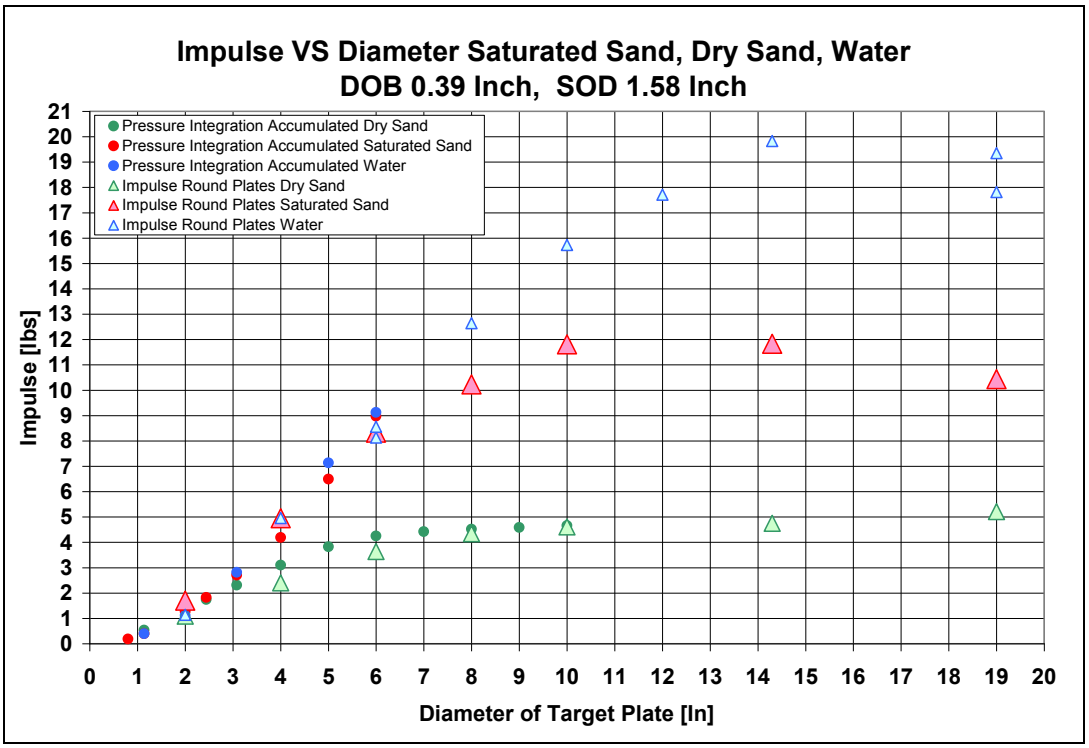

Figure 6.47 Impulse for the same stand-off distance using *saturated sand, dry sand, water* for accumulated pressure and impulse measurement

Combining the specific impulse results from the average pressure-time profiles and the plate tests, the specific impulse distribution over location from the target plate can be shown. The specific impulses for the plate tests need to be

calculated from the differences of impulse delivered to the round plates. **Figure 6.48** shows the trend lines used for *dry sand,* **Figure 6.49** for *saturated sand*, and **Figure 6.50** for *water* in order to plot the specific impulse distribution.

These trend lines can be used like described before to plot the specific impulse distribution of the combined test set data. Towards the center of the plate between 0 cm and the diameter of 5.08 cm (2 inches) the average pressure-time profiles are used in order to calculate the specific impulse. From the diameter of 5.08 cm (2 inches) to 15.24 cm (6 inches) for *saturated sand* and *water* both the pressure-time profiles and the round plate test data is used in order to calculate the specific impulse. In the case of *dry sand* the data overlaps from the diameter of 5.08 cm (2 inches) to 25.4 cm (10 inches). For increasing diameters only the round plate test data is used until the impulse for a 4.4 g charge is completely delivered to the target plate. The plots for the impulse as a function of location for the combined data are shown in **Figure 6.51** for *dry sand*, **6.52** for *saturated sand*, and **6.53** for *water*.

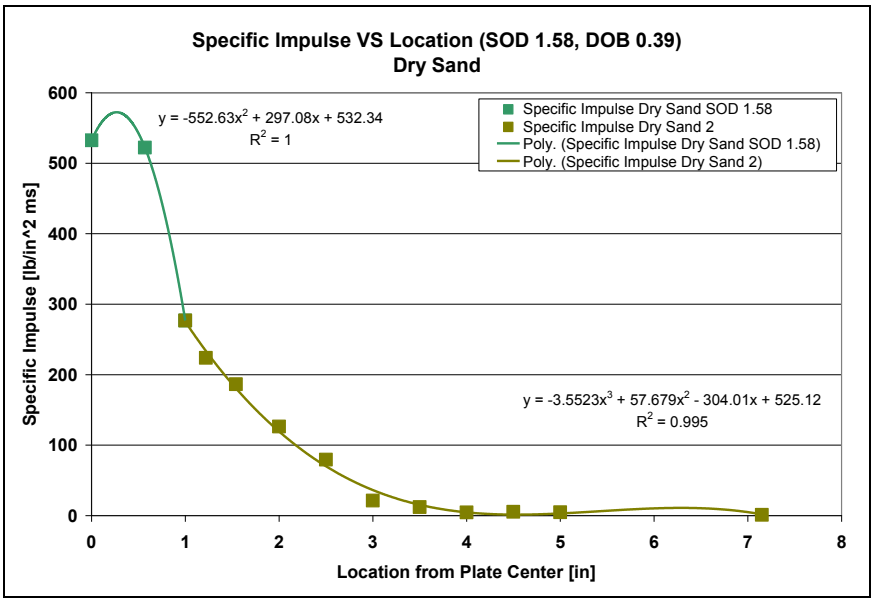

Figure 6.48 Specific Impulse distribution combined testing for *dry sand*

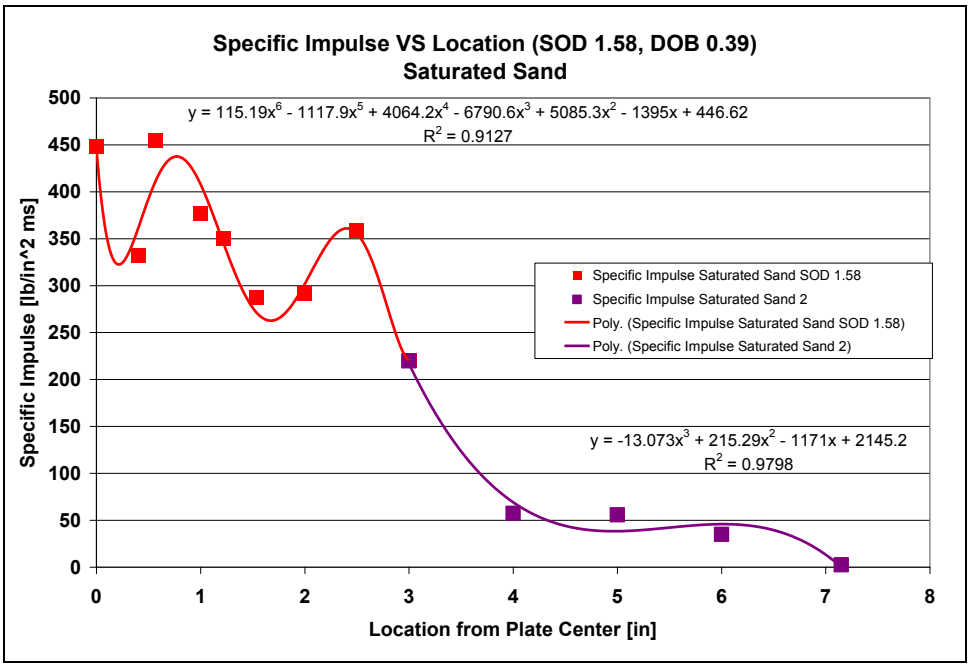

Figure 6.49 Specific Impulse distribution combined testing for *saturated sand*

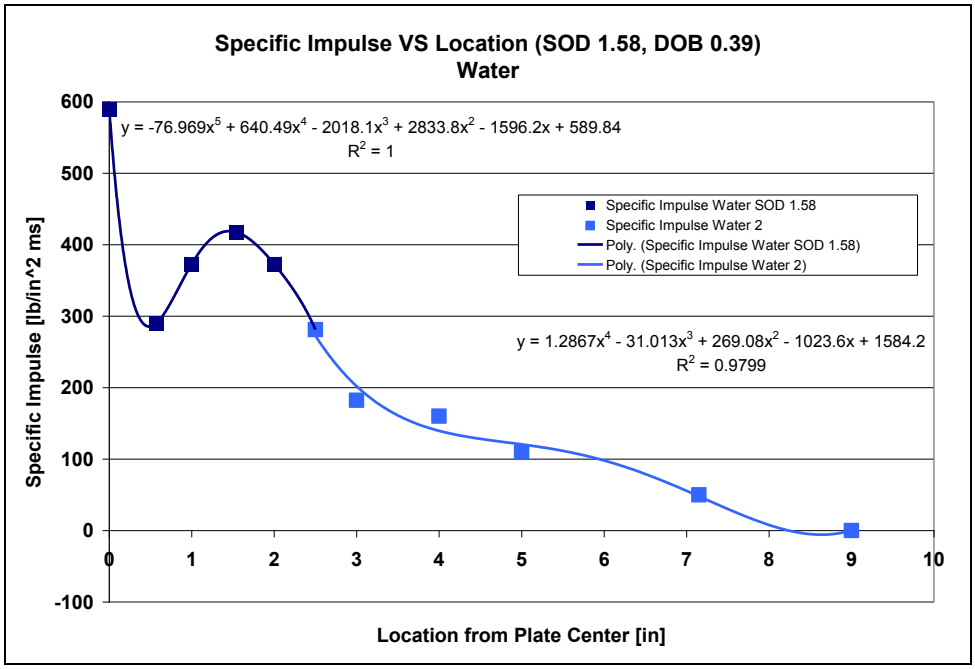

Figure 6.50 Specific Impulse distribution combined testing for *water*

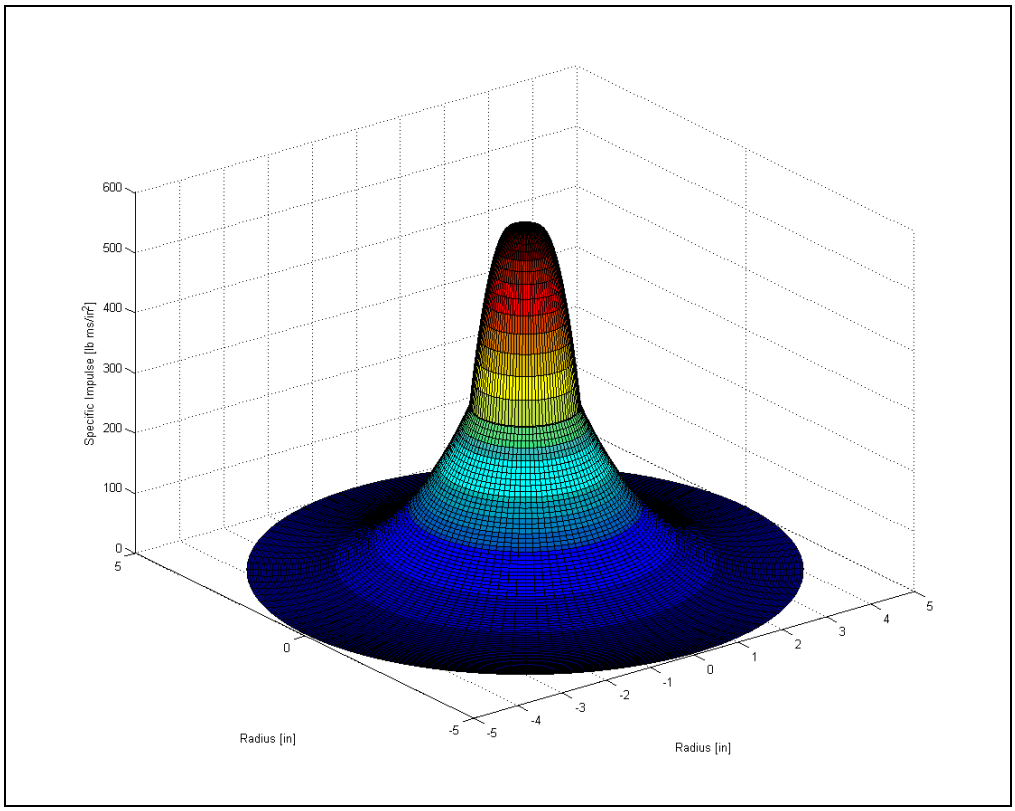

Figure 6.51 3-D plot for impulse for *dry sand* combined data

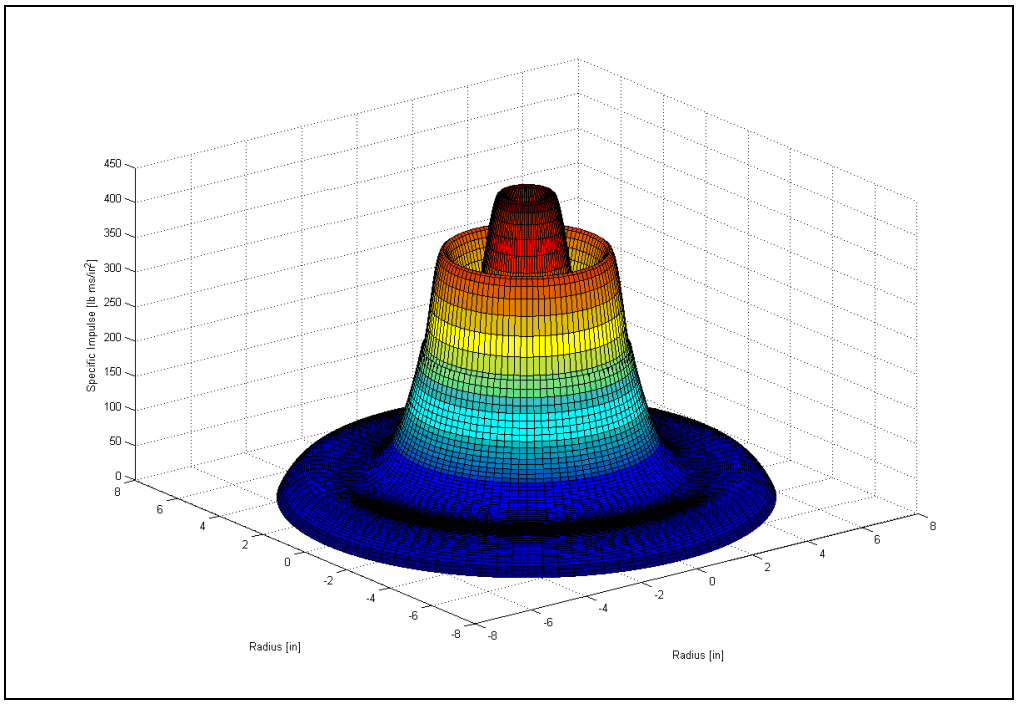

Figure 6.52 3-D plot for impulse for *saturated sand* combined data

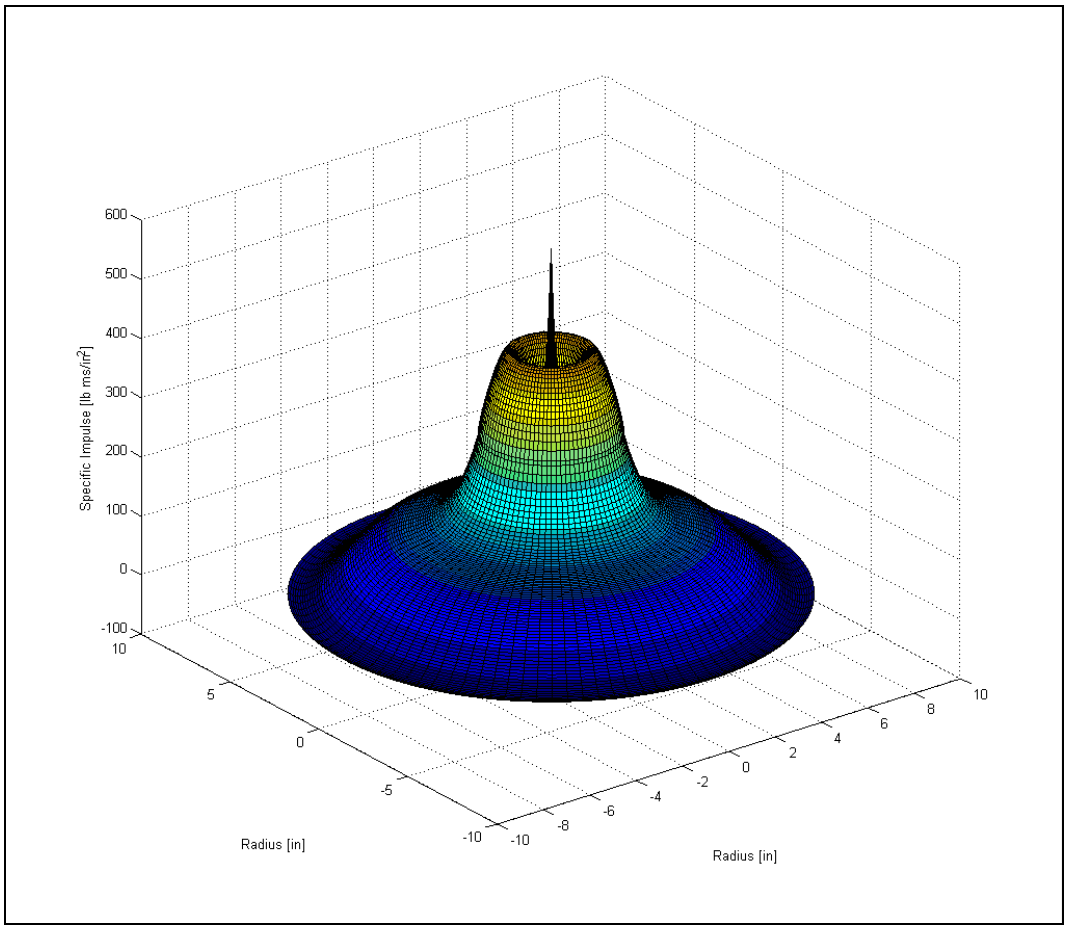

Figure 6.53 3-D plot for impulse for *water* combined data

6.6 Peak Pressure Results for Saturated Sand, Dry Sand, and Water at the Same SOD and DOB

In the following 3 different types of loading are compared for the same test conditions, a SOD of 4 cm (1.58 inches) and a DOB of 1 cm (0.39 inches). The loading is applied using *saturated sand*, *dry sand* and *water* as impacting media. Plotting the corresponding pressure-time profiles at the distance of 0 cm and 1.45 cm (0.57 inches) from the center of the plate reveals the differences between the 3 cases, see **Figure 6.54**.

At the location of 0 cm (0 inches), at the center of the plate, the processed average peak pressures for the *dry sand* and the *saturated sand* are very similar. The *water* shows the highest pressure value. The loading pulse for *dry sand* starts first and lasts the longest showing an oscillation after 0.06 milliseconds. Following next in time is the loading pulse for *water* which is slightly broader than the one for *saturated sand*.

At the location of 1.45 cm (0.57 inches) the average peak pressures for the *dry sand* and the *saturated sand* are still similar. The *water* shows the lowest pressure value. The loading pulse width is still broadest for *dry sand*, followed by *water* and than *saturated sand*.

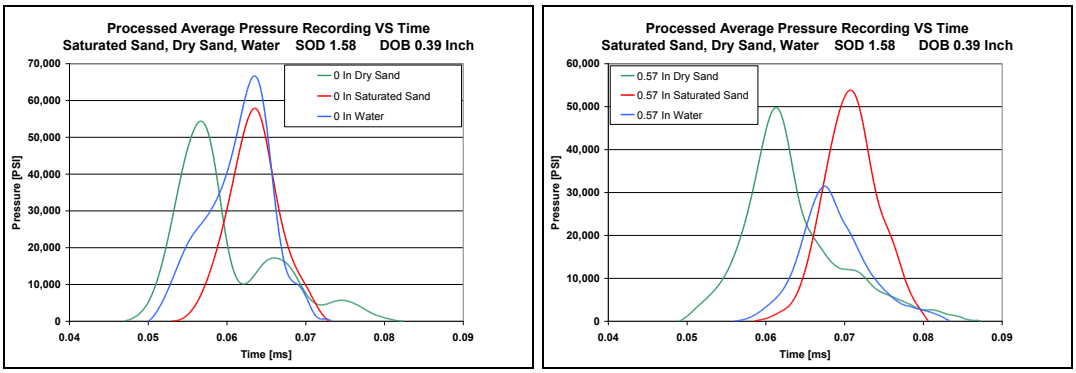

Figure 6.54 Average pressure-time profiles at 0 cm and 1.45 cm (0.57 inches) from the center of the plate for *water*, *saturated* and *dry sand*

At the location of 2.54 cm (1 inch), see **Figure 6.55**, the average processed peak pressures for the *dry sand* and *water* are practically the same. The *dry sand* shows the lowest pressure value. The loading pulse for *dry sand* and *water* start almost at the same time with the *dry sand* pulse width being broader.

At the location of 3.1 cm (1.22 inches), see **Figure 6.55**, the average peak pressures calculated for the *dry sand* is the lowest. The water pressure was not recorded at this location. The loading pulse for *dry sand* still starts first and is broad. As described earlier the *dry sand* tends to impact for a long time after the main impact took place since the loading characteristics are very different compared to cases where water is involved.

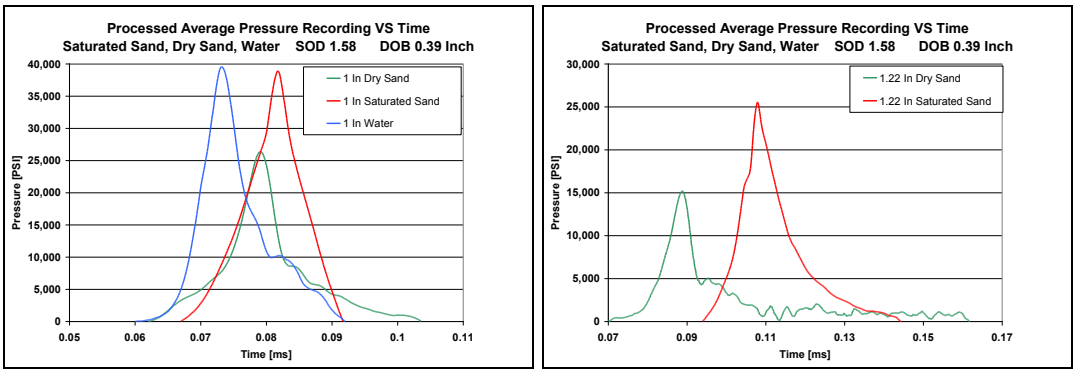

Figure 6.55 Average pressure-time profiles at 2.54 cm (1 inch) and 3.1 cm (1.22 inches) from the center of the plate for *water*, *saturated* and *dry sand*

At the location of 3.91 cm (1.54 inches), the average peak pressures for *water* are twice as high as for the *saturated sand*. The *dry sand* shows the lowest pressure value, see **Figure 6.56**. The loading pulse for *water* starts first from this location on, followed by *dry sand* and last *saturated sand*. Still the broadest pulse width is represented by the *dry sand*.

At the location of 5.08 cm (2 inches) the trend as described for the location of 3.91 cm (1.54 inches) is still the same and the time of arrival for the peak pressure for the *saturated sand* occurs even later, see **Figure 6.56**.

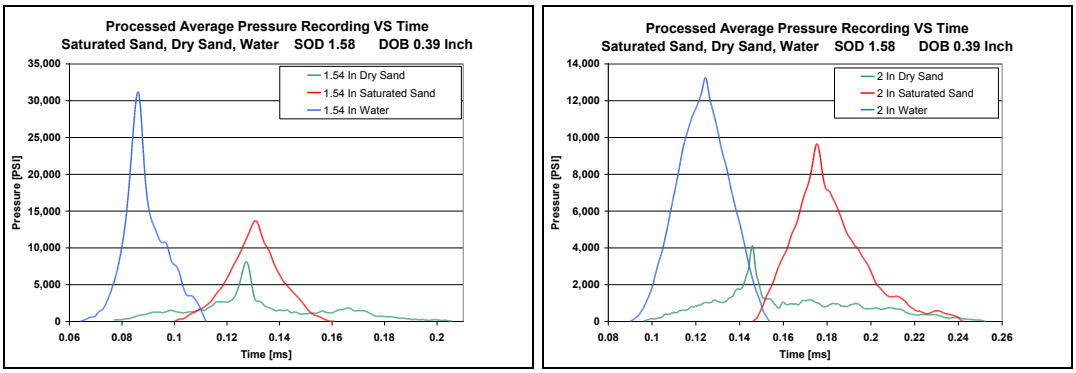

Figure 6.56 Average pressure-time profiles at 3.91 cm (1.54 inches) and 5.08 cm (2 inches) from the center of the plate for *water*, *saturated* and *dry sand*

At the location of 6.35 cm (2.5 inches) the loading pulse for *water* still starts first followed by a very broad pulse width for *dry sand*. The *saturated sand* pulse starts very late in time but still shows a peak, so does the profile for *water*. The loading for *dry sand* has a totally different character and does not show a pressure peak any more like it did in **Figure 6.56**.

At the location of 7.64 cm (3 inches) the pressure-time profiles have the same characteristics as seen at the location of 6.35 cm (2.5 inches) and the peak pressures drop further, see **Figure 6.57**.

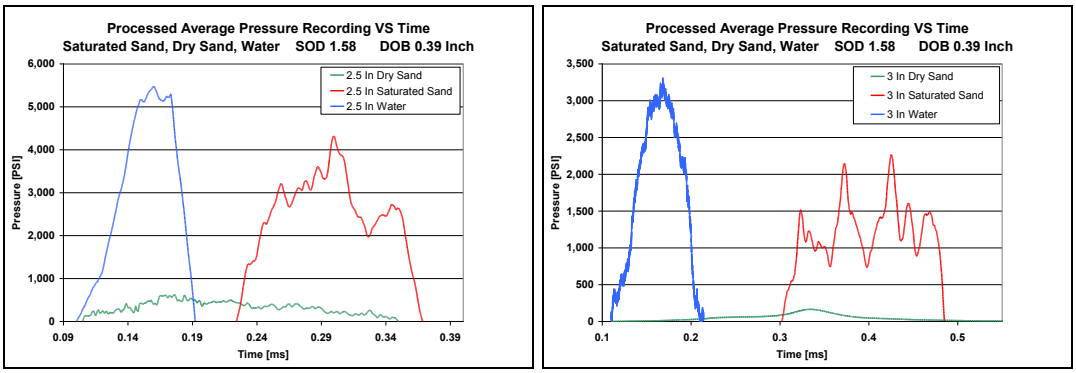

Figure 6.57 Average pressure-time profiles at 6.35 cm (2.5 inches) and 7.64 cm (3 inches) from the center of the plate for *water*, *saturated* and *dry sand*

Figure 6.58 contains the processed average peak pressure values for the above described cases where *saturated sand*, *dry sand* and *water* was used. It reflects the above described peak pressure distribution at each location calculated based on the measured values of the target plate. Using a different media for loading the target plate has an influence on the peak pressure keeping the test set-up constant.

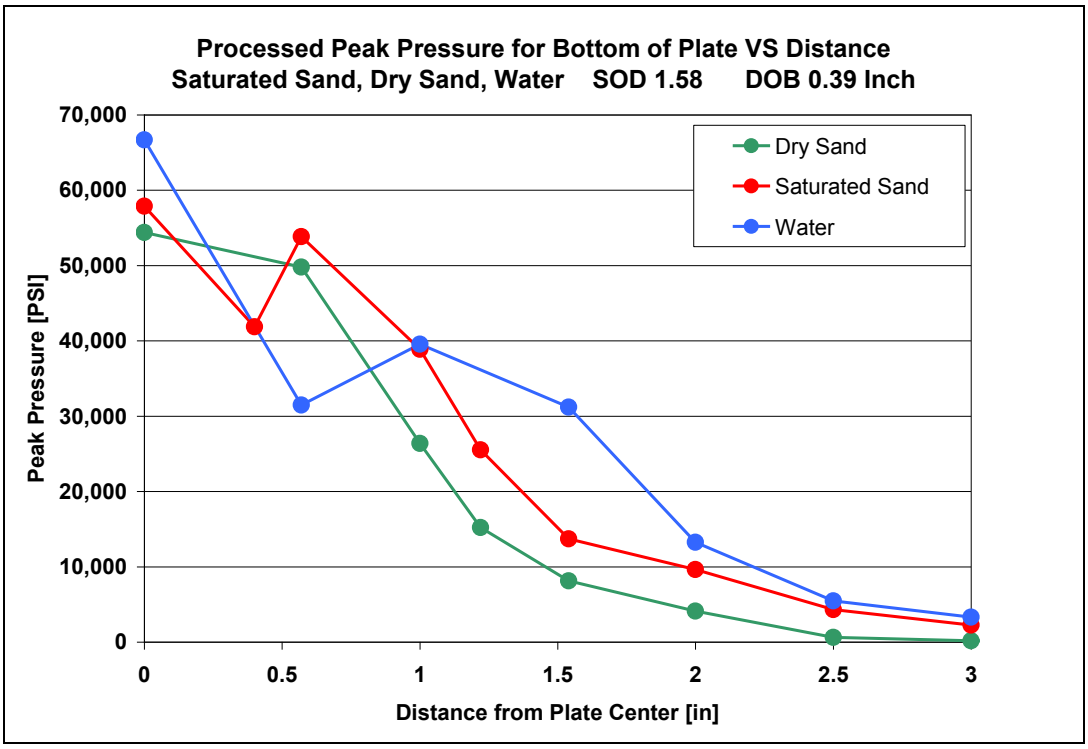

Figure 6.58 Processed average pressure values for the bottom of the target plate for *saturated sand*, *dry sand* and *water*

Comparing the measured average peak pressure values with the processed ones for *dry sand* reveals the differences at each location, see **Figure 6.59**. The processed values are larger at the location of 0 cm, 1.45 cm (0.57 inches) and 2.54 cm (1 inch) due to a significant larger logarithmic decrement calculated at these locations for *dry sand* (compare **Section 5**). At the next 2 locations (3.1 cm (1.22 inches), 3.91 cm (1.54 inches)) the processed peak pressure drops under the measured value due to the off-set correction based on the drift of the pressure-time profile. Similar corrections have been done to the *saturated sand* profiles at the same SOD, compare **Figure 6.16**. From the location of 5.08 cm (2 inches) on the processed values are identical with the measured values for *dry sand*.

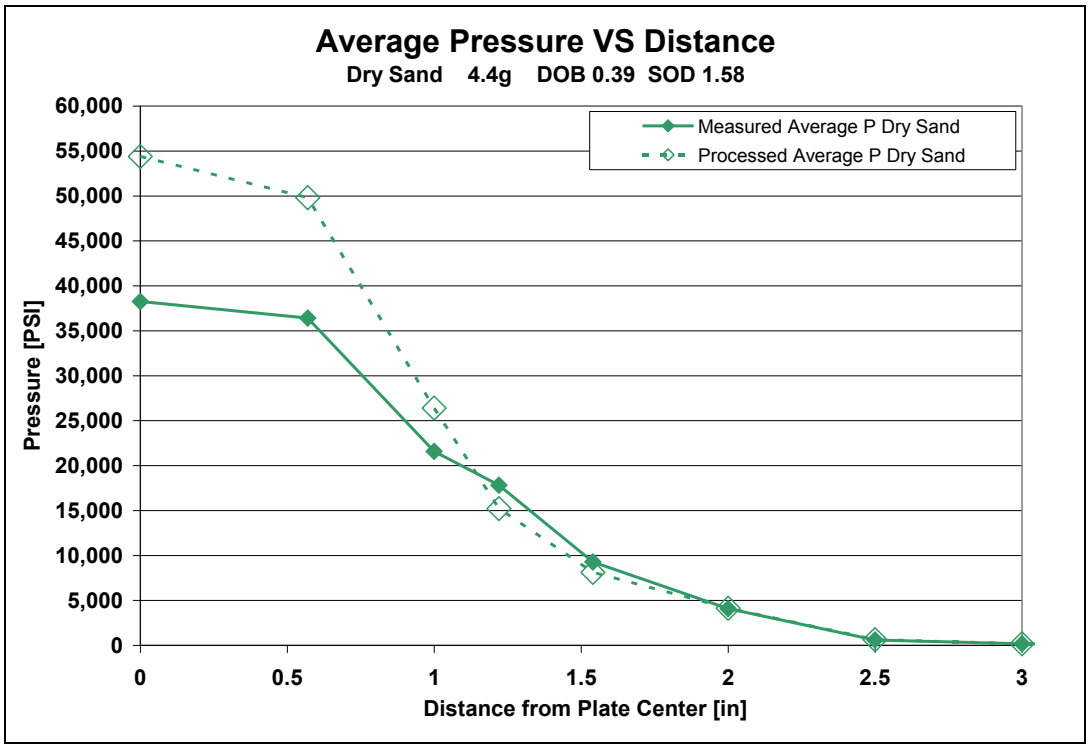

Figure 6.59 Processed versus measured average pressure values for the SOD of 4 cm (1.58 inches) in *dry sand*

Comparing the measured average peak pressure values with the processed ones for *water* shows the same trend as described before, see **Figure 6.60**. The processed values are larger at the location of 0 cm, 1.45 cm (0.57 inch), 2.54 cm (1 inch), and 3.19 cm (1.54 inches). From the location of 5.08 cm (2 inches) on the processed values are more or less identical with the measured values for *water*.

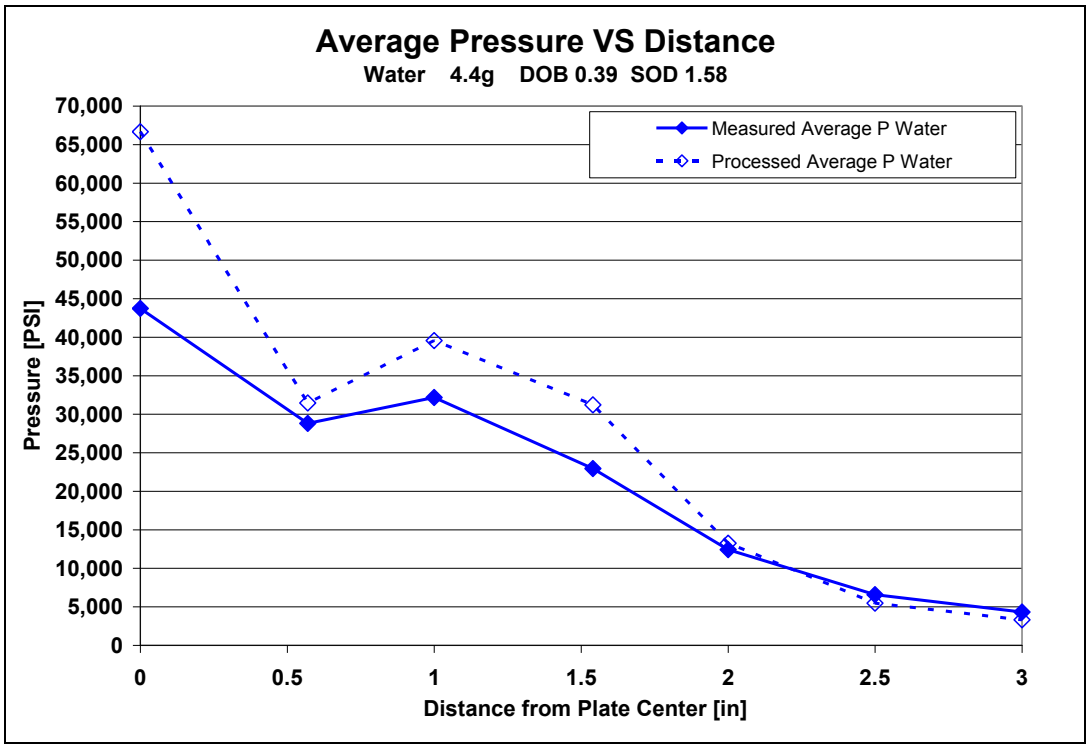

Figure 6.60 Processed versus measured average pressure values for the SOD of 4 cm (1.58 inches) in *water*

As shown in **Figure 6.61** the loading pulse widths are identical from the center of the plate up to the distance of 2.54 cm (1 inch). With increasing distance from the center the pulse width for *dry sand* starts to increase the most followed by *saturated sand*. *Water* shows the shortest loading pulse widths. From the location 6.35 cm (2.5 inches) on the loading pulse width starts increasing disproportionately high for *dry sand*.

Looking at all the measurements recorded for *dry sand*, the loading pulse widths increase even further, see **Figure 6.62**. The loading pulse widths are very long from the location of 7.62 cm (3 inches) on but the pressures applied are very low.

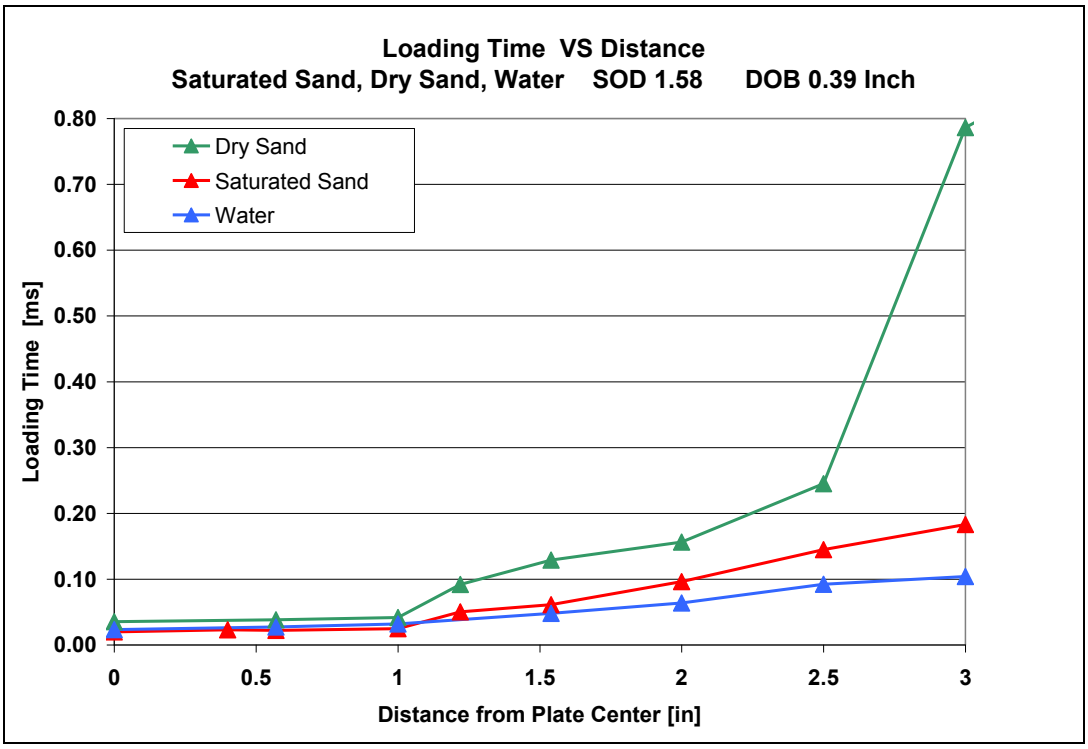

Figure 6.61 Loading time for pulse widths for same stand-off distances using *saturated sand*, *dry sand*, *water*

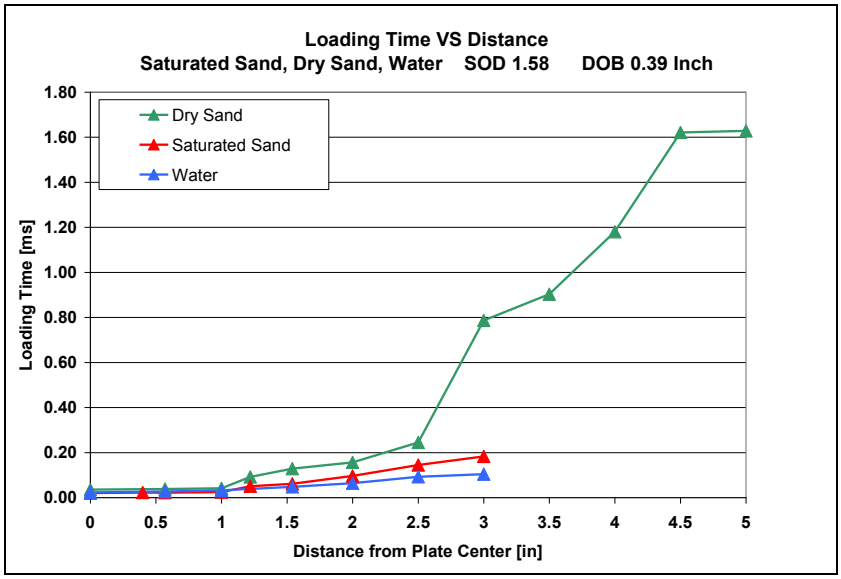

Figure 6.62 Loading pulse widths for same stand-off distances using *saturated sand*, *dry sand, water* in detail

6.7 Computed Results in Water Testing at the SOD of 4 cm (1.58 inches)

Numerous papers have been published **[15] – [20]** simulating the loading on a plate suspended directly above an explosive charge submerged in water or buried soil. Here some brief results on a target plate suspended over water will be shown. Results indicate that the plate loading mechanism of a buried charge in soil is similar to that one submerged in water. Using water instead of sand as a loading material has advantages for the computation. Sand is difficult to simulate and for water the properties are well known. The simulations were generated using the DYSMAS code (Dynamic System Mechanics Advanced Simulation).

Figure 6.63 shows results for a computed simulation in comparison of experimental results using Kolsky bars for a pressure measurement. The test specifics used were DOB 1 cm (0.39 inches), SOD 4 cm (1.58 inches), 4.4 g charge, and water. The computer simulation shows a steeper rise and fall of the pressure-time profile. Depending of the grid size used in the computation the peak pressure varies somewhat comparable with a sampling rate for an oscilloscope used in a pressure measurement. The tail shown in the measured pressure-time profile does not exist in the simulation. This was already discussed in earlier sections suggesting that this offset is caused by experimental circumstances and has nothing to do with an actual pressure applied to the target. Apart from that the data shows a very good fit.

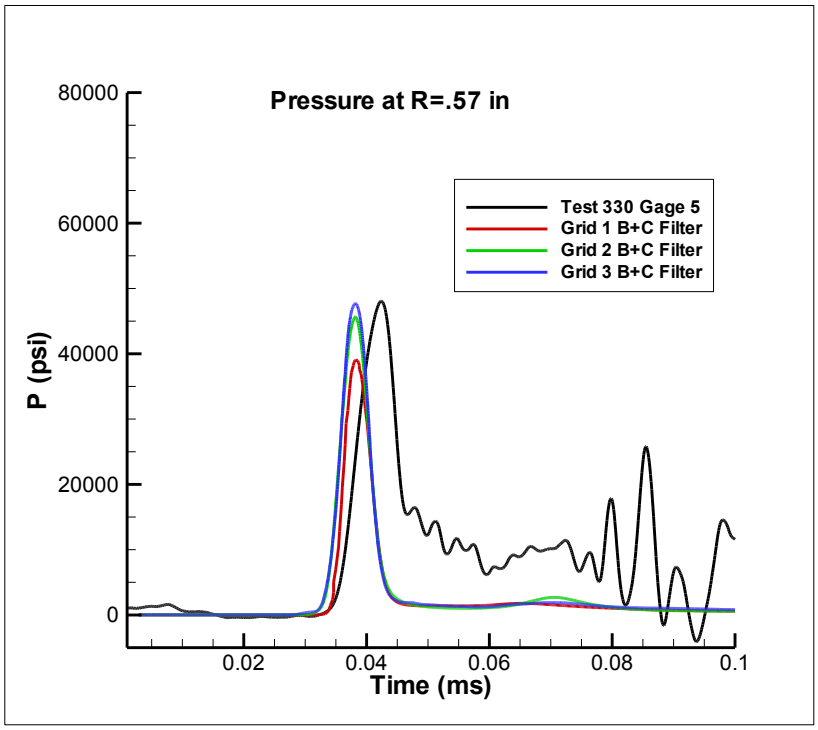

Figure 6.63 Computed and measured pressure-time profiles

The computer simulation shows the flow field in the water and the gas bubble in **Figure 6.64**. The gas bubble is driving the water front against the target plate and is confined by the water opening up against the target plate. The graph above the target plate in **Figure 6.64** shows the pressure-time profile at the same time. It is clearly visible that the impacting water forming a ring drives the pressure on the bottom of the target plate. The gas bubble does not transmit a noticeable pressure pulse to the target; see the pressure-time profile in **Figure 6.64**. The pressure transmitted at the time of 47.723 μs is 414 Mega Pascal (60,000 PSI).

Figure 4.65 shows the same simulation at a later time. The gas bubble is still confined and the pressure in the flow field and at the target bottom dropped significantly to 110 Mega Pascal (16,000 PSI) at the time of 101.05 μs, see pressure-time profile on top of the flow field.

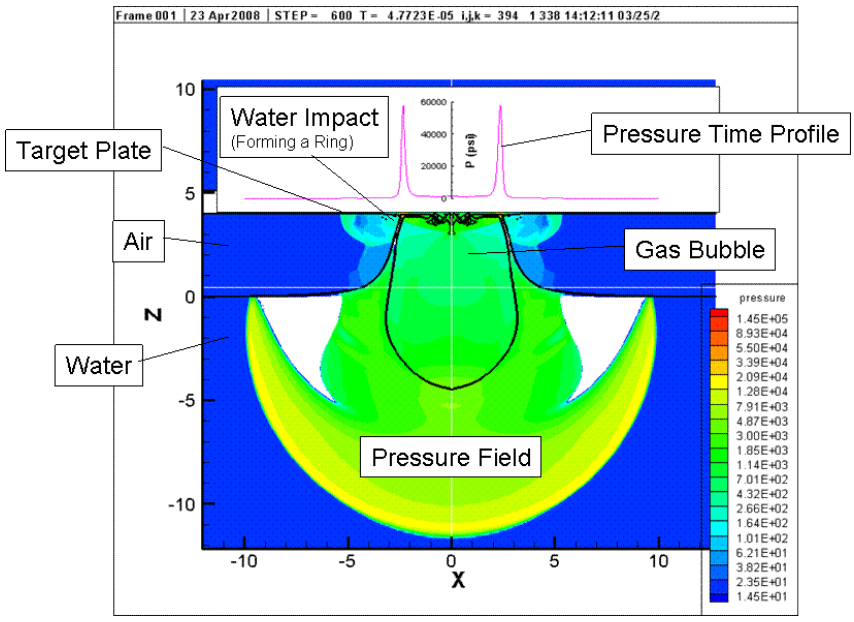

Figure 6.64 Computed pressure-time profile and expanding bubble at t=0.0477 ms

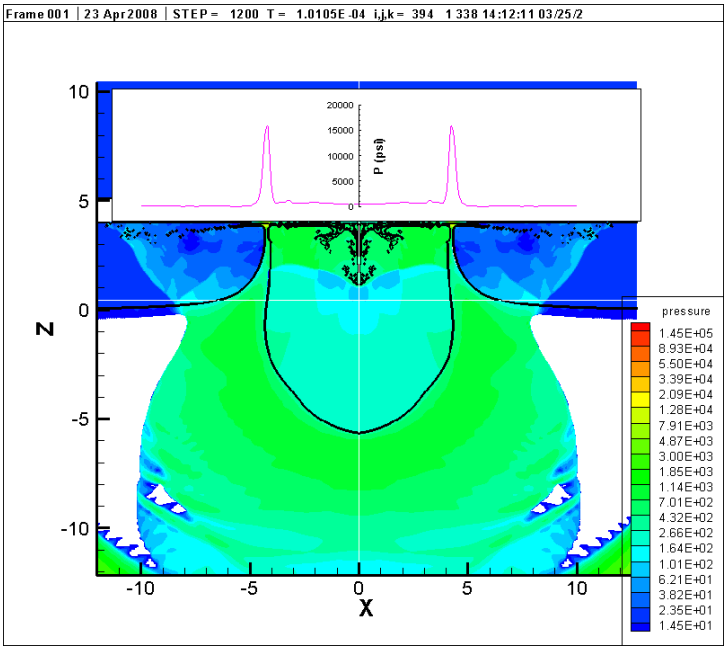

Figure 6.65 Computed pressure-time profile and expanding bubble at t=0.10105 ms

Chapter 7: Concluding Remarks

This report has presented the results of approximately 820 pressure – time profiles recorded (110 tests conducted) including approximately 60 tests on impulse, verification and visualization testing in order to establish the first database for pressure measurements on a vehicle bottom close to detonating IEDs. Approximately 300 tests have been conducted in order to develop and optimize the technique of pressure measurement using Kolsky bars.

Pressure – time profiles have been created which are new to the community of scientists. They can be used to evaluate and correlate hydro codes. The pressure – time profiles presented for the different materials used for loading the target plates and the different Stand-off Distances (SOD) for saturated sand are significant in order to design the bottom of an armored vehicle. The peak pressures at certain location on the bottom of a target plate have been determined which were unknown up to the present. The peak pressure applied lasts only an infinitesimal small amount of time. Overall more important is the pressure – time distribution in order to evaluate armored materials for the type of loading applied. In certain cases the time interval of the applied loading may be too small to shear the material as seen in the punch gage test series presented in this study. Qualitatively, the most insight was probably delivered by the visualization testing. This test method revealed the loading mechanisms for the different materials used and the different Stand-off Distances (SOD) for saturated sand.

The effects of Stand-off Distance (SOD) of the target and the variation of material impacting the target plate on pressure – time recordings have been examined in detail. Visualization testing was conducted to in order to match the loading applied on the bottom of the target plate and the pressure – time signals recorded in time. A technique to calculate the pressure - time profile at the bottom of the target plate has been developed. The pressure – time profiles have been integrated in order to calculate the specific impulse at certain locations. Then the cylindrical shell method

was used to calculate the impulse distribution on the bottom of the vehicle. The accumulated impulse over various circular target plate diameters was calculated. Calculated impulses were compared to impulses measured using different size round plates. Round plates in the impulse testing were preferentially used since the type of loading applied on the bottom of a target plate has a circular form. Additionally in order to model the impulse testing using a computer code, round plates are easier to use.

The loading applied to a target plate is considered as most severe using a saturated soil bed compared to any other mixture of soil containing a variety of moisture contents. The reason is believed to be the percentage of air filled voids in the soil mixture and is currently under investigation in the Dynamic Effects Laboratory. A saturated soil bed contains approximately 2% and a dry soil bed 30% of air filled voids. The effects of the change in SOD were investigated using a saturated sand test bed. The results showed that the peak pressure applied on a target plate directly above the charge over the entire charge diameter is 100% higher for the closest SOD compared to the largest SOD tested. Further away from the center of impact, the pressures measured on the target plate for all cases are very similar. The closest SOD shows the highest peak pressure of all cases.

The results for the specific impulse distribution directly above the charge show up to 500% higher values for the closer SOD compared to the largest SOD due to much longer loading times applied for the closest SOD. The values for the largest SOD decline fast but still stay above the values for the closest SOD with increasing distance from the center of the impact. The largest SOD shows the lowest specific impulse values as expected at all locations where measurements were taken.

The results for the accumulated impulse over plate size diameter show that the impulse delivered to a target plate with increasing plate size increases most for the closest SOD and least for the largest SOD. These results agree very well with tests conducted previously in the Dynamic Effects Laboratory at the University of Maryland.

The visualization tests revealed the differences in the loading mechanisms and were also used in order to verify the loading times for the Kolsky bars used for the pressure measurements.

The effect of change of soil bed was investigated using saturated sand, dry sand and water at the same SOD for all tests conducted. As previously mentioned the percentage of air filled voids changes drastically between dry sand and saturated sand. Water as a test bed was used primarily in order to develop a computer code since its properties are well known. The peak pressure values measured for the dry sand at all locations of the target plate stay well below the values for saturated sand. For water, the peak pressure values measured are largest at all locations besides at the location on the plate above the projected charge diameter. At this location (1.45 cm (0.54 inches)), the peak pressure measured for water is 40% lower compared to dry sand. A reason might be as noticed in the visualization tests for water, that the loading mechanism at the charge diameter shows a donut shape. The outer diameter of the charge equals the inner diameter of the donut. Since the loading mechanism shows this type of change only for the water testing, this might be an indication for the change in the pressure distribution at the bottom of the target plate.

The results for the specific impulse distribution show higher values above the charge for the dry sand compared to saturated sand even though the measured peak pressures are lower. This can be explained by the larger loading time at these locations compared to saturated sand. Further away from the center of impact the specific impulse values for dry sand decrease very fast compared to the other cases. The specific impulse shows up to 200% less value for dry sand at comparable locations. Again for the water results the specific impulse delivered is lowest for all cases above the projected charge diameter on the target plate.

The results for the accumulated impulse over plate size diameter show that the impulse delivered to a target plate with increasing plate size increases for all 3 cases very similar up to approximately 3 times the charge diameter. Then with increasing distance to the center of impact the accumulated impulse for dry sand starts to drop of rapidly. The water and the saturated sand values are almost the same for all the

locations, signals were recorded up to the diameter of 15.24 cm (6 inches) of a target plate. In previously conducted tests measuring the impulse it was shown that at approximately the plate diameter of 20 cm (8 inches) the values for saturated sand start to fall off. Approaching the target plate diameter of 35.5 cm (14 inches) for a 4.4 gram charge the impact is completely absorbed. Increasing the plate size does not increase the impulse further for a 4.4 gram charge. At that diameter the water has delivered a 40% higher impulse compared to saturated sand. Using a larger charge size increases the target diameter for total absorption of the impulse accordingly to the cube root scaling laws.

Again for this test series, the visualization tests revealed the differences in the loading mechanisms and were also used in order to verify the loading times for the Kolsky bars used for the pressure measurements. Additionally they gave some insight into the loading mechanisms for the impulse delivered to target plates.

In the past, the results from small scale tests conducted in the Dynamic Effects Laboratory at the University of Maryland have provided significant insight in testing procedures in order to predict full scale testing. In preparation for full scale testing they have proven to be a very helpful tool for the execution of full scale testing since technical issues are highlighted up-front. With tight budgeting small scale testing provides an economical solution in order to reduce costs for full scale testing. Predictions from results obtained by small scale tests for full scale tests have proven in the past a 90% accuracy. Since the peak pressure results from small scale tests to full scale tests scale one to one, the small scale results can directly be used at the appropriate scaled distance. The loading time needs to be scaled for the time using cube root scaling laws for the pressure – time profiles obtained in order to predict the loading time interval for full scale test results. For this research conducted, the large scale was based on a 4.5 kg charge (10 pounds). In order to scale-up the pressure – time profiles, a factor of 10.1 has to be used based on the cube root scaling for the weight ratios. Any other scaling factor can be used for scaling it up depending on the case required, keeping in mind that SOD and DOB need to be scaled to the same specifications.

Chapter 8: Future Work

As indicated in the section before, several problems encountered over the past 6 years need further to be investigated despite the approximately 500 tests conducted. The following areas should be revisited in order to verify or further investigate certain results.

In the area of impulse measurements, the round plates and saturated sand should be used in order to verify the results gained by the pressure measurements at the SOD 2 cm (0.39 inches) and 6 cm (2.38 inches).

Additionally it needs to be verified if the ratio of the plate mass over the explosive mass is the same for a different loading media than saturated sand. It was tested using saturated sand only, compare **Figure 5.34** in Section 5. In the past, tests have shown that the ratio plays a role in impulse testing. Characterizing a measured impulse as maximum impulse delivered to a target under certain test conditions implies testing at the so-called sweet spot. The sweet spot is defined by the maximum impulse absorbed by a target plate depending on the ratio of the plate mass over the explosive mass.

Recent results in dry sand testing using the round plates and different sand show deviations from old results, even though the sieve analyses of both sands show very close similarity. The question rises if a sieve analyses is not the only important point to look at but also maybe particle shapes play a significant role in dry sand loading.

For the pressure measurements, it would be desirable to measure the pressure at more locations between the center of impact and 2.45 cm (1 inch) on the target plate. It seems that there are significant differences found between low and high pressure areas. This might be important from the point of view for designing the armor plate on a bottom of a vehicle. It does not influence the total impulse calculation too much since the area applied to is very small and therefore does not change the impulse significantly.

Also it is desirable to investigate a different DOB in saturated sand, shallower and deeper in order to obtain results of the change of the pressure-time profiles with change of DOB.

An investigation of pressure – time profiles for a V-shaped bottom of a target plate supported by V-shaped Plexiglas plates in order to show the loading mechanisms would be desirable.

Recent tests conducted by using different types of soil have shown that the type of soil used does not drastically change the results for the impulse measured. What is more important is controlling the density of the soil in addition with the moisture content. The amount of air voids in the soil bed does influence the results significantly. It would be desirable to investigate how the pressure-time profiles change under these conditions.

More testing is required in order to investigate the fracturing happening in the acrylic sheets using water as impacting media. Neither the pressure-time profiles nor the total impulse plots show a significant enough difference compared to saturated sand at the location where fracturing occurs in order to explain the phenomenon.

References

(1) Fourney, W.L., Leiste, H.U., Bonenberger, R., Goodings, D., Explosive Impulse on Plates, International Journal for Blasting & Fragmentation, Vol. 9, Number 1, pp. 1-18, March 2005

(2) Fourney, W.L., Leiste, H.U., Hauck, A., Jung, D., Distribution of Specific Impulse on Vehicles Subjected to IED's, International Journal for Blasting & Fragmentation, Vol. 4, Number 2, pp. 117-134, October 2010

(3) Lamb, C., Schmidt, M., Fitzsimmons, B. (2009). MRAPs, Irregular Warfare, and Pentagon Reform. Joint Force Quarterly. 55 (4), 76-85

(4) Feickert, A., Mine-Resistant, Ambush-Protected (MRAP) Vehicles: Background and Issues for Congress, Congressional Research Service, January 2011

(5) Hopkinson, B., A Method of Measuring the Pressure Produced in the Detonation of High Explosives or by the Impact of Bullets, Philos. Trans. R. Soc. (London) A, 213, pp. 437-456, 1914

(6) Kolsky, H. (1949). An Investigation of the Mechanical Properties of Materials at Very High Rates of Loading, Proc. Phys. Soc. London, B62, p.676

(7) Taylor, L.C., Fourney, W.L., & Lathrop, D.P., Surface Instabilities from Buried Explosives, International Journal for Blasting & Fragmentation, Vol. 3, Number 3, pp. 241-268, December 2009

(8) Taylor, L.C., Fourney, W.L., Leiste, H.U., Cheeseman, B., Loading Mechanisms on a Target From Detonation of a Buried Charge, Proceedings of 24th International Symposium on Ballistics, New Orleans, LA, 22-26 September 2008

(9) Taylor, L.C., Fourney, W.L., Leiste, H.U, Soil Cap Density Distribution Resulting from Buried Explosions in Saturated Sand, International Journal for Blasting & Fragmentation, Submitted September 2011

(10) Lampson, C.W., Explosions in Earth in Effects of Impact and Explosion, Office of Scientific Research and Development, Washington, D.C. (1946)

(11) Morrey, C.B., Underground Explosion Theory in Operation Jangle, WT-369, Office of Technical Services, Department of Commerce, Washington, D.C., (1952)

(12) Chabai, A.J., On Scaling Dimensions of Craters Produced by Buried Explosives, Journal of Geophysical Research, Vol. 70, No. 20, pp 5075-5098 (Oct. 1965)

(13) Bartsch, H. J., Taschenbuch Mathematischer Formeln, Fachbuchverlag Leipzig, 19. Auflage, ISBN 3-446-21792-4, 2001

(14) Weisstein, E. W., Method of Shells, CRC Concise Encyclopidia of Mathematics, Second Edition, Chapman & Hall/CRC, ISBN-13 978-1584883470, 2002

(15) Dally, J. W., Bonenberger, R. J., Mechanic II Mechanics of Materials, College House Enterprises, LLC., ISBN-13 978-9792581-5-2, 2010

(16) Taylor, L. C., Fourney, W. L., Leiste, H. U., Pressures on Targets From Buried Explosions, International Journal for Blasting & Fragmentation, Vol. 4, Number 3, pp. 165-192, December 2010

(17) W.L. Fourney & U. Leiste, L,C. Taylor, Small Scale Testing to Investigate Air Blast Loading on Plates, International Journal for Blasting & Fragmentation, Vol. 3, Number 3, pp. 187-205, December 2009

(18) Andrew Wardlaw, William Fourney & Ulrich Leiste, Target Loading from a Submerged Explosion, International Journal for Blasting & Fragmentation, Vol. 2, Number 3, pp. 211-226, November 2008

(19) Kerley, Gerald I., Numerical Modeling of Buried Mine Explosions, ARL-CR-461, March 2001

(20) Donahue, L., Bouamoul, A., Dunbar, T. E., Numerical Modeling Approaches for Simulation of Landmine Blast Loading , Proceedings of the 76th Shock and Vibration Symposium, Destin, Florida, October 30th – November 3rd, 2005

(21) Wardlaw, A. B. Jr., Luton, J. A., Renzi, J. R., Kiddy, K. C., McKeown, R. M., The Gemini Euler Solver for the Simulation of Underwater Explosions, NSWC IH Tr 2005, November 2003

(22) Wardlaw, A. B. Jr., Illamin, R., Harris, G., Cavitation Modeling, Proceedings of the 73rd Shock Vibration Symposium, November 2002

(23) Wardlaw, A. B. Jr., Luton, J. A., Fluid-Structure Interaction Mechanisms for Close-in Explosions, Shock and Vibration Journal, 7, 2000, pp 265-275

(24) Szymczak, W. G., Platform Loading from Explosions in Saturated Sand Using a Visco-Plastic Model, International Journal for Blasting & Fragmentation, Vol. 9, Number 4, pp. 189-203, December 2005

(25) Fourney, W. L., Leiste, H. U., Bonenberger, R., Goodings, D. J., Mechanism of Loading on Plates due to Explosive Detonation, International Journal for Blasting & Fragmentation, Vol. 9, Number 4, pp. 205-217, December 2005

(26) Fourney, W. L., Leiste, H. U., Taylor, L., Pressures Acting on Targets Subjected to Explosive Loading, International Journal for Blasting & Fragmentation, Vol. 2, Number 2, pp. 167-188, 2008

(27) Szymezak, W., G., Leiste, H., U., Fourney, W., L., Yield Surfaces for Granular Flows Applied Explosively", International Journal for Blasting & Fragmentation, Vol. 3., Number 1, pp 43-72, 2009

(28) Fourney., W. L., Leiste, H. U., Taylor, L., Small Scale Testing to Investigate Air Blast Loading on Plates, International Journal for Blasting & Fragmentation, Vol. 3, Number 3, pp 187-206, 2009

(29) Wardlaw, A., Fourney, W. L., Leiste, H. U., Target Loading from a Submerged Explosion, Shock & Vibration 17, 3, pp317-328, 2010

(30) Sutton, M. A., Tiwari, V., Zhao, X., Deng, X., Fourney, W. L., Leiste, H. U., Bretall, D., Full-Field Deformation Measurements Under Explosive Loading Conditions Using Multi-Image Pattern Analysis, International Journal for Blasting & Fragmentation, Vol 4, Number 3, pp 193-205, December 2010

(31) Fox, D. M., Huang, X., Fourney, W. L., Leiste, H. U., Lee, J. S., The response of small scale rigid targets to shallow buried explosive detonations, International Journal of Impact Engineering. Vol. 38, Issue 11, pp. 882-891, November 2011

(32) Fourney., W. L., Leiste, H. U., Bonenberger, R., Goodings, D. J., Predicting Explosive Impulse by Means of Small Scale Tests, 31st Annual International Society for Explosives Engineering Meeting, Orlando, Fla. February 2, 2005

(33) Fourney., W. L., Leiste, H. U., Loading of Target Plates with Buried Explosives, ASME-International Mechanical Engineering Congress and Exposition (IMECE), Seattle WA, November 10-16, 2007

(34) Fourney., W. L., Leiste, H. U., Taylor, L. C., Pressures Acting on Targets Subjected to Explosive Loading, ASME-International Mechanical Engineering Congress and Exposition (IMECE), Seattle WA, November 10-16, 2007

(35) Fourney., W. L., Leiste, H. U., Taylor, L. C., Pressure Irregularities in the Loading of Vehicles by Buried Mines, 34th Annual International Society for Explosives Engineering Meeting, New Orleans, La., Volume II, (12 pages), January 2008

(36) Fourney., W. L., Leiste, H. U., Genson, K., Taylor, L. C., Geometrical Shaping of Vehicles for Reducing Impulse from Explosive Detonation, National Defense Industrial Association (NDIA), 2008 Warheads and Ballistics Classified Symposium, Monterey, California, 11-14 February 2008

(37) Fourney., W. L., Leiste, H. U., Taylor, L. C., Pressure Irregularities in the Loading of Vehicles by Buried Mines, 34th Annual International Society for Explosives Engineering Meeting, New Orleans, La. January 2008

(38) Fourney., W. L., Leiste, H. U., Taylor, L. C., Small Scale Mine Blast – Target Interaction, ARL Workshop, Aberdeen, Md., August 5, 2008

(39) Fourney., W. L., Leiste, H. U., Taylor, L. C., Loading Mechanisms from Shall Buried Explosives, ARL Workshop, Aberdeen, Md., August 5, 2008

(40) Fourney., W. L., Leiste, H. U., Taylor, L. C., Pressure Measurements in Small Scale Testing, ARL Workshop, Aberdeen, Md., August 5, 2008

(41) Fourney., W. L., Leiste, H. U., Taylor, L. C., Impulse Measurements with Shaped Bottoms, ARL Workshop, Aberdeen, Md., August 5, 2008

(42) Fourney., W. L., Leiste, H. U., Taylor, L. C., A Preliminary Study of Mitigation of Explosive Blast Effects on Vehicle Floorboards, ARL Workshop, Aberdeen, Md., August 5, 2008

(43) Fourney., W. L., Leiste, H. U., Taylor, L. C., Inverse Hybrid Method for Determining Explosive Loading on Plates Due to Buried Mines, ARL Workshop, Aberdeen, Md., August 5, 2008

(44) Fox, D. M., Fourney., W. L., Leiste, H. U., Taylor, L. C., Impulse Delivered to Concave Vehicle Shapes Due to Detonation of a Buried Mine, ARL Workshop, Aberdeen, Md., August 5, 2008

(45) Taylor, L. C., Fourney., W. L., Leiste, H. U., Loading Mechanisms from Shallow Buried Explosives, Ballistics Symposium, New Orleans, LA., September 2008

(46) Taylor, L. C., Fourney., W. L., Leiste, H. U., Loading Mechanisms from Shallow Buried Explosives, Modeling, Simulation, Testing, & Validation Symposium, Warren, MI., November, 2008

(47) Taylor, L. C., Fourney., W. L., Leiste, H. U., Exploring Target Loading from Explosions in Soil, Particle Mechanics in Extreme Environments, Feb. 2009, Vicksburg, MS

(48) Taylor, L. C., Fourney., W. L., Leiste, H. U., Diagnostics & Testing for Shallow Buried Explosives, Particle Mechanics in Extreme Environments, Feb. 2009, Vicksburg, MS

(49) Fourney., W. L., Leiste, H. U., Taylor, L. C., Investigation of Impulse Delivered To a Target Plate From a Buried Explosive, ISEE Explosives Meeting, Denver, CO. Feb. 2009

(50) Taylor, L. C., Fourney., W. L., Leiste, H. U., Comparison of the Response of Deforming and "Non-Deforming" Targets to the Explosion of a Charge Buried in Saturated Sand, 8th International Conference on Shock and Impact Loads on Structures, December 2nd-4th, 2009, Adelaide, Australia

(51) Fourney., W., L., Leiste, H., U., Hauck, A., Jung, D., Distribution of Impulse on Vehicles Subjected to IED's, IMPLAST 2010, Providence. R.I., October 12-14, 2010

(52) Taylor, L. C., Fourney., W. L., Leiste, H. U., Pressures on Targets From Buried Explosives, IMPLAST 2010, Providence. R.I., October 12-14, 2010

(53) Taylor, L. C., Fourney., W. L., Leiste, H. U., Pressures on Targets from Buried Explosions, PMME 2010

(54) Taylor, L. C., Fourney., W. L., Leiste, H. U., Response of Deformable Aluminum Targets to the Explosion of a Charge Buried in Saturated Sand, 2010 NDIA

(55) Taylor, L. C., Fourney., W. L., Leiste, H. U., Comparison of the Response of Deforming and "Non-Deforming" Targets to the Explosion of a Charge Buried in Saturated Sand (U), 11th Joint Classified Bombs/Warheads & Ballistics Symposium Monterey, California, 23-26 August 2010

(56) Taylor, L. C., Fourney., W. L., Leiste, H. U., Density Distribution in the Soil Cap Resulting from a Buried Explosion in Saturated Sand, Joint Classified Bombs/Warheads & Ballistics Symposium, Monterey, CA. August 8-11, 2011

(57) Fourney., W. L., Leiste, H. U., Bonenberger, R., Goodings, D. J., Impulse Loading on Plates due to Detonation of Explosives Beneath Saturated Soils, Report to U. S. Navy, Indian Head Division of NSWC, November 2004

(58) Fourney., W. L., Leiste, H. U., Bonenberger, R., Goodings, D. J., Impulse Loading on Plates due to Detonation of Explosives Beneath Soils and Clays, Report to U. S. Army, Aberdeen, Md., November 2004

(59) Fourney., W. L., Leiste, H. U., Bonenberger, R., Goodings, D. J., Measurements of Pressure Loading on Plates Due to Explosive Detonation, Report to NSWC – Indianhead Division, November 2005

(60) Fourney., W. L., Leiste, H. U., Bonenberger, R., Goodings, D. J., Reduction in Impulse Attributed to Geometric Bottom Shaping", Report to NSWC – Indianhead Division, November 2006

(61) Fourney., W. L., Leiste, H. U, Taylor, L. C., Genson, K., Geometrical Shaping of Vehicles for Reducing Impulse from Buried Explosions. A report to NATC on MRAP vehicles. August 2006

(62) Fourney., W. L., Leiste, H. U., Taylor, L. C., Small-Scale Model Testing in Investigations of Energetic Materials, Chapter 5, Simulation-Based Innovation and Discovery – Energetics Applications, Center for Energetic Concepts Development, 2011

(63) U.S. Department of Defense Photos

(64) Schmidt, R. M., Holsappel, K. A., Theory and Experiments on Centrifuge Cratering, Journal of Geophysical Research, Vol. 85, No. B1, pp 235-252 (Jan. 10th 1980)

(65) Sutton, M. A., Deng, X., Tiwari, V., Zhao, X., Department of Mechanical Engineering University of South Carolina and Fourney, W. L., Leiste, H. U., Dynamic Effects Laboratory University of Maryland, On the Scaling of Blast Loading Experiments for Buried Explosives, International Journal of Impact Engineering, Publication accepted for 2012